A software perspective on infinite elements for wave diffraction and wave forces on marine risers

Bettess, Jacqueline Anne

A Software Perspective on Infinite Elements for Wave Diffraction and Wave Forces on Marine Risers

by

Jacqueline Anne Bettess

A Thesis submitted in partial fulfilment
of the requirements for the degree of
Doctor of Philosophy

Information Technology Service

The University of Durham
2000

1 8 OCT 2000

Contents

v

LIST OF FIGURES

LIST OF TABLES

Abstract

This thesis describes work on the problem of the scattering of water waves by fixed objects. The method used to solve this problem is that of finite and infinite elements. In particular the development of a new wave infinite element is described. Various aspects of the wave scattering problem are considered, but always from the perspective of the numerical methods, the algorithms and the computer implementations used. These deal not only with the modelling of the wave equations, but also the pre and post processing of the finite element algorithms. This encompasses the generation of suitable finite element meshes, in an accurate and economical way, and the presentation of the results, particularly as accurate contour plots of the wave surface.

The first two chapters gives a brief introduction to water waves, and a summary of the basic concepts of finite and infinite elements. In the third chapter the new infinite element for waves, which is a development of an earlier infinite element, is described in detail, including the new mapping, the necessary shape functions and the integration of the element matrix. The earlier infinite element was restricted to the exterior of circular problems. For scattering objects of large aspect ratio this led to meshes with many finite elements, which performed no useful function, and which were computationally wasteful. The mapping in the new infinite element allows the mesh of infinite elements to be tailored to the shape of the diffracting body, without any observed loss of accuracy. It is therefore much more flexible and computationally efficient, because the infinite elements no longer need to be placed radially.

The next three chapters, concentrate on the computer science aspects of the implementation of the finite and infinite elements dealing with the linked list data structures for storage of the element information, the special purpose mesh generation programs, which make it possible to analyse a large range of practical scattering problems and the plotting programs for the display of the results. The chief work in chapter six is the implementation of the Akin and Grey accurate predictor-corrector contour plotting algorithm, with colour fill. The advantage of an accurate contour plotting algorithm is that any discontinuities in the contours represent discontinuities in the results, rather than plotting deficiencies.

Chapter seven shows results which validate the new infinite element, particularly on the problem of waves diffracted by an ellipse. In the remaining chapters eight to eleven, the emphasis is on a practical problem of the wave forces on groups of risers, which are the tubes which carry hydrocarbons from the sea-bed to the working areas of offshore platforms. The aim was to see if the forces on a group of risers were different from the sum of the forces on the individual risers, calculated on the assumption that the risers do not modify the wave field. The conclusion is that more detailed studies may well bring financial benefits to the companies operating offshore installations.

Acknowledgements

For Pete

With many thanks to Alan Craig for the right kind of supervision

Chapter 1

Introduction to surface waves

1.1 Preliminary

The literature on waves is enormous. The topic of this thesis is restricted to surface waves on water, although the results and methods described are also applicable to other fields. These include electro-magnetic waves, which encompass light waves, radio and radar, waves in elastic bodies, including earthquake waves and waves used for seismic explorations, and acoustic waves in air and water.

Even the restriction to surface waves on water involves an enormous body of work. Here the briefest of introductions is given, and the reader is referred to more comprehensive books on the topic, such as those of Lamb[87], Lighthill[91], Mei[96], Stoker[112], Kinsman[85], and Whitham[118]. Real physical waves involve many different effects, including surface tension, viscosity, breaking and other non-linear effects. In this thesis the waves considered are linear, and viscosity and surface tension are ignored.

1.1.1 Shallow water wave equations

In their simplest form the shallow water wave equations can be derived from a degeneration of the Navier-Stokes equations governing the movement of Newtonian fluids, a continuity (or conservation of mass) equation and a hydrostatic assumption. Figures 1.1 and 1.3 show the geometry of the problem. The free surface of the water, when undisturbed, is defined as the x, y plane, and the z direction is taken as vertically upwards, so as to form a right handed cartesian set of axes. A typical wavelength, is denoted by λ. The water depth, $h(x, y)$, is allowed to vary, with x and y, but is constant with time. (This excludes *tsunamis*, or earthquake or tidal waves.) The velocities in the x and y directions are denoted by $u(x, y, z, t)$ and $v(x, y, z, t)$ respectively. The velocities of fluid particles are functions of *position*, which is the *Eulerian* method of description of flows. Other important parameters are the acceleration due to gravity, g, and the wave elevation, $\eta(x, y, t)$, which varies in space and time.

1.1.2 Balance of momentum

The Navier Stokes equations can be written[87], page 577, in two dimensions, for the case of an *incompressible* fluid, and omitting body forces, in cartesian co-ordinates as
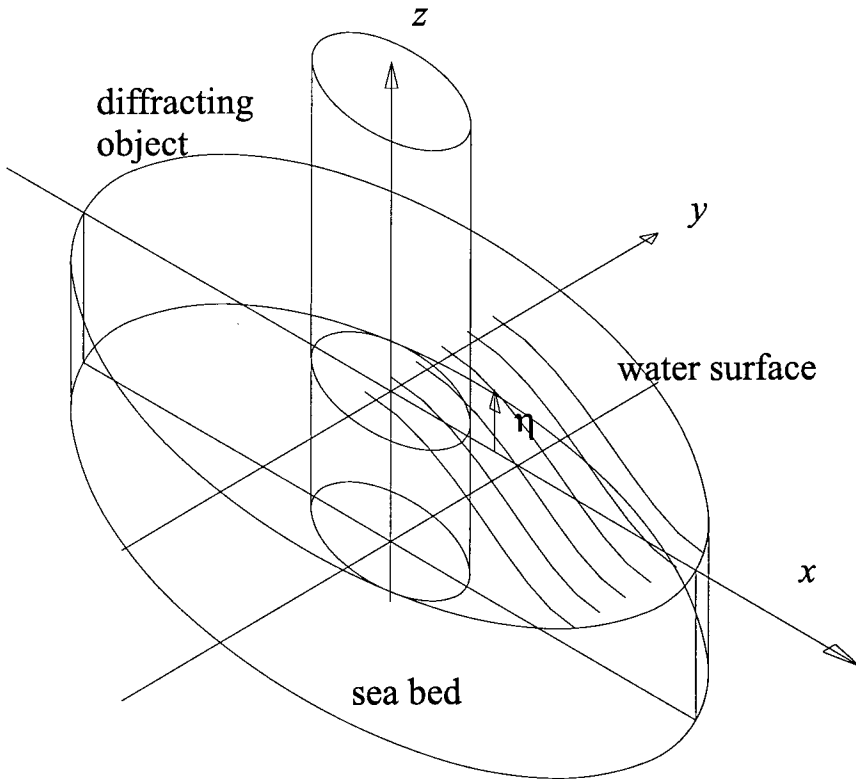
Figure 1.1   General arrangement of wave problem

$$\rho\left(\frac{\partial u}{\partial t} + \left[u\frac{\partial u}{\partial x} + v\frac{\partial u}{\partial y}\right]\right) = -\frac{\partial p}{\partial x} + \mu\left\{\frac{\partial^2 u}{\partial x^2} + \frac{\partial^2 u}{\partial y^2}\right\},$$

$$\rho\left(\frac{\partial v}{\partial t} + \left[u\frac{\partial v}{\partial x} + v\frac{\partial v}{\partial y}\right]\right) = -\frac{\partial p}{\partial y} + \mu\left\{\frac{\partial^2 v}{\partial x^2} + \frac{\partial^2 v}{\partial y^2}\right\},$$

1.1

where μ is the viscosity. The next step is to ignore the *convective* acceleration terms in equations 1.1. These are the terms in the square brackets. These terms express the accelerations of a particle, (even when there is no overall change in the pattern of flow), caused by its movement from a region of low to high velocity, as for example flow through a nozzle. They have been shown to be of less importance in waves and henceforth will be ignored. The second assumption is that the fluid is ideal, so it is incompressible and viscous effects are ignored, since these are also thought to be of little effect in most surface waves. That is all the terms including the viscosity, μ are now dropped. The final assumption, which can be relaxed later, is that the pressure, p is hydrostatic. The fluid is also assumed to be incompressible. The resulting form of the Navier-Stokes equations is

$$\rho\frac{\partial u}{\partial t} = -\frac{\partial p}{\partial x}, \qquad \rho\frac{\partial v}{\partial t} = -\frac{\partial p}{\partial y}, \qquad\qquad 1.2$$

and the pressure is given by

$$p = \rho g(\eta - z). \qquad\qquad 1.3$$

The expression for pressure 1.3, is substituted into equations 1.2, to give

$$\frac{\partial u}{\partial t} = -g\frac{\partial \eta}{\partial x}, \qquad \frac{\partial v}{\partial t} = -g\frac{\partial \eta}{\partial y}. \qquad\qquad 1.4$$

These equations express the balance of momentum in the x and y directions.

1.1.3 Conservation of mass

The equation of continuity, or conservation of mass states that if we consider a volume which is prismatic in plan, then the increase of fluid volume within the prism, is equal to the net inflow into the prism. If the prism is rectangular with plan dimensions δx and δy, as shown in Figure 1.2, then the equation can be derived as follows.
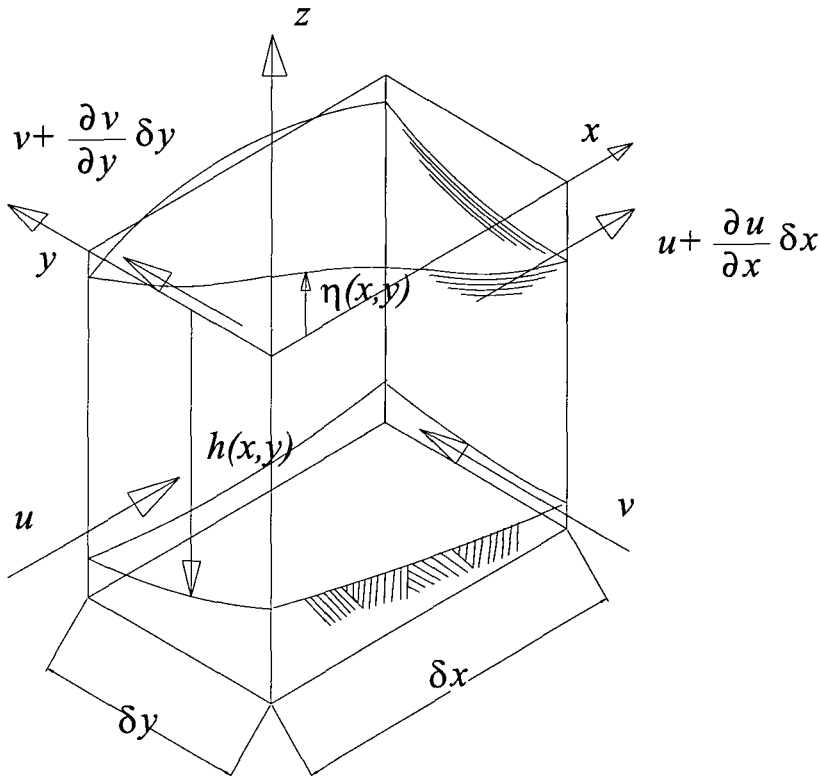
Figure 1.2 Element of fluid for conservation of mass

Consider first the outflow in the x direction. During a time δt, there will be a total volume outflow of

$$\left[-u \times h \times \delta y + \left(uh + \frac{\partial(uh)}{\partial x} \delta x \right) \times \delta y \right] \delta t = \frac{\partial(uh)}{\partial x} \delta x \times \delta y \times \delta t.$$

By a similar argument, the outflow in the y direction will be

$$\frac{\partial(vh)}{\partial y} \delta x \times \delta y \times \delta t.$$

During the same time interval, δt, the increase in volume will be

$$\frac{\partial \eta}{\partial t} \times \delta x \times \delta y \times \delta t.$$

On equating the inflow and the increase in volume and dividing by the area, we obtain

$$\frac{\partial \eta}{\partial t} = -\frac{\partial}{\partial x}(hu) - \frac{\partial}{\partial y}(hv). \qquad 1.5$$

This is the *continuity* equation.

1.1.4 Wave equation

At this stage various options are possible. The wave equation can be developed in terms of pressure, p, wave elevation, η, velocity potential, ϕ or the velocities, u and v can be retained.

The derivation in terms of the wave elevation, η, is very straightforward. Differentiate the continuity equation, 1.5, with respect to time, t, to give

$$\frac{\partial^2 \eta}{\partial t^2} = -\frac{\partial}{\partial x}\left(h\frac{\partial u}{\partial t} \right) - \frac{\partial}{\partial y}\left(h\frac{\partial v}{\partial t} \right). \qquad 1.6$$

Now use the momentum equations, 1.4, to eliminate the velocities, u and v, leaving the wave equation, 1.7, solely in terms of wave elevation, η.

$$\frac{1}{g}\frac{\partial^2 \eta}{\partial t^2} = \frac{\partial}{\partial x}\left(h\frac{\partial \eta}{\partial x} \right) + \frac{\partial}{\partial y}\left(h\frac{\partial \eta}{\partial y} \right). \qquad 1.7$$

This is the wave equation for varying water depth. For constant depth, h, it takes the form

$$\frac{1}{gh}\frac{\partial^2 \eta}{\partial t^2} = \frac{\partial^2 \eta}{\partial x^2} + \frac{\partial^2 \eta}{\partial y^2}.$$ 1.8

Now the shallow water wave equation will be developed in terms of the *Velocity Potential*. This is defined as a function, ϕ, such that its derivatives in the x, y and z directions, yield the corresponding wave particle velocities. Thus

$$\frac{\partial \phi}{\partial x} = u, \qquad \frac{\partial \phi}{\partial y} = v, \qquad \frac{\partial \phi}{\partial z} = w.$$ 1.9

The expressions for velocities can be substituted into the momentum equations in the x and y directions, 1.4.

$$\frac{\partial^2 \phi}{\partial t \partial x} = -g\frac{\partial \eta}{\partial x}, \qquad \frac{\partial^2 \phi}{\partial t \partial y} = -g\frac{\partial \eta}{\partial y}.$$ 1.10

Because the velocity potential is arbitrary, to within an additive constant, equation 1.10 can be integrated with respect to x or y, to give

$$\frac{\partial \phi}{\partial t} = -g\eta.$$ 1.11

Equation 1.11 is differentiated with respect to time and substituted into the continuity equation, 1.5, to give

$$\frac{1}{g}\frac{\partial^2 \phi}{\partial t^2} = \frac{\partial}{\partial x}\left(h\frac{\partial \phi}{\partial x}\right) + \frac{\partial}{\partial y}\left(h\frac{\partial \phi}{\partial y}\right).$$ 1.12

The equations can also be expressed in vector notation.

$$\frac{1}{g}\frac{\partial^2 \phi}{\partial t^2} = \nabla\left(h\nabla\phi\right), \qquad \frac{1}{g}\frac{\partial^2 \eta}{\partial t^2} = \nabla\left(h\nabla\eta\right).$$ 1.13

1.1.5 Wave parameters

Some of the parameters are illustrated in figure 1.3.

The wave speed, c is defined as $c = \omega/k$, where k is the wave number, given by $k = 2\pi/\lambda$, where λ is the wavelength. The period of the wave, T, is the time for a complete wave length to pass a chosen point, and it is related to the angular frequency, ω, by $\omega = 2\pi/T$. For shallow water waves, the wave speed, c, is given by $c = \sqrt{gh}$. This is also the group velocity, and all disturbances travel at the same speed in shallow water. For other depths the wave speed and group velocity are different.
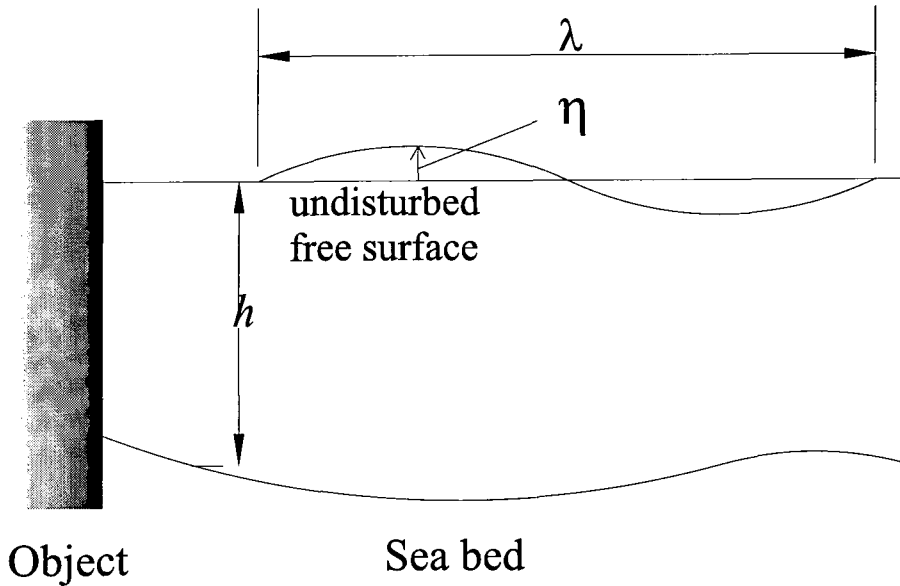
Figure 1.3   Wave geometry

1.2 Intermediate depths

If the assumption that the pressure is hydrostatic is abandoned the so-called *interme-diate* water depth theory is developed. This will not be explained in detail here, but is available in classical text books[85,87,96]. The theory predicts a vertical variation of pressure, and orbital velocities which vary as $\cosh k(h + z)/ \cosh kh$. In intermediate depths, the wave speed is no longer a constant and there is a relation between wave-length and wave speed. This is called the *dispersion relation*, because for any given wave shape, the separate parts will travel at different speeds and thus tend to disperse. The relation is given as

$$\omega^2 = gk \tanh kh. \qquad 1.14$$

The wave speed, c, is then given by $c = \omega/k$, which gives

$$c^2 = \frac{g}{k} \tanh kh. \qquad 1.15$$

The group velocity, c_g, is given by

$$c_g = \frac{1}{2}\left(1 + \frac{2kh}{\sinh 2kh}\right) c = nc, \qquad 1.16$$

where $n = (1/2)(1 + (2kh/\sinh 2kh))$.

For shallow water, $\tanh kh \approx kh$, so that $c = c_g = \omega/k = \sqrt{gh}$. For deep water, $\tanh kh \approx 1$, so that

$$\omega^2 = gk \qquad c = \frac{g}{\omega} = \sqrt{\frac{g}{k}}. \qquad\qquad 1.17$$

There are many more equations relating to various aspects of linear and non-linear waves, far too many to quote in full here. The reader is referred to refs 87, 89, 91, 118. Mehauté[89] gives tables of formulas for linear waves.

It is difficult to develop the necessary intermediate depth theory when the water depth, h is a function of position. However this was done, for the periodic case, by Berkhoff[27], using asymptotic expansions. The equation is given below, in section 1.3.

1.3 Periodic solutions

It is often convenient to consider periodic solutions of the wave equation, in which case the dependence of ϕ and all the other variables in the problem upon the time, t, can be taken to be of the form

$$\phi(x, y, z, t) = \phi(x, y, z)\exp(i\omega t), \qquad\qquad 1.18$$

where ω is the angular frequency, in radians per second. In this case the wave equation for shallow water given above as equation 1.12 becomes

$$\frac{\omega^2}{g}\phi = \frac{\partial}{\partial x}\left(h\frac{\partial\phi}{\partial x}\right) + \frac{\partial}{\partial y}\left(h\frac{\partial\phi}{\partial y}\right). \qquad\qquad 1.19$$

For the intermediate depth case the form of the wave equation is due to Berkhoff[27], and a full explanation of the asymptotic expansions is given by Bettess and Zienkiewicz[122]. The resulting wave equations are

$$\omega^2\frac{c_g}{c}\eta = \nabla\left(cc_g\nabla\eta\right) \quad\text{or}\quad \frac{c_g}{c}\frac{\partial^2\eta}{\partial t^2} = \frac{\partial}{\partial x}\left(cc_g\frac{\partial\eta}{\partial x}\right) + \frac{\partial}{\partial y}\left(cc_g\frac{\partial\eta}{\partial y}\right), \qquad 1.20$$

$$\frac{c_g}{c}\frac{\partial^2\phi}{\partial t^2} = \nabla\left(cc_g\nabla\phi\right) \quad\text{or}\quad \frac{c_g}{c}\frac{\partial^2\phi}{\partial t^2} = \frac{\partial}{\partial x}\left(cc_g\frac{\partial\phi}{\partial x}\right) + \frac{\partial}{\partial y}\left(cc_g\frac{\partial\phi}{\partial y}\right). \qquad 1.21$$

The above equations are valid for intermediate depths, i.e. the bed slopes are less than the water surface slopes. In equations 1.20 and 1.21, c is the wave speed, and c_g is the group velocity.

For constant depth, h, the equations reduce to the classical form of the Helmholtz equation, and it is this form which will mostly be used in this thesis.

$$\frac{\partial^2 \phi}{\partial x^2} + \frac{\partial^2 \phi}{\partial y^2} + k^2 \phi = 0.$$ 1.22

In periodic problems, equation 1.11 reduces to

$$i\omega\phi = -g\eta \qquad \phi = \frac{ig}{\omega}\eta \qquad \eta = -\frac{i\omega}{g}\phi.$$ 1.23

1.4 Bed friction

Bed friction as such is not relevant to the work in this thesis. Offshore installations are usually in water of such depth that the influence of the waves does not reach the sea-bed. In general for depths exceeding half the wave length, the wave motion on the bed is negligible and so can be neglected. The wave motion decays as $\cosh kz$, where k is the wave number, as mentioned in section 1.2. Thus at a depth of half a wavelength, motions will have reduced to $\cosh(2\pi/\lambda) \times (\lambda/2) = \cosh \pi \approx 0.08$. So at a depth of half a wavelength the influence of the waves will be less than one tenth of that at the surface. (This effect can be recalled when seeing films of divers working in deep water, where the motions always seem quite small). Of course strong tidal currents can still occur on the seabed. However the phenomenon of bed friction is still relevant to the energy absorption processes proposed in Chapter 9 and 10 for modelling the viscous losses around risers.

Even the concept of bed friction itself is a fiction, introduced to model in a relatively straightforward way the effects of a boundary layer at the bed.

The detailed mechanics of this layer are complicated, but it is often found satisfactory to model its effect on the rest of the flow as a friction force, related in a simple way to the slip velocity of the flow at the bed. The most generally accepted model for the friction force is that introduced by Chézy, which assumes that the force is related via Chézy's friction constant to the square of the velocity at the bed. The actual and assumed velocity distributions are sketched in Figure 1.4. In figure 1.4 the 'actual' velocity distribution is $u = y^{1/7}$, a crude appoximation to the true time averaged velocity profile for a turbulent boundary layer.

The momentum equation in the c direction becomes, with the addition of the Chézy friction force

$$\frac{\partial u}{\partial t} = -g\frac{\partial \eta}{\partial x} - g\frac{u|u|}{C_c^2 h}.$$ 1.24

The new term is non-linear. The absolute value of u is taken, because otherwise the force would sometimes act in the wrong direction, that is the opposite direction to the velocity. The Chézy constant can be related to the dimensionless friction factor by
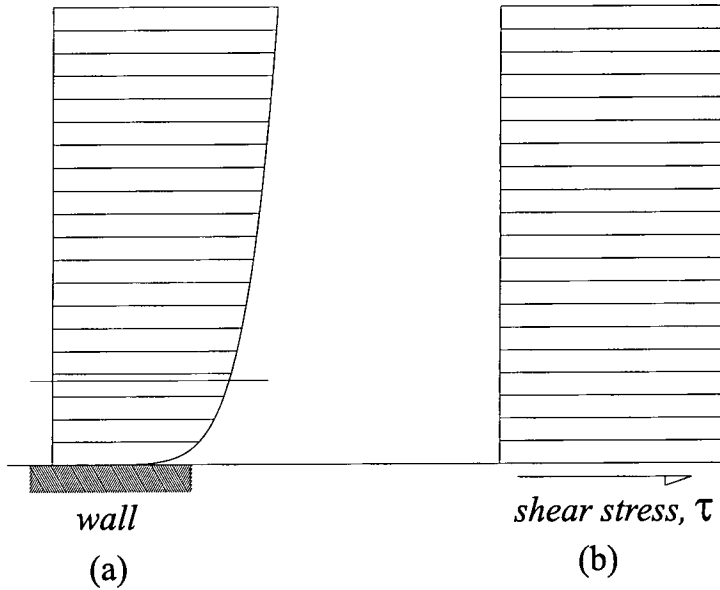
(a) 'actual' velocity distribution, with turbulent boundary layer,

(b) idealised velocity distribution, with friction force

Figure 1.4   Velocity distributions close to the bed

$$C_c = \sqrt{\frac{8g}{f}},$$ 1.25

where C_c is the Chézy factor and f is the friction factor or Darcy resistance coefficient.

One way out of the difficulties posed by the non-linearity of the friction term was proposed by Lorentz. This is to replace the non-linear term by a linear one which will dissipate the same amount of energy in one cycle of the periodic wave motion. The method will be used later, to dissipate the energy equivalent to the viscous drag force on the cylinder. The new linear constant is denoted by M and if the energies dissipated are equated, the equation

$$\int_0^T \frac{u^2 u dt}{C_c h} = \int_0^T (Mu) u dt$$ 1.26

is obtained in which T is the wave period. This gives an expression for M

$$M = \frac{8u_{max}}{3\pi C_c^2 h},$$ 1.27

where u_{max} is the maximum velocity at the bed at that point, in the wave cycle. The momentum equation can now be written

$$\frac{\partial u}{\partial t} = -g\frac{\partial \eta}{\partial x} - gMu.$$

1.28

With the continuity equation derived earlier, equation 1.5

$$\frac{\partial \eta}{\partial t} = -\frac{\partial}{\partial x}(hu) - \frac{\partial}{\partial y}(hv),$$

1.29

and the momentum equation for the y direction

$$\frac{\partial v}{\partial t} = -g\frac{\partial \eta}{\partial y} - gMv,$$

1.30

a new wave equation including friction can be found, as follows. The two momentum equations are multiplied by h and differentiated with respect to x and y to give

$$\frac{\partial}{\partial x}\left(h\frac{\partial u}{\partial t}\right) = -\frac{\partial}{\partial x}\left(gh\frac{\partial \eta}{\partial x}\right) - \frac{\partial}{\partial x}(ghMu)$$

and

$$\frac{\partial}{\partial y}\left(h\frac{\partial v}{\partial t}\right) = -\frac{\partial}{\partial y}\left(gh\frac{\partial \eta}{\partial y}\right) - \frac{\partial}{\partial y}(ghMv).$$

1.31

The continuity equation is differentiated with respect to t, thus

$$\frac{\partial^2 \eta}{\partial t^2} = -\frac{\partial}{\partial x}\left(h\frac{\partial u}{\partial t}\right) - \frac{\partial}{\partial y}\left(h\frac{\partial v}{\partial t}\right),$$

1.32

and the momentum equations are substituted, to give

$$\frac{\partial^2 \eta}{\partial t^2} = \frac{\partial}{\partial x}\left(hg\frac{\partial \eta}{\partial x}\right) + \frac{\partial}{\partial y}\left(hg\frac{\partial \eta}{\partial y}\right) + \frac{\partial}{\partial x}(hgMu) + \frac{\partial}{\partial y}(hgMv).$$

1.33

The original continuity equation can now be used, to rewrite the (hu) and (hv) expressions, in terms of $\partial \eta/\partial t$, to give

$$\frac{\partial^2 \eta}{\partial t^2} + gM\frac{\partial \eta}{\partial t} = g\left[\frac{\partial}{\partial x}(h\frac{\partial \eta}{\partial x}) + \frac{\partial}{\partial y}(h\frac{\partial \eta}{\partial y})\right].$$

1.34

For periodic problems $\eta(x, y, t) = \eta(x, y)\exp(i\omega t)$, giving

$$-\omega^2 \eta + i\omega M g \eta = g \left[\frac{\partial}{\partial x}(h\frac{\partial \eta}{\partial x}) + \frac{\partial}{\partial y}(h\frac{\partial \eta}{\partial y}) \right]. \qquad 1.35$$

This again can be used as the basis for a finite element model.

The chief difficulty is that the u_{max} value is not known before the calculation starts, and so M cannot be found. In practice the procedure is to guess u_{max} everywhere (possibly simply taking the incident wave as the velocity), and thus to estimate a starting value for M.

According to Ippen[81], 'The linearisation of the friction term in the dynamic equation received major attention in the studies connected with the closing off by a dyke of the Zuider-Zee through the famous physicist H. A. Lorentz and his committee. It was, however first suggested in 1909 by Prasil and Dubs, according to Einstein and Fuchs.' I have not been able to locate any of these references.

1.5 Boundary conditions

1.5.1 Total reflection

The condition that waves are totally reflected at a boundary is that the normal velocity, u_n, is zero, since there can be no flow through a rigid boundary. Thus

$$u_n = \frac{\partial \phi}{\partial n} = 0, \qquad \text{and} \qquad \frac{\partial \eta}{\partial n} = 0, \qquad 1.36$$

where n is the normal direction.

1.6 Exterior wave problems

1.6.1 Radiation conditions

Radiation conditions, in simple terms, express the concept that waves radiate away to infinity and do not return. They thus represent an energy loss to the system, and can be regarded as energy absorbers. The simple case of a radiation condition will be derived in one dimension and then simply quoted in two dimensions. We consider the one dimensional wave equation

$$\frac{\partial^2 \phi}{\partial t^2} = c^2 \frac{\partial^2 \phi}{\partial x^2}. \qquad 1.37$$

The d'Alembert solution to this wave equation is simply

$$\phi = f_1(x - ct) + f_2(x + ct). \qquad 1.38$$

In equation 1.38, $f_1(x - ct)$ can be seen to be a disturbance travelling in the positive x direction, and $f_2(x + ct)$ can be seen to be a disturbance travelling in the negative x direction. If the f_2 disturbance is excluded, then the expression 1.38 can be differentiated and f_1 can thus be eliminated giving

$$\frac{\partial \phi}{\partial x} = f_1'(x - ct) \qquad \text{and} \qquad \frac{\partial \phi}{\partial t} = -cf_1'(x - ct). \qquad 1.39$$

Thus

$$\frac{\partial \phi}{\partial t} + c\frac{\partial \phi}{\partial x} = 0. \qquad 1.40$$

Equation 1.40 gives the *exact* radiation condition for one dimensional waves. It can also be put in the periodic form

$$i\omega\phi + c\frac{\partial \phi}{\partial x} \qquad \text{or} \qquad \frac{\partial \phi}{\partial x} - ik\phi = 0. \qquad 1.41$$

Again this is exact for periodic problems. Unfortunately in two and three dimensions it is more difficult to formulate such precise boundary conditions, and for general waves they exist only as limits, of infinite series of products of operators.

In two and three dimensions for *periodic* problems there are forms of the radiation condition, as a *limit*, due to Sommerfeld[107,108] and Rellich[105]. The derivation is available in Courant and Hilbert[56]. For axi-symmetric waves in two dimensions there is a form of the condition which tends to an exact condition at large radii. For spherically symmetric waves in three dimensions there is an exact radiation condition. For transient problems, in two and three dimensions there are increasingly accurate radiation condition, in terms of the products of operators, due to Bayliss *et al*[21,22,23]. This can also be applied in periodic problems. All the radiation conditions are summarised in table 1.1, which follows the presentation of Bettess[44]. There has been a considerable amount of work on open boundary conditions and unbounded domains. This is too extensive to survey in detail here, but some of the material is summarised by Givoli[67].

1.7 Other wave theories

The work in this thesis deals exclusively with linear wave theory. However it was felt that the work should be set in the context of other, more advanced, wave theories. No single general theory deals with all surface waves on water.

Following LeMehauté for example, waves are usually characterised in terms of parameters. The most significant parameters are:

1. The wave height, H, which is the distance from crest to trough of the wave.

Dimensions		
1	2	3
General Boundary Conditions		
Transient		
$\frac{\partial \phi}{\partial x} + \frac{1}{c}\frac{\partial \phi}{\partial t} = 0$	$B_m \phi = 0, \quad m \to \infty$ $B_m = \prod_{j=1}^{m}\left(\frac{\partial}{\partial r} + \frac{1}{c}\frac{\partial}{\partial t} + \frac{2j-(3/2)}{r}\right)$	$B_m \phi = 0, \quad m \to \infty$ $B_m = \prod_{j=1}^{m}\left(\frac{\partial}{\partial r} + \frac{1}{c}\frac{\partial}{\partial t} + \frac{2j-1}{r}\right)$
Periodic		
$\frac{\partial \phi}{\partial x} + ik\phi = 0$	$\lim_{r\to\infty} \sqrt{r}\left(\frac{\partial \phi}{\partial r} + ik\phi\right) = 0$ or $B_m \phi = 0, \quad m \to \infty$ $B_m = \prod_{j=1}^{m}\left(\frac{\partial}{\partial r} + ik + \frac{2j-(3/2)}{r}\right)$	$\lim_{r\to\infty} r\left(\frac{\partial \phi}{\partial r} + ik\phi\right) = 0$ or $B_m \phi = 0, \quad m \to \infty$ $B_m = \prod_{j=1}^{m}\left(\frac{\partial}{\partial r} + ik + \frac{2j-1}{r}\right)$
Symmetric Boundary Conditions		
Transient		
$\frac{\partial \phi}{\partial r} + \frac{1}{c}\frac{\partial \phi}{\partial t} = 0$	$\frac{\partial \phi}{\partial r} + \frac{\phi}{2r} + \frac{1}{c}\frac{\partial \phi}{\partial t} = 0$ Axi-symmetric	$\frac{\partial \phi}{\partial r} + \frac{\phi}{r} + \frac{1}{c}\frac{\partial \phi}{\partial t} = 0$ Spherically symmetric
Periodic		
$\frac{\partial \phi}{\partial r} + ik\phi = 0$	$\frac{\partial \phi}{\partial r} + \left(\frac{1}{2r} + ik\right)\phi = 0$ Axi-symmetric	$\frac{\partial \phi}{\partial r} + \left(\frac{1}{r} + ik\right)\phi = 0$ Spherically symmetric

2. The wavelength, λ, which is the distance between two adjacent crossing points of the actual water surface and the undisturbed water surface.

3. The water depth, h, from the undisturbed free surface to the bed.

These parameters yield three key ratios, namely H/λ, which is called the *wave steepness*, H/h and λ/d.

Various assumptions are made which lead to more or less specialised wave theories and their applicability is illustrated in figure 1.5 which gives zones of applicability in terms of the dimensionless wave parameters, the dimensionless wave steepness, H/gt^2 and the dimensionless relative depth, d/gT^2. H_b is the breaking wave height.

Waves dealt with in this thesis are those where H is small compared to h and fall into the zones labelled Linear/Airy waves, and that labelled Shallow Water Waves. They

Deep Water
Breaking Limit
$H/\lambda = 0.14$

H_b

Shallow Water
Breaking Limit
$H/h = 0.78$

H/gT^2

Stokes 5

Or Stream Function 5

3

11 9 7 5

Linear / Airy

Or Stream Function 3

>11

Shallow
Water Waves

Intermediate depth waves

Deep
Water
Waves

0.05   0.02   0.01   0.005   0.002   0.001   0.0005   0.0002   0.0001   0.0005

0.001   0.002   0.005   0.01   0.02   0.05   0.1   0.2

h/gT^2
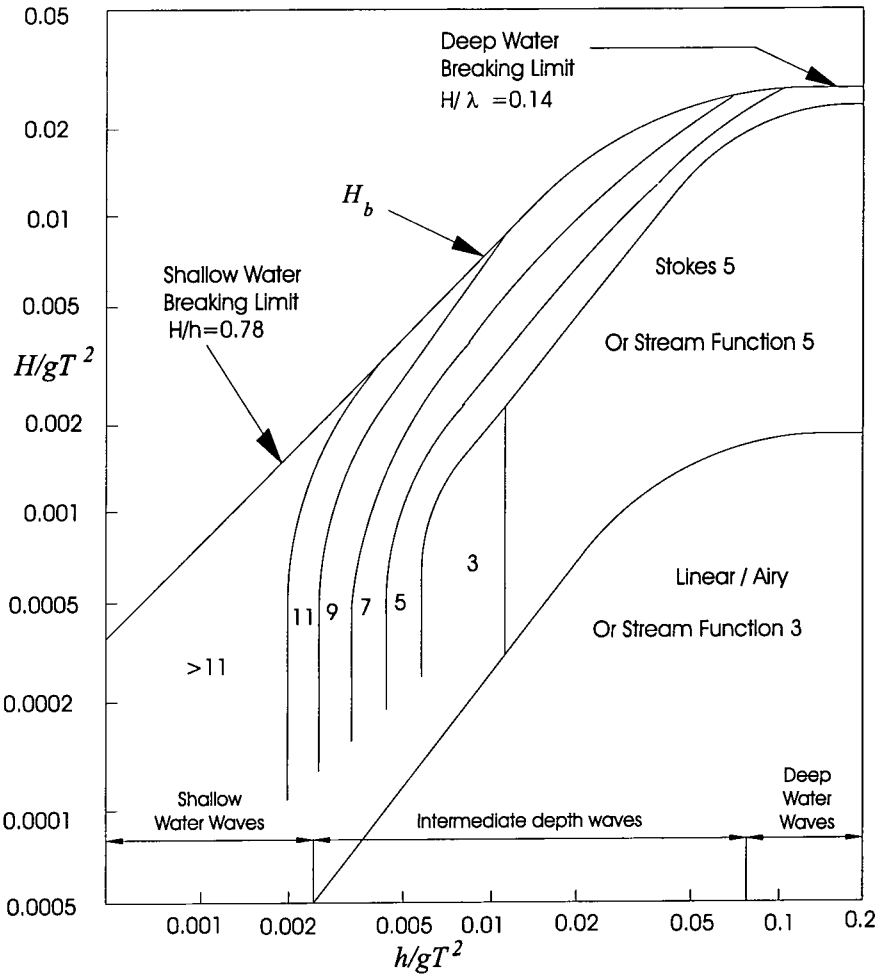
after the American Petroleum Institute publication API RP2A

Figure 1.5   Regions of applicability of various wave theories

are at the bottom of figure 1.5.

1.7.1 Small amplitude wave theories

This is the case dealt with in this thesis, where H/λ, H/h and λ/h are all small. Within this category the equations are all linear. If the water is shallow, $(h/\lambda < 0.05)$, then the pressure distribution is hydrostatic. For intermediate depths, $(0.05 < h/\lambda < 0.5)$ the pressure distribution behaves like $\cosh kz$. This corresponds to the Berkhoff theory, discussed in section 1.3. In deep water, $(h/\lambda > 0.5)$, the pressure distribution varies like $\exp -kz$, and the effect of the waves disappears at depths of the order of half the wavelength. All these types of wave can be analysed with the techniques discussed in this thesis.

1.7.2 Deep water, large amplitude waves - Stokes Theory

If the water is deep then H/h is small and λ/h is small. The important parameter is H/λ and if it is large, then the condition of zero pressure on the free surface can be expanded in a Taylor series, about the undisturbed water surface. This gives rise to a series of waves, first developed by Stokes. Depending on how many terms are retained in the expansions, then the theory is known as third order, fifth order and so on. Such waves are often used for design waves in calculation of fluid loading on offshore structures. Stokes fifth order waves, meaning that the series is expanded up to the fifth term, are particularly popular. It might be noted however that there is no proof that the series converges, and so a higher order solution does not necessarily imply a better solution.

1.7.3 Shallow water, large amplitude waves

The waves which fall into this class are the Cnoidal and Solitary waves. The important ratio in this case is H/h. The vertical accelerations become important, particularly under the wave crest and they affect the hydrostatic pressure distribution in the wave. These waves are important in for example canals, (the first observation of the solitary wave was by Scott-Russell and occurred on the Clyde canal, in Scotland), and in coastal areas.

The above are the main types of waves, but other waves on the surface of water exist, including trochoidal waves, flood waves, tidal waves, bores and roll waves. An important topic which conventional wave theory hardly touches, is the breaking of waves. More specialised texts deal with these in detail, see refs 118, 112 and 91. The statistical properties of waves in the ocean and the distribution of wave heights, periods and directions is also a topic outside the scope of this thesis.

1.8 Weighted residual and variational statements

Finite elements are usually developed from either weighted residual statements or variational statements, and in this section the appropriate forms for linear waves are developed.

1.8.1 Variational statement

For the shallow water wave equation, given earlier as equation 1.19, and repeated here

$$\frac{\omega^2}{g}\phi + \frac{\partial}{\partial x}\left(h\frac{\partial\phi}{\partial x}\right) + \frac{\partial}{\partial y}\left(h\frac{\partial\phi}{\partial y}\right) = 0, \qquad 1.42$$

the corresponding variational statment in a closed domain, Ω, is

$$\Pi = \oint_\Omega \frac{1}{2} \left[\frac{\omega^2}{g} \phi^2 - h \left(\left(\frac{\partial \phi}{\partial x} \right)^2 + \left(\frac{\partial \phi}{\partial y} \right)^2 \right) \right] d\Omega. \qquad 1.43$$

Making the functional Π stationary, with respect to variations in ϕ is equivalent to satisfying the Euler-Lagrange equations of the functional. Courant and Hilbert[59], volume 1, page 192, demonstrated these to be

$$\frac{\partial \Pi}{\partial \phi} - \frac{\partial}{\partial x} \frac{\partial \Pi}{\partial \left\{ \frac{\partial \phi}{\partial x} \right\}} - \frac{\partial}{\partial y} \frac{\partial \Pi}{\partial \left\{ \frac{\partial \phi}{\partial y} \right\}} = 0. \qquad 1.44$$

It can be verified by substituting the expression 1.43, for Π, into equation 1.44, that the shallow water wave equation is recovered. The natural boundary condition for such a functional can be shown to be (Courant and Hilbert[59], volume 1, page 209),

$$\frac{\partial \Pi}{\partial \left\{ \frac{\partial \phi}{\partial x} \right\}} \frac{dy}{ds} - \frac{\partial \Pi}{\partial \left\{ \frac{\partial \phi}{\partial y} \right\}} \frac{dx}{ds} = 0. \qquad 1.45$$

Equation 1.45 can be re-written as

$$\frac{\partial \phi}{\partial x} \frac{dx}{dn} + \frac{\partial \phi}{\partial y} \frac{dy}{dn} = 0, \qquad 1.46$$

which reduces to

$$\frac{\partial \phi}{\partial n} = 0, \qquad 1.47$$

where n denotes the normal to the boundary of the domain. This equation corresponds to perfect reflection (equation 1.23), so the variational statement, 1.42, is only valid for bounded domains, with perfectly reflecting boundaries. In this case, as will be discussed in chapter 2, the problem becomes an eigenvalue problem, namely given the geometry of the closed basin, including the water depth, what are the natural frequencies of oscillation of the water surface, and the corresponding mode shapes? This problem is not of direct concern in the present study. The form of the variational statement for scattering problems will be discussed in section 1.10.

1.8.2 Weighted residual statement

The weighted residual equation is derived by multiplying the differential equation by a weighting function and integrating over the problem domain. For a weighting function, W,

$$\int_{\Gamma} \left[W \left(\frac{\omega^2}{g} \phi + \frac{\partial}{\partial x} h \frac{\partial \phi}{\partial x} + \frac{\partial}{\partial y} h \frac{\partial \phi}{\partial x} \right) \right] d\Gamma = 0, \qquad 1.48$$

which after integration by parts this leads to

$$\int_{\Gamma} \left[W \frac{\omega^2}{g} \phi - \frac{\partial W}{\partial x} h \frac{\partial \phi}{\partial x} - \frac{\partial W}{\partial y} h \frac{\partial \phi}{\partial x} \right] d\Gamma = 0. \qquad 1.49$$

In equations 1.48 and 1.49 the potential, ϕ and the weighting function, W, are taken to be defined over the entire problem domain. The boundary terms are omitted in equation 1.49, although they are of importance, they will be discussed later. If the weighting function, W, is taken to be the same as the shape function which describes the variation of the velocity potential, then both the weighted residual and variational forms lead to identical equations. In this case 1.49 is the equivalent weighted residual statement to the functional 1.42. Because of this the weighted form will not be discussed further.

1.9 Incident and scattered waves

In extending the above ideas to scattering of waves in unbounded domains, there are two necessary extensions. One is the partitioning of the wave into incident and scattered components. An advantage of the linearity of the waves is that these wave components can be simply superposed. The second is the necessity for incorporating the radiation conditions in the variational statement, or the weighted residual statement.

1.9.1 Incident and scattered waves

The wave can be separated into an *incident* wave and a *scattered* wave. This gives

$$\phi_{total} = \phi_{incident} + \phi_{scattered}. \qquad 1.50$$

By 'scattered' is meant waves that have been scattered, diffracted, radiated or reflected from a fixed object in the water. From now on, the total potential will be written as ϕ and the incident wave potential as ϕ^i, and the scattered wave potential as ϕ^s. Radiation conditions were discussed in section 1.6. For our case, a two dimensional periodic wave problem, the radiation condition for the scattered wave is written

$$\lim_{r \to \infty} \sqrt{r} \left(\frac{\partial \phi^s}{\partial r} + ik\phi^s \right) = 0. \qquad 1.51$$

All outgoing waves must satisfy this condition, and obviously, any incident wave does not.

1.10 Variational formulation

The functional which gives equation 1.20 as its Euler-Lagrange equation was given earlier as equation 1.42. That functional gives incorrect boundary conditions for the scattering problem. In order to deal correctly with the boundary conditions, extra terms must be included on the boundary at infinity, to give equation 1.49.

First of all, the terms used in figure 1.6 are defined.

Γ_a	Boundary of scattering object
Γ_b	Boundary between total and scattered potential
Γ_c	Boundary of finite element mesh
Γ_d	Boundary at infinity
Ω_a	Domain of total potential (finite elements)
Ω_b	Domain of scattered potential (finite elements)
Ω_c	Domain of scattered potential (infinite elements)
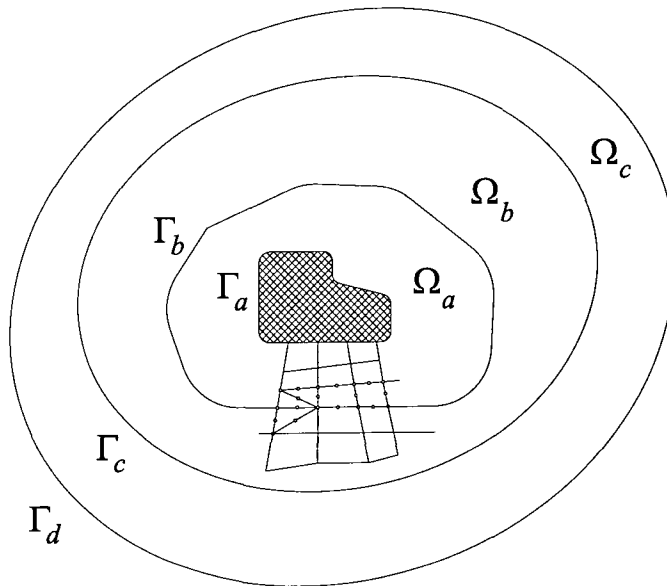
Figure 1.6   The scattering problem geometry

Ω is the entire domain exterior to Γ_a as far as infinity, denoted by Γ_d.

$$\Pi = \int\int_{\Omega} \frac{1}{2}\left[cc_g(\nabla\phi)^2 - \frac{\omega^2 c_g}{c}\phi^2 \right] dxdy$$

$$- \int_{\Gamma_d} cc_g\left(\phi - \phi^i\right)\nabla\phi^i.\mathbf{n}d\Gamma \qquad\qquad 1.52$$

$$+ \frac{1}{2}\int_{\Gamma_d} ikcc_g\left(\phi - \phi^i\right)^2 d\Gamma.$$

The natural boundary condition which arises on the inner boundary, Γ_a, is $\partial \phi / \partial n = 0$, which corresponds to complete reflection. On the exterior boundary, Γ_d, the boundary condition which arises is given by

$$\frac{\partial \phi}{\partial n} - \frac{\partial \phi^i}{\partial n} - ik(\phi - \phi^i) = \frac{\partial \phi^s}{\partial n} - ik\phi^s = 0. \qquad 1.53$$

This is the form required when the boundary tends to being infinitely distant.

The domain of the problem is now divided into inner and outer parts, as shown in figure 1.6. In the inner domain, termed Ω_a, between boundaries Γ_a and Γ_b, the equations must be dealt with in terms of the total potential, ϕ, since the boundary conditions on fixed objects are zero normal velocity. In the outer domain, termed Ω_b, between boundaries Γ_b and Γ_d, the variable must be the scattered wave potential, since the radiation condition is expressed in terms only of the scattered wave, and does not apply to the incident wave.

In the outer domain, Ω_b, the functional of equation 1.54 is again used, and the total potential is expressed in terms of ϕ^i and ϕ^s. Consider first only the integral over the domain. (The boundary terms will be introduced later.) It becomes

$$\Pi = \int \int_{\Omega_b} \frac{1}{2} \left[cc_g (\nabla(\phi^i + \phi^s))^2 - \frac{\omega^2 cc_g}{c} (\phi^i + \phi^s)^2 \right] dx dy. \qquad 1.54$$

The functional for the outer domain, equation 1.54, can now be simplified. The quadratic terms in ϕ^i are not subject to variation and can thus be discarded. As ϕ^i, corresponding to the known incident wave, is a solution of the wave equation, it can be transformed to a line integral along the boundary between the inner and outer domains, using Green's theorem in the plane, thus

$$\int \int \frac{1}{2} \left[cc_g (\nabla(\phi^i + \phi^s))^2 - \frac{\omega^2 cc_g}{c} (\phi^i + \phi^s)^2 \right] dx dy$$

$$= \int \int \frac{1}{2} \left[cc_g (\nabla(\phi^s))^2 - \frac{\omega^2 c_g}{c} (\phi^s)^2 \right] dx dy \qquad +$$

$$\int \int \left[cc_g \left\{ \left(\frac{\partial \phi^i}{\partial x} \frac{\partial \phi^s}{\partial x} \right) + \left(\frac{\partial \phi^i}{\partial y} \frac{\partial \phi^s}{\partial y} \right) \right\} - \frac{\omega^2 c_g}{c} \phi^i \phi^s \right] dx dy. \qquad 1.55$$

The last term of equation 1.55 is now considered. Using integration by parts, it can be written as

$$\int \int \left[cc_g \left\{ \left(\frac{\partial \phi^i}{\partial x} \frac{\partial \phi^s}{\partial x} \right) + \left(\frac{\partial \phi^i}{\partial y} \frac{\partial \phi^s}{\partial y} \right) \right\} - \frac{\omega^2 c_g}{c} \phi^i \phi^s \right] dx dy$$

$$= \int \int \left[cc_g \left\{ \frac{\partial}{\partial x} \left(\frac{\partial \phi^i}{\partial x} \phi^s \right) + \frac{\partial}{\partial y} \left(\frac{\partial \phi^i}{\partial y} \phi^s \right) \right\} \right] dx\,dy$$

$$- \int \int \left[cc_g \left(\frac{\partial^2 \phi^i}{\partial x^2} \phi^s + \frac{\partial^2 \phi^i}{\partial y^2} \phi^s \right) + \frac{\omega^2 c_g}{c} \phi^i \phi^s \right] dx\,dy. \tag{1.56}$$

The last term of equation 1.56 may be re-written as

$$\int \int \left[cc_g \left(\frac{\partial^2 \phi^i}{\partial x^2} + \frac{\partial^2 \phi^i}{\partial y^2} \right) + \frac{\omega^2 c_g}{c} \phi^i \right] \phi^s dx\,dy. \tag{1.57}$$

For constant depth, which also implies constant c and c_g, the term in square brackets in equation 1.55 is automatically zero, because, by definition, ϕ^i satisfies equation 1.20, the wave equation. The next step is to use Green's theorem in the plane, which states that

$$\oint (P dx + Q dy) = \int \int \left(\frac{\partial Q}{\partial x} - \frac{\partial P}{\partial y} \right) dx\,dy. \tag{1.58}$$

The integral in expression 1.56 can now be transformed using Green's theorem, so that

$$\int \int \left[cc_g \left\{ \frac{\partial}{\partial x} \left(\frac{\partial \phi^i}{\partial x} \phi^s \right) + \frac{\partial}{\partial y} \left(\frac{\partial \phi^i}{\partial y} \phi^s \right) \right\} \right] dx\,dy$$

$$= \oint cc_g \left[\frac{\partial \phi^i}{\partial x} \phi^s dy - \frac{\partial \phi^i}{\partial y} \phi^s dx \right] \tag{1.59}$$

$$= \oint cc_g \phi^s \nabla \phi^i . n d\Gamma.$$

The limiting form of these terms on the boundaries at infinity should be considered. However, as discussed by Astley *et al.*[13] they cancel with terms arising from the element integration and can be neglected, at any rate for infinite elements based on a variational principal or the equivalent Bubnov-Galerkin weighting, which is the case here.

The line integral arises on the boundary which is chosen to mark the division between two domains in which the variable is the total potential and the scattered potential. This is Γ_b in figure 2. At infinity, the field variable must be the scattered potential, and on the object which is diffracting the waves the field variable must be the total potential.

The part of the line integral on Γ_d in equation 1.59 cancels with the second term in equation 1.53 and the line integral on Γ_b remains as a 'forcing' term, giving the influence of the incident wave. The final form of the functional for the outer region, Ω_b is thus as given as

$$\mathrm{II} = \int\int_{\Omega_b} \frac{1}{2}\left[cc_g(\nabla\phi^s)^2 - \frac{\omega^2 cc_g}{c}(\phi^s)^2\right]dxdy$$
$$+ \int_{\Gamma_b} cc_g\left[\frac{\partial\phi^i}{\partial x}\phi^s dy - \frac{\partial\phi^i}{\partial y}\phi^s dx\right] \qquad 1.60$$
$$+ \frac{1}{2}\int_{\Gamma_d} ikcc_g(\phi^s)^2 d\Gamma.$$

1.11 Incident wave potential

The only incident wave considered in this study is the plane monochromatic wave. Other known waves are possible, for example the cylindrically symmetric wave defined by Hankel functions. In this case the incident wave elevation, η_i and potential, ϕ_i are given by

$$\eta_i = a_0 \exp\{ik\cos(\theta - \theta_i)\},$$
$$\phi_i = -\frac{iga_0}{\omega}\exp\{ik\cos(\theta - \theta_i)\}, \qquad 1.61$$

where a_0 is the incident wave amplitude, θ_i is the angle of incidence between the positive x axis and the direction of travel of the incident wave, and other parameters were defined in section 1.1.

Chapter 2

Introduction to Finite and Infinite Elements

2.1 Finite elements

Finite elements are now so universally used and so well understood that only the very briefest of outlines will be given here. Many excellent text books which describe the method are available. Zienkiewicz and Taylor[129,130] give a very comprehensive description of the method.

Finite elements were first applied in the 1950s to structures in the fields of Aeronautics and Civil Engineering. From the methods of structural analysis of frameworks and trusses, it was natural to consider the splitting of a continuum problem into elements. The usual procedure was to take values of the structural displacements at the vertex nodes of three node triangular and four node quadrilateral finite elements as unknowns and then to obtain the displacements anywhere within the element. Linear interpolation was used. Later more sophisticated elements with higher order interpolation were derived.

The assumed form of the displacements is an approximation. The displacements are substituted into the equilibrium and constitutive equations of the material. The next step is to use a weighted residual method in which the equations are 'weighted' by some function. This is often chosen to be the interpolation function itself, although other choices are possible. The weighted equations are then integrated over the problem domain, and often integration by parts is used to simplify the equations, and to reduce the requirements for continuity between elements. It is also possible to derive the finite element equations from variational statements. An example in elasticity is minimum potential energy. Critical factors in determining the accuracy of the solution are the fineness of the mesh, and the suitability of the element types chosen.

The finite element method has been developed to apply to many problems apart from structures. It is now used for, among other problems: electro-magnetic problems, torsion, viscous flows, compressible flows, metal forming, dynamic problems, shells, plasticity and of course waves, of pressure, elasticity, radio, and surface waves on water, the main topic of this thesis.

2.2 Finite elements for wave problems

In the application of finite elements to wave problems the field variable is taken to be the velocity potential, ϕ, (other valid choices include the pressure, p and the wave elevation, η.) In each finite element the potential is interpolated from the nodal values using the element shape function. In the present work two finite elements are used,

these being an eight node quadrilateral element, with quadratic polynomials and a six node triangular element. The details of the shape functions are given in many classical texts, for example Zienkiewicz and Taylor[129,130].

Within the finite element the velocity potential is obtained from

$$\phi = \sum_{i=1}^{n} N_i(\xi, \eta)\phi_i. \qquad 2.1$$

In equation 2.1 ϕ_i is the value of ϕ at the ith node. Thus the value of ϕ at any point within the element, or the problem domain, is represented by the finite set of nodal values of ϕ and the shape function polynomials, $N_i(\xi, \eta)$. It is possible to generate the well-known families of shape functions automatically using computer algebra, as has been done by the author[19,42].

The derivatives of the shape function are placed in the **B** matrix, which is called a 'strain' matrix in elasticity problems.

$$\mathbf{B} = \left\{ \begin{array}{c} \frac{\partial N_i(\xi, \eta)}{\partial x} \\ \frac{\partial N_i(\xi, \eta)}{\partial y} \end{array} \right\}. \qquad 2.2$$

The element 'stiffness' $\mathbf{k}_e$ and 'mass' $\mathbf{m}_e$, matrices can be then formed using the classical expressions, see for example Zienkiewicz[36]. The **D** matrix, which in elasticity problems relates the stresses to the strains, is here a two by two matrix containing the depth, h, or in Berkhoff's theory the wave speeds c and c_g

$$\mathbf{D} = \begin{bmatrix} h & 0 \\ 0 & h \end{bmatrix} \quad \text{or} \quad \mathbf{D} = \begin{bmatrix} cc_g & 0 \\ 0 & cc_g \end{bmatrix}, \qquad 2.3$$

for shallow water theory and Berkoff theory respectively. Thus

$$\mathbf{k}_e = \int_{\Gamma_e} \mathbf{B}^T \mathbf{D} \mathbf{B} d\Gamma_e \quad \text{and} \quad \mathbf{m}_e = \int_{\Gamma_e} \mathbf{N}^T \mathbf{N} d\Gamma_e. \qquad 2.4$$

2.3 Programming of wave finite elements

The code for a typical wave finite element can be written in a loose Algol type notation as shown below.

```
C finite element procedure C
parameters:  x,y, nodal coordinates, d properties,
gauss abscissæ and weights
BEGIN
     initialize element matrices kₑ and mₑ to zero
```

```
    FOR all gauss points DO
    BEGIN
         get gauss abscissa and weight, w
         call shape function procedure, returns
         N, ∂N/∂ξ, ∂N/∂η
         form Jacobian matrix J
```
$$\mathbf{J} := \begin{bmatrix} \partial \mathbf{N}/\partial \xi \\ \partial \mathbf{N}/\partial \eta \end{bmatrix} [\mathbf{x}, \mathbf{y}]$$
```
         Invert J to give J⁻¹
```
$$\mathbf{B} := \begin{bmatrix} \partial \mathbf{N}/\partial x \\ \partial \mathbf{N}/\partial y \end{bmatrix} := \mathbf{J}^{-1} \begin{bmatrix} \partial \mathbf{N}/\partial \xi \\ \partial \mathbf{N}/\partial \eta \end{bmatrix}$$
$$\mathbf{k}_e := \mathbf{k}_e + w\mathbf{B}^T\mathbf{D}\mathbf{B}$$
$$\mathbf{m}_e := \mathbf{m}_e + w\mathbf{N}^T\alpha\ \mathbf{N}$$
```
    END
END
```

For shallow water theory, the mass matrix constant α, would be $1/g$, and for Berkhoff theory the α would be c_g/c. These element matrices can be assembled into overall system matrices, so that

$$\mathbf{K} = \sum_{all\ elements} k_e \quad \text{and} \quad \mathbf{M} = \sum_{all\ elements} m_e, \qquad 2.5$$

where the summations in equations 2.5 are to take account of the numbering of the nodes. The problem is then in the classical eigenvalue form

$$\left(\mathbf{K} - \omega^2\mathbf{M}\right)\eta = 0,$$

where ω^2 represents the squares of the natural frequencies of oscillation and η represents the eigenvectors or mode shapes. This method was first applied to problems of the oscillation of closed harbours by Taylor, Patil and Zienkiewicz[114].

2.4 Infinite elements

Infinite elements are a means of extending the techniques of finite elements to deal with unbounded domain problems. Finite elements are intrinsically limited to finite domains. However many engineering problems are considered to be infinite in extent. This is despite the fact that all real engineering problems are finite. Because they may be of very great extent the engineer often prefers to assume that they are infinite. An example is the foundation of a dam or other building, which is bounded by the sphere of the earth. This is so large, relative to the size of the building, that the problem is usually regarded as unbounded.

There is now a considerable literature on infinite elements. The book by Bettess[44], of 1992, cites well over 200 references, the majority of which are on infinite elements, and

the number of papers has grown rapidly in the years since then. The survey given here, will necessarily be brief, and it draws on the papers by Bettess and Bettess[37,39,30].

2.5 Infinity

The concept of processes and numbers being infinite dates back to the very early days of mathematics, and the Greeks. I will not attempt to deal with this complex subject here.

2.6 Infinite continuum problems

The concept of solving problems in mechanics where the domain is supposed to extend to infinity, dates back at least to Newton[99], who lived between 1642 and 1727. Newton, in his Principia Mathematica discusses problems with an unbounded fluid. He mentions the unbounded fluid in such a casual way, without any justification that the reader gains the impression that this was a well-known and widely accepted assumption.

2.7 Green's functions

George Green was an English mathematician. He made several key contributions to the solution of continuum problems, including Green's first and second theorems, and the concept of Green's functions[71]. These functions give the influence of a point force or some other kind of unit load throughout the domain. Often the domain is unbounded. Although Green's functions will not be used directly in the infinite elements described in this thesis, the functions are important in indicating the way in which the solution can be expected to vary in the far-field and are thus clearly relevant to the work.

2.8 Numerical solutions for unbounded domain problems

One of the first attempts to produce numerical solutions to problems which were idealized as unbounded was Richardson's finite difference analysis of a dam and its foundation[109]. The actual dam was supposed to be the first Aswan dam, on the Nile, which is a gravity dam. Problems with the logarithmic behaviour of the displacements at infinity were avoided by working in terms of a stress function.

In the 1920's the idea of using the Green's function solutions in connection with a numerical procedure was developed by Trefftz[115], in the context of elasticity. The method has been greatly developed since, and is now commonly called the 'boundary integral' method, since it involves integrals along the boundary of the domain. The method, like other numerical methods has gained greatly in popularity since the widespread availability of computers. It is also called the 'boundary element method' when finite element type techniques are used. There are a number of textbooks dealing with the method, which explain it in detail, but it will not be dealt with here. One useful book, which relates the finite element and boundary element methods is by Beer and Watson[25].

The boundary integral method is virtually the only numerical method that does not require any special procedure for dealing with boundaries at infinity. This is because the Green's function can be selected to be valid throughout the space in question. It is usually easier, in fact, to find Green's functions for unbounded problems than for bounded ones. Of course, the correct Green's function has to be found for the problem in question. The boundary integral method is somewhat clumsy in dealing with non-linear problems. This is because it relies on the superposition of linear solutions. By the use of integrals over the domain, and a suitable iterative procedure, such non-linear problems can however be solved.

2.9 Development of infinite elements

The beginnings of infinite elements will be described, followed by the major developments. It is convenient to classify infinite elements as of *static* or *dynamic* type, as the methods needed for the two types are quite different. The original and simpler static infinite elements will be summarised briefly, only to the extent that their theory is needed for the dynamic infinite elements.

2.10 The first infinite elements

The first infinite element to be produced was that of Ungless[116,4] and Anderson, in 1973. They called their element an infinite finite element. This work existed as an M.Sc. thesis[116] but was not published until 1977[4], so that the first published work on infinite elements was a paper, by Zienkiewicz and Bettess, published in 1975[122].

The idea behind the element of Ungless and Anderson was the use of a shape function which varied as $1/(1+r)$ in the radial or r direction. As they remark, this is sufficiently simple for most of the manipulations to be handled analytically. Their infinite finite element is three dimensional and has a triangular base, which is defined to be in the local xy plane, and is extended from this base to infinity. It is therefore approximately a triangular prism in shape, with the z direction (which is defined as being perpendicular to the base) being infinite. Ungless and Anderson obtained good results in tackling the Boussinesq problem of elasticity.

The original formulation of infinite elements at Swansea was quite different. It is described in the two papers by Bettess[29,34]. The element domain is extended to infinity, using as a basis any original finite element. The shape function is then multiplied by a decay function which is appropriate for the particular problem type. Later periodic wave infinite elements were developed which included a periodic component[122,30].

In this type of infinite element the shape function is multiplied by a decay function, so that the desired behaviour at infinity is obtained. The first decay functions used by Bettess were of an exponential type, and typical terms in the infinite element matrices thus had the form of a polynomial multiplied by an $\exp(-r)$ term. These types of integrals can be found analytically, and so infinite elements of a rectangular form, which extended to infinity in one or more directions were developed. The elements were first

applied to some simple one dimensional examples and they were later applied to more complicated two dimensional and axi-symmetric problems, including problems of slow viscous flow (Stokes flow).

2.11 Infinite element classification

The succeeding infinite element formulations have followed two main lines of development. These have been:

- *mapping* of the element from finite to infinite domain.

- the use of *decay functions* in conjunction with the ordinary finite element shape function.

The *mapping* method is described in section 2.14, along the lines suggested by Zienkiewicz. Many mappings are possible, and opinions vary, but a widely held view is that the Zienkiewicz mapping is the best available, because of its simplicity and theoretical advantages.

The first mapped infinite element results were published by Beer and Meek[24] in 1981. The mapping which they used was specially devised. The geometry of the element is described by parametric 'mapping' of parent element to infinity in one local co-ordinate direction using shape functions which have a singularity at $\xi_n = +1$. Beer and Meek applied their new element to the determination of the stresses and displacements induced by an excavation in a pre-stressed medium. Beer and Meek also dealt with a spherical opening in an elastic solid. They applied these elements to the elasto-plastic analysis of tabular ore body extraction at the Mount Isa mine in Australia.

The theory of the Zienkiewicz form of mapped infinite element was first outlined in 1981[125], in a paper which surveyed all sorts of methods for exterior problems. The first results obtained using the new element were published in 1983[127].

The formulation of the Zienkiewicz mapped infinite element was rationalised by Marques and Owen[94], who gave tables of mapping functions for a range of two and three dimensional infinite elements. More details of the method are given in Marques and Owen[95] and in Owen and Hinton[101].

2.12 Decay function infinite elements

In these elements the appropriate behaviour at infinity is enforced by the use of a decay function, which is used to multiply the normal finite element shape function. Only a brief introduction will be given here, because the necessary theory is explained elsewhere[30,122] and because the decay function infinite elements, although used in this thesis, are not a major theme. The rôle of the decay function is to ensure that the behaviour of the element at infinity is a reasonable reflection of the physics of the problem. This usually means that the field variable must tend monotonically to its far field value. If the parent finite element shape function is written as $P_i(\xi, \eta)$ where ξ

and η are the local coordinates and the decay function is $f_i(\xi, \eta)$ where the subscript denotes the node number, then

$$N_i(\xi, \eta) = P_i(\xi, \eta) f_i(\xi, \eta).$$ 2.6

(no summation on i)

The decay function $f_i(\xi, \eta)$ must be unity at its own node, that is

$$f_i(\xi_i, \eta_i) = 1.$$ 2.7

In addition N_i must tend to the far field value at infinity. There is no requirement that the decay function takes any special value at other nodes. Whatever f is, the required derivatives of the element shape function can easily be established using the chain rule. For decay in the ξ direction only

$$\frac{\partial N_i}{\partial \xi} = \frac{\partial P_i}{\partial \xi} f_i + P_i \frac{\partial f_i}{\partial \xi} \qquad \text{and} \qquad \frac{\partial N_i}{\partial \eta} = \frac{\partial P_i}{\partial \eta} f_i.$$ 2.8

For decay in both ξ and η directions,

$$\frac{\partial N_i}{\partial \xi} = \frac{\partial P_i}{\partial \xi} f_i + P_i \frac{\partial f_i}{\partial \xi}$$ 2.9

and

$$\frac{\partial N_i}{\partial \eta} = \frac{\partial P_i}{\partial \eta} f_i + P_i \frac{\partial f_i}{\partial \eta}.$$ 2.10

Similar considerations apply in three dimensions. Obviously second derivatives can also be found if required and the extension to three dimensions is trivial. The ξ coordinate would normally be in the radial direction, away from the domain of interest, and is usually simply a constant multiplied by r, the radial coordinate. It is therefore simple to match ξ to $1/r$ or other known forms of decay.

2.13 Exponential decay functions

An obvious choice for the decay function, and the first to be used, is the function $\exp(-x)$. This has the advantage that it decays to zero faster than any polynomial and so dominates the polynomial behaviour as x is large and ensures convergence towards zero as x increases. It is also almost as easy to manipulate mathematically as a polynomial. The more precise expression for the decay function is

$$f_i(\xi, \eta) = \exp[(\xi_i - \xi)/L],$$ 2.11

for decay only in the positive ξ direction. The inclusion of ξ_i ensures that condition 2.7 holds.

It is possible for the decay length, L to vary within the infinite element. For the most likely case, that is decay in the ξ direction and variation of L in the η direction, the necessary expressions are

$$f_i(\xi, \eta) = \exp[(\xi_i - \xi)/L],$$

$$\frac{\partial f_i(\xi, \eta)}{\partial \xi} = \frac{-1}{L} \exp[(\xi_i - \xi)/L], \qquad\qquad 2.12$$

$$\frac{\partial f_i(\xi, \eta)}{\partial \eta} = \frac{-1}{L^2} \frac{\partial L}{\partial \eta} \exp[(\xi_i - \xi)/L](\xi_i - \xi).$$

It is necessary to interpolate for L in the η direction. There are many possibilities here and they cannot all be explored. No results obtained using such a variation in L have been reported in the literature to date, for exponential decay elements, but a similar technique has been used in wave envelope infinite elements, by Cremers and Fyfe[60,61], and it will be used later in this thesis for infinite wave elements.

Such exterior wave problems have been solved by a number of methods, including the use of finite and infinite elements. Another popular technique, not explored here, is that of linking finite elements to boundary integrals or series solutions. Pioneering papers in this field are by Berkhoff[26,27,28] and Chen and Mei[54,55] and a survey of coupling techniques was given by Zienkiewicz *et al.*[123].

2.14 Theory of mapped infinite elements

We now deal with the theory of mapped infinite elements.

2.14.1 Zienkiewicz mapped infinite element

The theory for this mapping is well known, but for reference will be briefly summarised here. Further details are given in references 44, 125, 127, 128, 38.

Consider first the geometry of the one-dimensional problem. The element extends from point x_1 through x_2 to x_3, at infinity, and x_0 being the 'pole' of the radial behaviour. This element is to be mapped onto the finite domain $-1 < \xi < 1$. This is shown in Figure 2.1. A suitable mapping expression was originally defined by Zienkiewicz *et al.*[122] (and further developed in refs. 127, 41, 129) as

$$x = \tilde{N}_0(\xi)x_0 + \tilde{N}_2(\xi)x_2, \quad x_2 > x_0, \qquad\qquad 2.13$$

where

$$\tilde{N}_0(\xi) = \frac{-\xi}{1-\xi} \qquad \tilde{N}_2(\xi) = 1 + \frac{\xi}{1-\xi}. \qquad\qquad 2.14$$

At

$$\xi = 1, \qquad x = \frac{\xi}{(1-\xi)}(x_2 - x_0) + x_2 = x_3 = \infty,$$

$$\xi = 0, \qquad x = x_2, \qquad\qquad 2.15$$
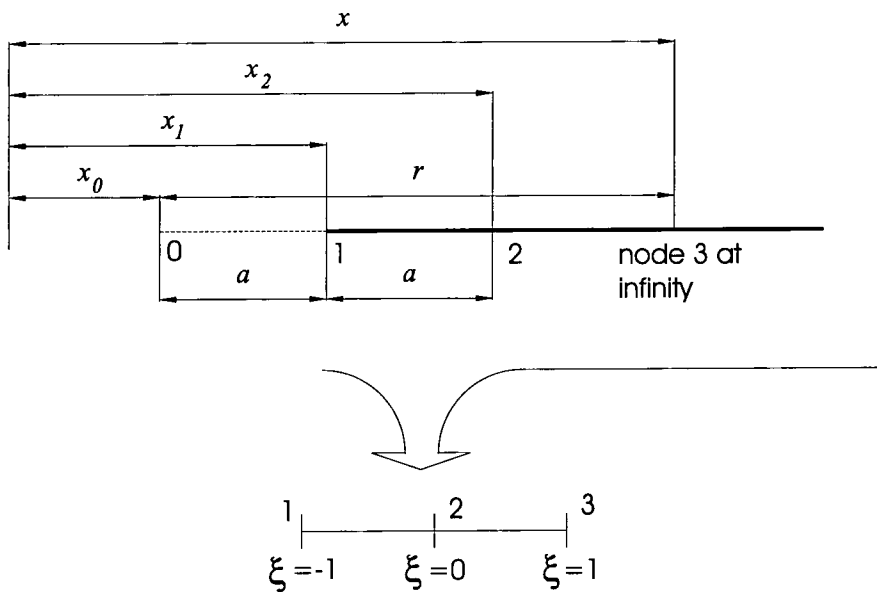
Figure 2.1   Zienkiewicz Infinite Element Mapping

$$\xi = -1 \qquad \text{and} \qquad x = (x_0 + x_2)/2 = x_1,$$

The point at $\xi = -1$ is to correspond to the point x_1, which is now defined to be midway between x_0 and x_2. Once the mapping relationship, equation 2.13, has been established the mapping can be written in terms of any two quantities from the set: x_0, x_1, x_2, a where $a = x_2 - x_1 = x_1 - x_0$. For example the mapping can be written as

$$x = (2x_1 - x_2)\tilde{N}_0 + x_2\tilde{N}_2. \qquad 2.16$$

A mapping between the infinite and finite domains has now been established. The next step is to see into what form polynomials in the finite, ξ, domain are transformed into in the unbounded x domain. Consider a polynomial, P,

$$P = \alpha_0 + \alpha_1\xi + \alpha_2\xi^2 + \alpha_3\xi^3 + \ldots, \qquad 2.17$$

which is typical of those used in finite element methods. The ξ to x mapping already obtained is

$$x = x_0 + \frac{2a}{(1 - \xi)}, \qquad 2.18$$

and its inverse is

$$\xi = 1 - \frac{2a}{(x - x_0)} = 1 - \frac{A}{x - x_0}. \qquad 2.19$$

Where $r = x - x_0$, these can be writen as

$$r = \frac{2a}{1 - \xi} \quad \text{and} \quad \xi = 1 - \frac{2a}{r} \quad \text{or} \quad r = \frac{A}{1 - \xi} \quad \text{and} \quad \xi = 1 - \frac{A}{r}, \qquad 2.20$$

where $A = 2a$. On substitution into the general polynomial, P, a new polynomial in inverse powers of r is obtained:

$$P = \beta_0 + \frac{\beta_1}{r} + \frac{\beta_2}{r^2} + \frac{\beta_3}{r^3} + \dots, \qquad 2.21$$

where the β_i can be determined from the α's and a. If the polynomial is required to decay to zero at infinity then $\beta_0 = 0$.

When placing the nodes of the element in the radial direction, it is necessary that they should conform to the mapping relation of equation 2.20. Otherwise the mapping will be inconsistent. The actual values are given in Table 2.1. If the example of the quadratic infinite element is considered, the following conditions must be met. If the first node is at a distance a from the 'pole' of the problem, then the midside node must be at a distance $2a$, in order to obtain the appropriate mapping.

For other nodes locations, the results may not necessarily be wrong. However results could be unpredictable.

ξ	-1	-1/2	-1/3	0	1/3	1/2	1
r	a	$4a/3$	$3a/2$	$2a$	$3a$	$4a$	∞

Table 2.1 Relation between ξ and r, for mapped infinite elements

Many exterior potential problems have solutions of the form of equation 2.21 and so a considerable benefit of the mapping given above is that such behaviour can be modelled using normal finite element polynomials. Accuracy can be increased by adding more terms to the series 2.17. The pole of the expansion of P is the point x_0. The finite element domain is used both for the definition of the shape function and for the numerical integration. This is one of the the main advantages of the algorithm. The element shape function routine is left unchanged, except for the inclusion of the wave component (see section 3.4). Of course the Jacobian matrix is calculated using the mapping given earlier as equation 2.13 and not using derivatives of shape functions.

An attractive alternative approach formulation was completely worked out by Marques and Owen[94,95]. In their formulation $\tilde{N}_0$ and $\tilde{N}_2$ are replaced by mapping functions M_1 and M_2 so that:

$$x = M_1 x_1 + M_2 x_2. \qquad 2.22$$

This now means that the mapping functions are handled in a more conventional manner. The forms of these functions can readily be worked out, and details are given by Marques and Owen, cited above and Bettess[44], and will not be repeated here. Further details of some interesting mapping effects and some corrections for three dimensional serendipity mapping functions are given by Kay and Bettess[84]. For a quadratic infinite

element the new mapping functions, M_1 and M_2 are shown in Table 2.2 and illustrated in Figure 2.2. The mapping functions for the 'last' node, the node at infinity, are not given, since the mapping functions for the node at infinity are not generally needed.

Mapping Function		$\xi =$	-1	0	1
M_1	$2 \times \tilde{N}_0(\xi)$	$-2\xi/(1-\xi)$	1	0	$-\infty$
M_2	$\tilde{N}_2(\xi) - \tilde{N}_0(\xi)$	$(1+\xi)/(1-\xi)$	0	1	∞

Table 2.2   Infinite Element Mapping Functions
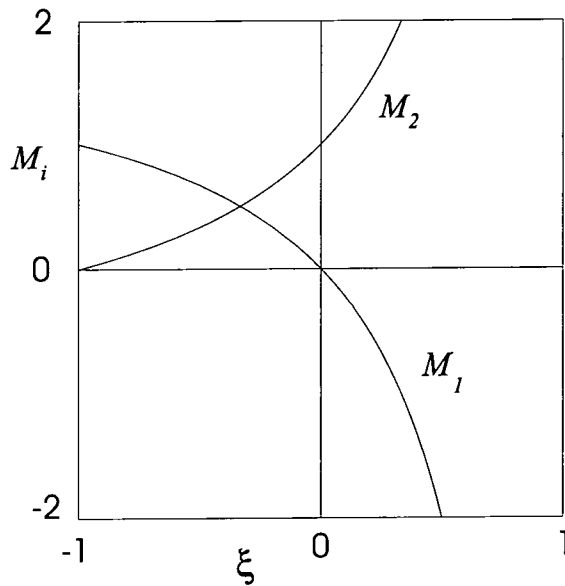
Figure 2.2   Quadratic Mapping Functions

If the conventional finite element shape functions are compared with the infinite element mapping functions, it can be seen that the only differences occur in the terms relating to $\xi = 1$, that is the terms at 'infinity'. These are the terms which involve $(1-\xi)$. The effect is seen in Table 2.3.

It can be seen that in the infinite element mapping functions, the term at infinity is inverted. The possibility of generating an open-ended set of infinite element mapping functions is therefore opened up. It is possible to generate sets of mapping functions,

Node Number, i	ξ_i	Quadratic Finite Element Parent Shape Functions P_i	Quadratic Infinite Element Mapping Functions M_i
1	-1	$-\xi \times (1 - \xi)/2$	$-\xi \times 2/(1 - \xi)$
2	0	$(1 + \xi) \times (1 - \xi)$	$(1 + \xi) \times 1/(1 - \xi)$
3	1	$\xi \times (1 + \xi)/2$	–

Table 2.3   Comparison of Infinite and Finite Element Functions

both Serendipity and Lagrange, for all square and cube finite element parent shapes to any desired order, just as for finite elements.

Mapping functions can be generated for infinite elements based on any of the well known finite elements. This is explained by Bettess[44,37,39,40], and Marques and Owen[94,95] and computer generated mapping functions can be produced as explained by Barbier, Bettess and Bettess[20].

As an example the mapping function for a quadratic six noded element is given below, as it will be used later in chapter 3. The particular infinite element used here is quadratic and has six nodes, those at infinity being removed. It is based on Lagrange polynomials and the mapping functions are easily constructed from the product of the finite element shape functions in terms of η and the infinite element mapping functions in the ξ direction, which are both given in table 2.4. The element is sketched in figure 2.3. For convenience the mapping functions for the six nodes are shown in table 2.4.

Node, i	ξ_i	η_i	M_i	$\partial M_i/\partial\xi$	$\partial M_i/\partial\eta$
1	-1	-1	$\eta(1 - \eta)\xi/(1 - \xi)$	$\eta(1 - \eta)/(1 - \xi)^2$	$\xi(1 - 2\eta)/(1 - \xi)$
2	0	-1	$-\eta(1 - \eta)(1 + \xi)/2(1 - \xi)$	$-\eta(1 - \eta)/(1 - \xi)^2$	$-(1 + \xi)(1 - 2\eta)/2(1 - \xi)$
3	0	0	$(1 - \eta^2)(1 + \xi)/(1 - \xi)$	$2(1 - \eta^2)/(1 - \xi)^2$	$-2\eta(1 + \xi)/(1 - \xi)$
4	0	1	$\eta(1 + \eta)(1 + \xi)/2(1 - \xi)$	$\eta(1 + \eta)/(1 - \xi)^2$	$(1 + \xi)(1 + 2\eta)/2(1 - \xi)$
5	-1	1	$-\xi\eta(1 + \eta)/(1 - \xi)$	$-\eta(1 + \eta)/(1 - \xi)^2$	$-\xi(1 + 2\eta)/(1 - \xi)$
6	-1	0	$-2\xi(1 + \eta)(1 - \eta)/(1 - \xi)$	$-2(1 - \eta^2)/(1 - \xi)^2$	$4\xi\eta/(1 - \xi)$

Mapping function and Derivatives. Infinite ξ / Finite η

Table 2.4   Lagrange 6 node Two dimensional Infinite Element
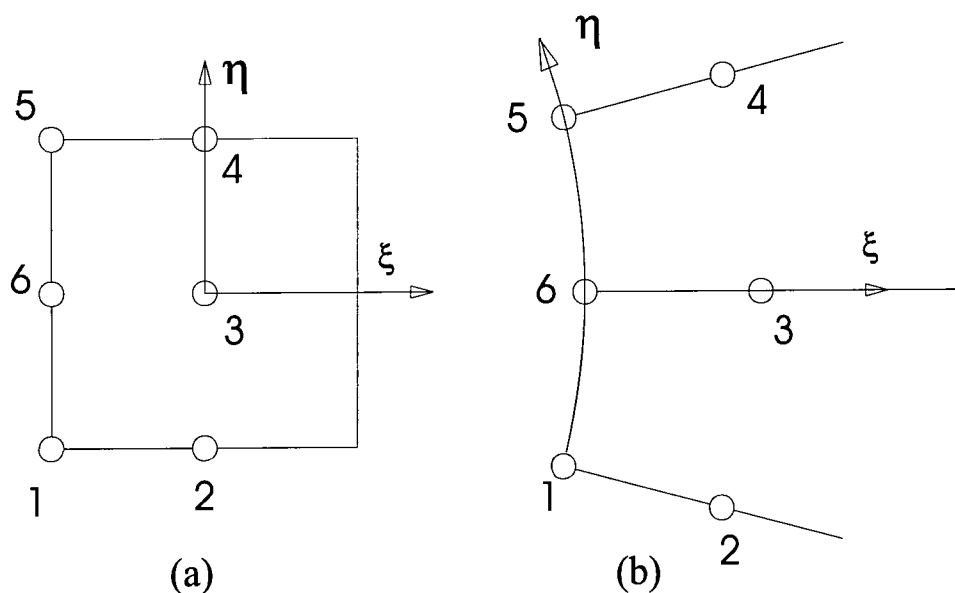
Figure 2.3   Lagrange 6 node Two dimensional Infinite Element

2.15 Periodic infinite elements for wave problems

The first infinite element for periodic wave problems was published by Zienkiewicz and Bettess[119]. This was followed by a more extensive paper[30], by the same authors. This first infinite element was based on an exponential decay of the wave amplitude. The element was effective in representing the effect of the exterior on the region of interest. Later elements which used the Zienkiewicz mapping for infinite elements were developed and these were described in refs. 124, 122, 38 and 125.

The mapped infinite elements can model very closely the appropriate decay of the wave amplitude with distance, and were thus an improvement over the exponential decay elements. These first infinite elements for waves were presented in variational terms, which is identical to the use of the Bubnov-Galerkin weighted residual method. Astley in a series of papers with co-workers, refs 5 to 10, showed that a complex conjugate weighting could also be used and this led to the possibility of simplifications in the infinite element formulation. Although this is an important development, it will not be pursued here. There are many issues which must be considered here, including the presence of terms at infinity and the rate of decay of the weighting function. In recent papers Astley has preferred to use steeper rates of decay in the weighting function, which eliminates terms at infinity, at the expense of an unsymmetrical element matrix. Since the terms at infinity make the element matrix unsymmetrical in any event, it is argued that this is an improvement. Some of these issues are discussed by Bettess[16]. The wave envelope infinite element also has some very attractive features in transient problems, which have been demonstrated by Astley[15,16].

Currently one of the better infinite elements for wave problems is that based on the

Zienkiewicz infinite element mapping, with the addition of the appropriate wave components, as described by Bettess *et al.* [38] and Zienkiewicz *et al.*[124,125], which was mentioned above. The original papers which demonstrated this element concentrated on circular problems. Although some elliptical diffraction problems were solved, the outer ring of infinite elements were placed in a circular mesh. The theory as originally presented does not allow for the infinite elements to be non-circular. In particular the mapping terms are taken to be constant, which implies circularity of the mesh of infinite elements. A reasonable criticism is that for problems which are not approximately circular, the requirement of a circular outer ring of infinite elements can lead to excessively large meshes of finite elements, with associated computational costs.

To address this perceived defect, Burnett[46] has developed a new type of wave infinite element, which can be placed in an elliptic or ellipsoidal mesh, leading to a much more economical solution, for problems of large aspect ratio. The Burnett infinite element uses a hyperbolic-elliptical co-ordinate system and creates semi-analytical infinite element matrices. Burnett terms the resulting approaches prolate and oblate geometries. Burnett's element uses analytical representations of the scattered wave, but is non-conforming.

Goransson and Davidson[68] present an extension of the original mapped wave infinite element of Bettess *et al.*[38], and apply it to the problem of a radiating sphere, for one wavelength. They deal in a terse and oblique manner with what appears to be a problem with variable mapping, but with no theory beyond that in ref. 38, except an extension to three dimensions.

Astley has presented several wave envelope infinite elements[14,16] in which the mapping varies from one element to the next, so that his infinite elements do not have to conform to the exterior of a circle or sphere. In some cases he uses a square finite-infinite element boundary. Astley demonstrates that the method gives good results. He does not, so far as I am aware, give explicit expressions for the derivatives of the shape functions with respect to the non- radial local co-ordinates or point out that these must be evaluated, although by implication he must do this.

Cremers and Fyfe, working with one of Astley's collaborators, Coyette, ref. 57 and alone, ref. 58, give the necessary theory for a variable order wave envelope infinite element and apply it to a range of problems in acoustics. They use essentially the same theory as Zienkiewicz *et al.*[38,125], except that they allow the mapping parameter to vary. They also use the wave envelope formulation. They also give explicit expressions for the shape function derivatives in local co-ordinates, s, and t, in their notation, corresponding to ξ and η in ref. 38 and in this paper. These permit variations in the mapping parameter.

2.16 Decay function periodic infinite elements

The first decay function periodic infinite element was developed by Bettess and Zienkiewicz[122], in 1975, immediately after the first decay function finite element for static

problems. The element was intended for the solution of exterior problems, governed by the Helmholtz equation,

$$\nabla^2 \phi + k^2 \phi = 0, \qquad\qquad 2.23$$

such as wave radiation and diffraction. The element had a special shape function formed from the product of the normal finite element shape function, an exponential decay function and a periodic function of the form $\exp(ikr)$, where r was the radius, $i = \sqrt{-1}$ and k is the wavenumber, $k = 2\pi/\lambda$, where λ is the wavelength. We will develop all the necessary theory for this element, and then look briefly at applications of similar infinite elements in other fields. It should be noted here that the element matrix is *complex* and that special numerical integration schemes are desirable. A sequel, also by Bettess and Zienkiewicz[30] described the necessary theory in more detail, and gave a large number of examples.

In static finite elements it is necessary that the shape function should represent a 'reasonable' behaviour for the field variable out to infinity. Usually this is a decay of type $1/r$ for example. In the periodic problem the behaviour is that of a wave, travelling outwards and gradually decaying. The extra component is the wave type behaviour. This can be achieved by using a product of three functions.

1. a standard shape function (as in static infinite elements)

2. a decay function (as in static infinite elements)

3. an oscillatory (wave) function

These functions are sketched in Figure 2.4. As in the static case there is a great deal of choice in the selection of a decay function. Exponential and reciprocal decay elements are again the obvious choices. All the work carried out to date has been on exponential decay type elements. For such elements the shape function $N_i(\xi, \eta)$ can be written as

$$N_j(\xi, \eta) = P_j(\xi, \eta) f_j(\xi) \exp(iks), \qquad\qquad 2.24$$

<div align="center">(no summation on j)</div>

assuming that ξ is the radial direction, extending to infinity. In equation 2.24 it is assumed that the decay, $f_j(\xi)$, is not a function of η. It is of course possible to remove this restriction. (For more details of choices for f_j, see Refs. 44, 34 and 37.) The derivatives of the shape function $N_j(\xi, \eta)$ are now found to be

$$\frac{\partial N_j}{\partial \xi} = \frac{\partial P_j}{\partial \xi} f_j \exp(iks) + P_j \frac{\partial f_j}{\partial \xi} \exp(iks) + P_i f_j ik \frac{\partial s}{\partial \xi} \exp(iks), \qquad 2.25$$

and

$$\frac{\partial N_j}{\partial \eta} = \frac{\partial P_j}{\partial \eta} f_j \exp(iks).$$

where s, a co-ordinate directly related to ξ the radial co-ordinate, is defined as follows.
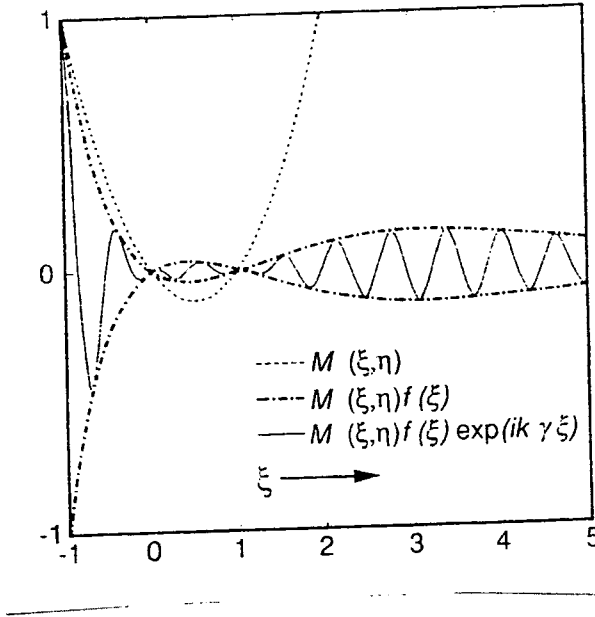
Various components from which the periodic decay function infinite element shape function is composed

Figure 2.4   Decay function infinite element shape functions

$$\frac{\partial s}{\partial \xi} = \sqrt{\left[(\frac{\partial x}{\partial \xi})^2 + (\frac{\partial y}{\partial \xi})^2 \right]} = \gamma. \qquad 2.26$$

This s co-ordinate, with the same metric as the x, y co-ordinate system must be introduced, because the wave number is a fundamental property of the problem and relates to the original x, y co-ordinates. The usual techniques, appropriate for finite elements are applicable to these infinite elements. They can be made isoparametric to a limited extent. As usual the Jacobian matrix **J**, can be found from the co-ordinates of the finite nodes and the *finite* element shape functions. That is

$$\mathbf{J} = \begin{bmatrix} \partial x/\partial \xi & \partial y/\partial \xi \\ \partial x/\partial \eta & \partial y/\partial \eta \end{bmatrix}, \qquad 2.27$$

$$\frac{\partial x}{\partial \xi} = \sum_{i=1}^{n} \frac{\partial P_i}{\partial \xi} x_i \qquad \frac{\partial y}{\partial \xi} = \sum_{i=1}^{n} \frac{\partial P_i}{\partial \xi} y_i,$$

$$\frac{\partial x}{\partial \eta} = \sum_{i=1}^{n} \frac{\partial P_i}{\partial \eta} x_i \qquad \frac{\partial y}{\partial \eta} = \sum_{i=1}^{n} \frac{\partial P_i}{\partial \eta} y_i.$$

The Jacobian matrix, $\mathbf{J}$, is inverted to give $\mathbf{J}^{-1}$. It can then be used to convert the shape function derivatives to global co-ordinates. Thus

$$\left\{ \begin{array}{c} \partial \mathbf{N}/\partial x \\ \partial \mathbf{N}/\partial y \end{array} \right\} = \mathbf{J}^{-1} \left\{ \begin{array}{c} \partial \mathbf{N}/\partial \xi \\ \partial \mathbf{N}/\partial \eta \end{array} \right\}. \qquad 2.28$$

The shape function derivatives with respect to local co-ordinates, ξ and η, are already known from equations 2.25. So far the procedure is very close to that for static infinite elements. Unfortunately the standard integration schemes described in Ref. 1, 63 and 113 are less than satisfactory for the periodic elements. This is because of the wave component in the integrand. Standard integration rules are designed to cope with polynomials, which are not good approximations to trignometric functions. It has been found in practice that the Gauss-Laguerre integration formula can be used for infinite elements for periodic problems, but large numbers of integration points (up to 32), had to be used. It is better to develop special integration formulas for these elements.

2.17 Integration of periodic infinite wave elements

The formulas are related to the Newton-Cotes type of formula. That is the integration abscissæ are chosen and the weights calculated. In the evaluation of infinite element matrices based on shape functions of the form of equation 2.24, the expressions which arise are of the form

$$\int_0^{\infty} f(x) e^{-\alpha x} e^{i\beta x} dx. \qquad 2.29$$

The first limit of integration may be non zero, depending upon the details of the parent finite element, but this can easily be accommodated by a change of variable. The constant α depends upon the chosen decay rate and β depends upon the wave number, k. Usually it will be $2k$. Equation 2.29 can also be written as

$$\int_0^{\infty} f(x) \exp(-\alpha + i\beta) x \, dx, \qquad 2.30$$

where $i = \sqrt{-1}$ and $\exp i\beta x = \cos \beta x + i \sin \beta x$. The procedure is to select integration abscissæ and then to generate Lagrange polynomials for each abscissa. The function $f(x)$ is then taken to be a linear combination of these polynomials and each polynomial is multiplied by $\exp(-\alpha + i\beta)$ and integrated, analytically, between the limits 0 and ∞. This integral gives the weight of that abscissa in the integration scheme. The whole

process is explained in detail in Appendix C, of reference 16, where tables of abscissæ and weights for 3, 4, 5 and 6 integration points are given.

2.17.1 Programming decay function wave infinite elements

The programming of infinite elements can be made fairly complicated if analytical integration is used, or if a finite element parent shape is not used. However, usually the coding is fairly simple even when wave elements are considered. As in section 2.3 we first consider the code for a typical *finite* element for Helmholtz equation, where the wave number, k, is specified, written in a loose Algol notation as shown below. $\mathbf{P}$ denotes the parent finite element shape function.

```
C finite element procedure C
parameters:  x,y,nodal coordinates,
gauss abscissae and weights
BEGIN
    initialize element matrix k to zero
    FOR all gauss points DO
    BEGIN
        get gauss abscissa and weight, w
        call shape function procedure, returns
        P, ∂P/∂ξ, ∂P/∂η
        form Jacobian matrix J
```

$$\mathbf{J} := \begin{bmatrix} \partial\mathbf{P}/\partial\xi \\ \partial\mathbf{P}/\partial\eta \end{bmatrix} [\mathbf{x}, \mathbf{y}]$$

```
        Invert J to give J⁻¹
```

$$\mathbf{b} := \begin{bmatrix} \partial\mathbf{P}/\partial x \\ \partial\mathbf{P}/\partial y \end{bmatrix} := \mathbf{J}^{-1} \begin{bmatrix} \partial\mathbf{P}/\partial\xi \\ \partial\mathbf{P}/\partial\eta \end{bmatrix}$$

$$\mathbf{k} := \mathbf{k} + w\mathbf{b}^T\mathbf{b} + k^2 w \ \mathbf{N}^T\mathbf{N}$$

```
    END
END
```

Now consider how this would be modified for a decay function wave infinite element.

```
C decay function infinite element procedure C
parameters:  x,y nodal coordinates,
gauss abscissae and weights
BEGIN
    initialize element matrix k to zero,
*1  call procedure to obtain integration abscissæ
    gauss in η direction,
    special integration rule, (equation 2.30)
    for ξ direction,
    FOR all integration points DO
```

```
    BEGIN
        get abscissa and weight, w
        call finite element shape function
        procedure, returns
```
$\mathbf{P},\ \partial\mathbf{P}/\partial\xi,\ \partial\mathbf{P}/\partial\eta$
```
        form Jacobian matrix J
```
$$\mathbf{J}:=\begin{bmatrix}\partial\mathbf{P}/\partial\xi\\ \partial\mathbf{P}/\partial\eta\end{bmatrix}[\mathbf{x},\mathbf{y}]$$
```
        Invert J to give J⁻¹
```
 *2   find γ from equation 2.26 (the element must be arranged so that γ is a constant on a given radial line)

*3   call decay function routine, returns

$\mathbf{f},\ \partial\mathbf{f}/\partial\xi,\ \partial\mathbf{f}/\partial\eta$

*4   form $\partial\mathbf{N}/\partial\xi, \partial\mathbf{N}/\partial\eta$ from $\mathbf{P},\partial\mathbf{P}/\partial\xi,\partial\mathbf{P}/\partial\eta$ and $\mathbf{f},\partial\mathbf{f}/\partial\xi,\partial\mathbf{f}/\partial\eta$ and the derivatives of $\exp(iks)$ using equations 2.25

$$\mathbf{b}:=\begin{bmatrix}\partial\mathbf{N}/\partial x\\ \partial\mathbf{N}/\partial y\end{bmatrix}:=\mathbf{J}^{-1}\begin{bmatrix}\partial\mathbf{N}/\partial\xi\\ \partial\mathbf{N}/\partial\eta\end{bmatrix}$$

$$\mathbf{k}:=\mathbf{k}+w\mathbf{b}^T\mathbf{b}+k^2 w\ \mathbf{N}^T\mathbf{N}$$

```
(Note that k is not simply a stiffness matrix, it includes both
 stiffness and mass effects - it is complex)
    END
END
```

The only modifications are marked *. They can each be accomplished by a call to a procedure: (*1) requires a procedure to set up appropriate integration abscissæ and weights as described above in an array; (*2) requires a simple calculation from equation 2.26 using **J**. (*3) requires a procedure to evaluate the decay function, $f(\xi,\eta)$, and its derivatives. This is about as complicated as a finite element shape function procedure; (*4) requires a procedure to implement equation 2.25, which typically requires about 10 lines of code. Of course, the shape function and element matrix must be declared as complex.

2.18 Periodic mapped infinite elements for wave problems

The necessary theory will be dealt with in Chapter 3, where the new infinite element is also described.

Chapter 3

A New Mapped Infinite Wave Element

3.1 Introduction

This Chapter describes the development of a new mapped infinite wave element. There is a very considerable literature on this topic, which was surveyed in Chapter 2.

Essentially the work of Astley and Cremers *et al.* is followed here, as it was described in section 2.15. The difference is that the Bubnov Galerkin or unconjugated method is used. The original shape functions of the Bettess and Zienkiewicz papers[38,125] are retained. One of the aims is to show how simple the necessary changes to the original formulation are. Following Cremers and Fyfe explicit expressions for the circumferential (or η) derivatives of the shape functions are given showing their dependence upon the mapping parameter. In addition in recent work Astley[16] extends his wave envelope infinite elements to the oblate and prolate geometries proposed by Burnett[49] and Burnett and Holford[50,51] in three dimensional acoustics problems.

The work on the new mapped infinite wave element has three main aspects:

(i) The extension of the previous theory of the mapped infinite wave elements to the case when the elements are not placed strictly radially, which is dealt with in this Chapter.

(ii) A comparison of the accuracy of the infinite wave elements for a problem which has an analytical solution, but is not circular.

(iii) The presentation of a large number of accurate solutions to the problem of waves diffracted by an ellipse, for reference by future researchers. Aspects (ii) and (iii) are dealt with in Chapter 7.

It will be shown that the relatively simple extension of the orignal mapped wave element theory of Zienkiewicz, Bettess *et al.*[38,128] enables the method to be used for wave diffraction problems of large aspect ratio. In particular it will be demonstrated that the new infinite elements are accurate, even when the finite element mesh is long and thin. In this case the circle circumscribing the *finite* element mesh, or that circumscribing the diffracting object will intersect the infinite elements. There are proofs available demonstrating the convergence of the solutions to these scattering problems, outside a circle due to Karp[83] and Wilcox[119]. The necessary background wave theory was dealt with in Chapter 1.

3.2 Theory of mapped periodic infinite elements

We now deal with the application of the mapped infinite element to periodic wave problems. The Zienkiewicz and Marques and Owen mappings were described in section 2.14. Here the effect of the wave component on the infinite elements is discussed. First the classical theory is rehearsed, and then the quite simple extensions are described.

Many exterior wave problems have solutions in which the wave amplitude decays like $1/r$ and an advantage of the mapping given in section 2.14 is that such a decay can be accommodated. In the two dimensional case considered here, however, the amplitude decays approximately as $1/\sqrt{r}$, and in this case a special procedure is used to deal with this term. In general, accuracy can be increased by adding extra terms to the series 2.17. An advantage of this approach is that the finite element domain is used for the definition of the shape function and for the numerical integration, which is thus carried out over a finite domain. As we shall see special integration procedures are still needed.

As mentioned in section 2.14 the particular infinite element used here is quadratic and has six nodes, those at infinity being removed. It is based on Lagrange polynomials and the mapping functions are easily constructed from the product of the finite element shape functions in terms of η and the infinite element mapping functions in the ξ direction. The functions were given and the element sketched in chapter 2, figure 2.3 and tables 2.4.

3.3 Introducing the wave component

Three dimensional exterior wave problems turn out to be simpler than two dimensional ones, because the solutions are dominated by terms of the form e^{ikr}/r, and the $1/r$ behaviour is already in the shape function.

The shape function of the parent finite element, $P(\xi, \eta)$, is simply multiplied by the exponential term.

$$N(\xi, \eta) = P(\xi, \eta) \exp(ikr). \qquad\qquad 3.1$$

In two-dimensional exterior domains the asymptotic solution to Helmholtz's equation can be described by a series of combined Hankel and trigonometric functions, the simplest solution to Helmholtz's equation being $H_0(kr)$.* For large r the zeroth-order Hankel function oscillates roughly like $\cos(kr) + i\sin(kr)$, where k as defined above is the wave number, while decaying in magnitude as $r^{-1/2}$. We will use a series of terms $1/r$, $1/r^2$ etc., generated by the mapping, multiplied by $r^{1/2}$ and the periodic component $\exp(ikr)$ in order to model the $r^{-1/2}$ decay.

---

* This is not the place to explore the convergence characteristics of such a series. But it should be noted that for waves diffracted by arbitrary bodies a series solution may not converge.

The shape function is therefore the original shape function described earlier, multiplied by the additional wave terms, giving

$$N(\xi,\eta) = P(\xi,\eta)r^{1/2}\exp(ikr),$$ 3.2

which as can be seen is slightly more complicated than equation 3.1. We will therefore work out the theory for the simpler three dimensional case, before moving to the two dimensional case. The three dimensional theory was first given by Bettess *et al.*[38] and that for two dimensions by Zienkiewicz *et al.*[128]. Preliminary sketches of the theory, without results were given in ref. 125.

3.4 Three dimensions

The mapping in equation 2.20 is repeated here as

$$r = \frac{A}{1-\xi},$$ 3.3

where $A = 2a$, and the shape function will become

$$N(\xi,\eta) = P(\xi,\eta)\exp\left[\frac{ikA}{1-\xi}\right],$$ 3.4

where $P(\xi,\eta)$ is the shape function of the parent finite element. An important point to be mentioned is that if the shape functions are to be continuous between finite and infinite elements, the absolute value should be unity and the phase must be made zero at $\xi = -1$ (the boundary with the standard finite elements). At $\xi = -1$, the value of the shape function $N(\xi,\eta)$ is

$$N(-1,\eta) = P(-1,\eta)\exp\left[\frac{ikA}{2}\right].$$ 3.5

To ensure continuity, a factor $\exp(-ikA/2)$ is introduced so that the shape function becomes

$$N(\xi,\eta) = P(\xi,\eta)\exp\left[\frac{-ikA}{2}\right]\exp\left[\frac{ikA}{1-\xi}\right] = C.P(\xi,\eta)\exp\left[\frac{ikA}{1-\xi}\right],$$ 3.6

where

$$C = \exp\left[\frac{-ikA}{2}\right],$$ 3.7

and its derivatives are

$$\frac{\partial N}{\partial \xi} = C \exp\left[\frac{ikA}{1-\xi}\right]\left[\frac{\partial P}{\partial \xi} + PikA\frac{1}{(1-\xi)^2}\right] \qquad 3.8$$

and

$$\frac{\partial N}{\partial \eta} = C\frac{\partial P}{\partial \eta}\exp\left[\frac{ikA}{1-\xi}\right]. \qquad 3.9$$

The functional corresponding to Helmholtz's equation in three dimensions is given by

$$F = \int_\Omega \left[\left(\frac{\partial \phi}{\partial x}\right)^2 + \left(\frac{\partial \phi}{\partial y}\right)^2 - k^2\phi^2\right]d\Omega - \int_\Gamma \phi\frac{\partial \phi}{\partial n}d\Gamma, \qquad 3.10$$

(see section 1.8.1). In forming the element matrix, it is necessary to integrate this functional, (or, equivalently, a weighted residual) over the element domain. In the first extended paper on this element ref. 65, in which the numerical integration was discussed at length, there was some uncertainty about the evaluation of the function at infinity, because it is not obvious that the terms in the domain integral should be zero on the boundary at infinity. It was later shown by Astley, Clark and Bettess[13] that in forming the integral over the element domain the contribution at infinity can be neglected, because the terms will always cancel with the line integral at infinity. The argument will not be repeated here. More details are given in ref. 44.

3.4 Two dimensions

For the more complicated, two dimensional form, which includes an extra $\sqrt{r}$ term, equation 3.2, can be written as

$$N(\xi,\eta) = P(\xi,\eta)\left[\frac{A}{1-\xi}\right]^{1/2}\exp\left[\frac{ikA}{1-\xi}\right], \qquad 3.11$$

as explained in equation 3.2. As before the shape functions must be continuous between finite and infinite elements. At $\xi = -1$, the value of the shape function $N(\xi,\eta)$ is

$$N(-1,\eta) = P(-1,\eta)\left[\frac{A}{2}\right]^{1/2}\exp\left[\frac{ikA}{2}\right]. \qquad 3.12$$

To ensure continuity, a factor $(2/A)^{1/2}\exp(-ikA/2)$ is introduced so that the shape function becomes

$$N(\xi, \eta) = P(\xi, \eta) \left[\frac{2}{A}\right]^{1/2} \left[\frac{A}{1-\xi}\right]^{1/2} \exp\left[\frac{-ikA}{2}\right] \exp\left[\frac{ikA}{1-\xi}\right]$$

$$= C.P(\xi, \eta) \left[\frac{A}{1-\xi}\right]^{1/2} \exp\left[\frac{ikA}{1-\xi}\right], \qquad 3.13$$

where

$$C = \left[\frac{2}{A}\right]^{1/2} \exp\left[\frac{-ikA}{2}\right]. \qquad 3.14$$

The derivatives can now be evaluated after some slight manipulation as

$$\frac{\partial N}{\partial \xi} = C \times \left\{\frac{\partial P}{\partial \xi} + \frac{P}{2(1-\xi)} + \frac{ikAP}{(1-\xi)^2}\right\} \times \exp\left[\frac{ikA)}{(1-\xi)}\right] \times \left[\frac{A}{(1-\xi)}\right]^{1/2} \qquad 3.15$$

and

$$\frac{\partial N}{\partial \eta} = C \times \frac{\partial P}{\partial \eta} \times \exp\left[\frac{ikA}{(1-\xi)}\right] \times \left[\frac{A}{(1-\xi)}\right]^{1/2}. \qquad 3.16$$

3.5 Numerical integration over the element domain

In the formation of the element matrix, integrals involving the products of polynomials and trignometrical functions arise. In refs 125 and 128 a scheme is devised which enables these integrals to be efficiently and accurately evaluated. The most difficult case which arises is of the form

$$\int_b^\infty \frac{cosx}{x} dx, \qquad 3.17$$

and in this case tables and computer functions are available for the integration. All the other terms which arise can be reduced, using integration by parts to the same form. Readers are referred to the above references for complete details. A computer code is available on disc with reference 44. It might be noted by readers that, contrary to some recent statements[49],[97] in the literature, it is not an essential feature of the numerical integration process that a matrix inversion should be carried out. This just happens to be the way that it was implemented in ref. 128. This step may be eliminated at the expense of some slightly different programming. This is shown in Appendix B.

3.6 New mapped wave infinite element

The theory described above gives the previous formulation. The new formulation consists of allowing the mapping to vary within each element. It should be noted that this does not compromise inter infinite element compatibility, since all the mappings are still determined by the nodes. It simply means that the constant A, equation 2.20, varies within the element. A is now determined on each radial line from the positions of the nodes. It is interpolated between these values.
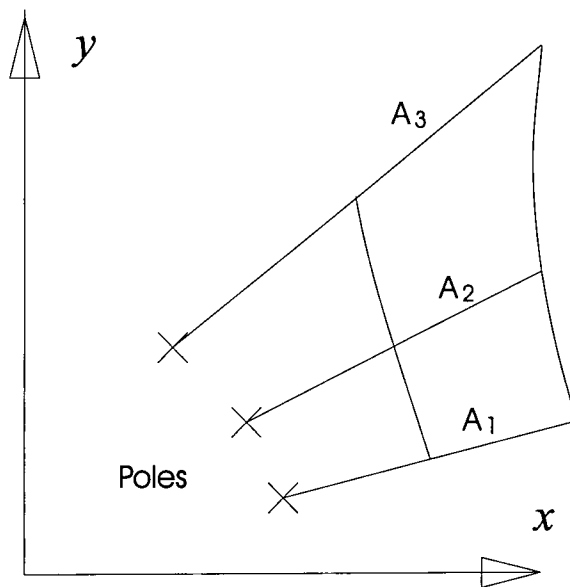
Figure 3.1   Variable Mapping in the New Infinite Mapped Wave Element

The first step is to write $A = A(\eta)$. This allows different infinite elements to have different 'poles', and different rates of decay, while remaining conforming, as shown in figure 3.1. Within the infinite element, the parameter A is interpolated in the η direction. The values of A are determined on the lines $\eta = -1, 0, +1$, (for a quadratic element). On each line the x and y co-ordinates are used to determine A, from the mapping function, table 2.4. Let these values be labelled A_1, A_2 and A_3. Then in the interior of the infinite element, at a location η, the value of A, and its derivatives, are given by

$$A = \sum_{i=1}^{3} N_i A_i \qquad \text{and} \qquad \frac{\partial A}{\partial \eta} = \sum_{i=1}^{3} \frac{\partial N_i}{\partial \eta} A_i, \qquad\qquad 3.18$$

where N_i are the one dimensional quadratic shape functions

$$N_1 = -\frac{\eta}{2}(1 - \eta), \quad N_2 = 1 - \eta^2, \quad N_3 = \frac{\eta}{2}(1 + \eta).$$

It is also convenient to define a variable, $\alpha = 2kA$. Now the only alteration to the shape function derivative is an additional term in the η derivative (equation 3.16). The shape function and derivatives are thus

$$N(\xi, \eta) = P(\xi, \eta)\left[\frac{2}{A(\eta)}\right]^{1/2}\left[\frac{A(\eta)}{1-\xi}\right]^{1/2}\exp\left[\frac{-ikA(\eta)}{2}\right]\exp\left[\frac{ikA(\eta)}{1-\xi}\right]$$

$$= C.P(\xi, \eta)\left[\frac{A(\eta)}{1-\xi}\right]^{1/2}\exp\left[\frac{ikA(\eta)}{1-\xi}\right], \qquad 3.19$$

where

$$C = \left[\frac{2}{A(\eta)}\right]^{1/2}\exp\left[\frac{-ikA(\eta)}{2}\right], \qquad 3.20$$

$$\frac{\partial N}{\partial \xi} = C \times \left\{\frac{\partial P}{\partial \xi} + \frac{P}{2(1-\xi)} + \frac{ikA(\eta)P}{(1-\xi)^2}\right\} \times \exp\left[\frac{ikA(\eta)}{(1-\xi)}\right] \times \left[\frac{A(\eta)}{(1-\xi)}\right]^{1/2}, \quad 3.21$$

$$\frac{\partial N}{\partial \eta} = C \times \left[\frac{\partial P}{\partial \eta} + \left\{\frac{ik}{2} \times \frac{1+\xi}{1-\xi} \times P \times \frac{\partial A(\eta)}{\partial \eta}\right\}\right]$$

$$\times \exp\left[\frac{ikA(\eta)}{(1-\xi)}\right] \times \left[\frac{A}{(1-\xi)}\right]^{1/2}. \qquad 3.22$$

The only new term is the term involving $\partial A(\eta)/\partial \eta$, which is indicated in equation 3.22 by placing it in $\{\}$. However A is no longer constant for the element or problem, and is a function of η.

3.7 Integration scheme

Because the integration weights are dependent upon A, unfortunately it is now necessary to evaluate them for all the different values of A used in the analysis, instead of only once. Only the part of the process which depends upon the wave number need be repeated. The determination of the integration abscissæ and the associated polynomials can be done once and for all. The remaining work, the evaluation of the complex

weights, is not a large computational overhead, and does not affect the solution times to a large extent. It would, however, be good to find a way to avoid this extra computation. The rest of the evaluation of the element matrix and its use in the program, remains unchanged.

3.8 Programming

The main structure of the program follows that published by Bettess and Bettess as a report[31]. Conventional numerically integrated eight node quadrilateral and six node triangle finite elements are used. The solver is the Bruce Irons frontal solver modified to deal with complex arithmetic. All the real variables are stored in eight bytes and the complex numbers are stored in sixteen bytes. The program has been modified to run on a PC using the Salford Fortran compiler, and the program is compatible with Fortran 77. It has also been run on workstations using the f77 (UNIX) compiler. Most of the wave program and all the mesh generation and post processing programs have been written by the author. The elliptical meshes seen in the figures in the results section were generated by a custom-written mesh generator.

3.9 Total and scattered potential

It was explained in section 1.10 that the essential change from total to scattered potential leads to a line integral on a boundary. This integral is evaluated from the incident wave, which is known. The line integral leads to a 'right hand side' term, which forces the wave response. The user may select the location of this boundary, subject to certain limitations.

This line integral may be evaluated by integrating the expression given in the right hand half of equation 1.59, along the chosen boundary. The scattered potential, ϕ^s is of course omitted. The process utilises the usual iso-parametric mapping techniques, to evaluate the expression along the edge of the appropriate finite element, making up a segment of the boundary.

The values of c and c_g are found from the depth, and the dispersion relation, for a given frequency. This involves the use of the Newton-Raphson method to solve the non-linear dispersion relation. If the depth is constant, this need only be done once, and in any event the process converges very rapidly.

The element of distance dx is found from $(\partial x/\partial \xi)d\xi$, where ξ is taken to vary along the edge of the element, and $\partial x/\partial \xi$ is found in the usual way from the derivatives of the element shape functions and the nodal co-ordinates. ϕ_i is a known function and is readily determined from equation 1.59 for a plane wave. Gauss-Legendre integration in one dimension is used to evaluate the 'forcing' term.

In addition to the line integral there is a change of nodal variable at the nodes on

the boundary between total and scattered potential. This change of nodal variable is carried out as follows. We consider the finite element shown in figure 3.2. The nodes are partitioned into two sets, 1 and 2, in which the first set of nodes, numbered 1, 8 and 7 are in terms of the total potential and the second set of nodes numbered 2, 3, 4, 5 and 6 are in terms of the scattered potential. Initially the variable at all nodes is the scattered potential. The element matrix can thus be written
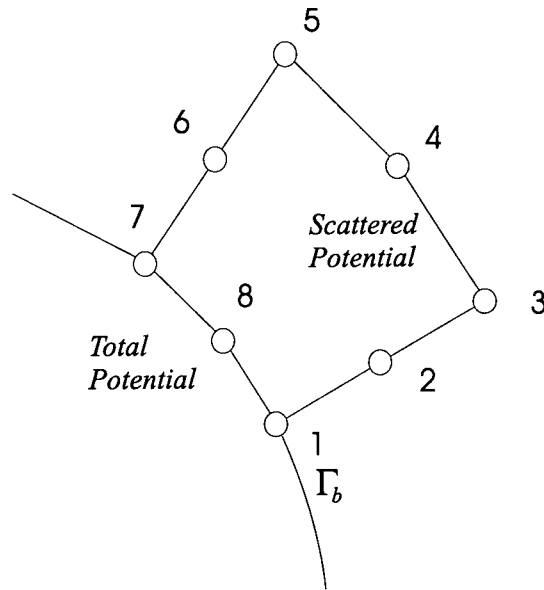
Figure 3.2   Partitioning of nodal variables at total and scattered potential boundary

$$\begin{bmatrix} k_{11} & k_{12} \\ k_{21} & k_{22} \end{bmatrix} \begin{Bmatrix} \phi_{s1} \\ \phi_{s2} \end{Bmatrix}.$$ 3.23

The condition that

$$\phi = \phi_i + \phi_s \qquad \text{or} \qquad \phi_s = \phi - \phi_i$$ 3.24

is now applied, so that the element matrix can now be written as

$$\begin{bmatrix} k_{11} & k_{12} \\ k_{21} & k_{22} \end{bmatrix} \begin{Bmatrix} \phi_1 \\ \phi_{s2} \end{Bmatrix} - \begin{bmatrix} k_{11} \\ k_{21} \end{bmatrix} \{ \phi_{i1} \}.$$ 3.25

It can be seen that the effect of the change in nodal variable is to generate as set of nodal 'forcing' terms for the nodes on the interface boundary, which arise from the

terms in the element matrix and the known nodal values of ϕ_i. These are generated and inserted in the appropriate place in the overall system matrix right hand side. They are of course complex, because ϕ_i is complex.

3.10 Infinite elements

There are essentially three changes to the infinite element code as published on the computer disc available with ref. 44. These are:

1. The introduction of the calculation of the parameter A on three separate radial lines within the quadratic element.

2. The use of the above values, with a simple quadratic shaped function to interpolate for $A(\eta)$ and $\partial A(\eta)/\partial \eta$, for any given value of η within the element.

3. The modification of the infinite element routine to re-calculate the integration absiccæ and weights for each different η value.

4. The addition of a single extra term in the element shape function derivative evaluations, from equation 3.22.

Chapter 4

Data structures in wave program

4.1 Introduction

Data structures of various kinds are widely used in Computer Science. Descriptions are given by Knuth[86] and Page and Wilson[102] of many different kinds of data structure which are used in compilers, operating systems, graphics software, large scale finite element packages and other applications. This chapter describes a simple set of Fortran subroutines which can be used with little effort to store finite element data in a very flexible manner. The advantages and disadvantages can be summarized as

Advantages

- Data array sizes do not have to be estimated before compilation.

- A trade off between memory and time requirements can be decided by the user.

- Complex relationships between data can be explored.

- Variation in number of nodes per element do not lead to wasted storage.

- The data structure makes the transfer of information between programs straightforward.

Disadvantages

- Access to data will usually be slightly slower.

- Programming is more complicated.

- The data structure routines occupy memory.

4.2 Basic concepts of the data structure

It is assumed that the data structure has an unlimited supply of storage locations available. This can be thought of as a large Fortran singly dimensioned array. In systems with virtual memory facilities this is easy to implement by declaring a very large Fortran array. The data stored in the structure are arranged so that it is possible, with the use of pointers, to access and explore the complex relationships between them. A pointer is a number in some location in the array which gives another location in

the array. For example in Figure 4.1 the contents of location 4 point at location 11. The data structure routines described below can be used as a 'black box' for storing and accessing finite element data in a very flexible manner.
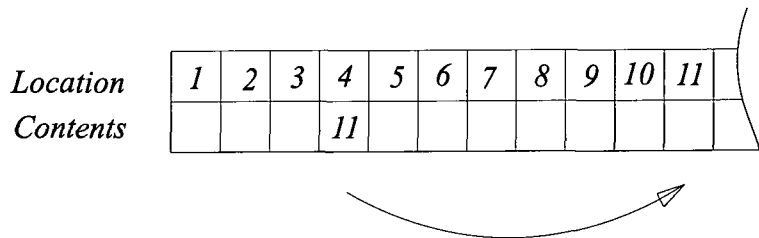
Figure 4.1   Example of data structure pointer

4.3 Detailed description of the data structure

4.3.1 Software paging

A direct access disc file is mapped onto a fixed area of memory in such a way that to the user, it appears as if the amount of memory available is as large as the disc file. The access is implemented by a Fortran function NO(I). The contents of the Ith word of the disc file can be transferred to a memory location called K, by writing

```
K = IB( NO(I))
```

The function NO will make any necessary disc transfers and deliver the contents of the required location in IB, the Fortran array which is in memory. Similarly, the contents of a location called K can be stored in location I in the data structure by writing

```
IB( NO(I)) = K
```

The chosen mapping from memory to disc is extremely simple, because more sophisticated algorithms are probably not worth the increased execution time. The mapping is shown in figure 4.2.

The memory is divided into a set of pages for the purpose of transfer to disc. Originally, the memory allocated was 1000 32 bit words, divided into 10 pages of 100 words each, and the direct access disc file was 1000 pages of 100 words each. All these parameters are readily changeable, and can be chosen to suit the computer system being used.

4.3.2 The components of the data structure

The first two sections of the data structure are fixed and permanent. They are the title block, which holds the problem title, and the pointer block, which holds pointers to

3 pages

Memory

Disc
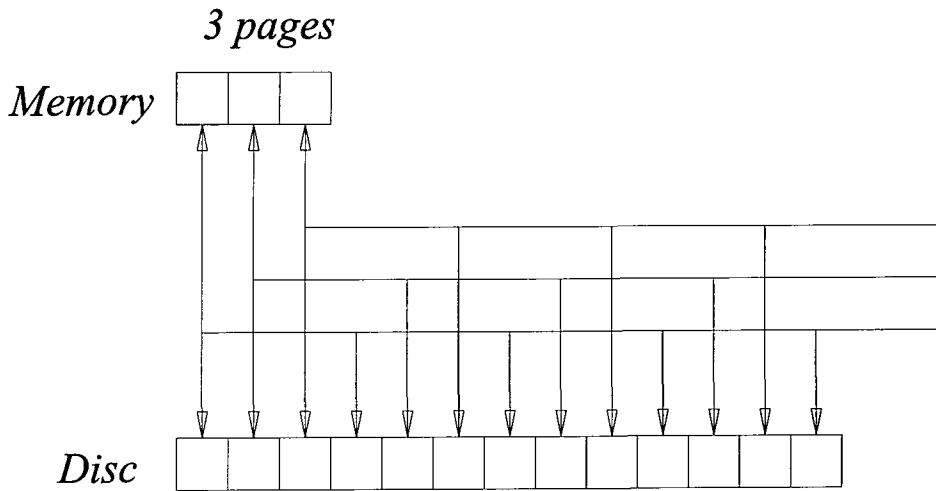
Figure 4.2   Paging mapping function

element data, node data and so on. The other parts of the data structure, called entries, can appear in any part of the array. There are node entries, element/node entries, element entries. The node entry holds the node number, the node co-ordinates, a spare word and a pointer to the first element/node entry for that node. The element entry holds the element number and the element type and a pointer to the first element/node entry for this element. The element/node entry holds the element number, the node number and a pointer to the next element/node entry for this node.

4.3.3 How to use the housekeeping routines

Instead of reading data into arrays, the user puts the data into the data structure and retrieves data from it by calling subroutines. The subroutines are briefly described below and the parameters are described in detail in the listings in Appendix 1. These routines assume that integer and real variables occupy 4 bytes each in the data structure.

- **PUTNOD** inserts a node entry into the data structure. It must be called once for every node. Before calling **PUTNOD** for the first time, the pointer **IPN** must be set equal to the initial address of the node entries, i.e. **IPN** =**IAN** and thereafter **IPN** will be incremented automatically and should not be re-set. It is advisable to insert the nodes in numerical order to increase the speed of accessing node information.

- **GETNOD** retrieves a node entry from the data structure. It works fastest when the node entries are held in numerical order.

- **PUTEL** inserts an element entry into the data structure and also sets up the element/node entries which define all the element/node connections. It should be called once for every element. Before the first call, the pointers **IPE** and **IPEN** must

be set i.e. `IPE=IAE`; `IPEN=IAEN`. As with `PUTNOD`, the pointers are incremented automatically and again it is advisable to insert the elements in numerical order.

- `GETEL` retrieves an element entry from the data structure. It saves a lot of time if the elements have been inserted in numerical order.

- `NODELS` returns the elements connected to a node.

- `ELNODS` returns the nodes defining an element.

- `PUTDIS` inserts the displacements for an element into the data structure. They are inserted in node number order (this assumes all node numbers exist from 1 to `NN`), and the node number is not stored with the displacement. This method does involve inserting the displacements for a node more than once, but it eliminates any searching to see if the displacements are already there.

- `GETDIS` retrieves all the displacements for an element. The displacements are assumed to be in node number order.

4.3.4 An example

Data structures are really best understood by reference to examples. Figure 4.3 shows a hypothetical finite element mesh, in three dimensions, with a wide variety of element types. The data is listed in Table 4.1 along with a list of elements connected to each node. The data structure representation of the mesh in Figure 4.4 shows some sample links.

The first 30 locations are reserved for basic data, with only the number of nodes and the number of elements being used here. The next ten locations are reserved for pointers, the first four of which point to the node data, the element data, the element/node data and the end of the data. A node entry holds the node number, the three co-ordinates and the pointer to the first entry of element/node data for that node. From there, each element/node entry points to the next element/node entry for that node until the pointer points back to the node entry (indicated by a negative pointer).

The element entries hold the element number, the number of nodes for that element and a pointer to the first entry of element/node data for that element. Since the number of nodes connected to that element is known, the element/node entries follow in sequence.

The element/node entries are accessed when pointed to by a node or element entry. They can be used to find the nodes connected to each element or the elements connected to each node.
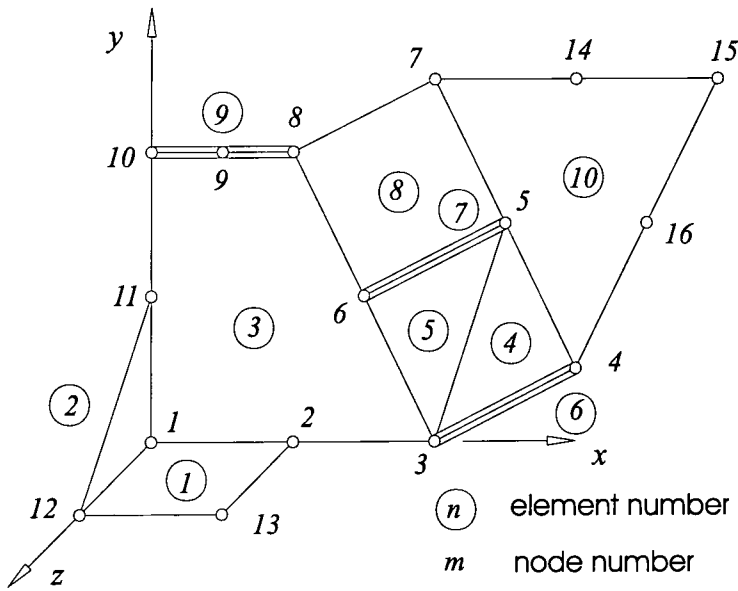
Figure 4.3 Example finite element mesh

Data

16	10						
1	0.0	0.0	0.0
2	2.0	0.0	0.0
3	4.0	0.0	0.0
4	6.0	1.0	0.0
5	5.0	3.0	0.0
6	3.0	2.0	0.0
7	4.0	5.0	0.0
8	2.0	4.0	0.0
9	1.0	4.0	0.0
10	0.0	4.0	0.0
11	0.0	2.0	0.0
12	0.0	0.0	2.0
13	2.0	0.0	2.0
14	6.0	5.0	0.0
15	8.0	5.0	0.0
16	7.0	3.0	0.0

Node	Elements			
1	3	2	1	
2	3	1		
3	6	5	4	3
4	10	6	4	
5	10	8	7	5 4
6	8	7	5	3
7	10	8		
8	9	8	3	
9	9	3		
10	9	3		
11	3	2		
12	2	1		
13	1			
14	10			
15	10			
16	10			

4	12	13	2	1			
3	12	1	11
8	1	2	3	6	8	9	10 11
3	3	4	5
3	3	5	6
2	3	4	
2	6	5	
4	6	5	7	8
3	8	9	10
6	4	16	15	14 7 5

Table 4.1 Listing of the test data & List of elements connected to each node

Figure 4.4 Contents of Data Structure

Location

Initial data:

Location					
1	16	10	0	0	0
6	0	0	0	0	0
11	0	0	0	0	0
16	0	0	0	0	0
21	0	0	0	0	0
26	0	0	0	0	0

Pointers:

31	(illegible)	(illegible)	(illegible)	(illegible)	0
36	0	0	0	0	0

Node data:

Location					
41	1	0.0	0.0	0.0	236
50	2	2.0	0.0	0.0	239
59	3	4.0	0.0	0.0	259
68	4	6.0	1.0	0.0	311
77	5	5.0	3.0	0.0	326
86	6	3.0	2.0	0.0	290
95	7	4.0	5.0	0.0	323
104	8	2.0	4.0	0.0	302
113	9	1.0	4.0	0.0	305
122	10	0.0	4.0	0.0	308
131	11	0.0	2.0	0.0	257
140	12	0.0	0.0	0.0	227
149	13	2.0	0.0	0.0	218
158	14	6.0	5.0	0.0	320
167	15	8.0	5.0	0.0	317
176	16	7.0	3.0	0.0	314

Element data:

Location			
185	1	4	215
188	2	3	227
191	3	8	236
194	4	3	260
197	5	3	269
200	6	2	278
203	7	2	284
206	8	4	290
209	9	3	302
212	10	6	311

Element/Node data:

Location			
215	1	12	-140
218	1	13	-149
221	1	2	-50
224	1	1	-41
227	2	12	215
230	2	1	224
233	2	11	-131
236	3	1	230
239	3	2	221
242	3	3	-59
245	3	6	-86
248	3	8	-104
251	3	9	-113
254	3	10	-122
257	3	11	233
260	4	3	242
263	4	4	-68
266	4	5	-77
269	5	3	260
272	5	5	266
275	5	6	245
278	6	3	269
281	6	4	263
284	7	6	275
287	7	5	272
290	8	6	284
293	8	5	287
296	8	7	-95
299	8	8	248
302	9	8	299
305	9	9	251
308	9	10	254
311	10	4	281
314	10	16	-176
317	10	15	-167
320	10	14	-158
323	10	7	296
326	10	5	293

End of data: 329

Chapter 5

Mesh generation software

5.1 Introduction

Several special purpose mesh generators were created by the author to generate the meshes of finite and infinite elements used in this study. The mesh generators were constructed over a period of years. There are a number of advantages of special purpose generators versus commercial mesh generators, such as ABAPRE, or PATRAN. These are as follows:

- The meshes can be defined using a very small number of input parameters, far smaller than those required by ABAPRE or PATRAN, where the user must define a geometrical hierarchy of points, lines and surfaces to define the geometry, followed by mesh seeds and mesh densities, before creating the actual mesh. Also this has to be done for each mesh created, unless a special script is written, in which case one is, in effect writing a computer program, but in a special, limited, language.

- The entire program is under the user's control, and can be modified by almost anyone, since it is written in Fortran, and has a relatively simple structure.

- The program can be run on any computer from PCs to mainframes and special purpose computers, providing that a Fortran compiler is available.

- The programs are extremely fast, only requiring seconds to run, whereas commercial packages typically take minutes to obtain the software licences and check them and to create the windows environment for the code to execute. Indeed, if there is a limited number of licences available, it may not be possible to run the code, if the licences are reserved by other users.

- The programs are cheap, there are no recurrent licence costs, which can be substantial, even with academic concessions, for packages such as ABAPRE and PATRAN.

- The program can be made freely available to industrial and academic collaborators, at the discretion of the author.

- The work was initiated in the 1970s, in the days before many general purpose mesh generators were available.

5.2 Mesh generators

Several special mesh generators have been written by the author for particular wave problems which have arisen. The programs are as follows:

- A cylindrical mesh generator, SMACREA

- A rectangular mesh generator, SMAGEN

- A generator for regular rectangular arrays of cylinders (or risers), CYLGEN

The programs and their capabilities will now be briefly described, in order. Details of the data preparation needed to use the programs are given in Appendix A.

5.3 The cylindrical mesh generator, SMACREA

This mesh generator will actually generate a wide range of meshes based on cylinders, and cylindrical type shapes. The motivation for the program structure and capabilities was originally the set of problems which Chen and Mei studied[50,51,52,53], and for many of which they had analytical solutions. However the class of geometries for which the mesh generator can be used was made as general as possible without sacrificing simplicity.

The user of the program defines the radii at which the nodes are to be placed, and also the depths of the water at these radii, (r_i, h_i, where i runs from the inner nodes to the outer nodes). The wave program, SMAWAVE, then interpolates quadratically in the radial direction for the depth, using standard finite element techniques. In the circumferential direction the depth at a given radius stays constant. The radius at which the finite elements are to start is thus defined, being r_1. The angles in the circumferential direction, α, β and γ are also defined. These data fix the geometry of the problem as shown in figure 5.1.

To fix the mesh details, the number of subdivisions in both radial and circumferential directions in all sectors is also defined, as described in Appendix A. The user also gives some check data, giving the extent of the finite and infinite element mesh and some of the wave data, such as frequency, ω and and acceleration due to gravity, g. These data are simply passed through to the wave program. The data are quite compact, only occupying a few lines. After checking the data for internal consistency, the program generates all the mesh data in a form which is completely compatible with the wave program. Further information on data preparation for the wave program is given in Appendix A and in the comments in the program itself.

The mesh generation concept of SMACREA is as follows. All meshes are essentially circular or elliptical. From now on, the meshes will be referred to as circular, although all the meshes described can also be generated as ellipses. The mesh can form a complete circle, or can extend to any angle up to 360°. In the case of the complete 360°, an option allows the mesh to be connected, or disconnected. A flag, BFLAG, is read in, which is TRUE if the breakwater is present and FALSE if the breakwater is absent. The

Elevation of section through problem

Plan of problem
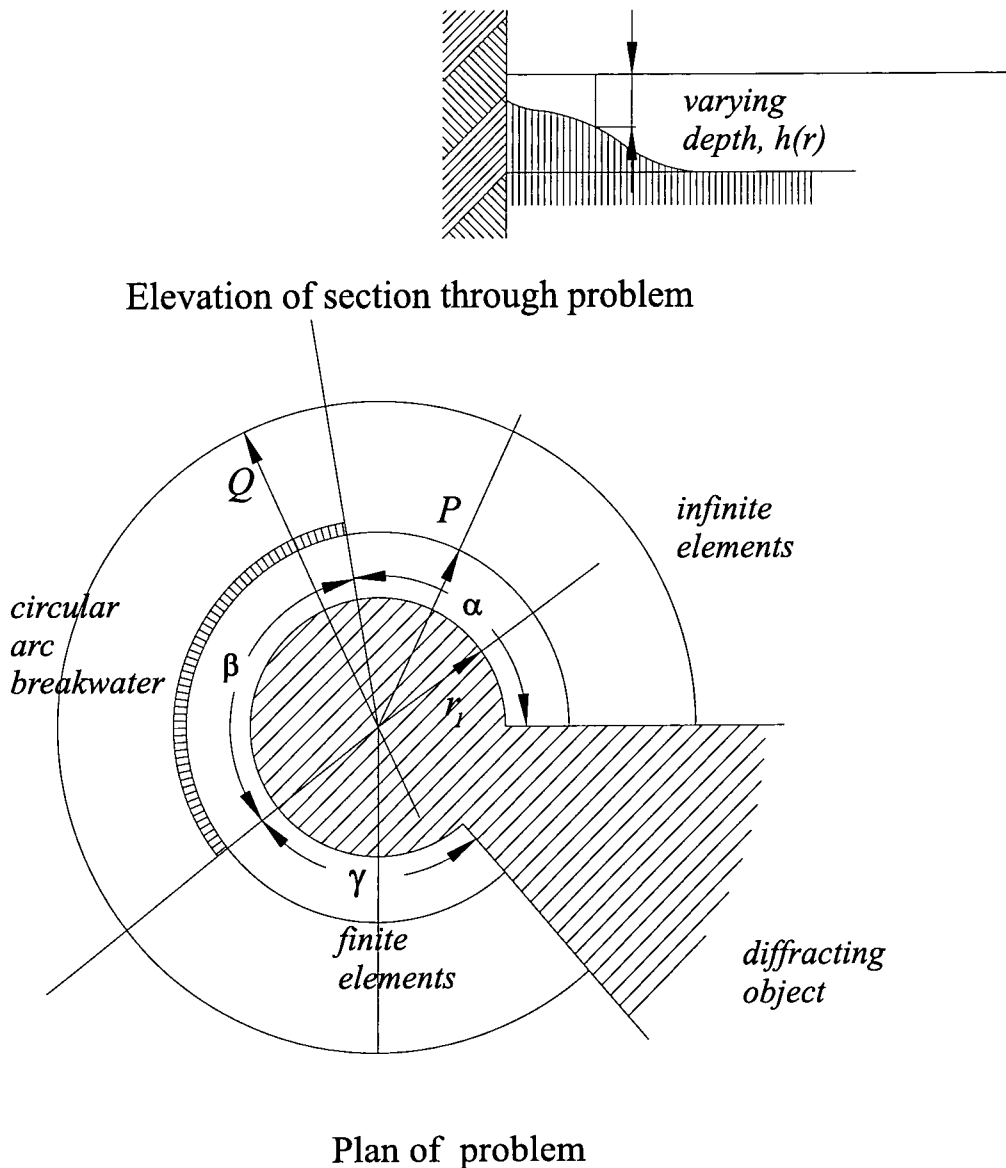
Figure 5.1   General geometries of SMACREA meshes

FALSE case would apply to a cylinder, in the water, and the TRUE case to a semi-infinite breakwater, extending from the origin to infinity along the positive x axis, as will be seen later. The centre of the mesh is the origin, $x = 0$, $y = 0$. The breakwater must always lie along the axis $y = 0$, $x > 0$, but this is still completely general, because the angle of incidence of the incoming wave can be set to any chosen value.

The first set of nodes are at $r = r_1$, and r_1 can be zero, or some positive value, giving an initial finite radius. At some larger radius, $r = P$, where $P > r_1$, a circumferential breakwater of zero thickness may be included. This subtends the angle β, and β can extend through any angle up to 360°. The circumferential breakwater is absent if

$\beta = 0$. Q is the outermost radius of the problem.

The general circular geometry case is shown in Figure 5.1. The mesh is divided into 3 radial sectors. The sectors are defined by the angles α, β and γ. The domain is the exterior of a wedge, with a circular section at its tip, and a breakwater forming an arc of a circle.
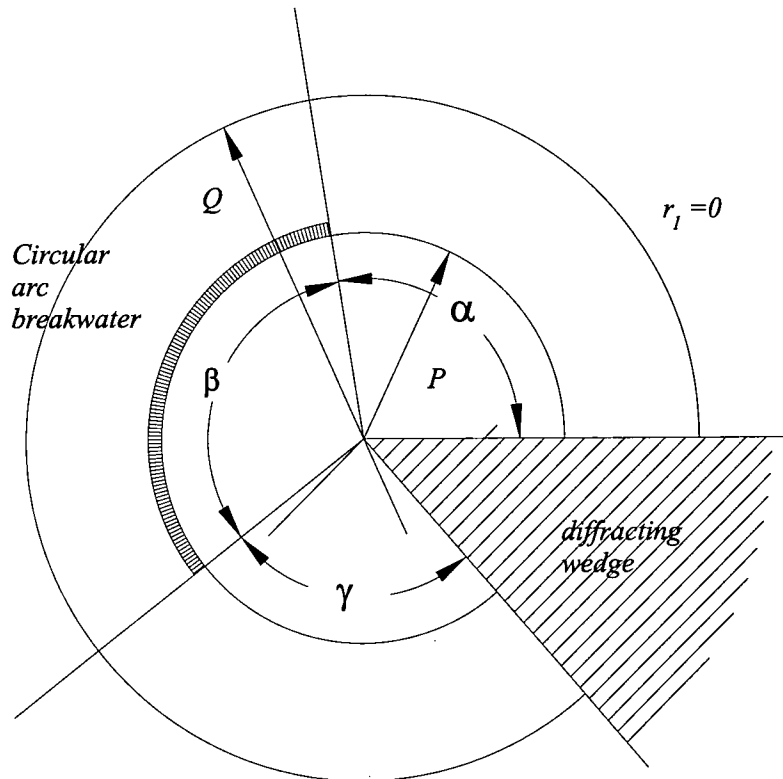
Figure 5.2   SMACREA meshes with zero inner radius

If the inner radius, r_1 is shrunk to zero, then the mesh takes the form shown in Figure 5.2, which is essentially wave diffracted by a wedge and a breakwater in the form of a sector of a circle, subtending an angle, β.

5.4 Varying depth with radius

The user is allowed to input the depth at each node, along a given radius, and this depth is then used for all nodes at that radius. This is a small amount of data to input, and allows the program to generate meshes for a large variety of problems, such as a parabolic shoal, studied by Berkhoff[26,27,28], and an island on a parabolic shoal, which is a classical problem discussed by Bettess *et al.*[36], Zienkiewicz *et al.*[122,128] and many others. It also enables the study of a breakwater on a parabolic shoal, studied by Bettess, Liang and Bettess[36], for which there is no analytical solution.

5.5 Induced singularities at re-entrant corners

The quadratic finite elements can have the midside nodes moved to their quarter points in order to induce singularities. There is some discussion of the rationale of this in the book by Bettess[44], page 140, and the paper by Bettess, Liang and Bettess.[36].

5.6 Program logic

The program generates the elements and nodes sector by sector, progressing in an anti-clockwise direction and starting from the positive x axis. As the nodes are generated the presence or absence of the circumferential breakwater is noted, and this leads to nodes with the same co-ordinates on the two sides of the breakwater (if present) which is assumed to be of zero thickness.

The program maintains the correct nodal numbering by having variables which store the necessary increments, between sectors of elements and between the elements in each sector. By changing the value of the increment the circular breakwater can be included or omitted. The details of the logic are too complicated to give here, but the code is available.

A subroutine, ELNOD is called for each element. One of the subroutine parameters is INOD, the number of the first node in the element. The first node is always that closest to the origin, with the smallest anti-clockwise angle from the positive x axis. The element type is also passed to this subroutine. This gives the number of nodes in the element. Some other incremental parameters enable all the node numbers for the element to be constructed.

The program uses an input file, for the data and two output files. One of these gives diagnostic information, and all the generated data. The other produces the finite element data in exactly the form expected by SMAWAVE. This can be used by SMAWAVE with no further intervention.

Different types of infinite elements, with either 9 nodes or 6 nodes, as described in Chapters 2 and 3 can be accommodated. The type of infinite element is selected by using a variable in the input data, see Appendix A. After generating all the sectors, if $\alpha + \beta + \gamma = 360°$, the program looks at the breakwater indicator. If this is FALSE, the nodes on the last edges of the last sector of elements are overwritten with those on the first edges of the first sector of elements, thus closing the mesh. The program has approximately 720 lines and is written in Fortran. It has been run on a wide variety of computers from PCs to mainframes.

5.7 Elliptical mesh generation

The mesh generator which had originally been for circular meshes and variants on circular meshes was extended to deal with the case of elliptical cylinders. This was to test the new element of Chapter 3. The essential difference from the circular mesh generator is that the aspect ratio of the ellipse is included in the data. If the mesh is

non-circular, then the co-ordinates of the mesh points are developed from the classical elliptical cylindrical co-ordinate system, given by

$$x = \alpha \cosh u \cos v, \qquad y = \alpha \sinh u \sin v, \qquad 5.1$$

where v is the angular co-ordinate, $(0 \geq v \geq 2\pi)$ and u is the radial co-ordinate and the focii of the ellipse are located at $y = 0$, $x = \pm\alpha$. The original circular co-ordinates are modified so that the diffracting cylinder is changed into an ellipse, of a specified aspect ratio. This fixes the location of the foci of the ellipse. The remaining co-ordinates are modified so as to lie on con-focal ellipses of larger radius. The original co-ordinates along the line $x = 0$ are retained and the others are altered to conform to this. The geometry is shown in Figure 5.3.
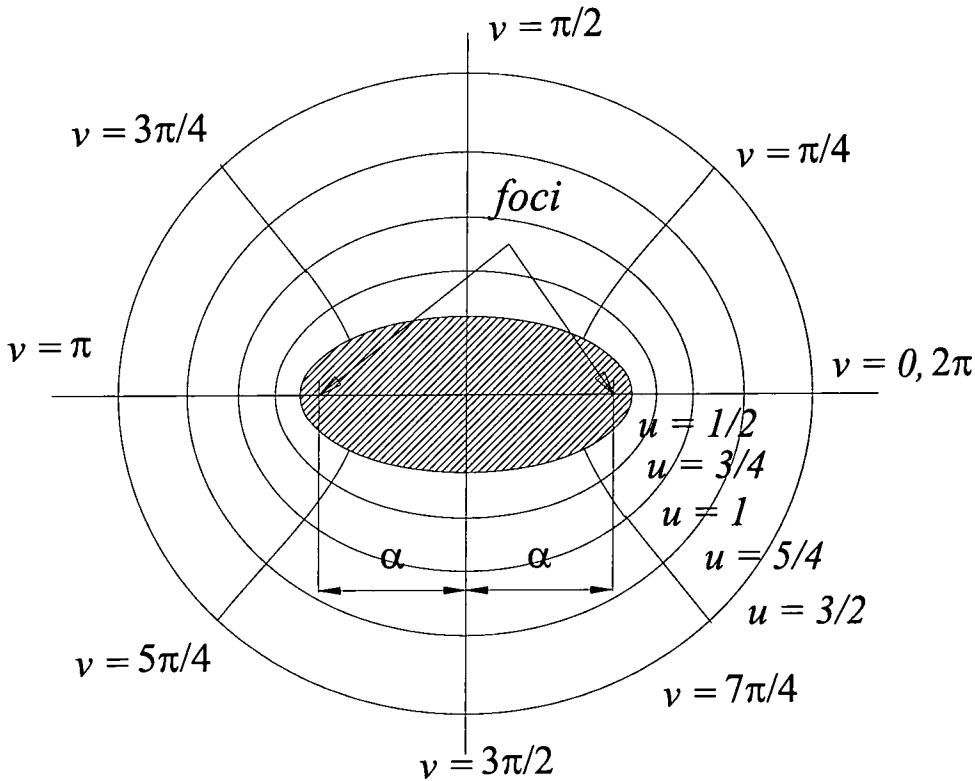
Figure 5.3 SMACREA mesh for elliptical cylinder

The theory is as follows:

We start by finding α, the key parameter in equation 5.1 from the given data. The values of a and b, the lengths of the ellipse semi-axes, are found from the eccentricity, e, specified by the user, thus

$$a = r_1 \times (1 + e) \qquad \text{and} \qquad b = r_1. \qquad 5.2$$

An eccentricity, $e = 0$, corresponds to a circle and $e = 1$ corresponds to an ellipse of aspect ratio 2. As before, r_1 is the radius of the diffracting cylinder. From equation 5.2, we have

$$a = \alpha \cosh u \qquad \text{and} \qquad b = \alpha \sinh u. \qquad 5.3$$

On squaring

$$a^2 = \alpha^2 \cosh^2 u \qquad \text{and} \qquad b^2 = \alpha^2 \sinh^2 u. \qquad 5.4$$

Equations 5.4 can be manipulated to give

$$\cosh^2 u - \sinh^2 u = \frac{a^2 - b^2}{\alpha^2} = 1, \qquad 5.5$$

and so

$$\alpha = \sqrt{a^2 - b^2}. \qquad 5.6$$

The next step is to determine u. First put $v = \pi/2$, to maintain co-ordinate spacing on the line $v = \pi/2$ or $x = 0$. (This is an arbirtrary choice, $y = 0$ could also have been chosen.) The radius, r of the given point in its original cylindrical polar co-ordinates is calculated from Pythagoras theorem as

$$r = \sqrt{x^2 + y^2}. \qquad 5.7$$

On the line $x = 0$, we have from equation 5.1

$$y = \alpha \sinh u \qquad \text{and thus} \qquad \sinh u = y/\alpha = g \quad (say). \qquad 5.8$$

Hence

$$\cosh u = \sqrt{1 + g^2}. \qquad 5.9$$

If, in order to find $\exp u$, we now write an expression for the sum of $\sinh u$ and $\cosh u$, thus

$$\sinh u + \cosh u = \frac{1}{2}\left(e^u - e^{-u} + e^u + e^{-u}\right) = e^u = g + \sqrt{1 + g^2}, \qquad 5.10$$

then by taking logs, we obtain the expression for u,

$$u = \log\left[g + \sqrt{(1 + g^2)}\right]. \qquad 5.11$$

Finally v is simply given from the angle subtended by the point in original cylindrical co-ordinates,

$$v = \tan^{-1}(y/x). \qquad 5.12$$

Now, because u and v and α are known, (from equations 5.12, 5.11 and 5.6 respectively), the x and y co-ordinates of the point can be found from equations 5.1. This is the basis of the transformation code given below.

```
      subroutine prntxy(r1,r2,nod,xxx,yyy,dj,rj,th,ecc1,elltyp,j,nr,inftyp)
      double precision dj, ecc, ecc1, rj, th, xxx, yyy, r1, r2,
    1 rrr, fact, uuu, vvv, alpha, aaa, bbb, gash
      double precision xnr1,xnr2,ynr1,ynr2
      common /coords/ xnr1,xnr2,ynr1,ynr2
```

```
      integer nod, elltyp, j, nr, inftyp
      rrr = sqrt(xxx * xxx + yyy * yyy)
      if(elltyp.eq.1) then
C
C***Simple 'stretch version of mapping'
C
      ecc = 0.0D0
      fact = (rrr - r2) / (r1 - r2)
      if(rrr.lt.r1) fact = 1.0d0
      if(rrr.gt.r2) fact = 0.0d0
      fact = fact * fact
      ecc = ecc1 * fact
      write(6,1015) r1, r2, rrr, xxx, yyy, ecc
 1015 format( ' r1 = ',e13.5,' r2 = ',e13.5,' rrr = ',e13.5/
     2 ' xxx = ',e13.5,' yyy = ',e13.5,' ecc = ',e13.5)
      xxx = xxx * (1.0d0 + ecc)
      endif
      if(elltyp.eq.2) then
C
C***Second version
C
      if(abs(ecc1).lt.0.1e-6) go to 195
      bbb = r1
      aaa = r1 * (1.0d0 + ecc1)
      alpha = sqrt(aaa * aaa - bbb * bbb)
      gash = rrr / alpha
      gash = gash + sqrt(gash * gash + 1.0d0)
      uuu = log(gash)
      vvv = atan2(yyy, xxx)
      xxx = alpha * cosh(uuu) * cos(vvv)
      yyy = alpha * sinh(uuu) * sin(vvv)
  195     continue
      endif
C
C*** Modified November 1995 to ensure elliptical co-ords for infinite
C*** elements are in ratio of 1:15
C*** i.e.  if J=NR+1, then (x(nr)=x(nr-2))/(x(nr-1)-x(nr-2)) = 15
C*** we need to keep x(nr-1) and x(nr-2) so that we can adjust x(nr)
C*** Similarly for the Y co-ords
      if(j.eq.nr-2) then
      xnr2=xxx
      ynr2=yyy
      endif
      if(j.eq.nr-1) then
        xnr1=xxx
        ynr1=yyy
C*** Adjust infinite element co-ord when J=NR
      endif
      if(j.eq.nr) then
        if(inftyp.eq.3) then
```

```
      xxx=15.0*(xnr1-xnr2)+xnr2
      yyy=15.0*(ynr1-ynr2)+ynr2
    else
      xxx=2.0*(xnr1-xnr2)+xnr2
      yyy=2.0*(ynr1-ynr2)+ynr2
    endif
  endif
  write(6,1014) nod, xxx, yyy, dj, rj, th
  write(7,1014) nod, xxx, yyy, dj, rj, th
1014 format(I5,5f10.6)
  return
  end
```

The original version of the elliptical mesh generator simply scaled the co-ordinates. (This is the 'stretch' version in the above code.) Although this converts a circular cylinder into an elliptical one, it is not completely satisfactory. The second and more logical method uses the mapping given above, given as equation 5.1. The program has to deal with two types of infinite element, the early exponential infinite element and the mapped infinite element. This means two options have to be catered for in the placing of the radial co-ordinates for the infinite elements.

5.8 Special cases

The number of special cases is enormous, and by no means all of them have been generated and solved. However some of the more important cases that have been used will now be listed.

5.8.1 Circular cylinder, in water of constant depth

In this case β is set to zero, and $\alpha + \gamma = 360°$. Usually $\alpha = \gamma = 180°$, and $\beta = 0$. This excludes the circumferential breakwater. The radial breakwater is excluded by putting BFLAG = FALSE, which dictates that the mesh should close. The cylinder is, of course, a very important case. The resulting cylinder mesh is shown in Figure 5.4. The depths at each nodal radius, h_i are set to the constant depth value.

5.8.2 Parabolic (or other profile) shoal

In this case β is set to zero, and $\alpha + \gamma = 360°$. Usually $\alpha = \gamma = 180°$. This excludes the circular breakwater. The radial breakwater is excluded by putting BFLAG = FALSE, which dictates that the mesh should close. The depths vary in line with the parabolic, or other required depth profile. The initial radius, r_1, is set to zero. The mesh is shown in Figure 5.5. The problem was first tackled by Berkhoff[26,27,28], and was repeated by Bettess and Zienkiewicz[122,30].
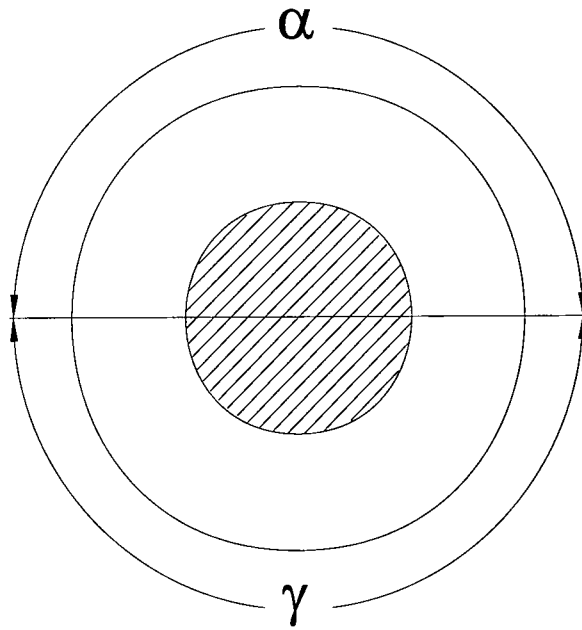
Figure 5.4   SMACREA mesh for circular cylinder
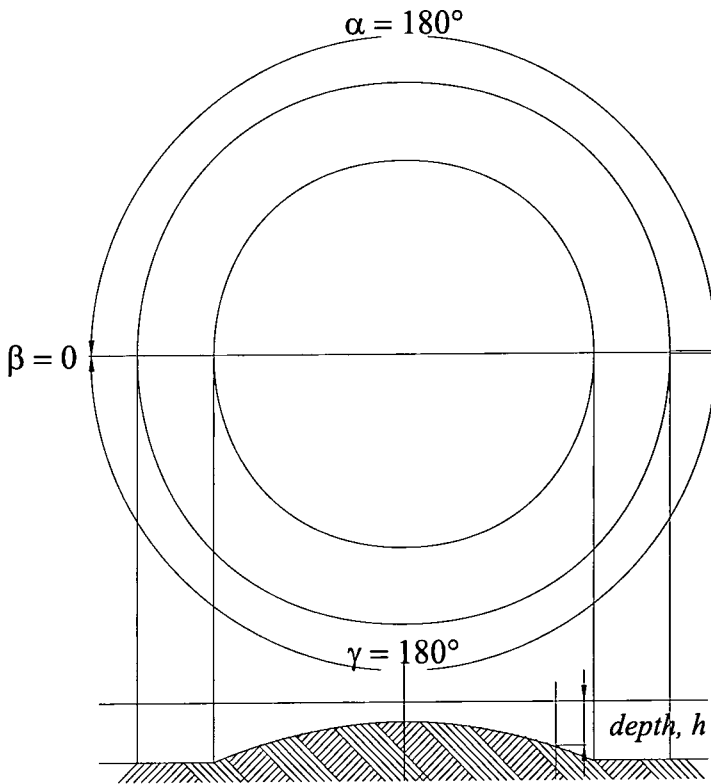
Figure 5.5   SMACREA mesh for parabolic shoal

5.8.3 Circular island on parabolic shoal
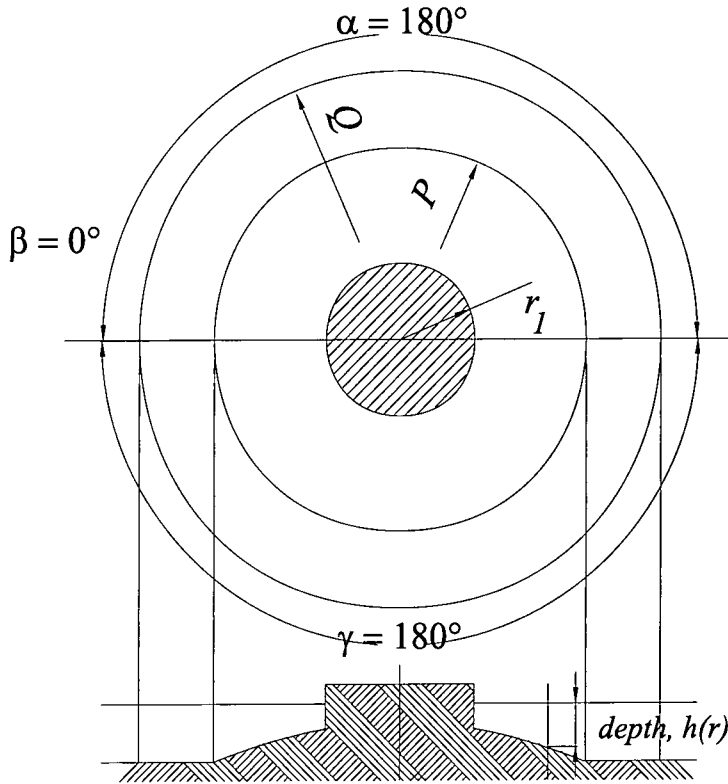
Figure 5.6   SMACREA mesh for circular cylinder, on parabolic shoal

In this case β is set to zero, and $\alpha + \gamma = 360°$. Usually $\alpha = \gamma = 180°$. This excludes the circular breakwater. The radial breakwater is included by putting BFLAG = TRUE, which dictates that the mesh should *not* close. The initial radius, r_1, is set to the cylinder radius. The depths vary in line with the parabolic, or other required depth profile. The mesh is shown in Figure 5.6. The problem was first tackled by Homma[78], who gave an analytical solution, in terms of Bessel and Hankel functions, and by Vastano and Reid[117], who solved it using finite differences.

5.8.4 Semi-infinite breakwater in water of constant or varying depth

In this case β is set to zero, and $\alpha + \gamma = 360°$. Usually $\alpha = \gamma = 180°$. The circular breakwater is thus excluded. The radial breakwater is included by putting BFLAG = TRUE, which dictates that the mesh should *not* close. This means that there are two sets of nodes along the line $y = 0$, which are not connected. Such meshes are shown in the paper by Bettess, Liang and Bettess[36]. As in the case of the circular cylinder, the depths can also be made to vary in line with the parabolic, or other required depth profile. The meshes for the two cases are shown in Figures 5.7. and 5.8.
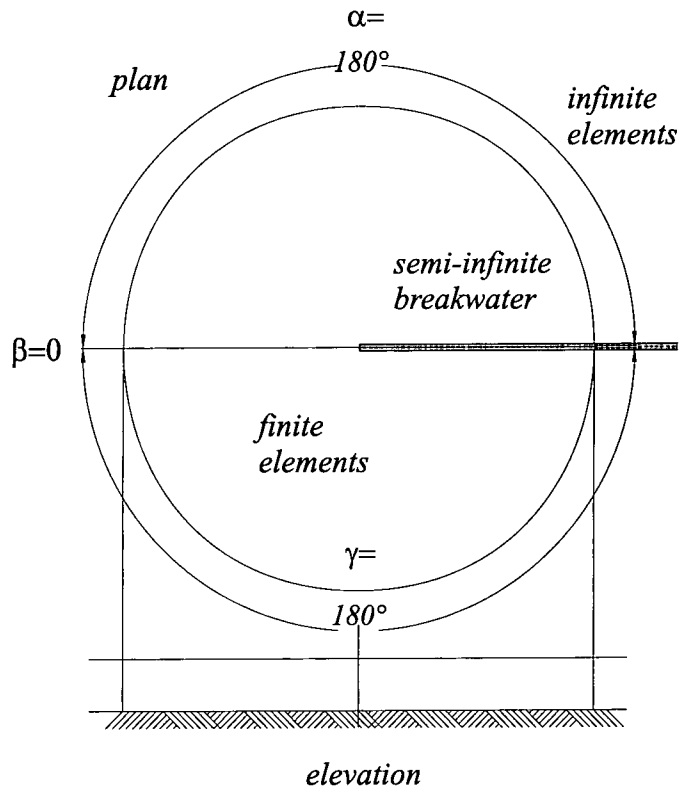
Figure 5.7   SMACREA mesh for semi-infinite breakwater, with constant depth
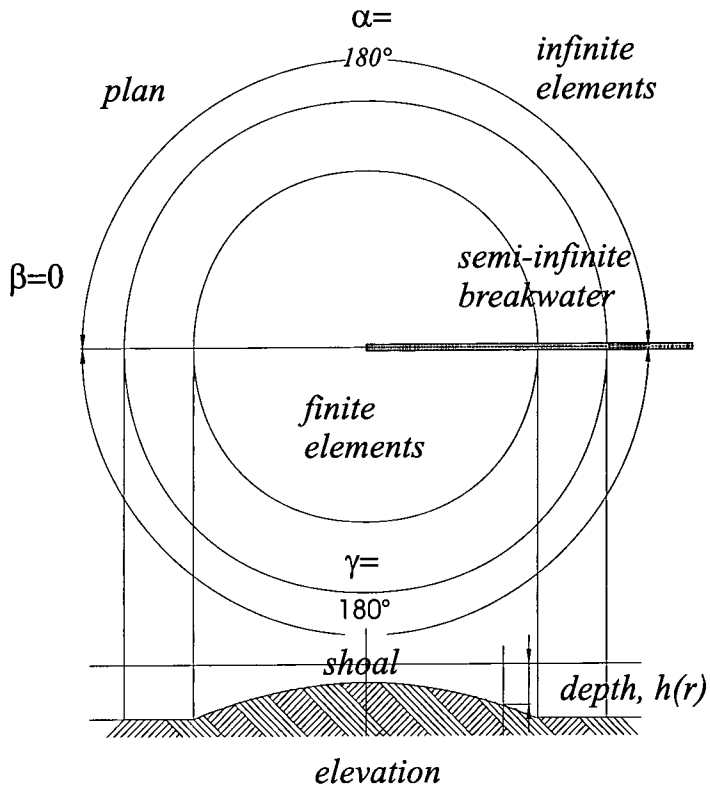
Figure 5.8   SMACREA mesh for semi-infinite breakwater, with varing depth
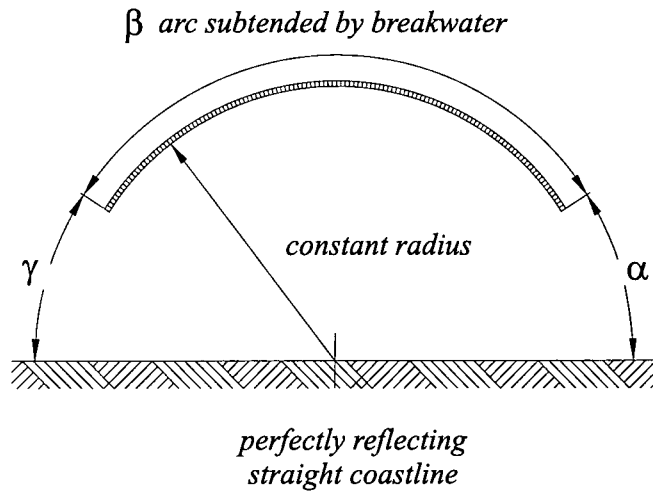
Figure 5.9   SMACREA mesh for breakwater as an arc of a circle

5.8.5 Breakwater in the form of the arc of a circle

This is the case of a breakwater in the form of an arc of a circle adjacent to straight infinite coastline. α is set to some non zero angle, such at 25°, and $\alpha + \beta + \gamma = 180°$. Also $\alpha = \gamma$. The non-zero value for β causes the generation of the breakwater in the form of an arc of a circle. This problem is used as a test case by Chen and Mei[54,55], and they quote an analytical solution in the form of Bessel and Hankel functions. The problem was also tackled by Bettess and Zienkiewicz[30] using the present mesh generator. The mesh is shown in Figure 5.9.

5.8.6 Porous wall around cylinder

This is the case of a porous breakwater in the form of an entire circle. This is the form which was used in the analysis of the offshore concrete gravity structure, designed for the Ekofisk field. The parameters α and γ are both set to 0°, and $\beta = 360°$. The problem was considered in the paper by Zienkiewicz *et al.*[124]. The type of meshes that can be generated is shown in figure 5.10. In this particular case special six node finite elements for the porous wall were used. These are not available in SMACREA, and so the mesh had to be finalised by hand. However the basic mesh was created using SMACREA. The mesh is shown in Figure 5.10.

5.9 Papers in which the program SMACREA has been used

SMACREA has been used to generate finite element meshes, which have been used in the following papers, among others:

1. Bettess and Zienkiewicz, ref. 30. This has been a strongly influential paper, and it was the first to use infinite elements in wave diffraction and refraction problems. *All* the finite and infinite element meshes in the paper were generated
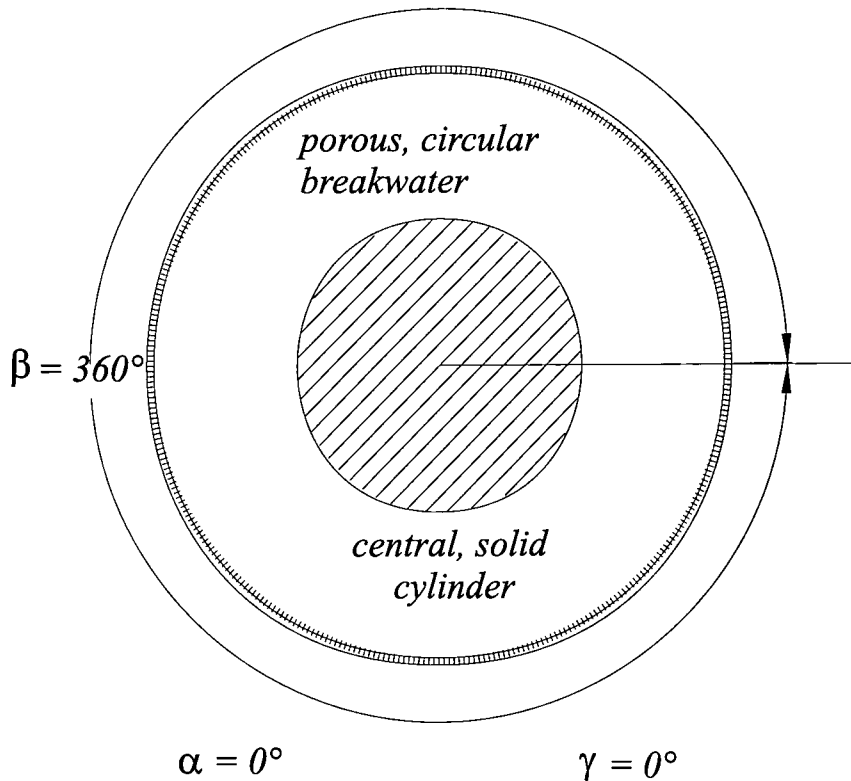
Figure 5.10   SMACREA mesh for cylinder surrounded by porous circular breakwater

using SMACREA, with the exception of the mesh for the Chen and Mei problem of the Atlantic Generating Station, which had a complicated geometry, which did not fall within the scope of the program, and the case of the rectangular harbour in an infinite coastline.

2. Bettess, Liang and Bettess, ref. 36. This paper was a study of the diffraction of waves by a semi-infinite breakwater, and in it comparisons were carried out between the results obtained using finite and infinite elements, and those obtained using an analytical solution based on Fresnel integrals. All the meshes generated in this paper were created using either of the SMACREA, or SMAGEN (see below), programs written by the author.

3. Zienkiewicz, Bettess and Kelly, ref. 124. Most of the two dimensional finite and infinite element meshes used in this paper were generated using SMACREA, and the three dimensional meshes were adapted by hand from the two dimensional meshes.

5.10   The rectangular mesh generator, SMAGEN

This mesh generator actually generates a wide range of meshes based on rectangular shapes. The user defines the abscissæ and ordinates at which the nodes are to be

placed, for the x and y directions, and also the depths of the water at these locations. The number of subdivisions is also defined. The data are quite compact, only occupying a few lines. After checking the data for internal consistency, the program generates data which are ready to be processed by the wave program.

Essentially a rectangle of finite elements, all 8 node quadrilaterals, is created. The mesh of elements is surrounded with a layer of infinite elements. These are oriented parallel to the x and y axes, except at the corners of the mesh. Here the corner node of the finite element mesh is pulled in slightly, and two infinite elements are placed going out radially.

The mesh may have a semi-infinite breakwater, lying along the positive x axis. The mesh generator was developed to produce the results given in Ref. 36. The general arrangement of the mesh is shown in Figure 5.11.
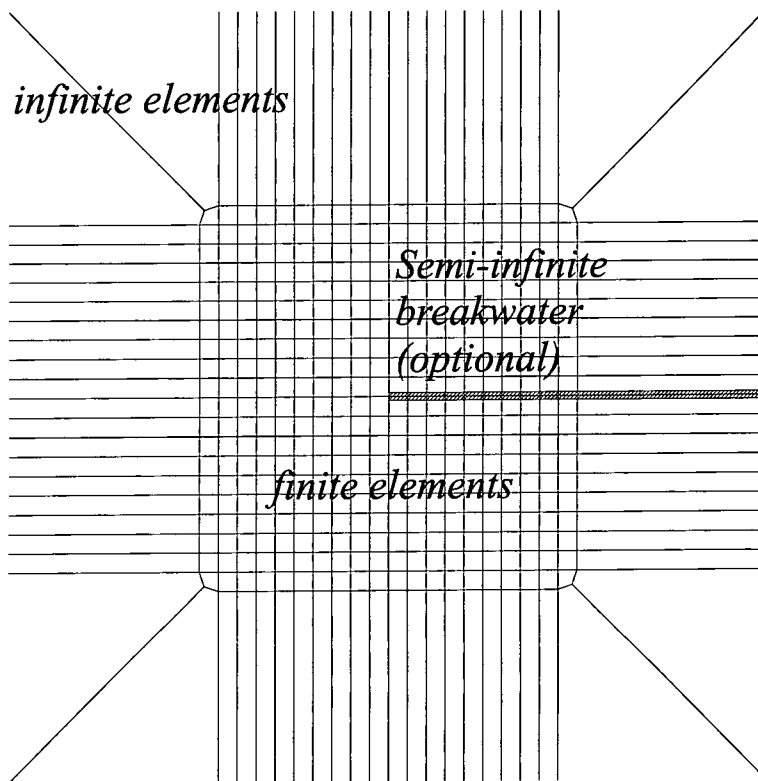
Figure 5.11   SMAGEN general arrangement of the mesh

Further information on the program is given in Appendix A on software and in the comments in the program itself.

5.11 The riser mesh generator, CYLGEN

The riser mesh generator has the capability of generating a two dimensional mesh of finite and infinite elements around any rectangular array of risers. The conditions are that the risers must all have the same diameter, and must all be equally spaced. This is clearly a highly specialised mesh generator and it can only be applied to rectangular arrays of cylinders, but it effects great reductions in effort for such problems. The number of elements around each riser is under the control of the user. In addition the user can control the number of finite elements beyond the domain of the risers, and the location and extent of the mesh of infinite elements. Examples with 4 and 6 risers are shown in figures 8.20 and 8.31, but there is no limitation to the number of risers in the mesh. Figure 5.13 shows a fine mesh of finite and infinite elements with 12 risers, which was not used in this study. Details on the use of the program are given in appendix A. The user defines the density of the mesh around each riser, both circumferentially and radially. The rectangular area containing this single riser is then filled with distorted eight node quadrilateral finite elements. This is shown in the meshes in Chapter 8 and also in figure 5.12.
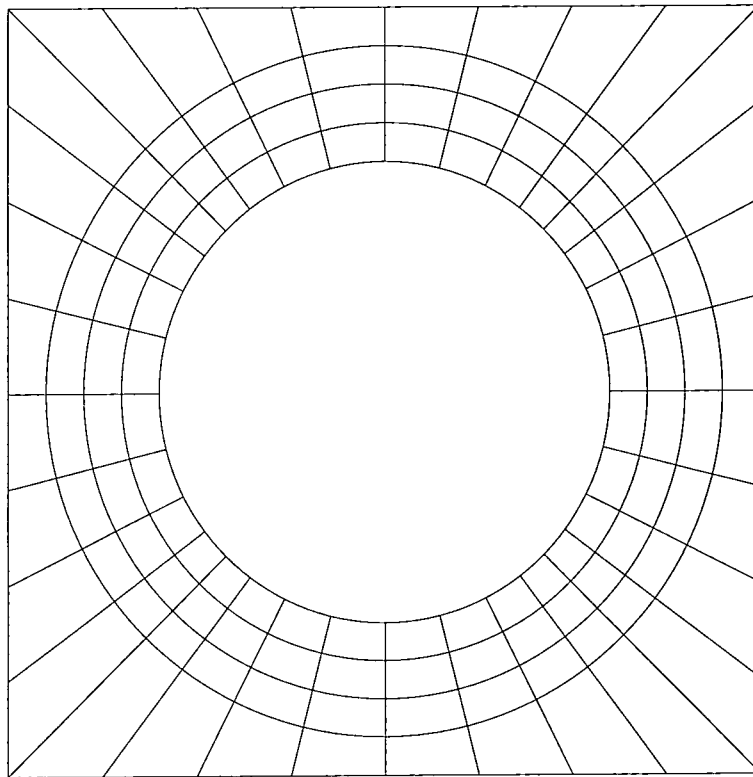
Figure 5.12   CYLGEN arrangement of a block of mesh around a riser

The blocks of mesh around each riser are then assembled into a rectangular array of risers. The extent of this depends upon how many risers the user has specified in

each of the x and y directions. The user also defines how many finite elements should surround the mesh of risers before the start of the infinite elements. This is shown in Figure 5.13, and similar meshes can also be seen in Chapters 8 and 9.

5.12 Program logic for CYLGEN

The finite elements are generated in each block surrounding each riser, or cylinder, processing radially and then circumferentially. The processing starts along the sector of elements along the line in the positive x direction progressing outwards from the element touching the cylinder, for each node and element, until the sector is completed. The sectors are then processed in the anti-clockwise direction, until all the elements in the block, together with their associated nodes, have been generated. The blocks are processed in the x and then the y directions. This process continues until all the finite elements surrounding the cylinders have been generated. Finally the surrounding ring of infinite elements is generated, with special provision at the corners of the mesh. At these locations, just as in SMAGEN, the nodes on the diagonals are pulled in slightly, to enable the generation of two infinite elements which fill in the corner in a kind of mitred effect. The resulting mesh is sketched in figure 5.13. The main logical complication in the mesh generation is ensuring compatibility of node numbering between the blocks of the mesh. This is achieved by maintaining incremental counters within the program.
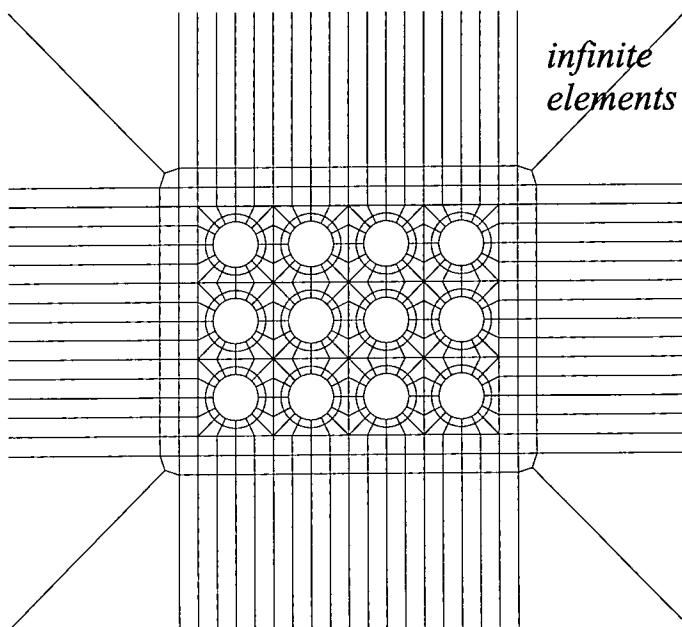
Figure 5.13   Typical CYLGEN mesh layout

5.13 Band width and front width minimisation

To maintain the simplicity of the logic, no attempt was made to order the elements to minimise either the bandwidth or the frontwidth. This sometimes leads to large front or bandwidths, so a bandwidth and frontwidth minimising program was written based on the reverse Cuthill-McKee algorithm. It is not claimed that this is a sophisticated implementation of the algorithm, or that this is currently the best algorithm, but the advantage was to have a program which would take the input in a specified format and would output the re-ordered mesh in the format for the SMAWAVE program. It achieves satisfactory reductions in the execution time of the program SMAWAVE, which, in any event runs very quickly. The bandwidth and frontwidth minimiser is called BWFWMIN.FOR, standing for BandWidth, FrontWidth MINimiser.

The algorithm is very well-known, but will be briefly rehearsed here. The mesh is first searched for the node with the fewest connections to other nodes. (Several nodes may have the same minimal connectivity, but this is not important, and any one of them may be selected). All the nodes which connect to this first node are labelled in sequence. When all these nodes are exhausted, then all the nodes connected to these nodes are numbered in sequence. This algorithm is repeated until all nodes have been re-numbered. Nodes retain the first number which they are given, thus there is no back-tracking of nodes which have already been numbered. Finally the order of nodes is reversed, since there is a proof that the reversed numbering cannot be worse than the original re-numbering, and may be better. The program has to maintain tables of connectivity of the nodes, but is essentially straight-forward. The front width minimisation simply put the elements in the order in which the nodes are re-numbered. That is the first element is that which connects to the node with the fewest connections. The next elements are those which connect to this first element, and the next elements are those which connect to this set. Again the process carries on until all elements have been dealt with.

This program accepts the output from CYLGEN and processes it to re-number the nodes, or re-order the elements, at the users choice. The resulting output file is completely compatible with SMAWAVE, satisfying one of the main motives for writing the program.

Chapter 6

Plotting programs for wave results

Several special purpose plotting programs were created to plot contours of wave heights and elevations around a cylinder or ellipse. A program to plot the actual mesh was also written, but this is very straightforward, and will not be descibed in any detail here. It only requires the nodal numbers for each element, and the co-ordinates of each node. Each edge of each element was divided into 10 segments, and the iso-parametric mapping was used to generate the global co-ordinates of the ten points, so that the element edges would be correctly curved in the plot. The use of ten points seemed to model the edge with sufficient accuracy to appear curved to the naked eye, for all applications attempted. The contour plotting program is more complicated, and will be now be described in more detail.

6.1 Theory of contour plotting

Various techniques are available for plotting contours of finite element results. One option which is often used is to divide the finite element into a large number of triangles and to treat the field variable to be plotted in each triangle as varying linearly. This means that points on the contour can be found on two of the three sides of the triangle, and joined with a straight line. While this method is very quick, it can sometimes hide discontinuities in the slope of the coutour. The method used in this work attempts to follow the contour as accurately as possible, using a predictor corrector method.

6.2 The predictor corrector contour method

The method does not originate with the author. It was first published in 1977 by Akin and Gray[2], and improved by them in 1979[3]. It was later programmed by H. Y. Leung, as part of a final year undergraduate project in the Department of Civil Engineering, University College, Swansea[90]. The student was given assistance in his work by his supervisor, Dr. Bettess, and myself, as the systems manager of the departmental computer. The theory below draws on the paper by Akin and Gray, and on Mr. Leung's dissertation. We now consider the main steps in the method which are as follows:

Consider an isoparametric finite element as shown in Figure 6.1. Let the field variable be ϕ. Then we can express the value of ϕ, at any point (ξ, η), as

$$\phi(\xi, \eta) = \sum_{i=1}^{n} N_i(\xi, \eta)\phi_i, \qquad 6.1$$

where ξ and η are the usual local co-ordinates, $N_i(\xi, \eta)$ is the element shape function, n is the number of nodes in the element, and ϕ_i is the value of ϕ at the ith. node. The
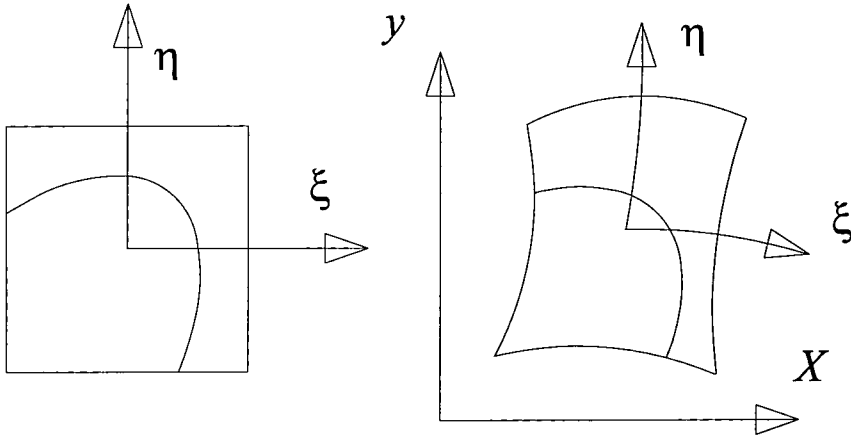
(a) local co-ordinates   *(b) global co-ordinates*

Iso-parametric Element with contour line, in local and global co-ordinates

Figure 6.1   Element in local and global co-ordinates

contour can be expressed as

$$\phi = k, \qquad\qquad 6.2$$

where k is the constant value along the contour. This implies that

$$\Delta\phi = 0, \qquad\qquad 6.3$$

and hence that

$$\frac{\partial\phi}{\partial\xi}d\xi + \frac{\partial\phi}{\partial\eta}d\eta = 0, \qquad\qquad 6.4$$

where $d\xi$ and $d\eta$ are components of a distance Δs, tangent to the contour, as shown in Figure 6.2

6.2.1   The predictor step

If the contour makes an angle θ with respect to the ξ axis, then

$$d\xi = \Delta s \times \cos\theta \quad \text{and} \quad d\eta = \Delta s \times \sin\theta. \qquad\qquad 6.5$$

Let the point already determined on the contour be denoted by (ξ_j, η_j). Then the co-ordinates of the next point can be written approximately as

$$\xi_{j+1} = \xi_j + \frac{\Delta s}{\nabla}\frac{\partial\phi}{\partial\eta}$$

$$\eta_{j+1} = \eta_j - \frac{\Delta s}{\nabla}\frac{\partial\phi}{\partial\xi}, \qquad\qquad 6.6$$
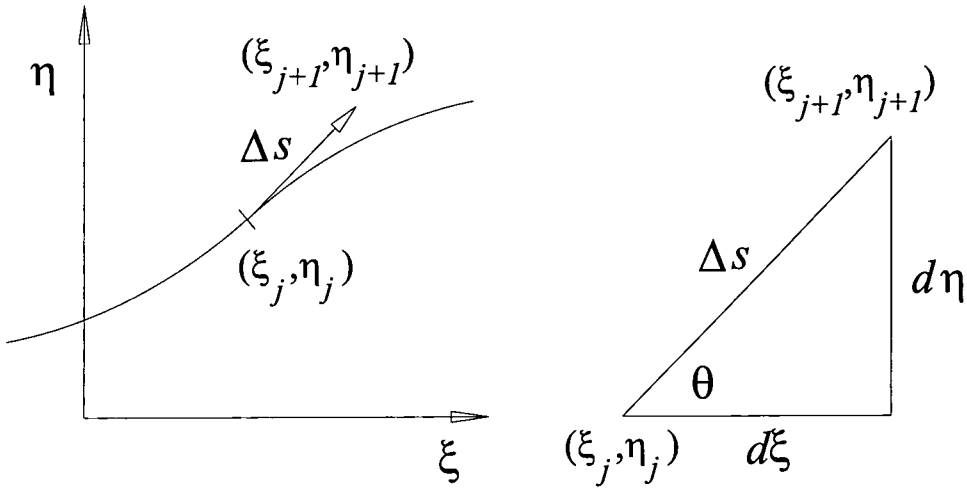
Figure 6.2 Details of the contour and increment

where

$$\nabla = \sqrt{\left(\frac{\partial \phi}{\partial \xi}\right)^2 + \left(\frac{\partial \phi}{\partial \eta}\right)^2}.$$ 6.7

The values of $\partial \phi / \partial \xi$ and $\partial \phi / \partial \eta$ are obtained by differentiating equation 6.1 to obtain

$$\frac{\partial \phi}{\partial \xi} = \sum_{i=1}^{n} \frac{\partial N_i}{\partial \xi} \phi_i$$

$$\frac{\partial \phi}{\partial \eta} = \sum_{i=1}^{n} \frac{\partial N_i}{\partial \eta} \phi_i.$$ 6.8

Equation 6.6 is derived simply by considering the gradients of the field variable, ϕ, in the ξ and η directions, and using the geometry shown in figure 6.2. Thus the co-ordinates of the new point on the contour, ξ_{j+1}, η_{j+1} can be explicitly found. In principle the algorithm described above can be used to trace all the points within an element along a given contour, starting from a known point on the edge of an element, or within the element. However, because the element of length Δs is finite, the value obtained at the end of the increment will usually be slightly different from the required contour value, k. So a second step is introduced into the algorithm, which corrects for the location of the end point of the increment of contour length.

6.2.2 The corrector step

In their second paper Akin and Gray[3] state that the a simple correction step can be added in the direction normal to the contour line, to reduce the amount of deviation.

They give, without derivation, the correction equation as

$$\xi_{j+1,cor} = \xi_{j+1} - \frac{1}{\nabla^2}\frac{\partial \phi}{\partial \xi}\left[\phi(\xi_{j+1},\eta_{j+1}) - k\right]$$

$$\eta_{j+1,cor} = \eta_{j+1} - \frac{1}{\nabla^2}\frac{\partial \phi}{\partial \eta}\left[\phi(\xi_{j+1},\eta_{j+1}) - k\right].$$

6.9

In equation 6.9, the subscript *cor* denotes corrected values. I have not attempted to verify the derivation of the correction equation. It appears to be based on the local gradients of the field variable, and it certainly works.

6.2.3 Stopping criteria and co-ordinates

To stop the contour a check is carried out to see if the the co-ordinates are within the domain of the finite element. All calculations are carried out in local (ξ, η) co-ordinates, with a final transformation to the global co-ordinates being carried out immediately before plotting takes place. This uses the normal iso-parametric transformation

$$\left\{\begin{array}{c} x(\xi,\eta) \\ y(\xi,\eta) \end{array}\right\} = \sum_{i=1}^{n} N_i(\xi,\eta) \left\{\begin{array}{c} x_i \\ y_i \end{array}\right\},$$

6.10

where x_i, y_i are the co-ordinates of the ith node of the finite element. In practice it has been found that a value of $\Delta s = P/160$, where P is the perimeter of the contour, has been found satisfactory. This value is suggested by Akin and Grey[3]. The contour lines have been as accurate as the plotting device can discriminate.

6.3 Contour starting points

Contours either start and end on the edges of the element, or are completely closed within the element.

6.3.1 Edge starting and ending points

On the edges of the linear, three node element, and the bi-linear four node elements, the field variable is linear in ξ or η* In quadratic elements the field variable is quadratic in ξ or η. For higher order elements the variation is cubic or higher. In each case the variation of the field variable can be written in a polynomial form, such as

$$P(\xi) = \sum_{i=0}^{n} \alpha_i \times \xi^i,$$

6.11

where n is the highest order encountered in the element, and α_i are polynomial coefficients which depend upon the nodal values, ϕ_i. The calculation of the polynomial coefficients from the nodal values is straightforward. It is carried out here using a matrix inversion, although this is not essential.

---

* The method may be applied without loss of generality using area co-ordinates, or other methods of modelling the variation in triangular elements.

The polynomial, $P(\xi)$, is equated to the contour value, k, that is

$$(\alpha_0 - k) + \sum_{i=1}^{n} \alpha_i \xi^i = 0, \qquad\qquad 6.12$$

and the resulting equation is solved for the values of ξ, which correspond to the start and end points of the contours. For linear, quadratic and cubic equations, closed form solutions are used and for higher order equations a Newton-Raphson iteration is used. All the elements used in this thesis are quadratic, and so only a simple expression for the roots of a quadratic equation is needed. No more than two contour start and finish points can occur on any element edge.

6.3.2 Closed contours

It is possible for quadratic and higher order elements to contain completely closed contours within the element. It is also possible for the contour value to be higher than the highest value encountered on any of the element edges. And it is possible for the contour value to be lower than the lowest value encountered on any of the element edges. It is therefore necessary to modify the search for contours within the element to take account of this effect. The internal contours are sought along the diagonals of the elements. It has been found in practise that this is sufficient. The contour increment has to be chosen to be small enough to ensure that closed contours do actually close, and do not degenerate into non-closing spirals. With the values chosen in this program this has not been a problem. The plotting of the closed contour has to have a termination after a finite number of steps, as otherwise it would continue indefinitely.

6.4 Plotting

When contours are plotted as lines it suffices to retain a list of the (ξ, η), or (x, y) co-ordinates of the points defining the contour. A simple loop of the form, draw a straight line from (x_i, y_i) to (x_{i+1}, y_{i+1}) then is enough to draw the contour. Labelling of the contour with values is slightly more complicated.

6.5 Programming

The program written by the Mr. Leung is the basis of the plotting codes used here. The program incorporated, in a modified form, the predictor-corrector subroutine, LCONTR, given by Akin and Gray[3]. The program of Mr. Leung has been extensively modified by the present author, because the original code was written for a PDP 11/40, and the plotting library PLOT10. It was also in several independent sections, since the program was too large to run on the PDP. The first section did all the calculations and produced a file of co-ordinates of points on contours. The second section interacted with PLOT10, and did the actual plotting, on Tektronix 4010, 4014 graphical display devices, or the tektronix 4662 plotter. The programs have been modified, unified and changed to use the GINO graphics library. A very important change has been the development of routines to produce colour fill, since the original code only drew line

contours. Colour fill requires a considerable change to the contour logic.

6.6 Colour Fill

For the present work the contour program was upgraded to produce colour filled contour plots, using the GINO graphics library. This introduces considerable plotting complications. It no longer suffices to retain all the points defining a single contour. The points on the adjacent contour must also be retained. The GINO graphics library, like many graphics libraries has a feature of filling a polygon, provided the polygon points are ordered in the desired sequence to define the edges of the polygon. The main problem with the colour fill algorithm are the many special cases. Some of these are sketched in figure 6.3, and are listed below:

1. The fill area is defined entirely by element edges.

2. The fill area is defined by a contour line starting and ending on the same edge and parts of four edges.

3. The fill area is defined by a contour line starting and ending on two adjacent edges and parts of three adjacent edges.

4. The fill area is defined by a contour line and part of three adjacent edges.

5. The fill area is defined by a contour line and part of one edges.

6. The fill area is defined by a two contour lines and part of one edge.

7. The fill area is defined by two contour lines and parts of two edges, which are adjacent.

8. The fill area is defined by two contour lines and parts of two edges, which are not adjacent.

9. The fill area is defined by two contour lines at adjacent vertices and parts of four edges.

10. The fill area is defined by two contour lines at opposite vertices and parts of four edges.

11. The fill area is defined by three contour lines at adjacent vertices and parts of four edges.

12. The fill area is defined by four contour lines at vertices and parts of four edges.

13. The fill area is defined solely by a closed contour.

14. The fill area is defined solely by two closed contours.

15. The fill area is defined solely by two closed contours, one between opposite edges and the other at a vertex.

16. The fill area is adjacent to a saddle point.
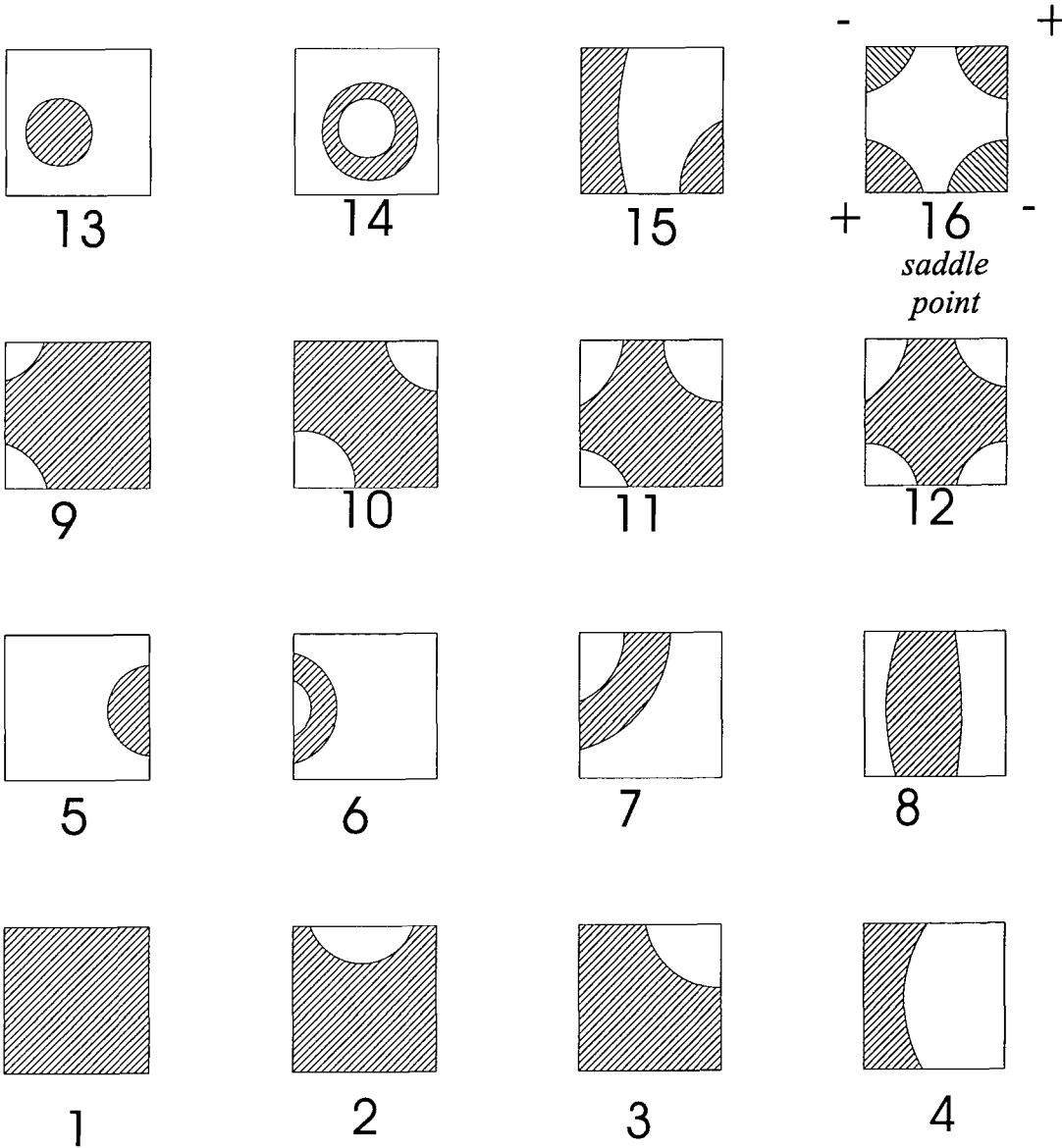
Figure 6.3   Colour fill special cases

The cases for the triangular element are simplified versions of those for the quadrilateral, and will not be descibed in detail. Fewer special cases arise. Some of the cases described above are actually dealt with easily, since the colour is applied in layers, and this can deal with cases 6, 7 and 13, provided the contours are increasing in value and the plotting proceeds from the lowest valued contour.

The program deals with saddle points routinely as these are just a combination of special cases. For example, the case shown in fig 6.3 (16) is a combination of the inverse of 10 for the lowest value, followed by 10 itself and completed by the inverse of 10 again for the highest value.

Other pathological cases arise when a contour edge point is very near the vertex of the element. However, by selecting tolerances appropriate to the mesh size, the program deals with these cases without problem.

6.7 Conclusions

Despite the difficulties and special cases arising from this contour plotting method compared with the technique of subdivision into triangles, the resulting plots have a number of advantages. In particular the plot shows the actual contour to within the accuracy of the plotting increment, Δs, and the plotting device. This means that any discontinuities are a feature of the solution being plotted, and need to be investigated and appraised. Too many conventional contour plotting algorithms leave discontinuities in the plot, which the user has to accept, and which mask any real discontinuities in the solution. Other plotting algorithms smooth all the results, giving a deceptively bland feel to the resulting plot. Both of these extremes have their hazards.

Chapter 7

Ellipse problem using new infinite element

7.1 Background theory

In this section the analytical solutions, or sources for them, are given.

7.1.1 Circular cylinder diffraction

The problem of waves diffracted by a cylinder was first solved by Havelock[*] who developed a solution for water of infinite depth[77]. The key to the solution is the representation of the monochromatic incident wave as a series of Bessel functions. The scattered wave can be developed from this solution, term by term. It is relatively straightforward to extend Havelock's solution to the case of intermediate depth and this was done by MacCamy and Fuchs[93].

Havelock's solution for the total velocity potential is given by

$$
\phi = \frac{g a_0}{\omega} \exp[i\omega t + kz] \left\{ J_0(kr) + 2 \sum_{n=1}^{\infty} i^n J_n(kr) \cos n\theta \right\}
$$
$$
- \frac{g a_0}{\omega} \exp[i\omega t + kz] \left\{ b_0 H_0^{(2)}(kr) + 2 \sum_{n=1}^{\infty} i^n b_n H_n^{(2)}(kr) \cos n\theta \right\},
$$

7.1

where $\omega^2 = gk$ and $b_n = J_n'(ka)/H_n^{'(2)}(ka)$, r and θ are the cylindrical co-ordinates and a is the radius of the circular cylinder. $H_n^{(2)}(kr)$ is the Hankel function of the second kind, given by $H_n^{(2)} = J_n - iY_n$, where J_n and Y_n are the Bessel functions of order n. The first term in equation 7.1 represents the incident wave potential and the second term is the scattered wave potential.

The solution of MacCamy and Fuchs is given by

$$
\phi = \frac{g a_0}{\omega} \exp[i\omega t] \frac{\cosh[k(h+z)]}{\cosh kh} \left\{ J_0(kr) + 2 \sum_{n=1}^{\infty} i^n J_n(kr) \cos n\theta \right\}
$$
$$
- \frac{g a_0}{\omega} \exp[i\omega t] \frac{\cosh[k(h+z)]}{\cosh kh} \left\{ b_0 H_0^{(2)}(kr) + 2 \sum_{n=1}^{\infty} i^n b_n H_n^{(2)}(kr) \cos n\theta \right\},
$$

7.2

---

[*] Sir Thomas Henry Havelock, F.R.S., was the Professor of Pure and Applied Mathematics 1928 - 45, and sub-rector 1937 - 45, at King's College, Durham University, which provides a pleasing link with my first degree and this thesis.

where Havelock's term $\exp kz$, corresponding to deep water, has simply been replaced by the term $\cosh[k(d+z)]/\cosh kh$, corresponding to intermediate depth water.

7.1.2 Elliptical cylinder diffraction

The case of the elliptical cylinder is considerably more difficult than that of the circular cylinder, and the solution must be developed in terms of Mathieu functions. Peter Bettess acquired some computer code for generating Mathieu functions written by Clemm[58] and this was modified to execute on modern computers and a program was written in conjunction with Mr. Christos Atalianis, as his final year undergraduate project in the Department of Marine Technology, Universtiy of Newcastle upon Tyne. This program used the Mathieu functions to evaluate the wave elevations and velocity potentials and wave forces for an elliptical cylinder. The results were published originally as Mr. Atalianis's final year undergraduate project[17]. Some results were subsequently published in Dr. Atalianis's Ph. D. thesis[18]. Background on the Mathieu functions and their evaluation on a computer are given in references 48, 58, 72, 80, and 98. The use of Mathieu functions to solve the ellipse diffraction problem is described in references 18, 52, 53, 120 and 121. Unfortunately the analytical expressions are too long and involved to reproduce here. The evaluations are carried out by summing appropriate Mathieu function series. The reader is referred to references 17, 18, 52, 53, 120 and 121 for further details.

The program which evaluates the analytical results can deal with a wide range of aspect ratios of the ellipse, and can produce wave velocity potential and wave elevation at a range of points on and around the ellipse.

7.2 Circular cylinder wave diffraction results

A single case of a circular cylinder of radius, a and wave number k, for $ka = 4.0$ was considered. This choice implies a ratio of wavelength to element length of 15.0 on the cylinder surface. On the boundary between the finite and infinite elements the corresponding ratio is approximately 5.8, which is not unrealistically fine or so coarse that the finite element model would introduce large errors. The mesh is shown in figure 7.1.

The analytical results were obtained by evaluating the Havelock solution. Figure 7.2 shows the results for the wave elevations on the cylinder surface and figure 7.3 shows the errors in the real, and imaginary parts of the wave elevation, again on the cylinder surface. Figures 7.4 and 7.5 show contour plots of the real and imaginary parts of the wave elevations. The results, as expected are highly accurate. The maximum error in the wave elevation is less than 1%.
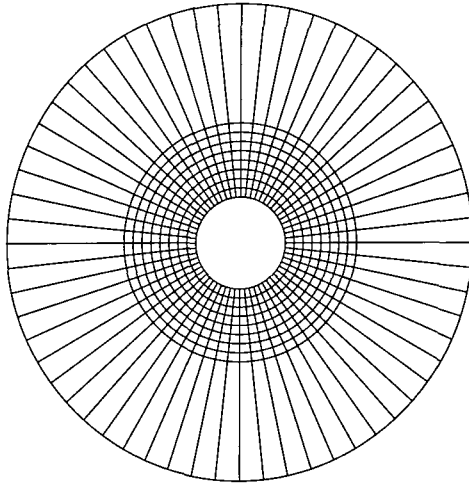
Figure 7.1   Circular cylinder mesh

7.3   Elliptical cylinder wave diffraction

The following ellipses were considered:

Aspect ratios: 2:1, 4:1 and 10:1.

In each case two meshes of finite and infinite elements were used. The coarse mesh consisted of two concentric circles, the first containing finite elements and the second infinite elements. There are 2 radial elements and 24 circumferential elements.

The fine meshes contain more finite and infinite elements, both radially and circumferentially. There are 9 elements radially and 60 circumferentially. The three coarse meshes are shown in figure 7.6, and the fine meshes in figure 7.7.

There are many parameters in the ellipse problem: the product of wavenumber and major axis, the aspect ratio of the ellipse and the angle of incidence. Clearly a systematic variation of all these parameters is not possible in a relatively short chapter. Instead, for each of the problems defined above, waves of unit amplitude were considered incident at the single angle of 30° to the major axis of the cylinder. The major axis of the ellipse was taken to be a, and a single ka value, where k is the wave number was considered, that of $ka = 4.0$. For each case a coarse and a fine mesh were used, with the same number of elements for each ellipse. This should indicate how the new element deals with problems as they depart further from the circular case.

The results are reported in several ways:

1. Plots of the real and imaginary parts of the wave elevation, on the elliptical cylinder surface.
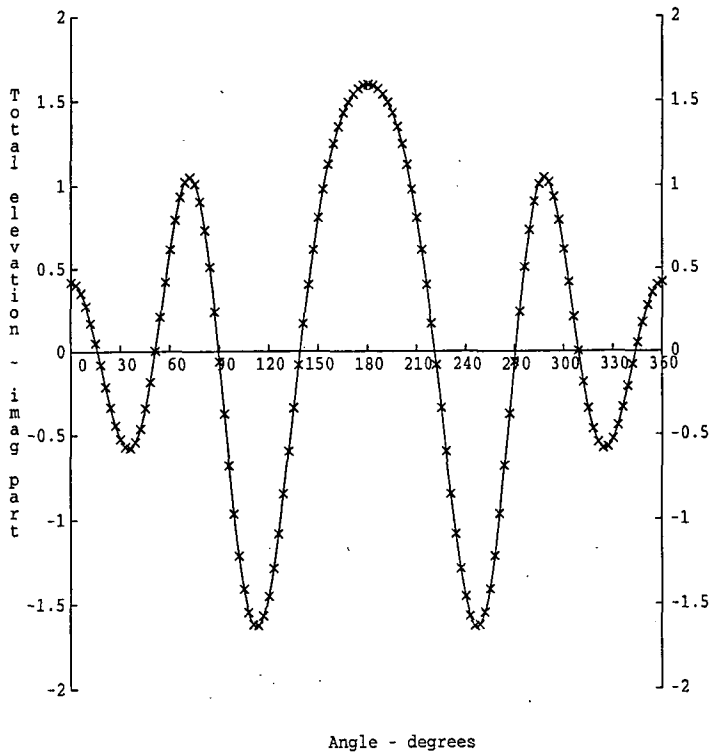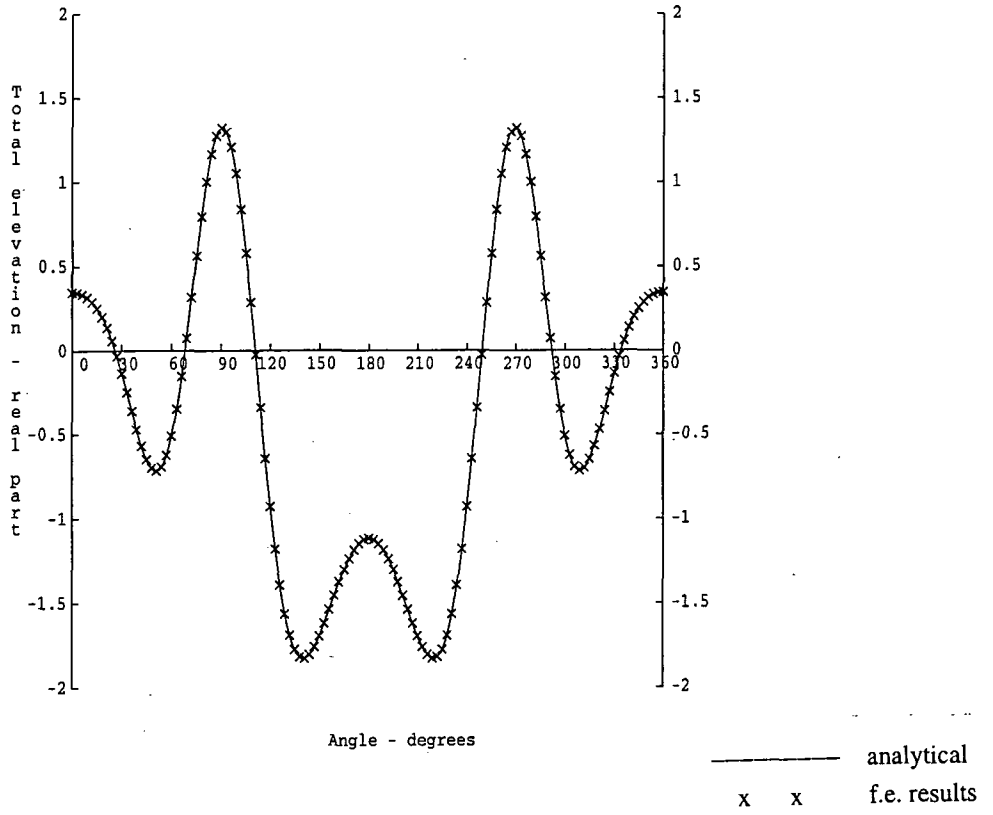
Figure 7.2   Wave elevations on the cylinder surface - real and and imaginary parts
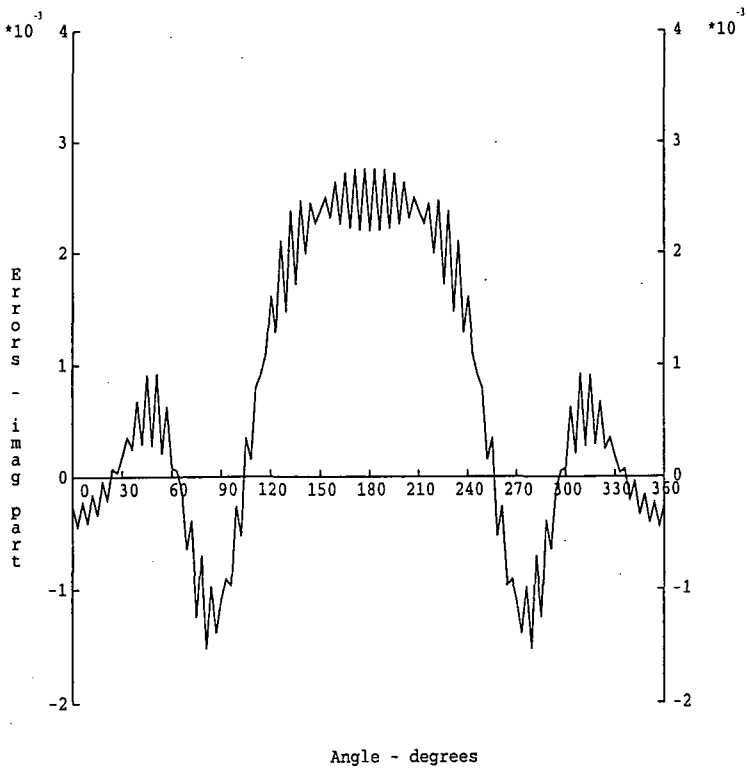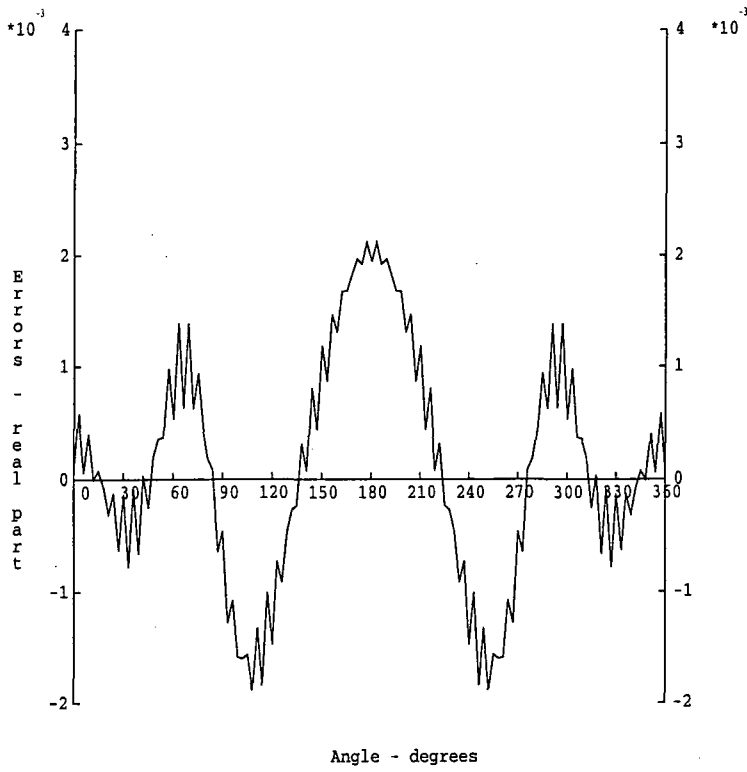
Figure 7.3 Errors in wave elevations on the cylinder surface - real and imaginary parts
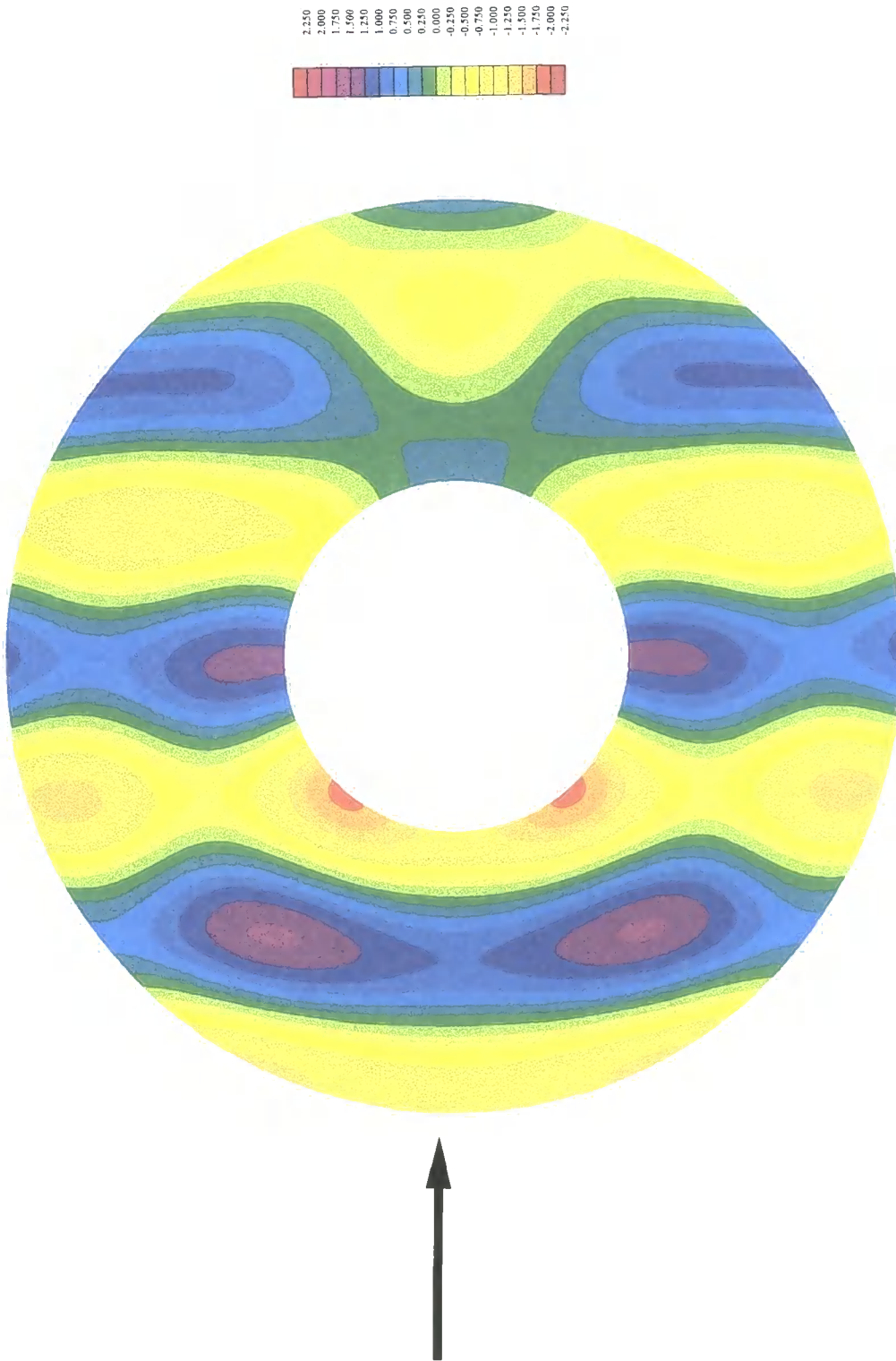
Figure 7.4   Contour plot of wave elevations - real part
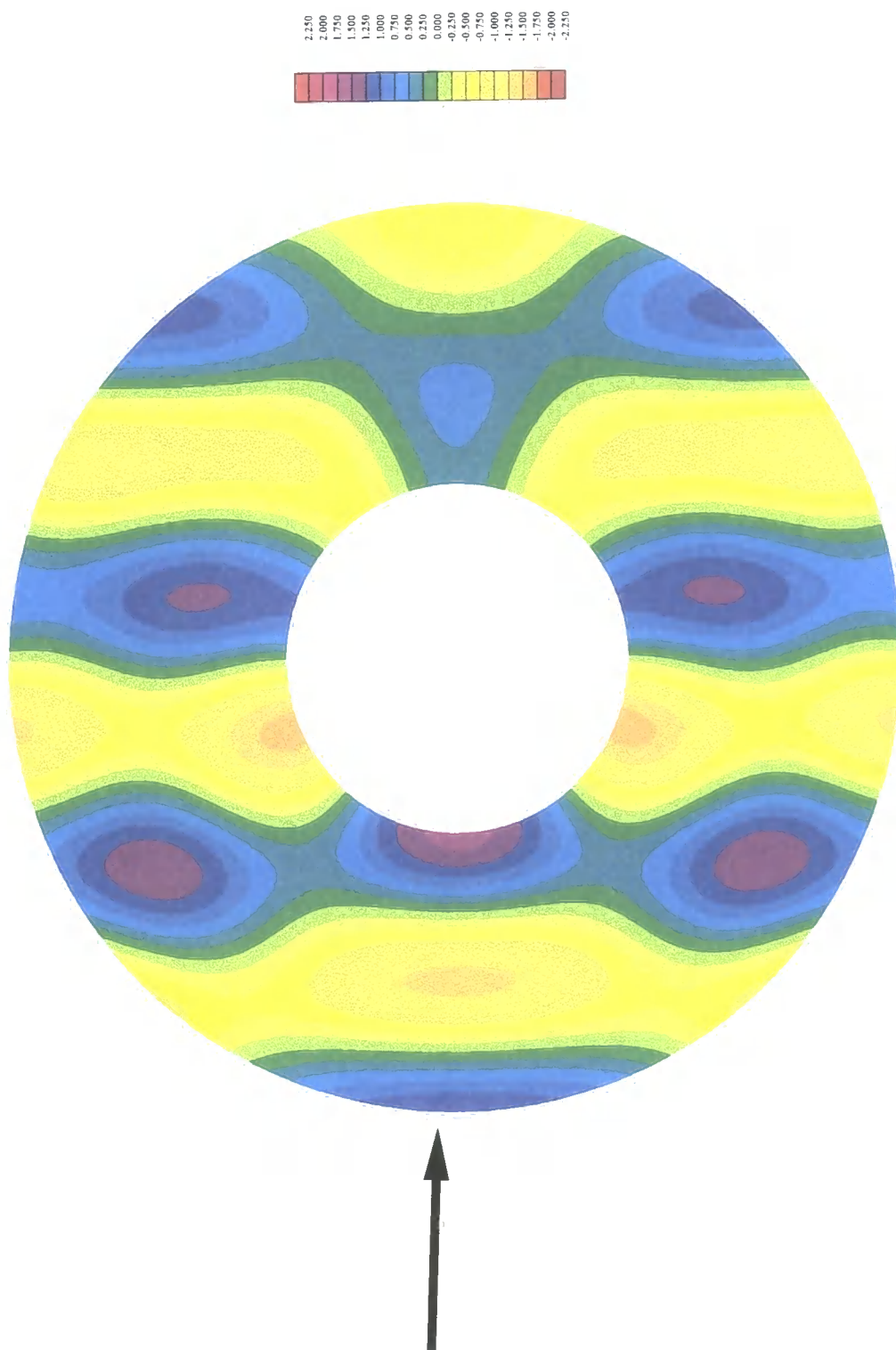
Figure 7.5   Contour plot of wave elevations - imaginary part
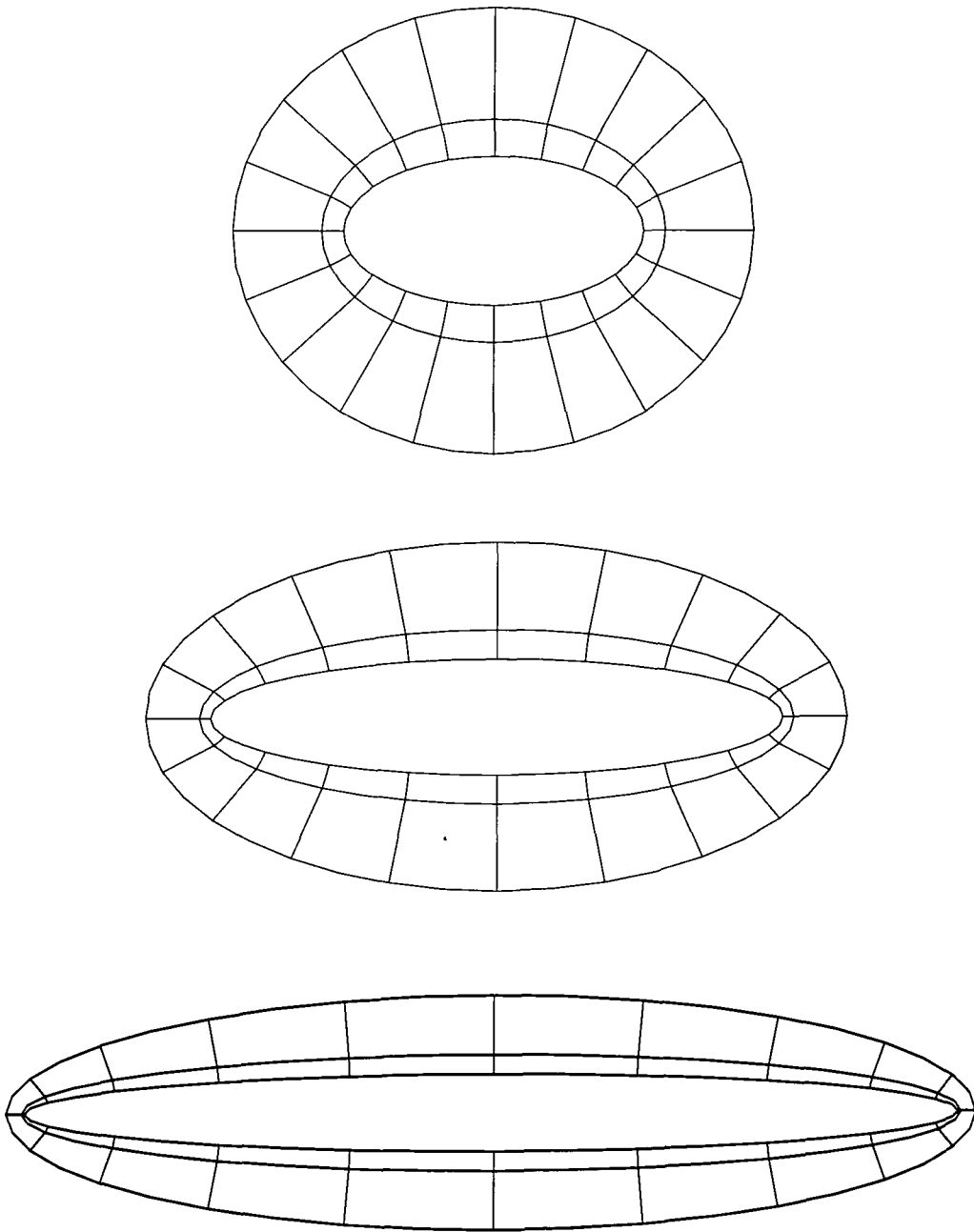
Figure 7.6   Ellipse coarse meshes - aspect ratios 2:1, 4:1 and 10:1
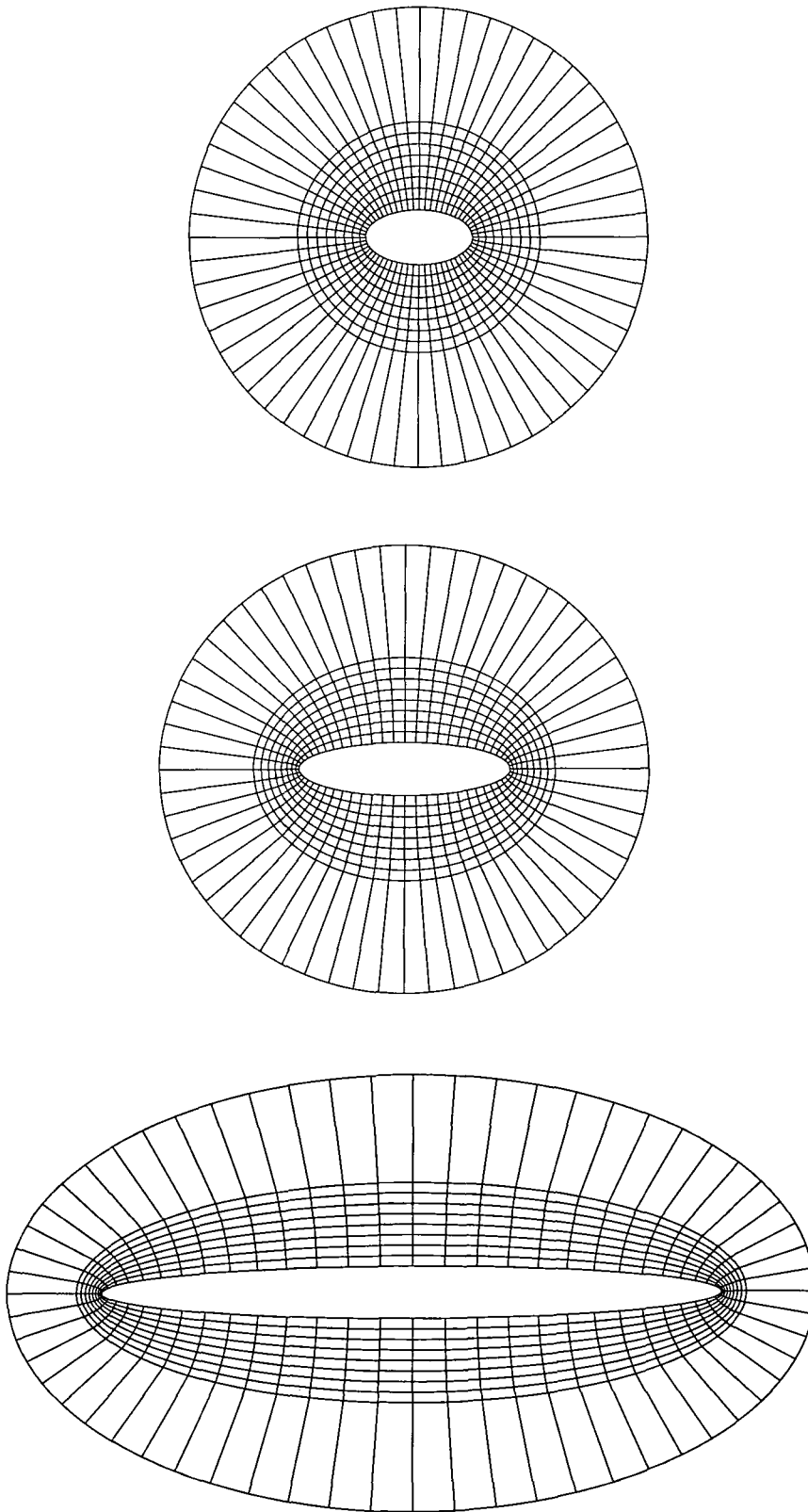
Figure 7.7   Ellipse fine meshes - aspect ratios 2:1, 4:1 and 10:1

2. Plots of the errors in the real and imaginary parts of the wave elevation, on the elliptical cylinder surface, and other concentric elliptical co-ordinate lines, around the cylinder.

3. Contour plots of the real and imaginary parts of the wave elevation, in the finite element mesh in the vicinity of the cylinder.

7.3.1 Ellipse of aspect ratio 2:1

The meshes are shown in Figures 7.6 and 7.7. Figure 7.8 shows the real and imaginary components of the wave elevation on the surface of the cylinder. Figure 7.9 shows the errors in the real and imaginary part of the numerical solution around the ellipse, for this coarse mesh. The angles measured around the ellipse are, in all cases, the local elliptical co-ordinate, (variable v in equation 5.1), and not the angle subtended from the centre of the ellipse. The errors on the ellipse surface can be seen to have a maximum value of about 0.5%, of the incident wave amplitude.

Figure 7.10 shows the errors on several other radii, obtained with the finer mesh, to demonstrate the change in the errors with radius. The maximum error is of the order of 0.15%. Figures 7.11 and 7.12 show contour plots of the wave elevations, generated by the fine mesh solution, illustrating the real and imaginary values of the wave elevation.

7.3.2 Ellipse of aspect ratio 4:1

The meshes are shown in Figures 7.6 and 7.7. Figure 7.13 shows the real and imaginary components of the wave elevation on the surface of the cylinder. Figure 7.14 shows the errors in the real and imaginary part of the numerical solution around the ellipse. The errors on the ellipse surface can be seen to have a maximum value of about 2%.

Figure 7.15 shows the errors from the finer mesh. The maximum error is of the order of 0.6%. Figures 7.16 and 7.17 show contour plots of the real and imaginary parts of the wave elevations, again generated by the fine mesh solution.

7.3.3 Ellipse of aspect ratio 10:1

The meshes are shown in Figures 7.6 and 7.7. Figure 7.18 shows the real and imaginary components of the wave elevation on the surface of the cylinder. Figure 7.19 shows the errors in the real and imaginary part of the numerical solution around the ellipse. The errors on the ellipse surface can be seen to have a maximum value of about 14%.

Figure 7.20 shows the errors from the finer mesh. The maximum error is of the order of 0.9%. Figures 7.21 and 7.22 show contour plots of the real and imaginary parts of the wave elevations, generated by the fine mesh solution.
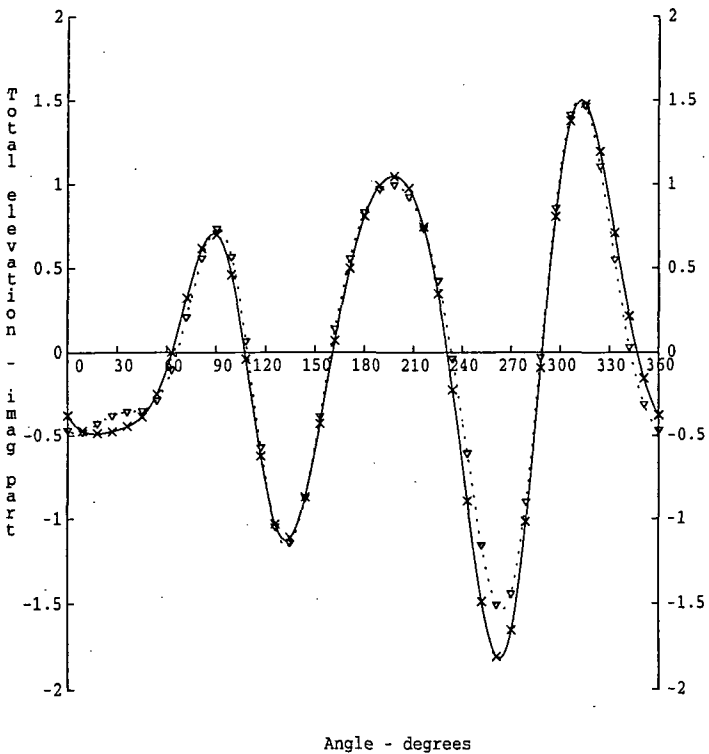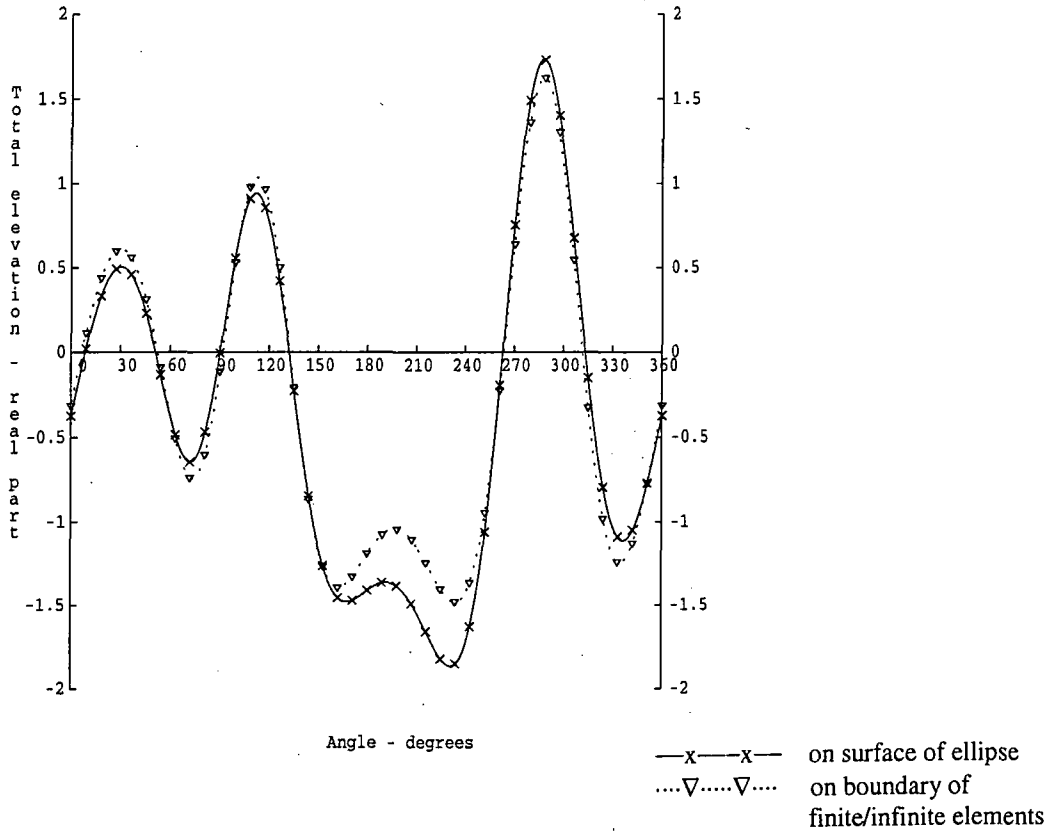
Wave elevations on surface of the ellipse - real and imaginary parts for aspect ratio of 2:1 and coarse mesh (contour plots are Figures 7.11a and 7.12a)

Figure 7.8   Wave elevations for ellipse of aspect ratio 2:1 and coarse mesh
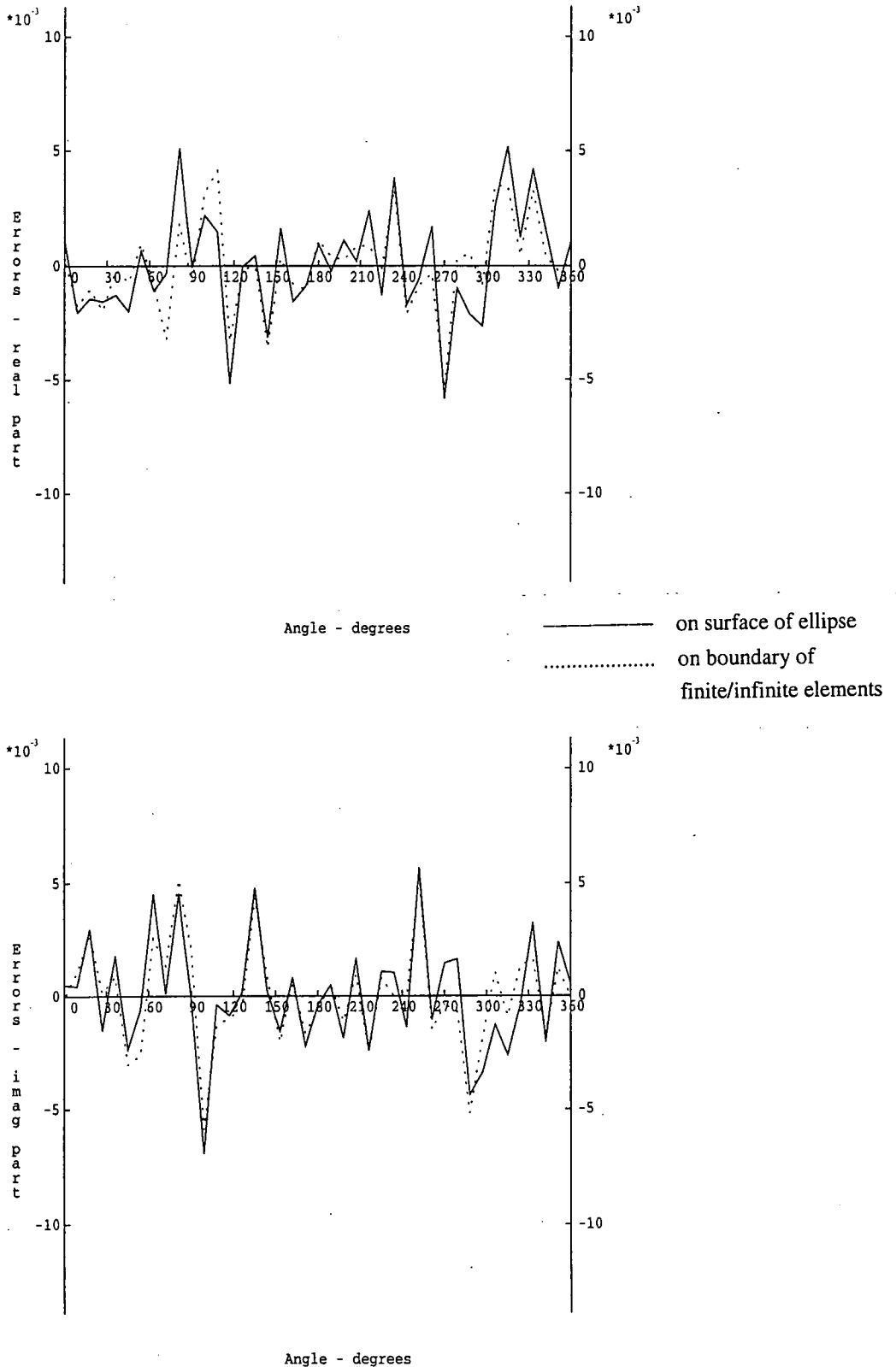
Errors in wave elevations on surface of the ellipse - real and imaginary parts for aspect ratio of 2:1 and coarse mesh

Figure 7.9   Errors in wave elevations, coarse mesh, 2:1 ellipse
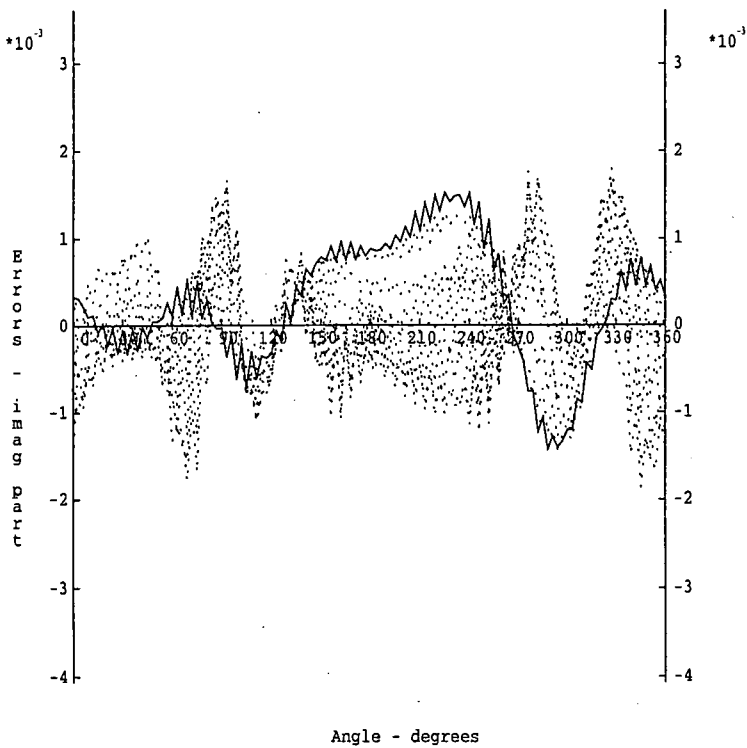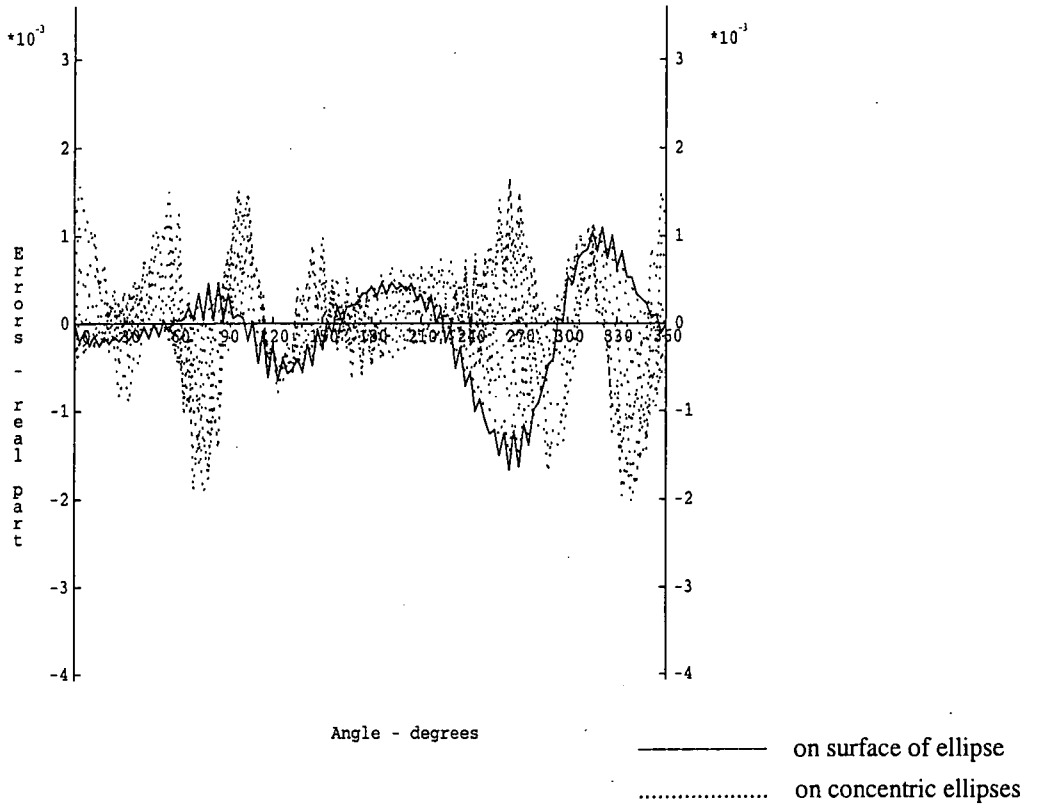
Errors in wave elevations around ellipse - real and imaginary parts for aspect ratio of 2:1 and fine mesh

Figure 7.10   Errors in wave elevations, fine mesh, 2:1 ellipse
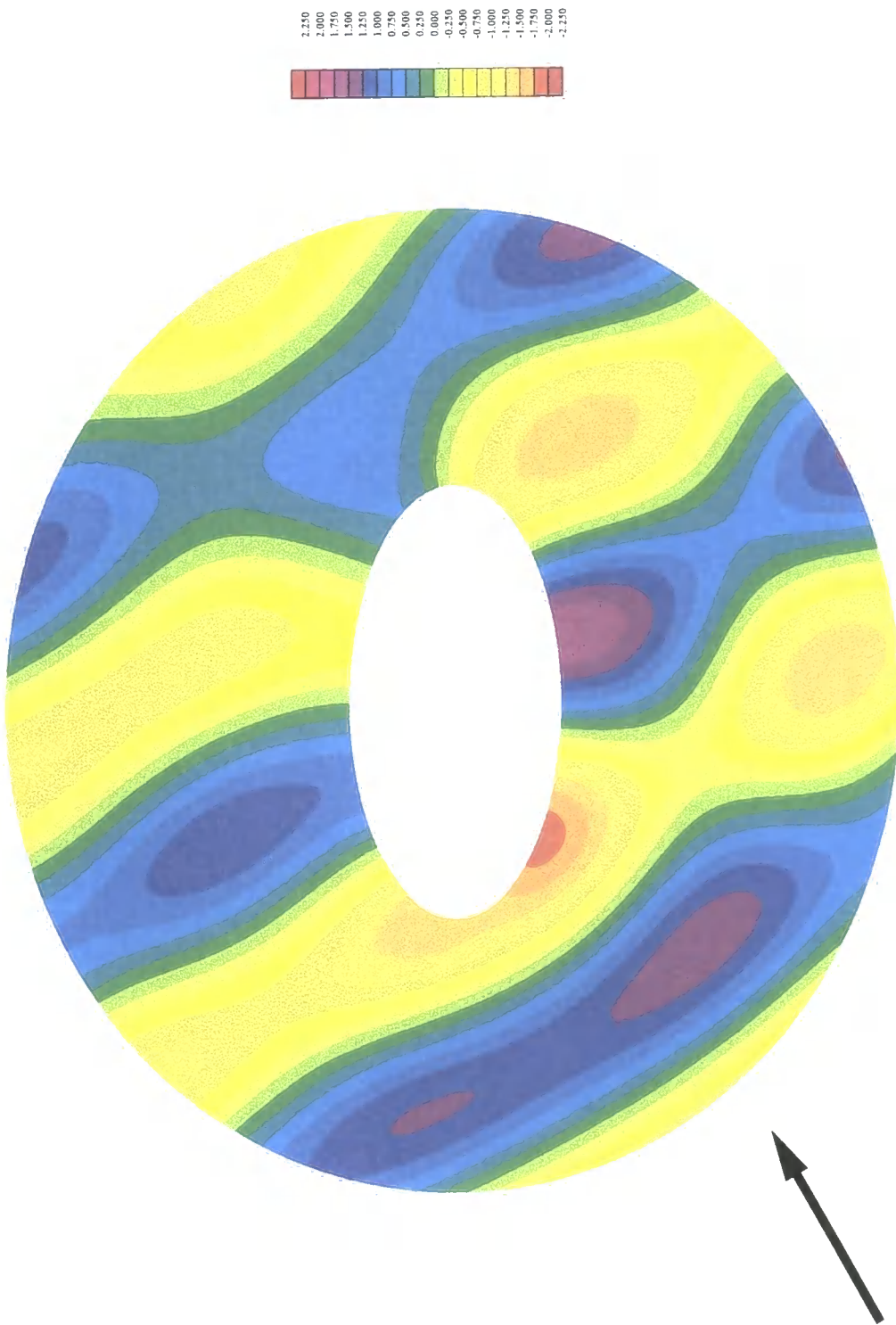
Figure 7.11 Contour plot of wave elevations - real part, aspect ratio 2:1, fine mesh
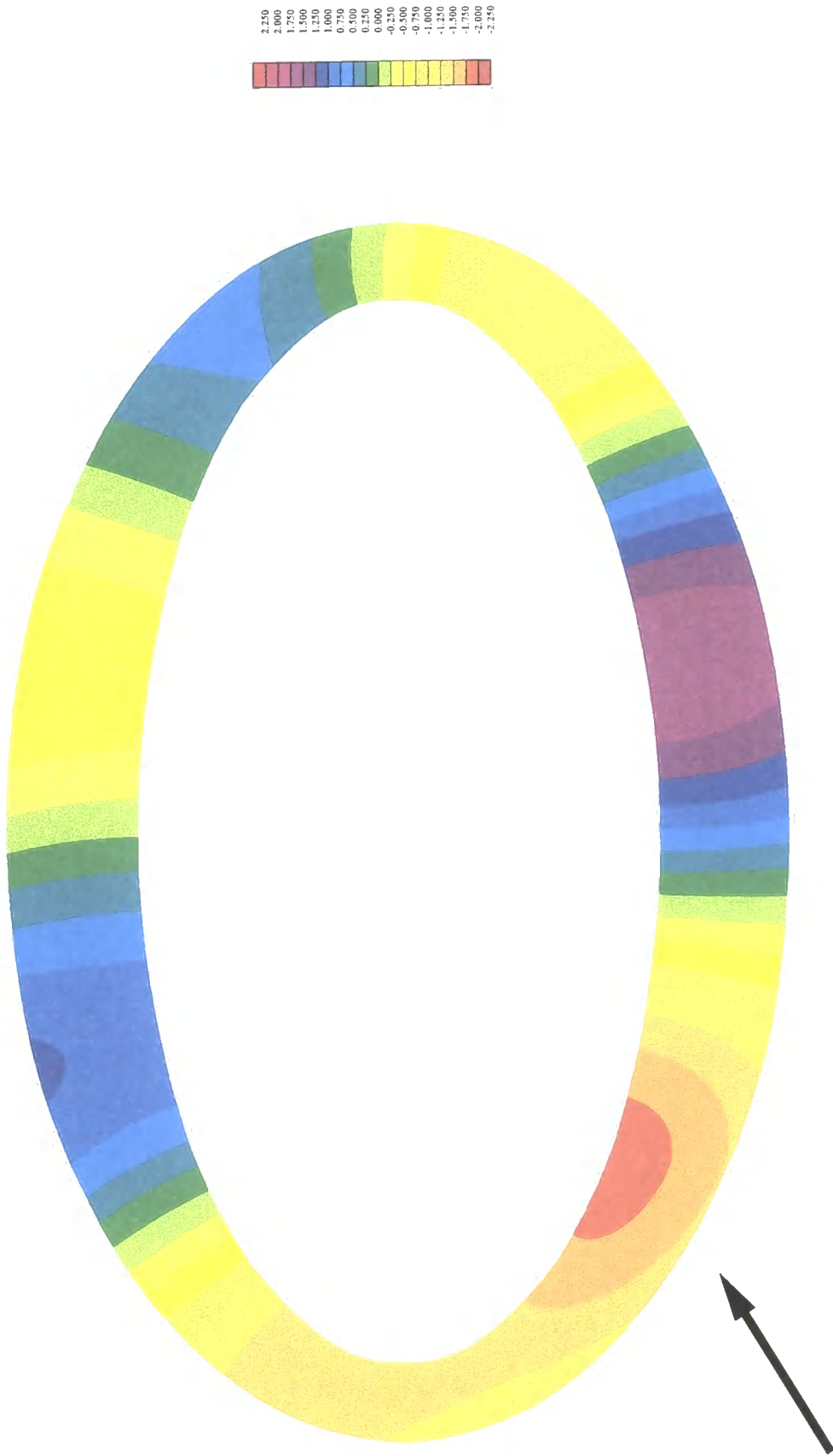
Figure 7.11a Contour plot of wave elevations - real part, aspect ratio 2:1, coarse mesh
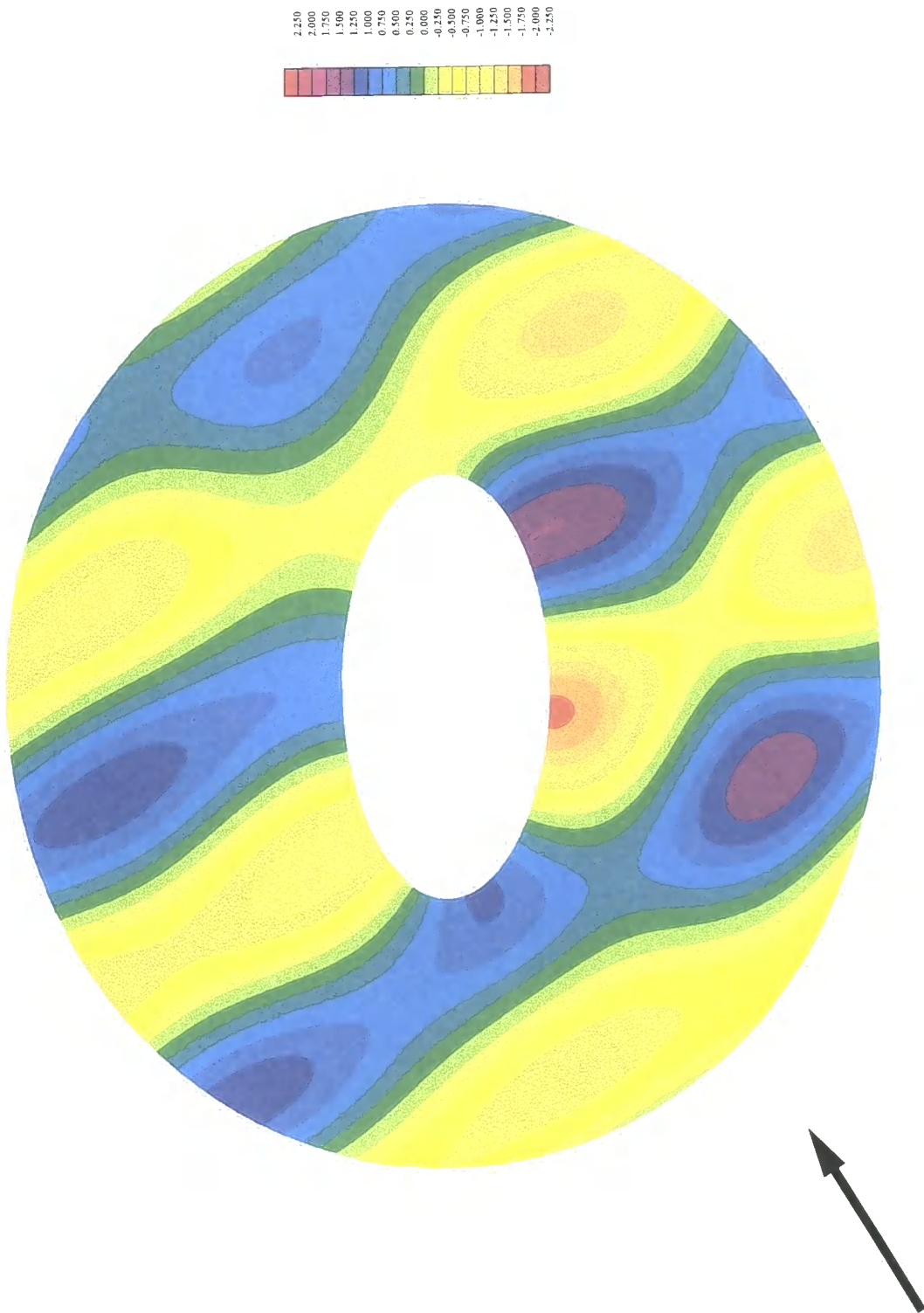
Figure 7.12   Contour plot of wave elevations - imaginary part, aspect ratio 2:1, fine mesh
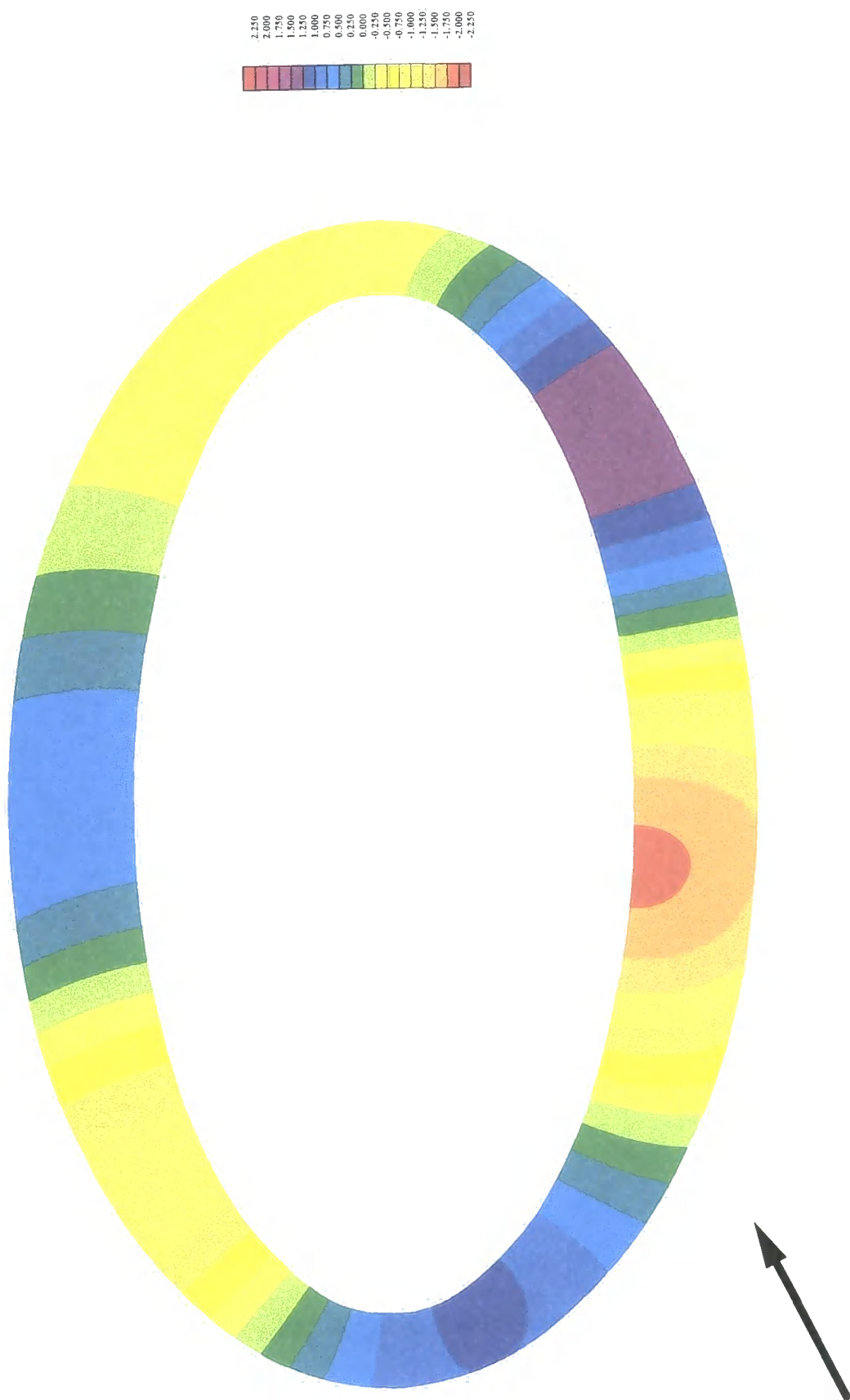
Figure 7.12a Contour plot of wave elevations - imaginary part, aspect ratio 2:1, coarse mesh
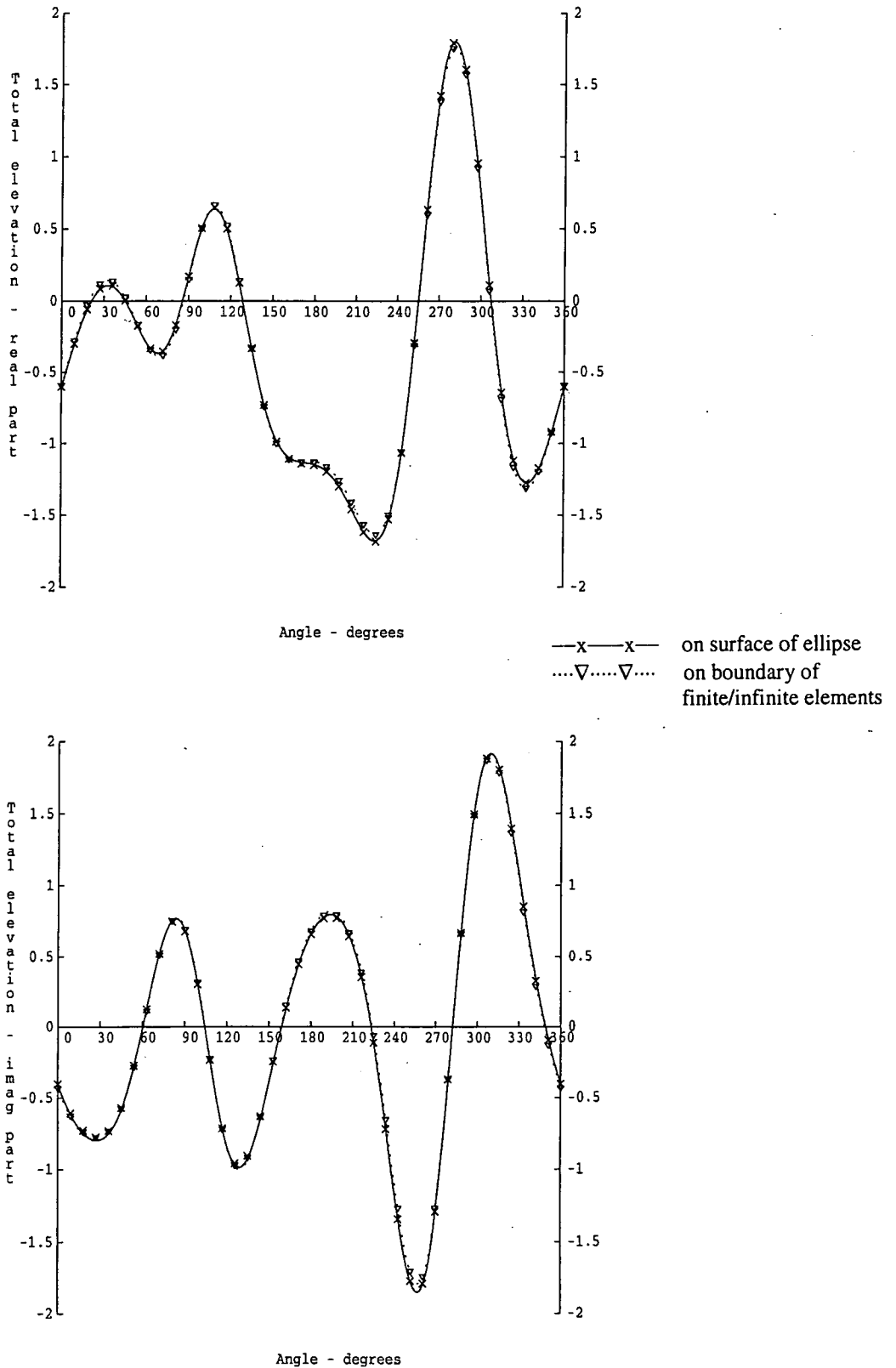
Wave elevations on surface of the ellipse - real and imaginary parts for aspect ratio of 4:1 and coarse mesh (contour plots are Figures 7.16a and 7.17a)

Figure 7.13 Wave elevations for ellipse of aspect ratio 4:1 and coarse mesh
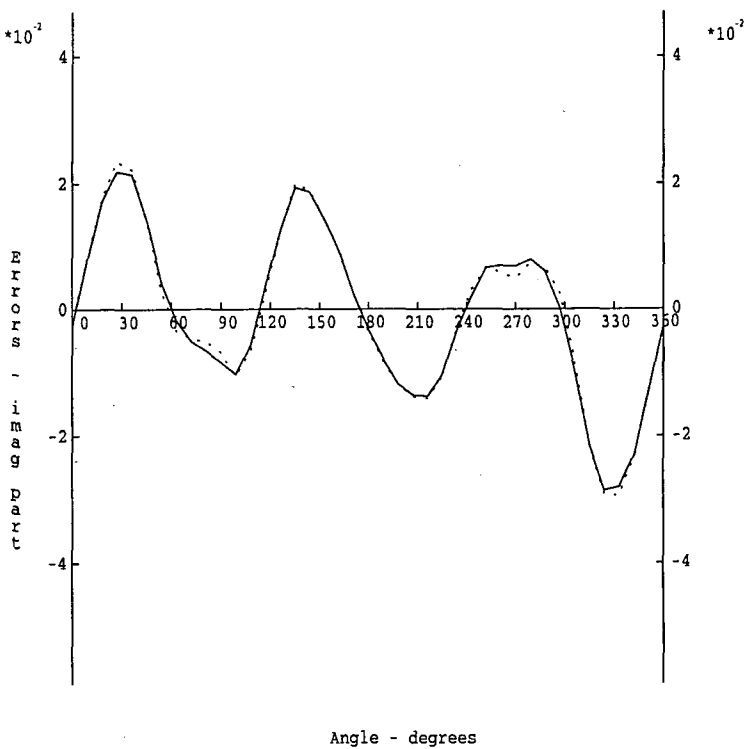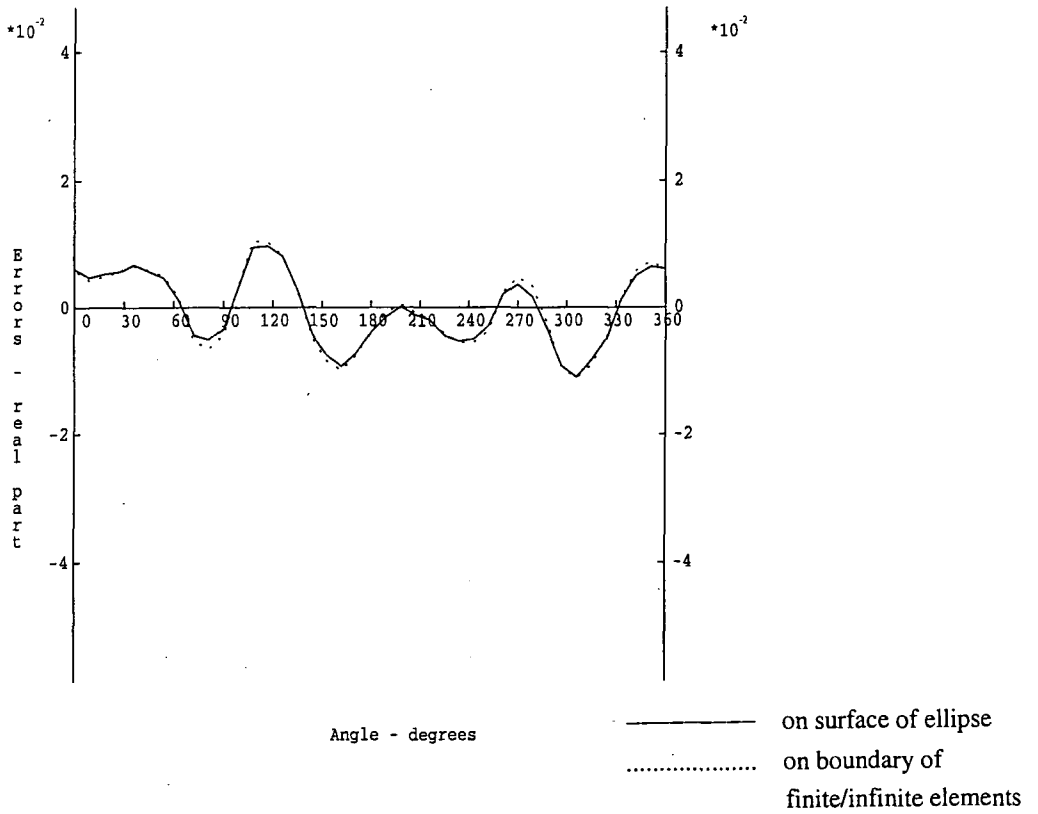
Errors in wave elevations on surface of the ellipse - real and imaginary parts for aspect ratio of 4:1 and coarse mesh

Figure 7.14 Errors in wave elevations, coarse mesh, 4:1 ellipse
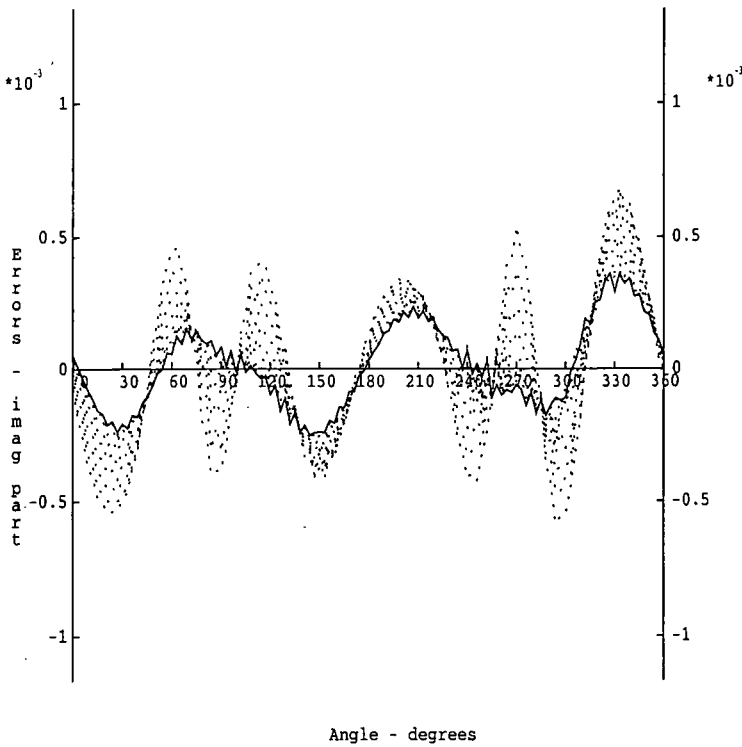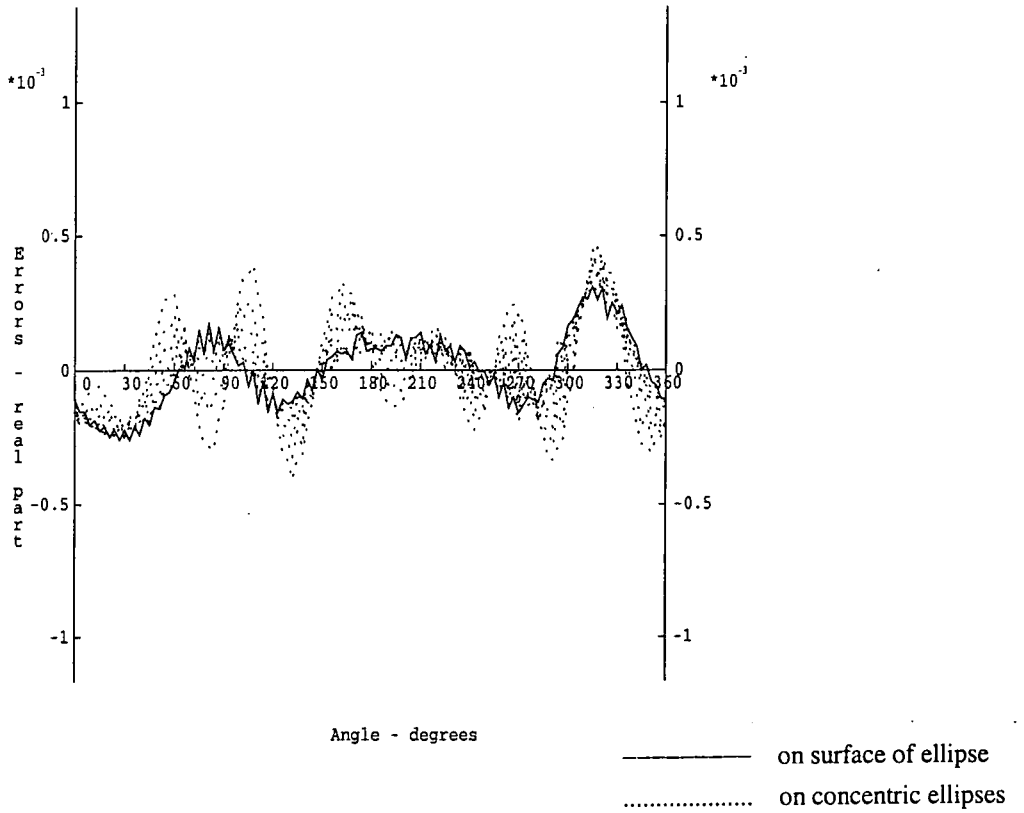
Errors in wave elevations around ellipse - real and imaginary parts for aspect ratio of 4:1 and fine mesh

Figure 7.15 Errors in wave elevations, fine mesh, 4:1 ellipse
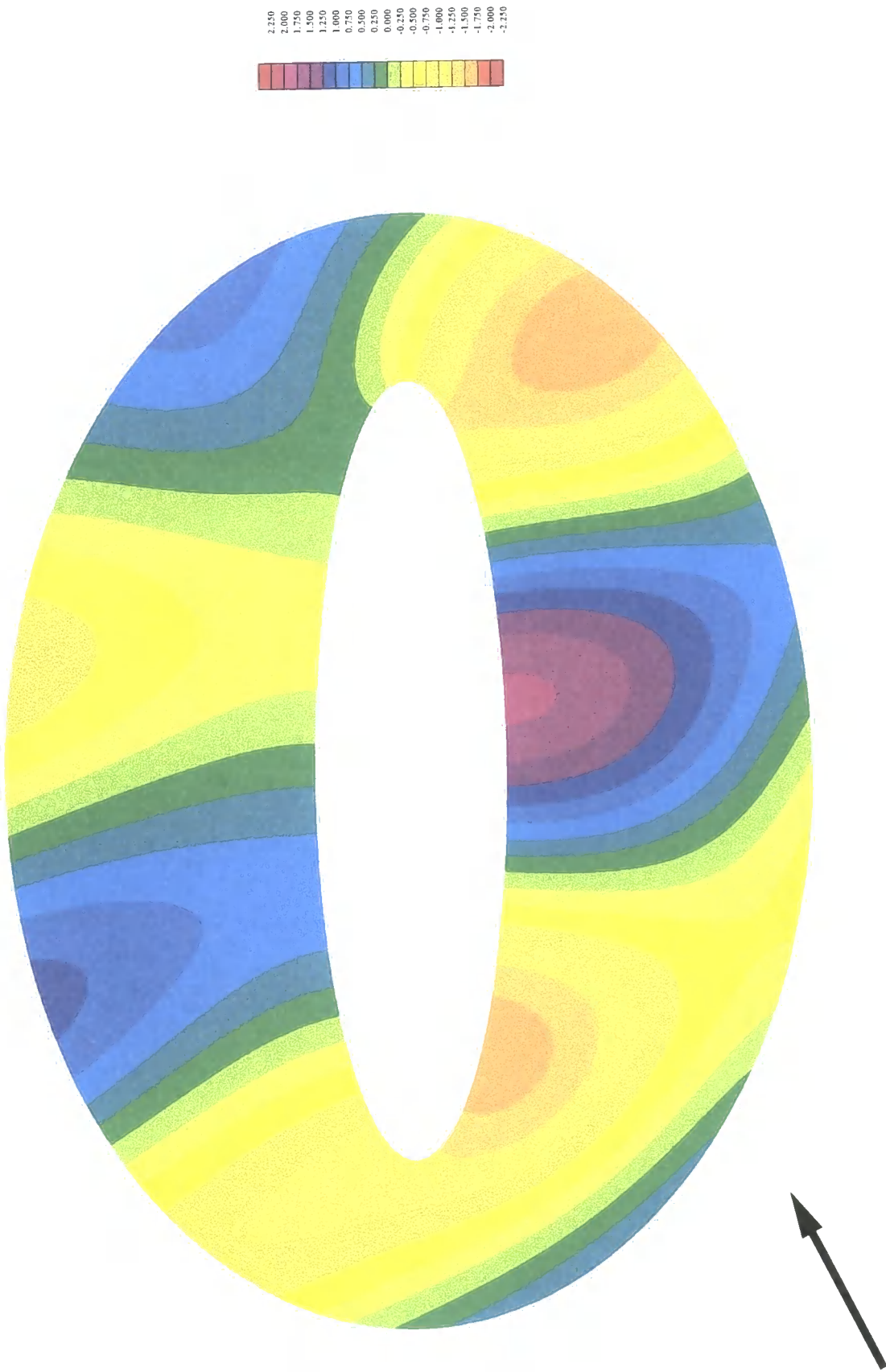
Figure 7.16   Contour plot of wave elevations - real part, aspect ratio 4:1, fine mesh
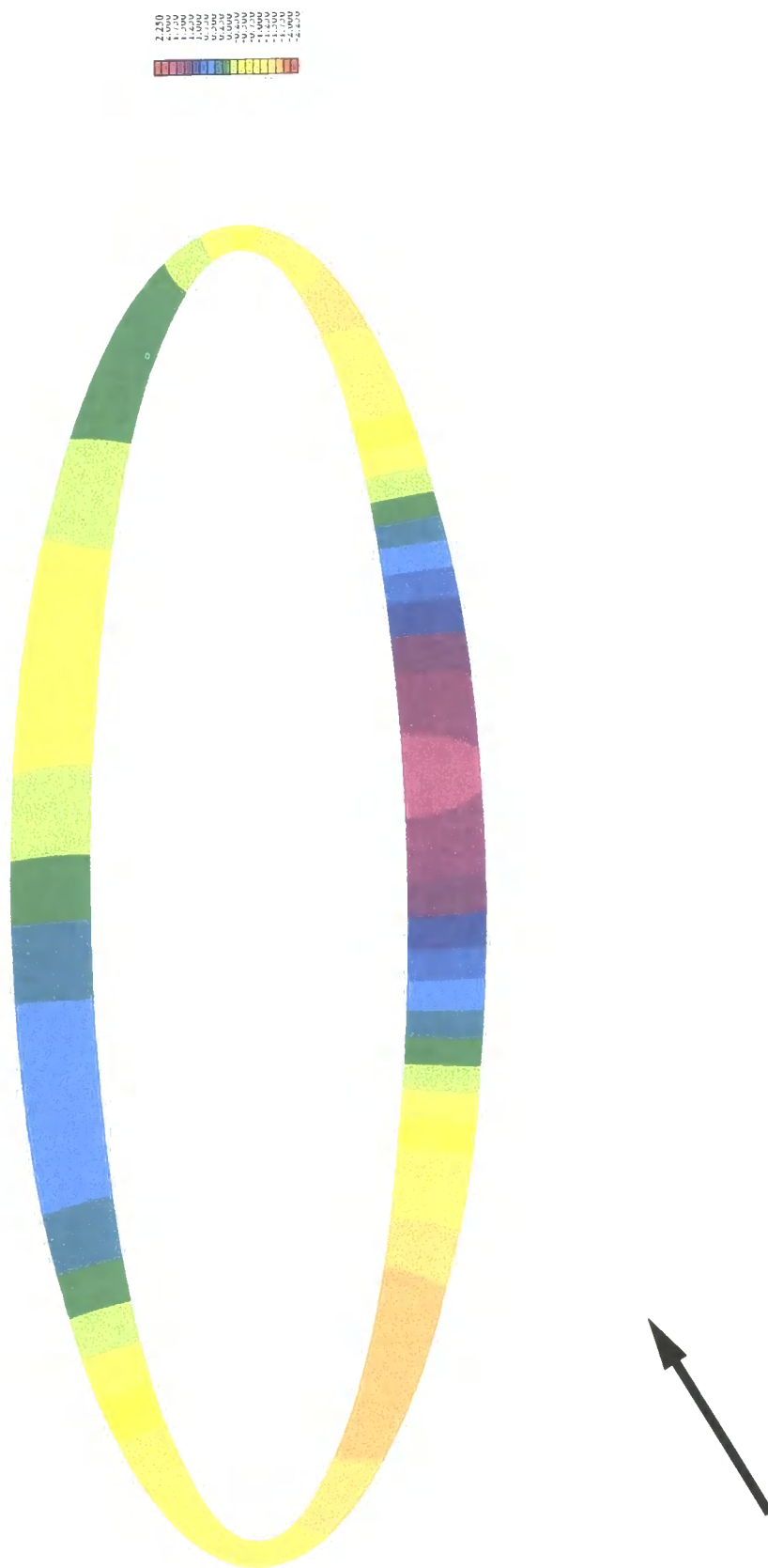
Figure 7.16a Contour plot of wave elevations - real part, aspect ratio 4:1, coarse mesh
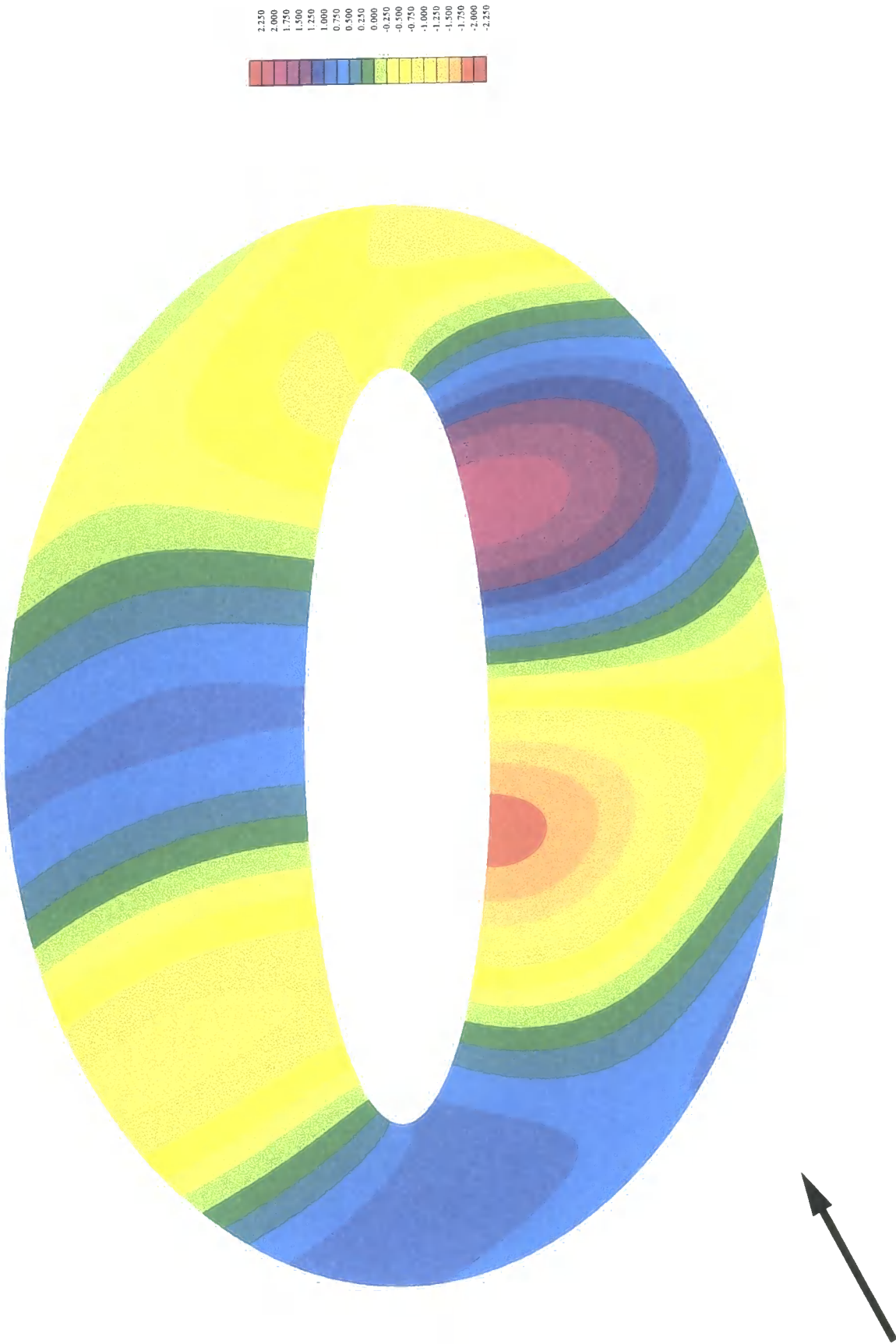
Figure 7.17 Contour plot of wave elevations - imaginary part, aspect ratio 4:1, fine mesh

Figure 7.17a Contour plot of wave elevations - imaginary part, aspect ratio 4:1, coarse mesh
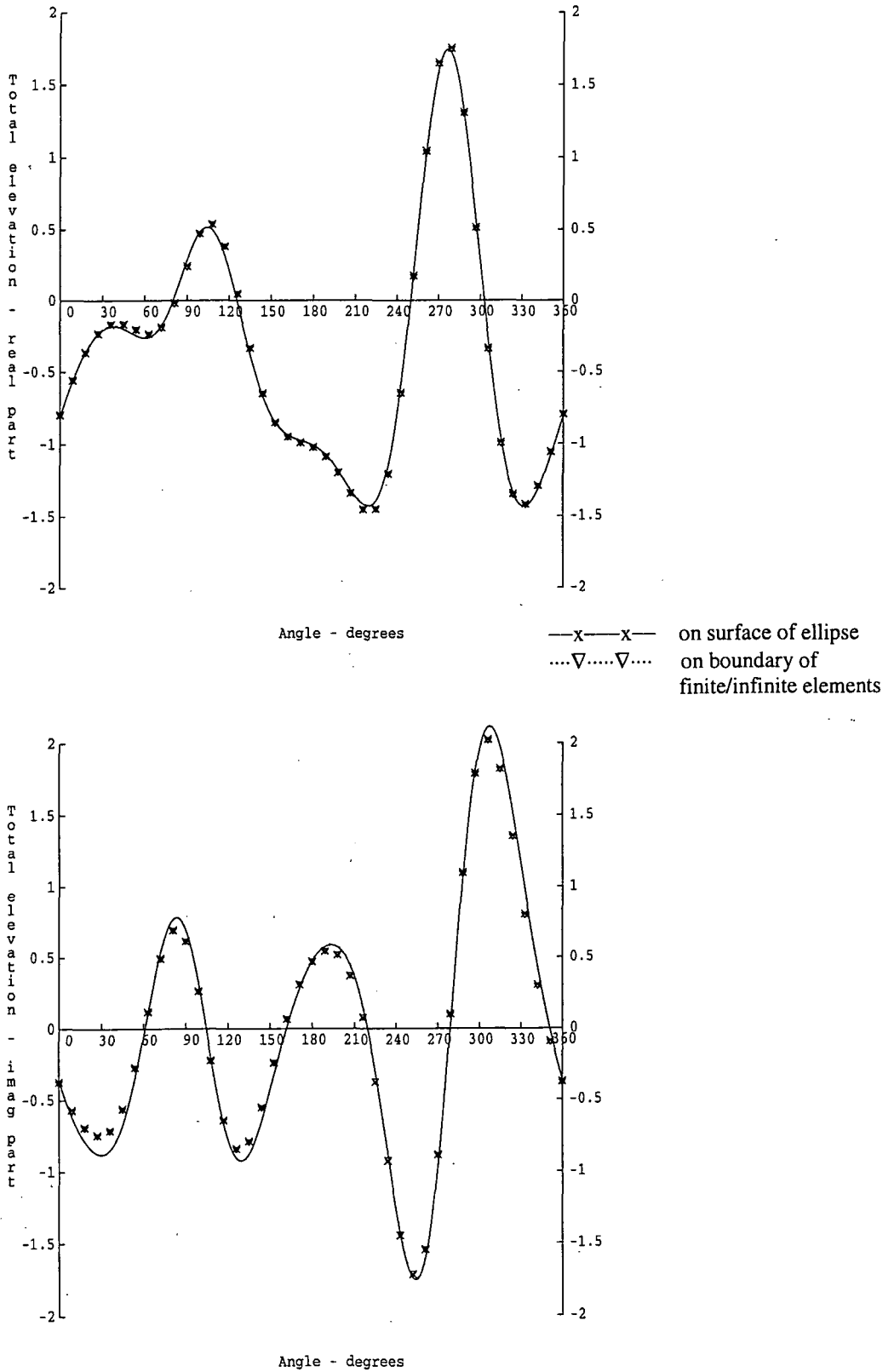
Wave elevations on surface of the ellipse - real and imaginary parts for aspect ratio of 10:1 and coarse mesh

Figure 7.18 Wave elevations for ellipse of aspect ratio 10:1 and coarse mesh
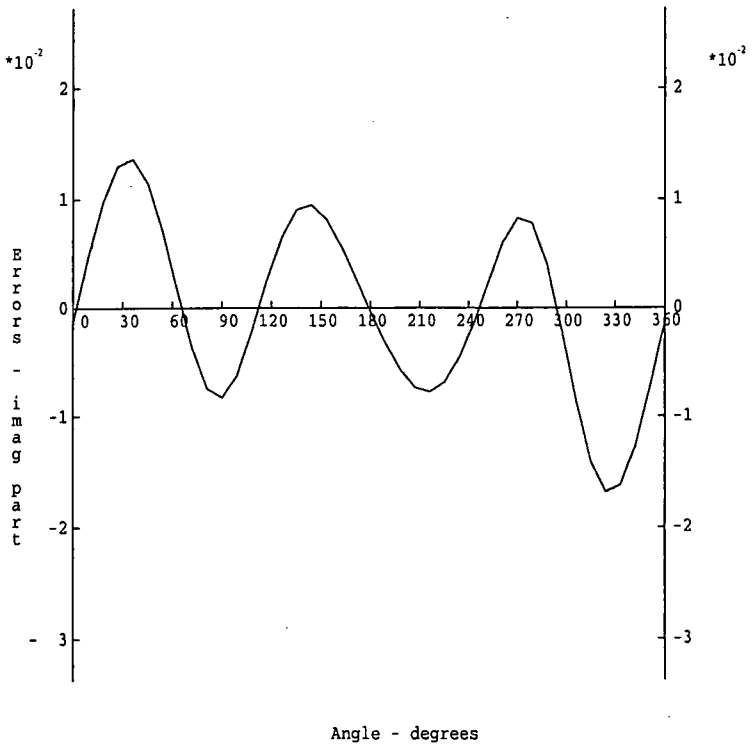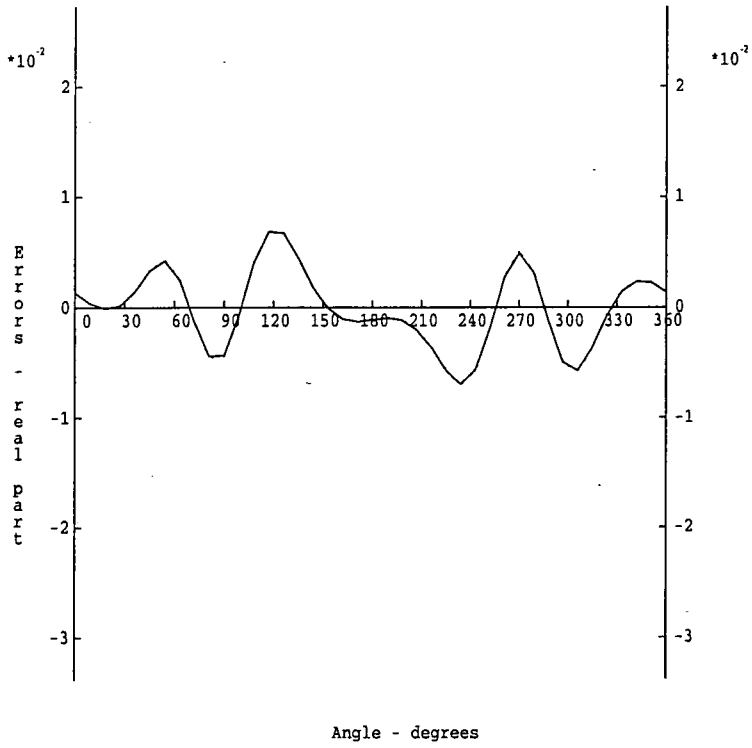
Errors in wave elevations on surface of the ellipse - real and imaginary parts for aspect ratio of 10:1 and coarse mesh

Figure 7.19   Errors in wave elevations, coarse mesh, 10:1 ellipse
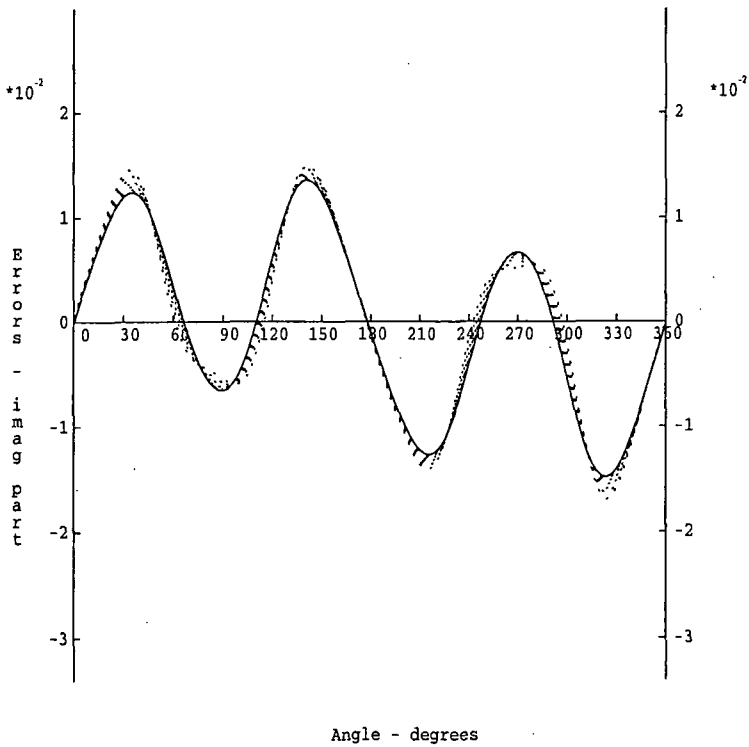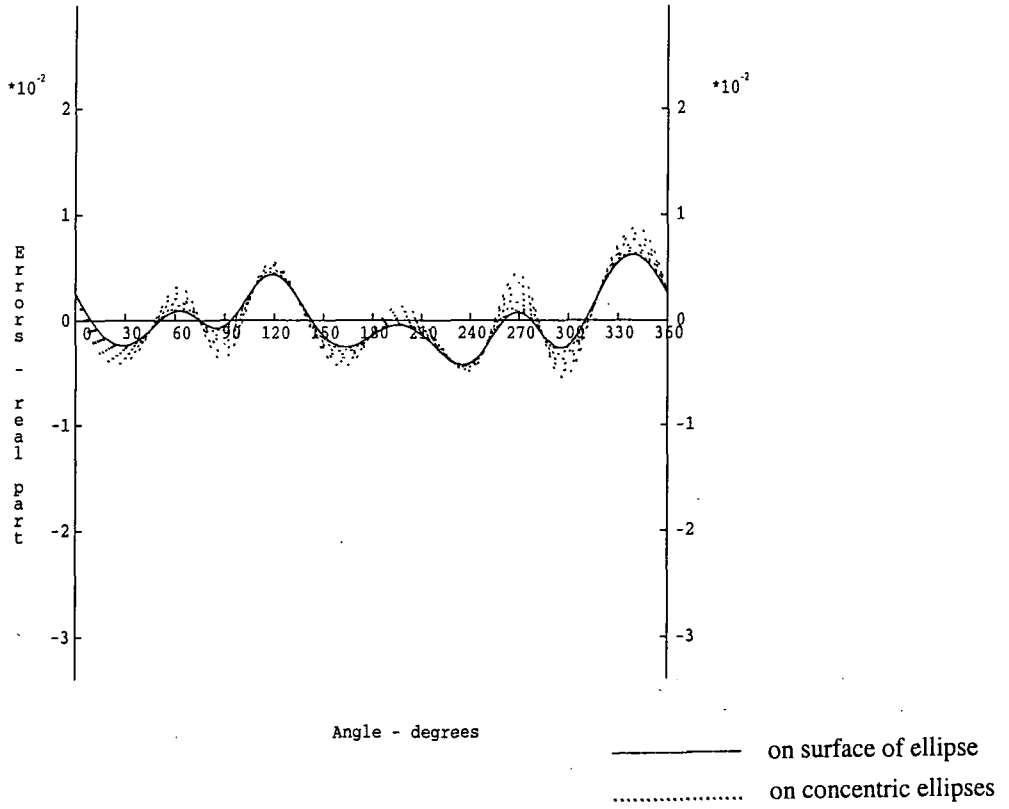
Errors in wave elevations around ellipse - real and imaginary parts for aspect ratio of 10:1 and fine mesh

**Figure 7.20** Errors in wave elevations, fine mesh, 10:1 ellipse
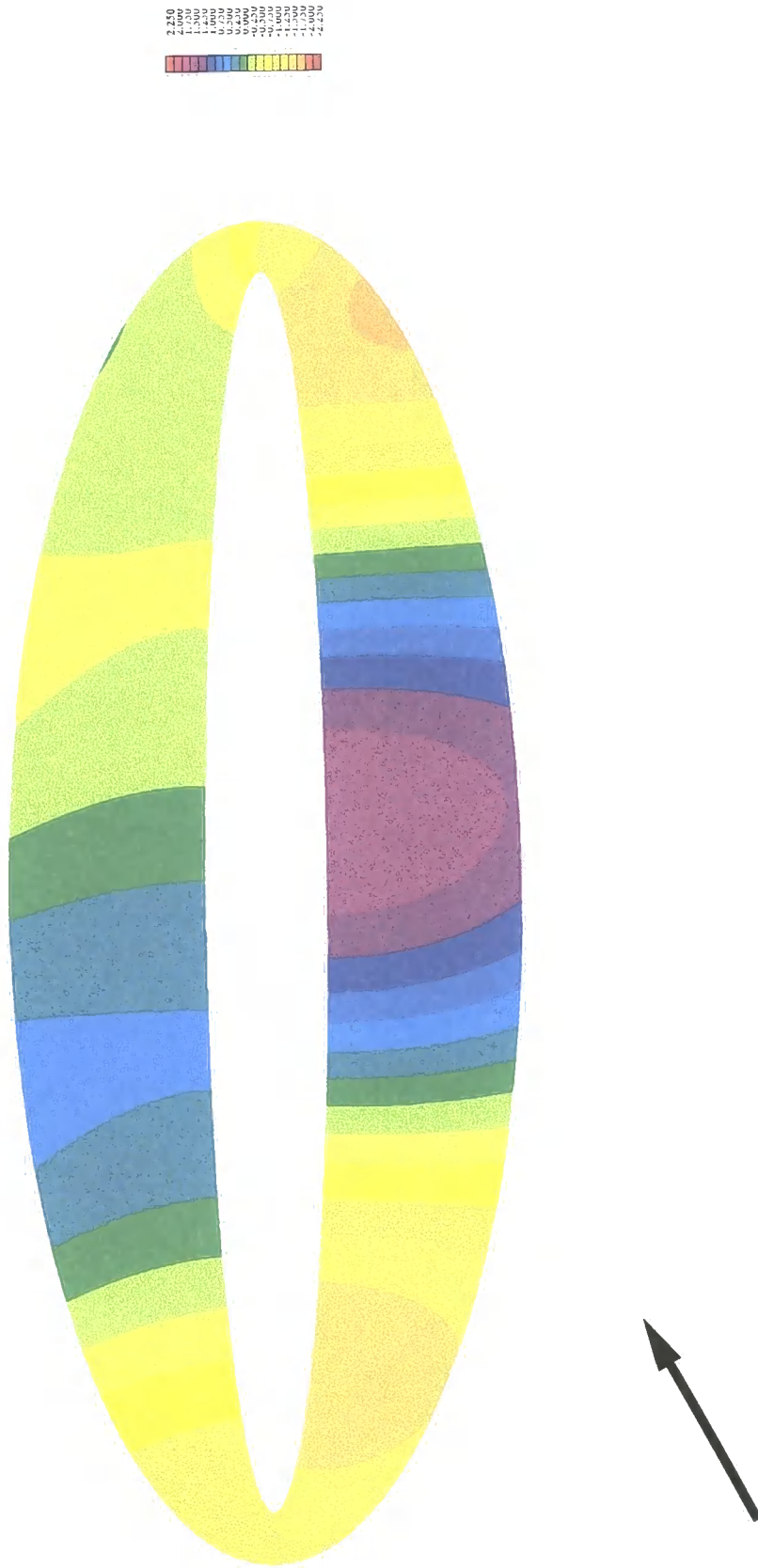
Figure 7.21 Contour plot of wave elevations - real part, aspect ratio 10:1, fine mesh

Figure 7.22 Contour plot of wave elevations - imaginary part, aspect ratio 10:1, fine mesh

7.4   Discussion

In general the finite and infinite element results are very accurate. There seems to be little influence on the accuracy of the results, for the fine mesh, as the aspect ratio of the ellipse is increased, for a given ka value. There is no noticeable deterioration in the results when the aspect ratio is such that the circle circumscribing the ellipse intersects the infinite elements.

In the limit the ellipse of infinite aspect ratio might be expected to behave like a slender breakwater, and special provision might be needed for the singularities at the breakwater tips. See, for example ref. 36. There is no indication that this is a problem with the ellipses considered here.

7.5   Conclusions

The results demonstrate that the new infinite element, together with conventional finite elements for wave problems, gives accurate results for the diffraction of waves around an ellipse, even for the case of ellipses of large aspect ratios.

The results further demonstrate that infinite elements do not need to be restricted to problems in which a circumcircle around the scattering object can be drawn entirely within the finite element mesh. The results show that the new infinite element can be used with *some* confidence in problems with large aspect ratios. It is of course still possible that two dimensional diffraction problems could be bounded by an ellipse, yet not converge in a hyperbolic-elliptical co-ordinate system. It would be desirable to test the elements on problems such as diffraction of waves by two cylinders, (and other problems with internal reflections), using an elliptical interface between the finite and infinite elements. However, this is beyond the scope of the present study. The techniques described in this thesis are easily extended to three dimensions, and to higher order infinite elements, having more terms in the multi-polar expansion.

Chapter 8

The riser problem and diffraction modelling

This chapter describes the development of a method for the assessment of the effects of wave induced flows past risers. It is intended that it could form the basis of a design procedure. The method uses finite and infinite element techniques to model the diffraction of the waves around the risers. The conventional finite element matrices are modified, by means of empirical constants, derived from a knowledge of the viscous flow, in order to model its dissipative effects. Estimates of the velocity field are thus possible, together with wave force calculations, based on Morison's equation.

8.1 Introduction

The aim of this chapter is to arrive at a logical but simple method for the determination of wave induced fluid flows and associated forces on groups of risers. Risers are the steel cylinders which are used to convey hydrocarbons, and related equipment between the topsides of offshore installations and the sea bed. They are supported over this span by riser support frames, which transmit any forces acting upon the risers into the rest of the jacket structure. The risers will normally be subject to the action of waves.

Risers form a very important part of most offshore installations. A typical jacket structure might have a rectangular array of say 10 risers by 5 risers. The wave forces on an individual riser might not be large, in comparison with the total wave force on the structure, but in aggregate they make a significant contribution to the total wave force.

The risers are relatively long and thin. Their diameters are small relative to the wave length. Individually they will only experience small wave diffraction effects, but considered as a group, they will tend to diffract the waves. They will also be acted upon by viscous, bluff body effects. Figure 8.1 shows a typical offshore jacket structure with an array of risers.

It must be said at the outset, that while the possibility of a complete computer simulation of the flows around a group of risers is just about within the bounds of what is feasible, using the largest computers, to the knowledge of the author no such simulation has been carried out. It would, in any event, be far too expensive as a routine design tool. Such a numerical model would need to incorporate free surface effects, waves, diffraction, radiation, and so on, and separated viscous flow at high Reynolds Numbers and a range of Keulegan-Carpenter numbers. These tasks are quite difficult, for a single riser, or cylinder, and prohibitively complicated for an array of risers.
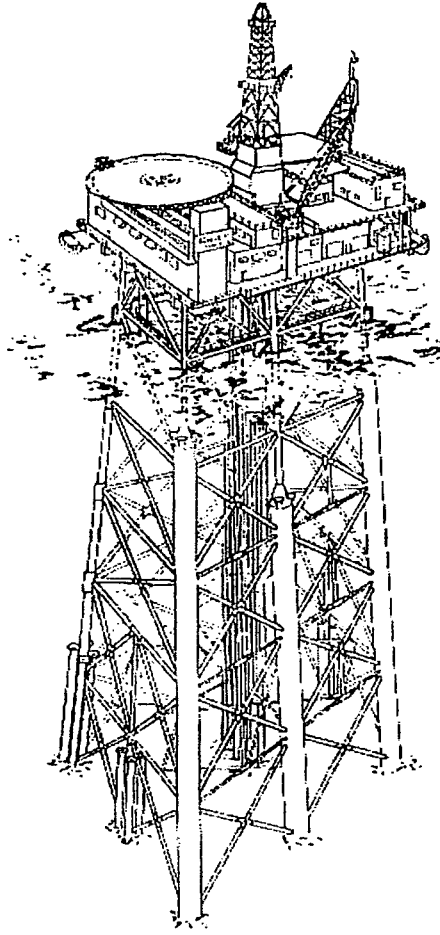
Figure 8.1   Typical offshore jacket structure

The two defining parameters for the flow are the Reynolds Number, R_e, which is named after the great nineteenth century engineer, Osborne Reynolds, and the Keulegan Carpenter number, K. These are defined as follows:

$$R_e = \frac{U_m D}{\nu} = \frac{U_m D \rho}{\mu} \qquad \text{and} \qquad K = \frac{U_m T}{D}.$$

In the above equations U_m is the peak velocity, T is the wave period, D is the diameter of the cylinder, and ν is the kinematic viscosity, given by the normal viscosity, μ divided by the fluid density, ρ. Thus $\nu = \mu/\rho$.

From these parameters the flow regime around the cylinder can be classified as shown in Table 8.1.

The aim of the study was to arrive at a rational procedure for designers, based on an empirical approach, and the simplest 'reasonable' numerical model. The scheme arrived

K	$D/\lambda < 0.20$	$D/\lambda > 0.20$
$K > 25$	Drag dominated flow regime. Morison's Equation with C_M and C_D values required for computing wave forces. Drag coefficient is function of Reynold's number. For $R_e > 1.5 \times 10^6$, $C_M = 1.8$, $C_D = 0.62$ For $10^5 < R_e < 1.5 \times 10^6$, $C_M = 1.8$, C_D varies from 1.0 to 0.6	
$5 < K > 25$	Intermediate regime between drag and inertia domination. Morison's equation applicable but published C_M and C_D values exhibit wide scatter. Flow behaviour and consequent loading complex and uncertain. For $R_e > 1.5 \times 10^6$, $C_M = 1.8$, $C_D = 0.62$	
$K < 5$	Inertia dominated flow regime. Morison's Equation or diffraction theory for computing forces $C_M = 2.0$ Effect of C_D is negligible	Morison's Equation unsuitable for computing wave forces. Diffraction theory required.

C_M inertia coefficient, C_D drag coefficient.

$$R_e = \frac{U_m D}{\nu} \qquad K = \frac{U_m T}{D}.$$

U_m peak velocity, T wave period, ν kinematic viscosity, R_e Reynolds number, K Keulegan Carpenter number.

Table 8.1   Classification of flow regimes past cylinders

at utilises a finite and infinite element model to predict the wave pattern, modified by the diffraction effects, and with approximate adjustments to account for viscous energy losses. The method enables the prediction of the modified wave velocities, and associated wave forces, generated from Morison's equation.

8.2 Flow past risers

There are three main effects to be considered in the modelling of the riser array.

- Wave diffraction
- Viscous drag effects
- The interaction of the first two effects

The first two effects will be considered in turn.

8.3 Diffraction modelling

In effect three approches are possible here. They will be considered in turn.

8.4 'Exact' modelling

By exact modelling is meant the detailed geometrical modelling of each and every riser, and the determination of the diffraction effects using an accepted and accurate solution method. This would be either the analytical solution of Linton and Evans[42], which is based on the truncation and summation of infinite series, or a fine finite and infinite element mesh. It will be shown later that such a method does give very accurate results, in the sense that they agree closely with those from the Linton and Evans model. 'Exact' modelling would be the more accurate, and preferable solution. Its disadvantage is that it is more computationally intensive, and it would require a very fine mesh, with associated computational load and data preparation problems. In this work some exact modelling is carried out, using a mesh of finite and infinite elements which incorporates the riser array.

8.5 Permeable wall modelling

The effect of the array of risers can be likened to permeable walls, through which the water, though obstructed, can flow. Such permeable walls can be modelled in a simple way, by making a rather approximate assumption. This is that the velocity of flow through the wall is proportional to the difference in head between the two sides of the wall. Such an approach has been used to predict flow through permeable walls of the type used in the 'Doris' design of gravity platform.[152].

8.6 Modified permeability

The preferred approach will be to modify the permeability of a region of the finite element mesh, so as to approximate the diffraction behaviour of the riser cylinders.

8.7 Changes in the wave equation

In this method a new wave equation is generated which models, in an approximate way, the presence of the cylinders. The usual derivation of shallow water wave theory was given in Chapter 1.

Again consider a small element of water, extending from the bed to the undisturbed free surface, with dimensions $\delta x \times \delta y \times h$, where h is the water depth. The element is shown in Figure 1.2.

The equation for horizontal momentum can be developed as follows. The elementary volume is given by

$$\delta x \times \delta y \times h. \tag{8.1}$$

The force due to the pressure gradient in the x direction is given by

$$-\frac{\partial p}{\partial x}\delta x \delta y \beta h, \tag{8.2}$$

where β is the percentage of the domain not occupied by the risers, as in Figure 8.2
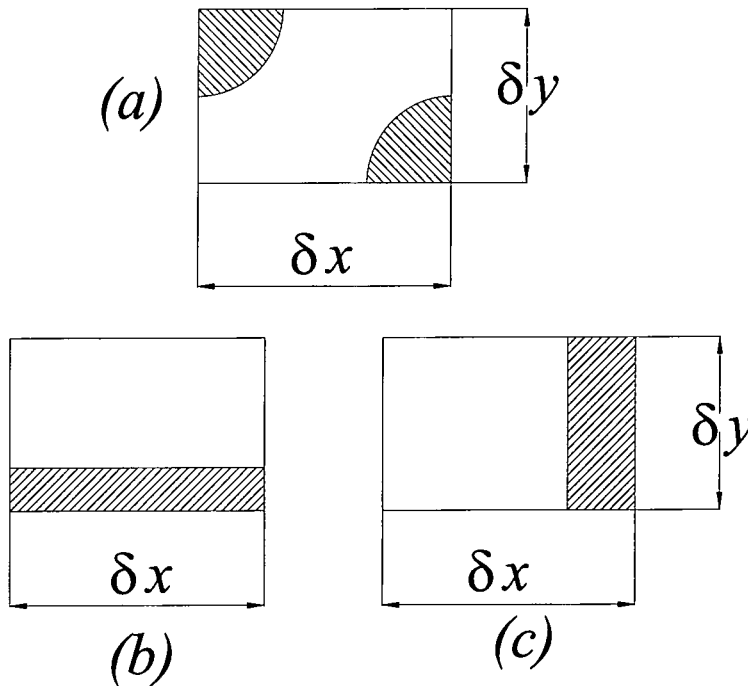
Area not occupied by risers $= \beta \delta x \delta y$

(a) example of true riser layout, (b) assumption for x direction momentum, (c) assumption for y direction momentum. In (a), (b) and (c) the shaded areas are equal

Approximation of elementary volume of riser zone

Figure 8.2   Elementary volume of riser zone

From Newton's second law, and using the hydrostatic relation,

$$p = \rho g(\eta - z). \tag{8.3}$$

The x direction momentum equation is

$$\frac{\partial u}{\partial t}\beta = -g\frac{\partial \eta}{\partial x}\beta \tag{8.4}$$

and that for the y direction is similarly

$$\frac{\partial v}{\partial t}\beta = -g\frac{\partial \eta}{\partial y}\beta, \qquad 8.5$$

where β is a constant, which models the effect of the 'blockage' of the section, by the presence of an obstruction. The left hand side of the equation is multiplied by a factor β because the elementary volume of fluid is now $\beta\delta x\delta yh$. The right hand side is also multiplied by a factor β because the elementary area over which the pressure acts is now $\beta\delta yh$. Apart from the introduction of β, everything is exactly as before.

Clearly, in the above equations, β simply cancels. In physical terms, there is less of an area for the horizontal pressure gradient to act over, but also there is less fluid for it accelerate. The two effects cancel. This is not to say that β disappears, since it will still be relevant at the interface between the partially blocked wave elements, and the completely free elements.

The continuity equation is next derived. The rate of flow into the elementary volume is given by

$$\beta\frac{\partial(uh)}{\partial x}\delta x\delta y + \beta\frac{\partial(vh)}{\partial y}\delta x\delta y, \qquad 8.6$$

and this can be equated to the rate of increase of volume, given by

$$\frac{\partial \eta}{\partial t}\delta x\delta y\beta. \qquad 8.7$$

Thus the continuity equation is obtained

$$\frac{\partial \eta}{\partial t}\beta = -\frac{\partial}{\partial x}\left(hu\right)\beta - \frac{\partial}{\partial y}\left(hv\right)\beta. \qquad 8.8$$

On substition of the momentum equations, 8.4 and 8.5, we finally obtain the wave equation.

$$\frac{\partial^2 \eta}{\partial t^2}\beta = g\left[\frac{\partial}{\partial x}(h\frac{\partial \eta}{\partial x}) + \frac{\partial}{\partial y}(h\frac{\partial \eta}{\partial y})\right]\beta. \qquad 8.9$$

Clearly the β term can be simply cancelled, in this case. *However* if elements which are to model the 'obstructed' or lower permeability zone, corresponding to the area of the risers, are to be used in conjunction with elements modelling the unobstructed fluid zone, then β must be retained. This point is explained more fully in Appendix E.

8.8 Numerical testing

The diffraction of the waves was modelled using finite and infinite elements, by the methods described in this thesis.

8.9 Diffraction by single cylinder

As a test of the program a problem of the diffraction of waves by a cylinder for a wave number, $k = 2$ was considered. Two different meshes of elements were used. The first was a cylindrical mesh of elements, generated automatically by the mesh generator SMACREA. This program is described in Chapter 5. The second was a mesh generated by the mesh generator, CYLGEN, also described in Chapter 5. CYLGEN is a mesh generator specially developed to deal with meshes of finite and infinite elements surrounding arrays of risers. In this case it was used to generate the mesh around a single cylinder, or riser. In both cases the radius of the cylinder was set to unity.
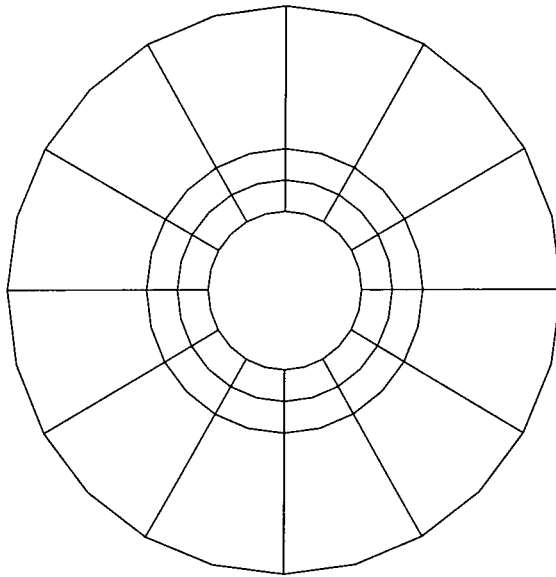
Diffraction of waves by solid cylinder, cylindrical mesh of finite and infinite elements

Figure 8.3   Cylindrical mesh

Figure 8.3 shows the mesh of finite and infinite elements generated by SMACREA, with a cylindrical polar type mesh. Figures 8.4 and 8.5 show contour plots of the real and imaginary components of the wave elevation in the vicinity of the cylinder. In addition, in figure 8.6 the two components of the wave elevation are plotted as functions of the angle around the cylinder for both meshes, and compared with the theoretical elevations. These theoretical elevations are generated by the program CYL, which evaluates the MacCamy and Fuchs solution[93]. The agreement is so close that the differences between the analytical and finite and infinite element results can hardly be discerned on the plots. The errors are shown in figure 8.7.
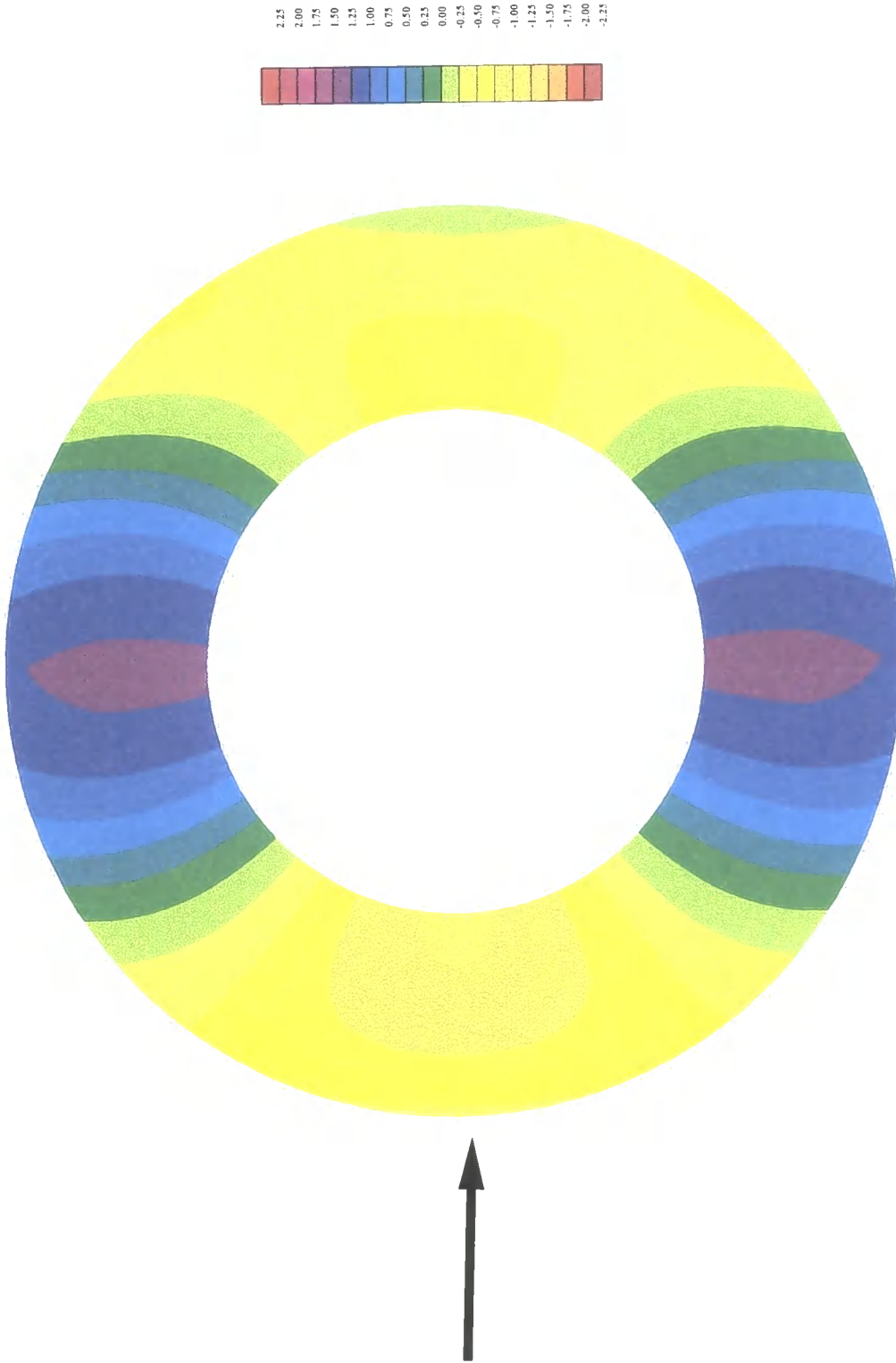
Figure 8.4   Real part of wave elevations - cylindrical mesh
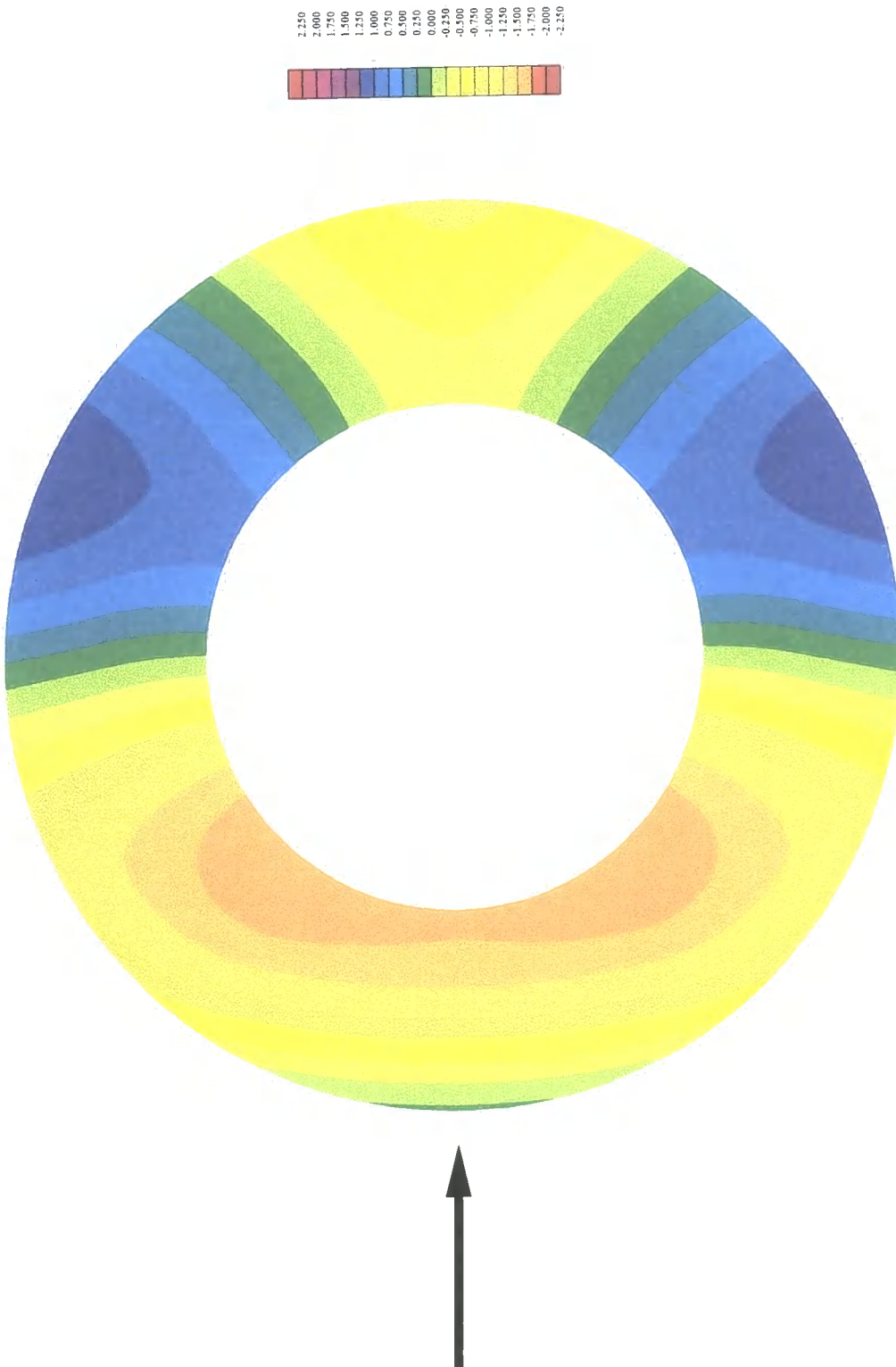
Figure 8.5 Imaginary part of wave elevations - cylindrical mesh
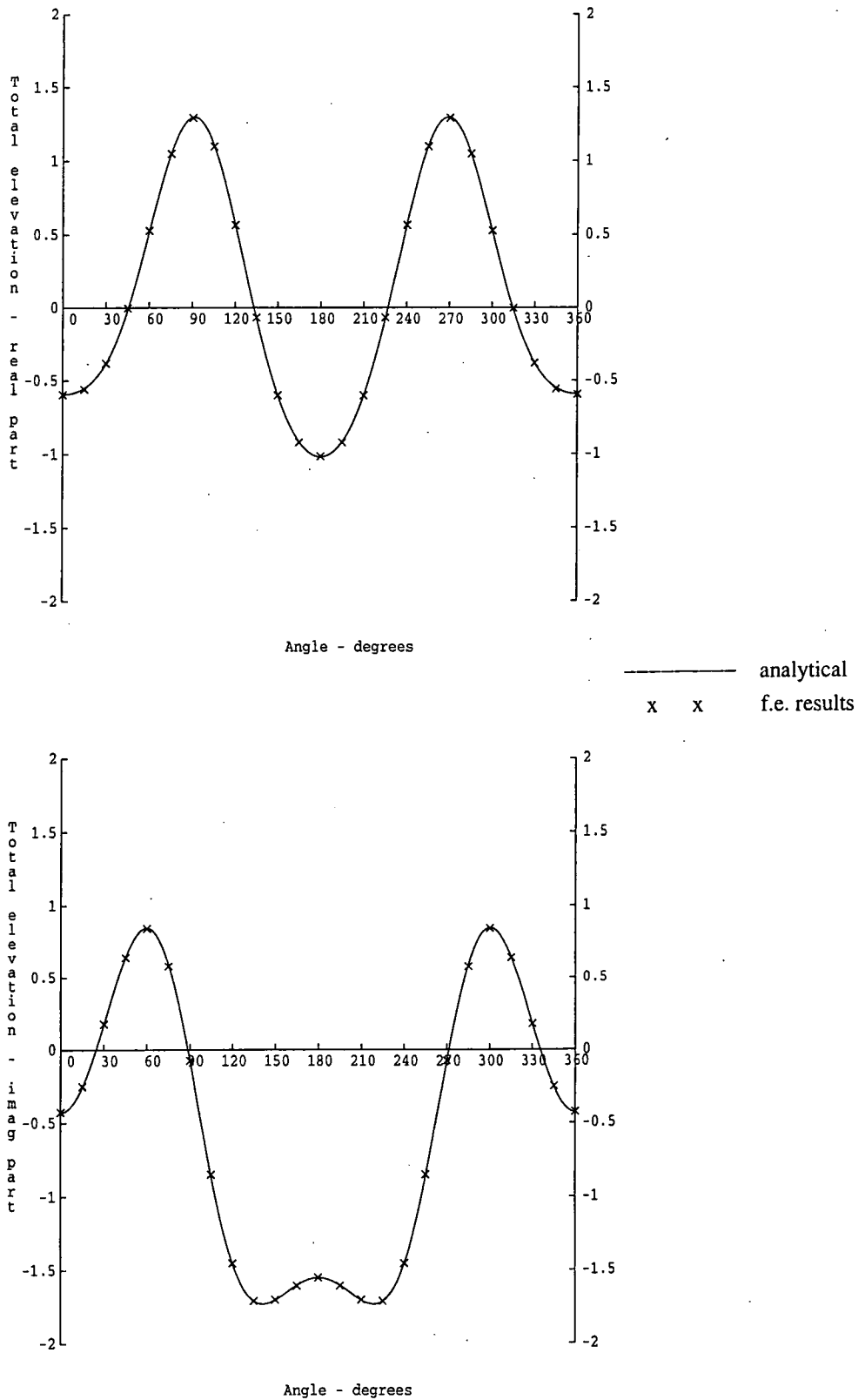
Wave elevations on surface of the cylinder - real and imaginary parts

Figure 8.6 Wave elevations on surface of the cylinder
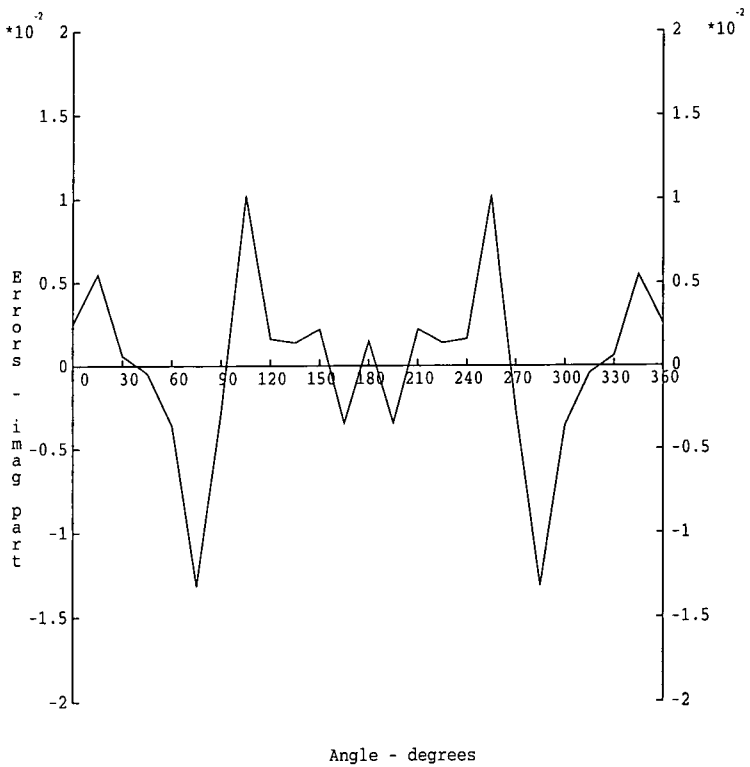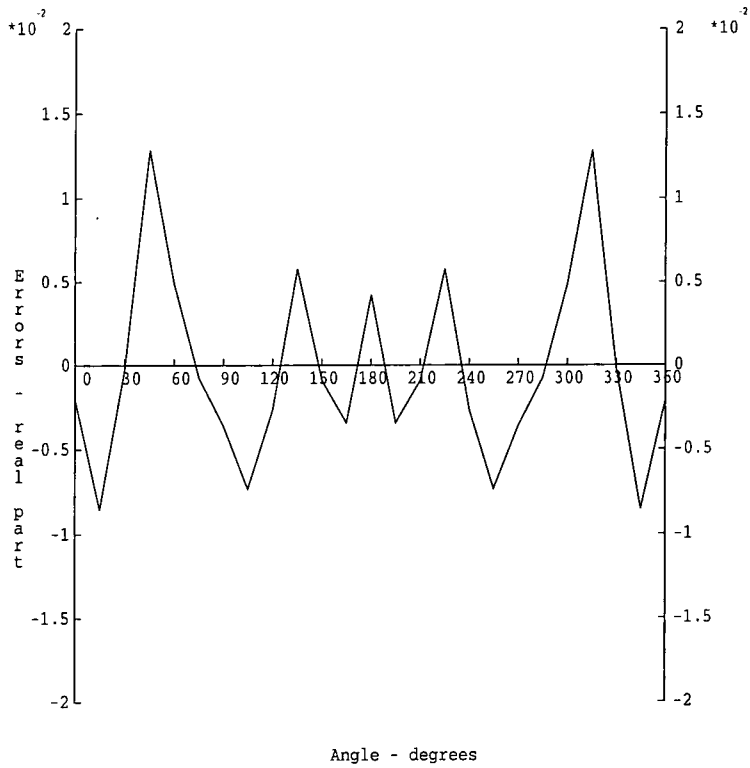
Errors in wave elevations on surface of the cylinder - real and imaginary parts

Figure 8.7   Errors in wave elevations on surface of the cylinder

Figures 8.8 to 8.12 repeat the above results, but with a part orthogonal and part radial mesh used for the arrays of risers, although in this case only the one riser is present. Again the accuracy is excellent.

Altogether the results give confidence in both the finite and infinite element wave diffraction progam, and in the mesh generators. The next step is to investigate the numerical validity of the reduced permeability effect derived above.
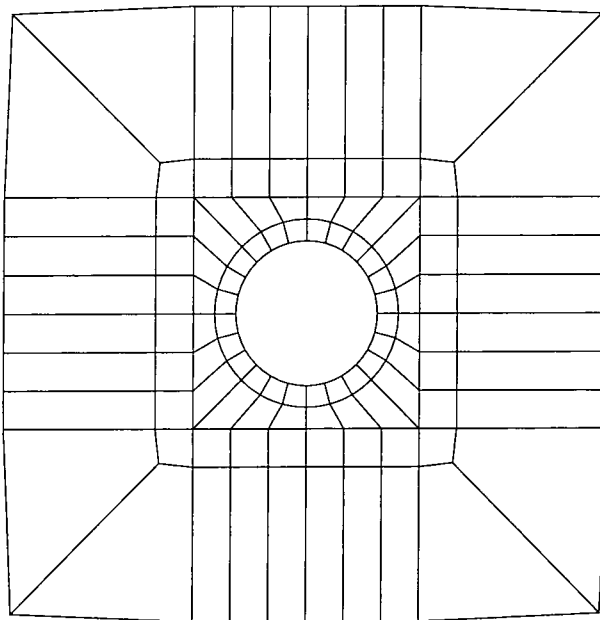
Diffraction of waves by solid cylinder, rectangular mesh of finite and infinite elements

Figure 8.8   Rectangular mesh

8.10   Reduced permeability

If equation 8.9 represents a good model of the effect of some sort of region with a high density of cylinders or risers, then we should be able to confirm at least its limiting behaviour, by solving a cylinder problem, with an outer cylinder, with modified permeability. That is we consider the diffraction of waves by a rigid cylinder. We first generate a mesh of finite and infinite elements about the cylinder, and confirm that the exact analytical solution, due to McCamy and Fuchs[93] is recovered. This was described in the previous paragraph. Next we replace the outer annulus of the cylinder with fluid elements, as shown in figure 8.13, which would normally lead to a different
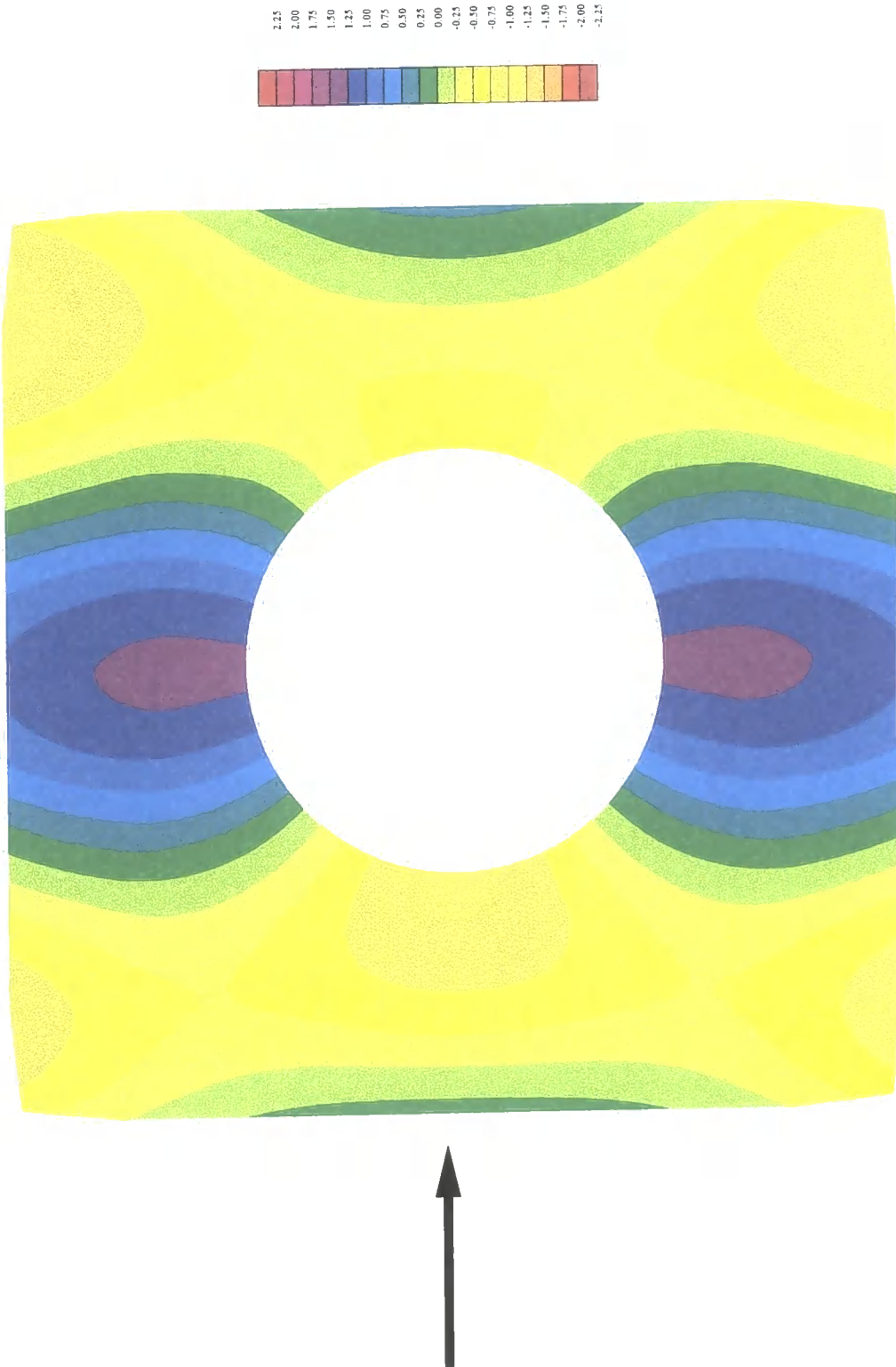
Figure 8.9   Real part of wave elevations - rectangular mesh
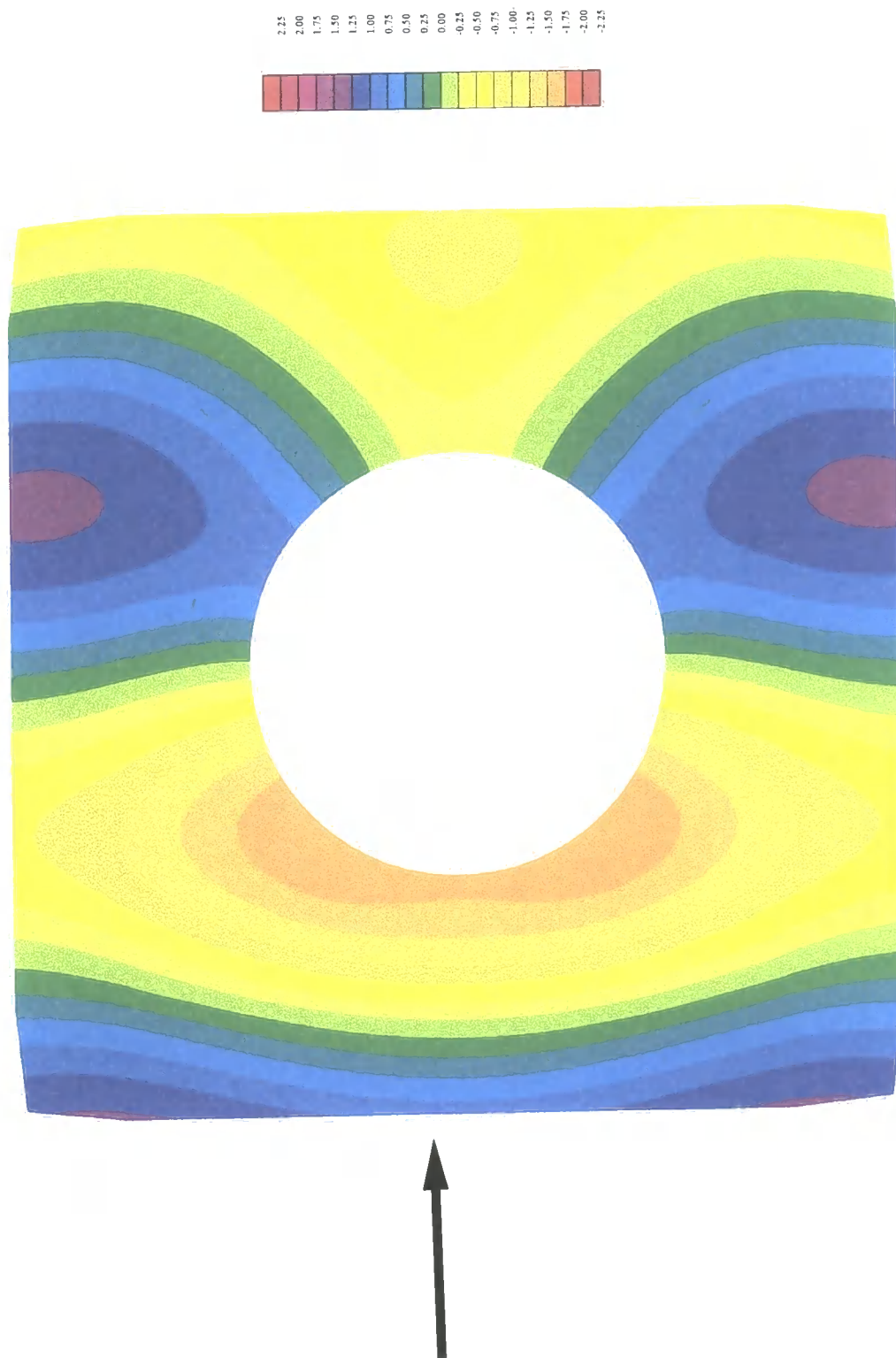
Figure 8.10   Imaginary part of wave elevations - rectangular mesh
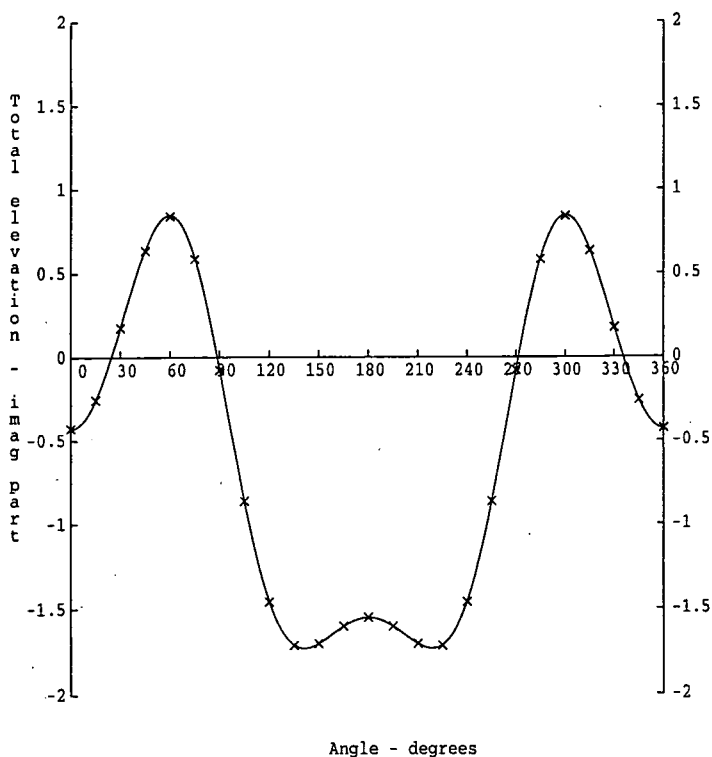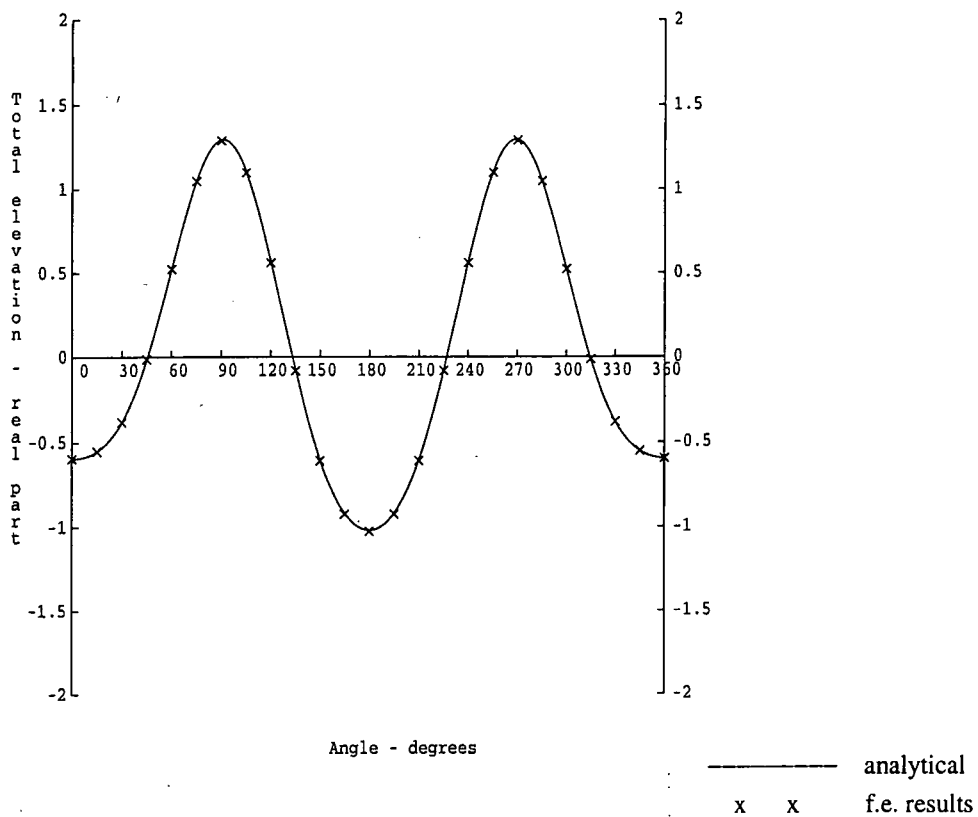
Wave elevations on surface of the cylinder - real and imaginary parts

Figure 8.11 Wave elevations on surface of the cylinder - rectangular mesh
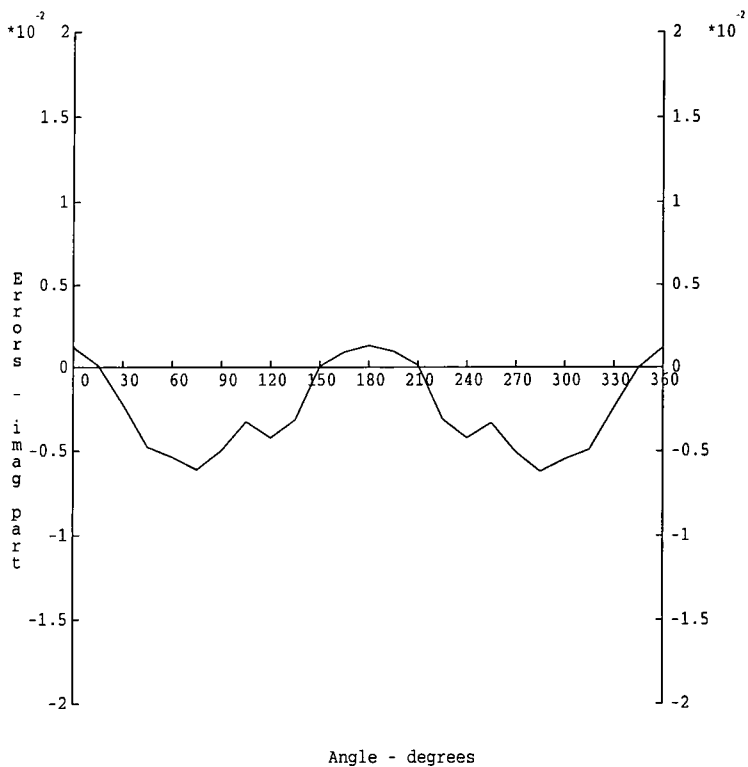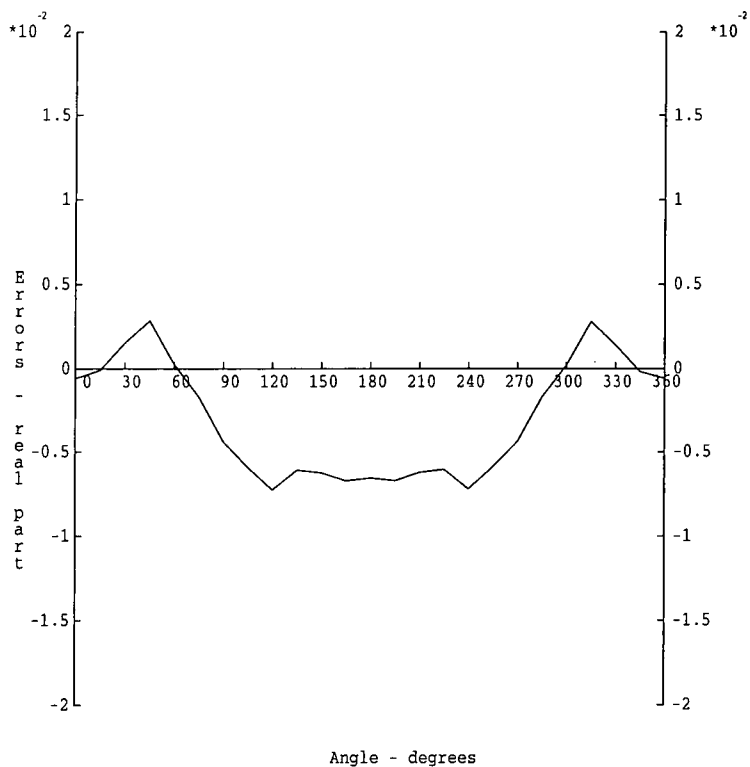
Errors in wave elevations on surface of the cylinder - real and imaginary parts

Figure 8.12   Errors in wave elevations on surface of the cylinder - rectangular mesh

diffraction solution. This would be the solution for a cylinder of smaller diameter. But the elements modelling the outer annulus of the cylinder are given an artificially low permeability, or in the nomenclature above, β is made small, in this case 0.01.
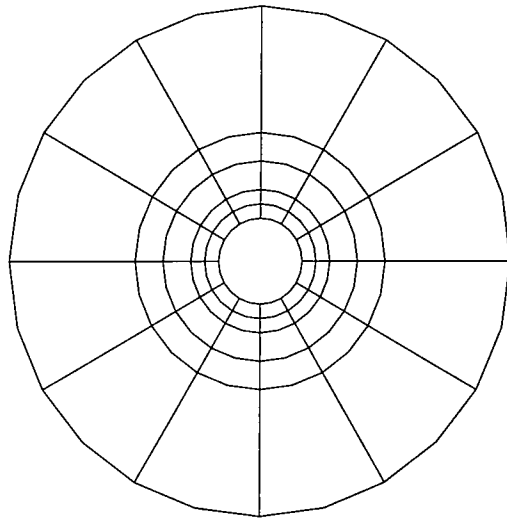
Diffraction of waves by solid and partly permeable cylinder, cylindrical mesh of finite and infinite elements. Inner layer permeability is 0.01

Figure 8.13   Cylindrical mesh for composite cylinder

A necessary condition for the above theory to be correct is that the original (large diameter) cylinder solution should be recovered. The results from the above numerical experiment are shown in figures 8.14 to 8.17 and the results confirm that the model is satisfactory in this respect. This does not, of course, prove that the model is universally accurate. But they validate, at least in the limit, the modified permeability approach.
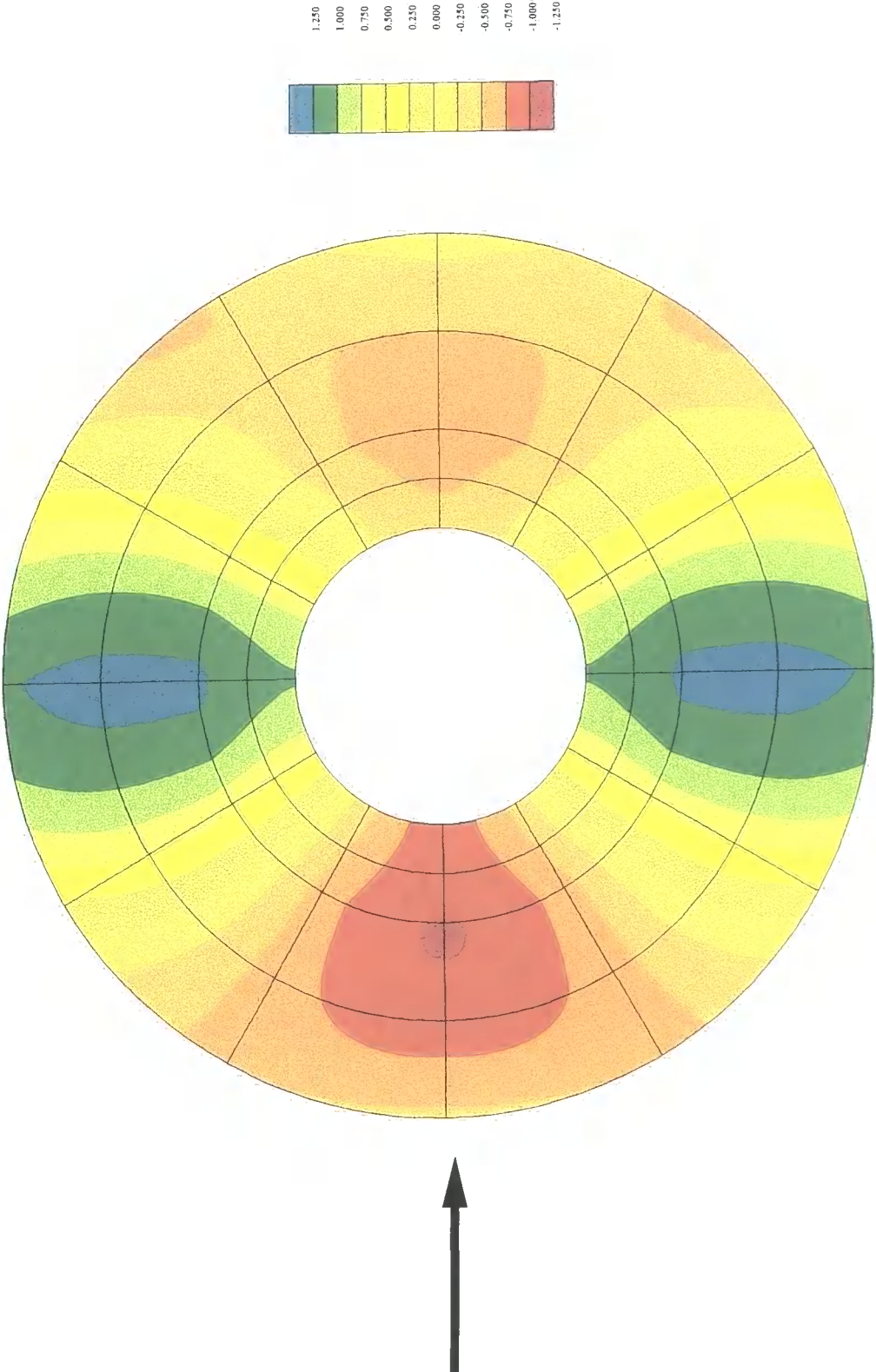
Figure 8.14   Real part of wave elevation - composite cylinder
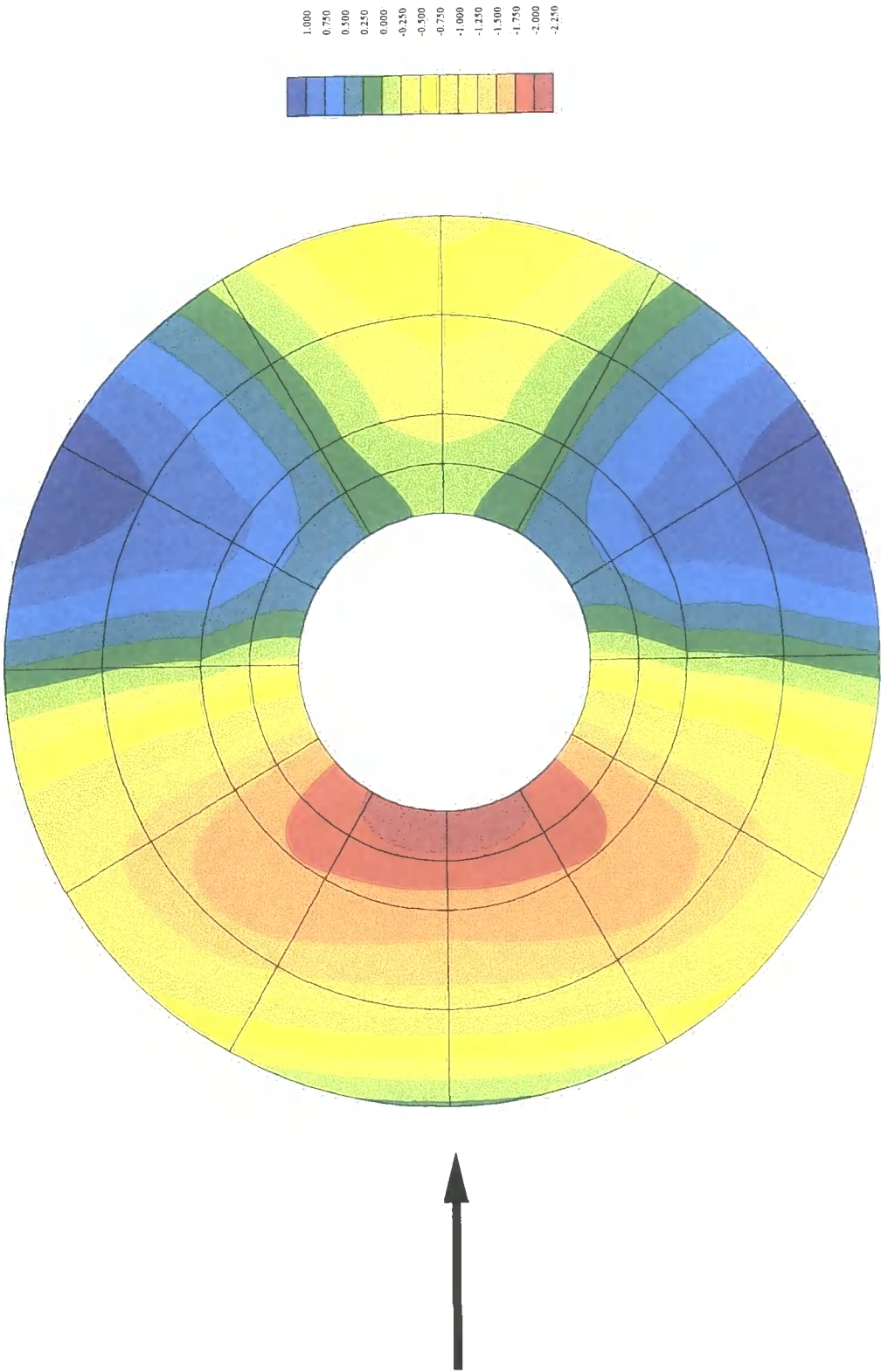
Figure 8.15   Imaginary part of wave elevation - composite cylinder
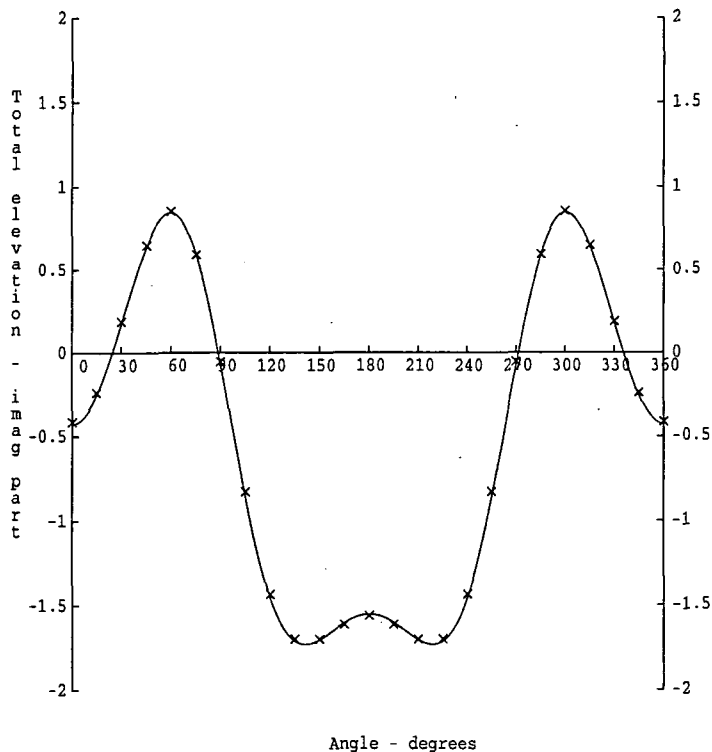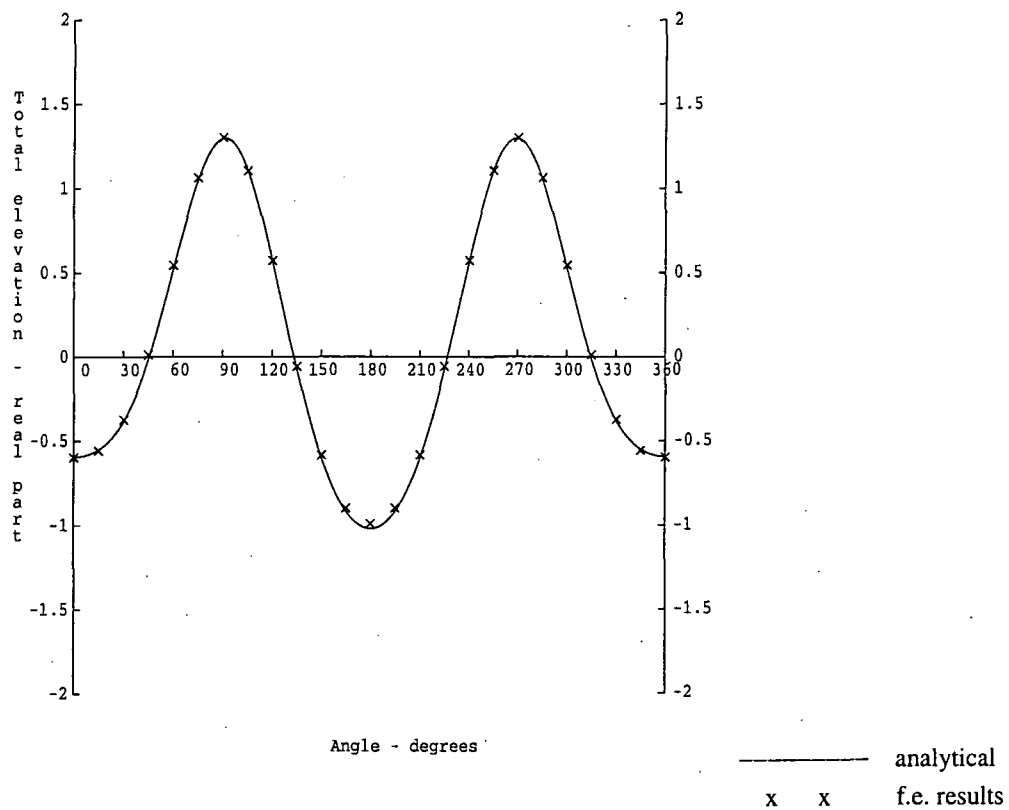
Diffraction of waves by partly permeable cylinder, wave elevations on surface of the cylinder - real
and imaginary parts

Figure 8.16   Wave elevations on surface of the cylinder - composite cylinder
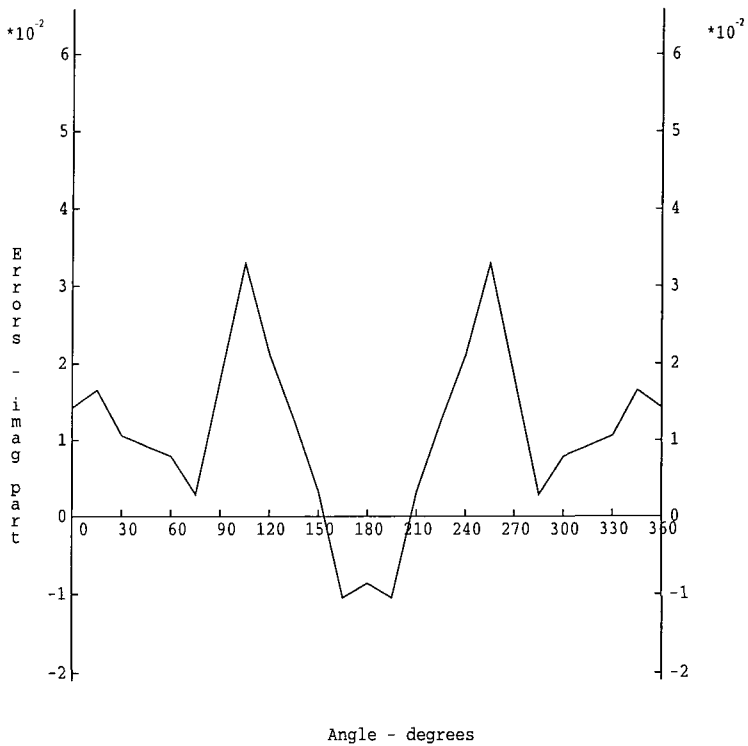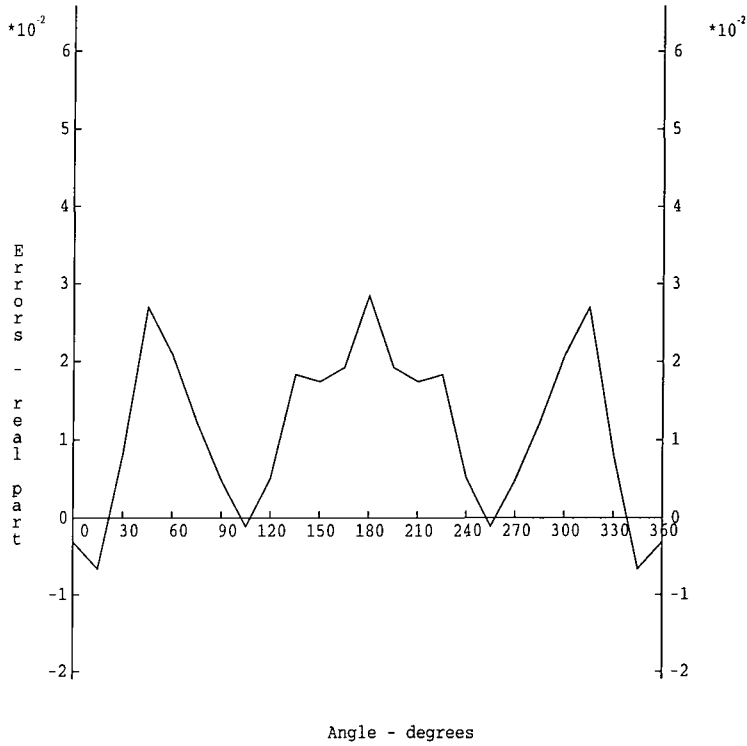
Diffraction of waves by partly permeable cylinder, errors in wave elevations on surface of the cylinder - real and imaginary parts

Figure 8.17   Errors in wave elevations on surface of the cylinder - composite cylinder

8.11 Wave diffraction by multiple cylinders

As a further test, this section is devoted to a comparison of the finite and infinite element results with the series results of Linton and Evans[92]. Linton and Evans have published a series solution for the diffraction of waves by an array of cylinders. The cylinders can be arbitrary in their location and diameter, and extend from the free surface to the sea bed. Their method is essentially an extension and generalisation of the method of Havelock[77] and MacCamy and Fuchs[93]. It involves matrix inversion to find the values of a number of coefficients. In their paper they give a series of contour plots of the absolute values of wave elevations in the vicinity of the cylinders. In particular they consider an array of four cylinders located at the corners of a square, with a range of wave directions and wave lengths. These results will be generated using the finite and infinite element program, as a check.

In order to compare with Linton and Evans[92], two sorts of finite and infinite element meshes were generated around an array of four cylinders, which Linton and Evans had considered, and the contour plots of the wave elevations were compared. The two meshes used are shown in figures 8.18 and 8.19.

Figures 8.20 to 8.28 show reproductions of the Linton and Evans contour plots, together with contour plots derived from the present finite and infinite element solutions. All of the results are plotted over the same area $(-3.0 \leq x/h \leq 3.0 \quad \text{and} \quad -3.0 \leq x/h \leq 3.0)$ and using the same contour interval.

Figures 8.21 and 8.22 show results for a coarse and fine mesh for the case of an incident wave of 45° and $kh = \pi$. The results show very good agreement with those of Linton and Evans shown in Figure 8.20. The change in mesh density makes very little difference to the values of the elevations. It should be noted that the Linton and Evans contour plots show small assymmetries in places. This effect is probably due to the contour plotting algorithm used by Linton and Evans.

Similarly, figure 8.28 shows very good agreement with the Linton and Evans results in figure 8.27 for the case of an incident wave of 0° and $kh = 2\pi/5$. However, the case of an incident wave of 0° and $kh = 2\pi/3$ compared in figures 8.23, 8.24 and the case of an incident wave of 0° and $kh = 2\pi/4$ compared in figures 8.25, 8.26 show marked differences. In both sets of results, the general form of the contours is similar, but the peaks are in different places. Also in figure 8.26 there is a trough at the right which does not appear in figure 8.25. On looking more closely at these two sets of Linton and Evans results, it does seem strange that there are peaks after the first pair of cylinders rather than before them, as in the case shown in figure 8.27. In figure 8.26, the results show a standing wave to the left of the left-most cylinders of the correct form and wavelength. One would expect this effect as the incident waves will be partially reflected from the cylinders. The Linton and Evans results show no such effect.

These results need further investigation to determine the cause of the discrepancies especially as two sets of results show good agreement.
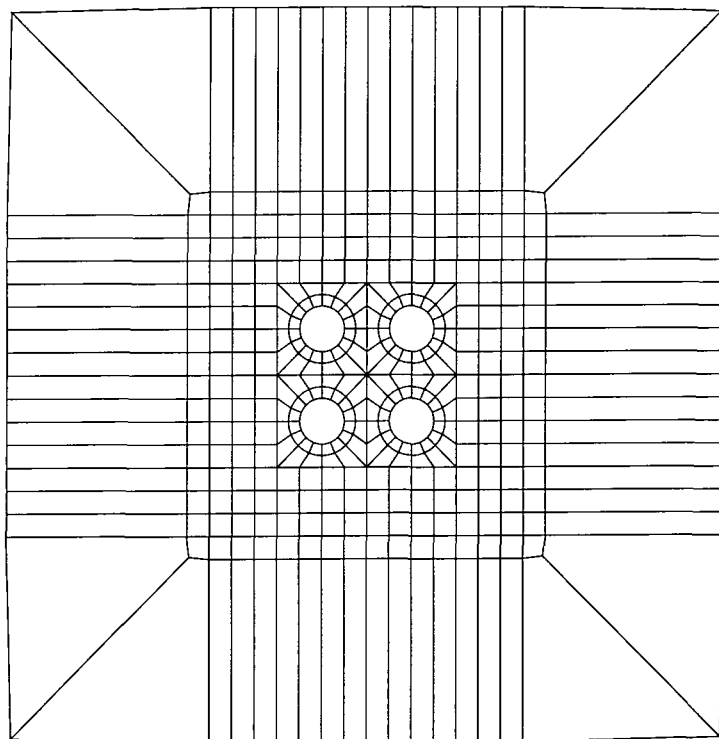
Figure 8.18 Coarse rectangular mesh for array of square cylinders
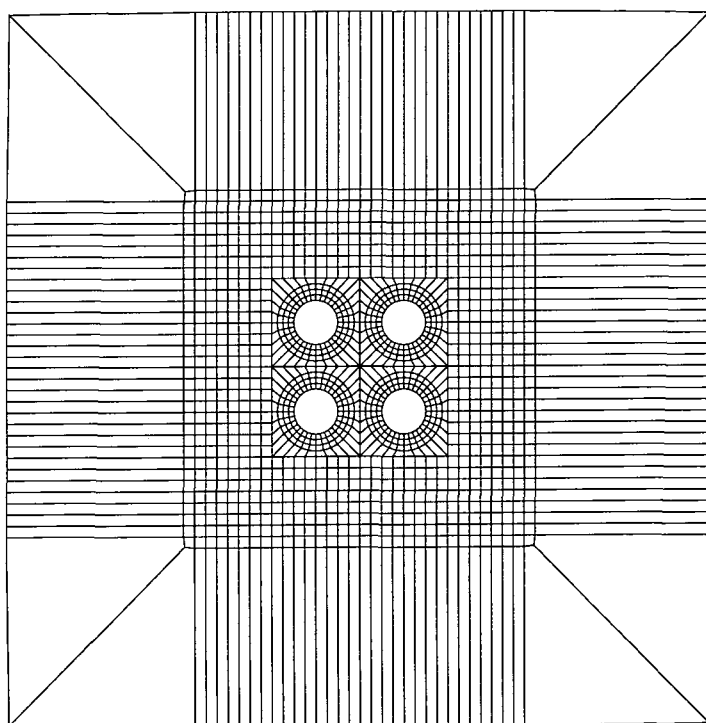
Figure 8.19 Fine rectangular mesh for array of square cylinders
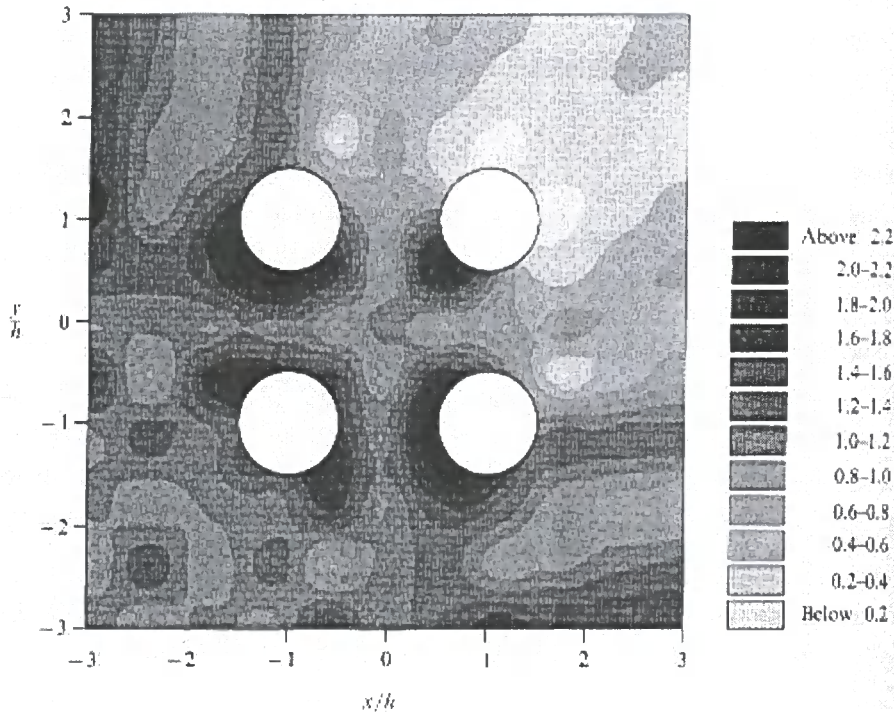
Diffraction of wave by a square array of vertical circular cylinders

Linton & Evans results, incident wave 45°, kh = π

Figure 8.20 Linton and Evans results. Absolute part of wave elevations, $\theta = 45°$, kh = π
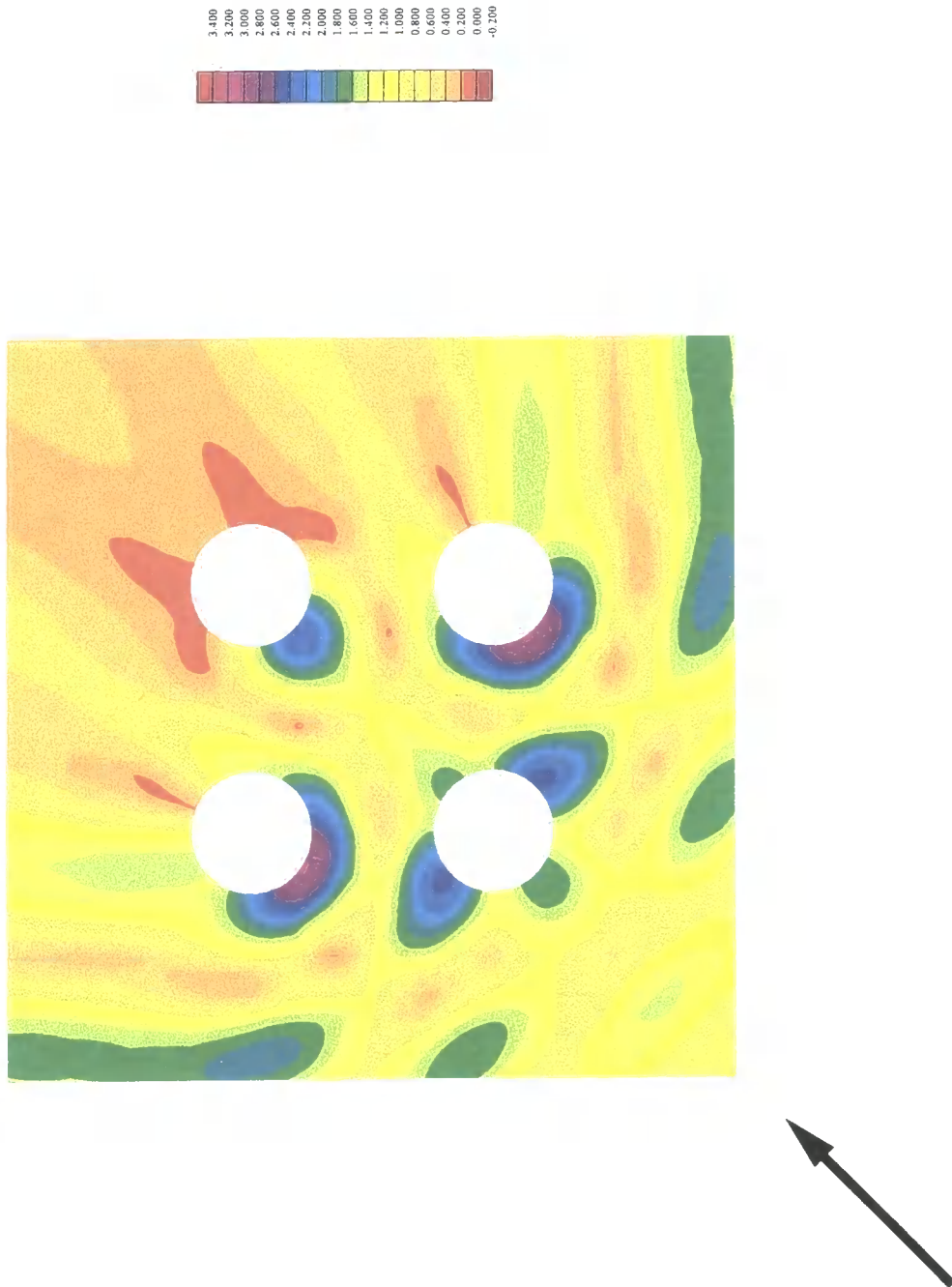
Figure 8.21 Coarse mesh, absolute part of wave elevations, incident wave = 45, kh = pi
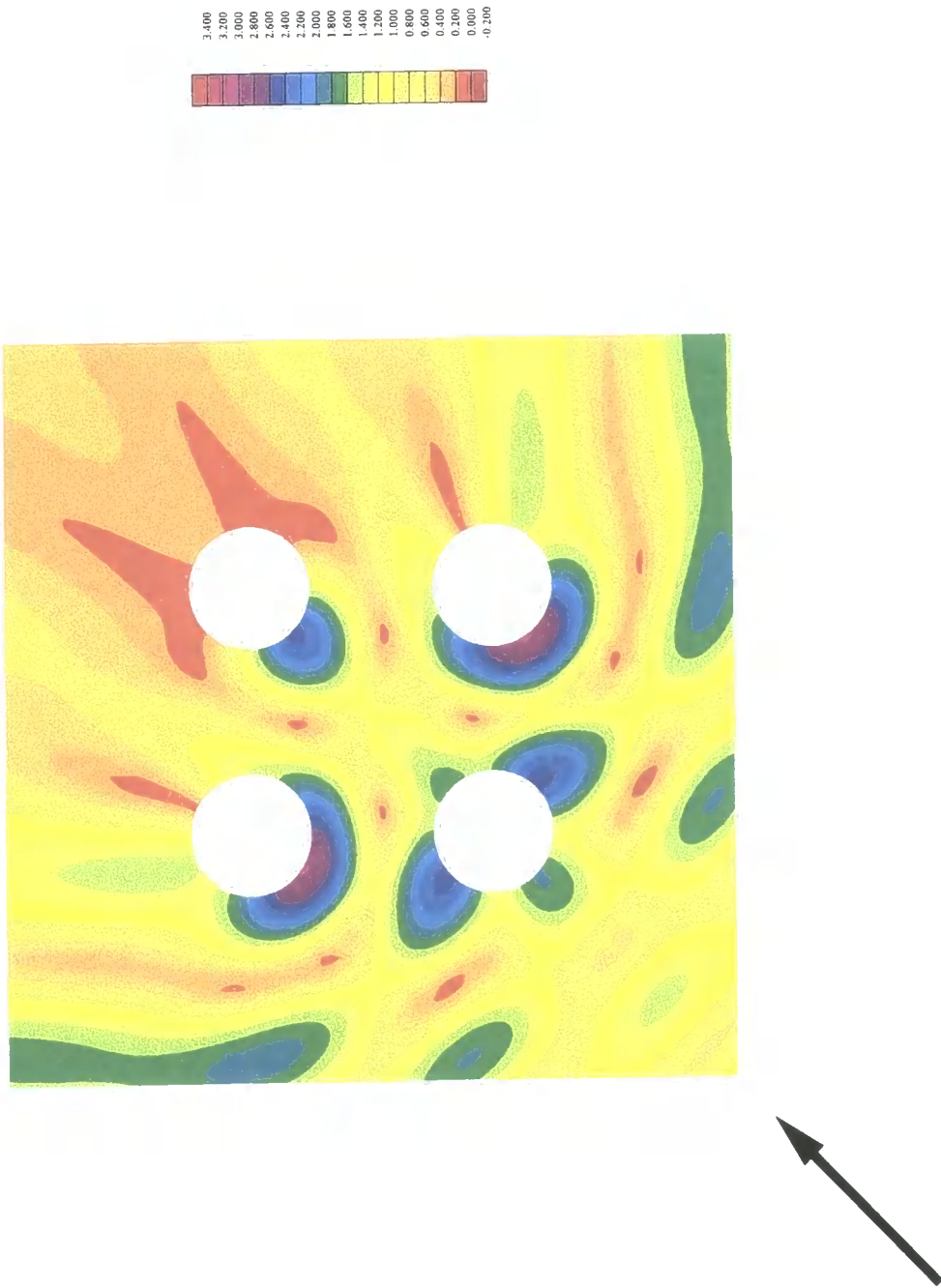
Figure 8.22 Fine mesh, absolute part of wave elevations, incident wave = 45, kh = pi
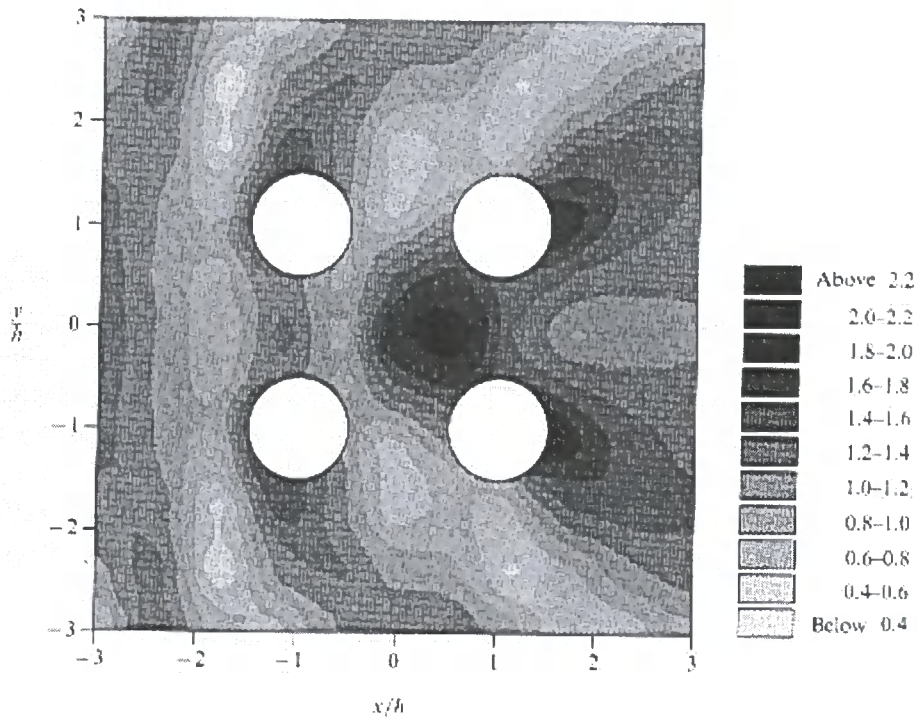
Diffraction of wave by a square array of vertical circular cylinders

Linton & Evans results, incident wave $0°$, $kh = 2\pi/3$

Figure 8.23 Linton and Evans results. Absolute part of wave elevations, $\theta = 0°$, $kh = 2\pi/3$
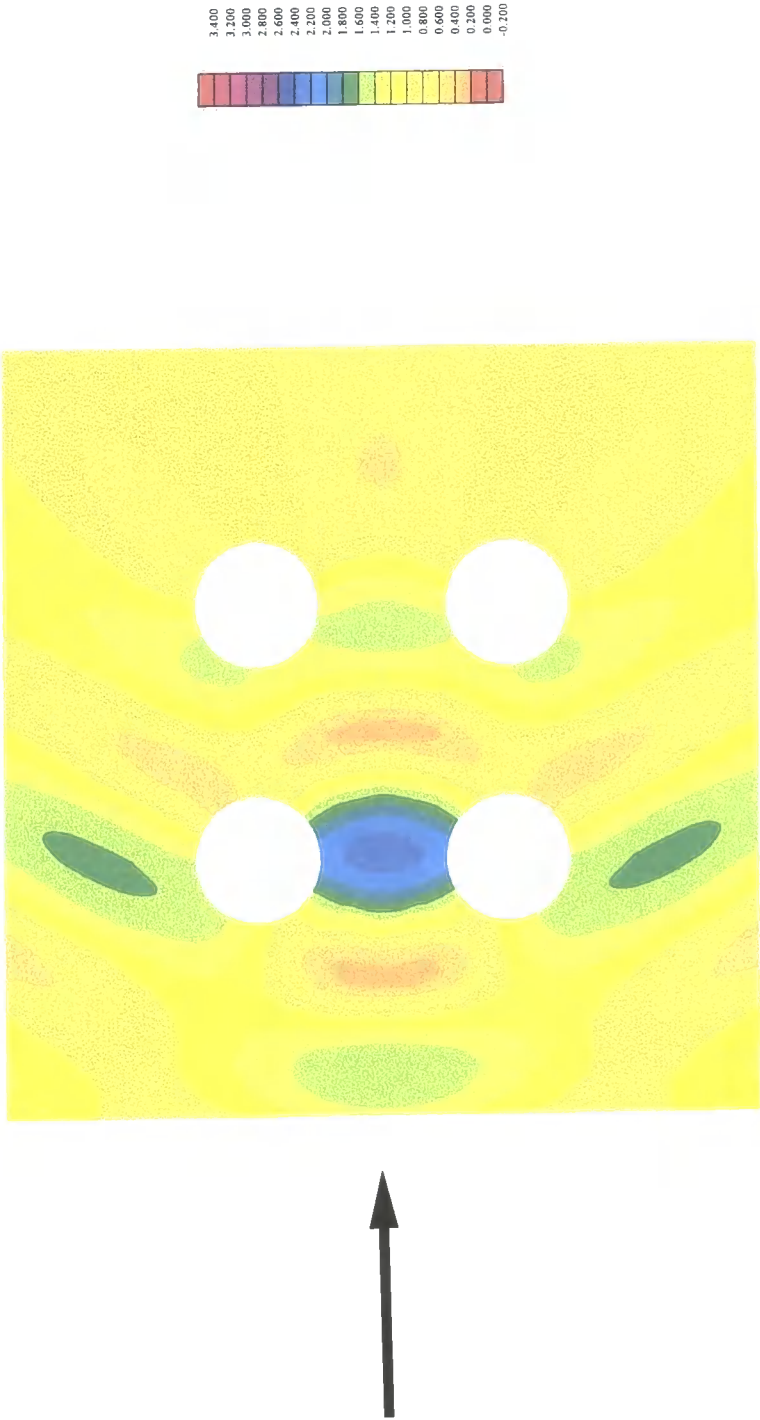
Figure 8.24 Coarse mesh, absolute part of wave elevations, incident wave = 0, kh = 2pi/3
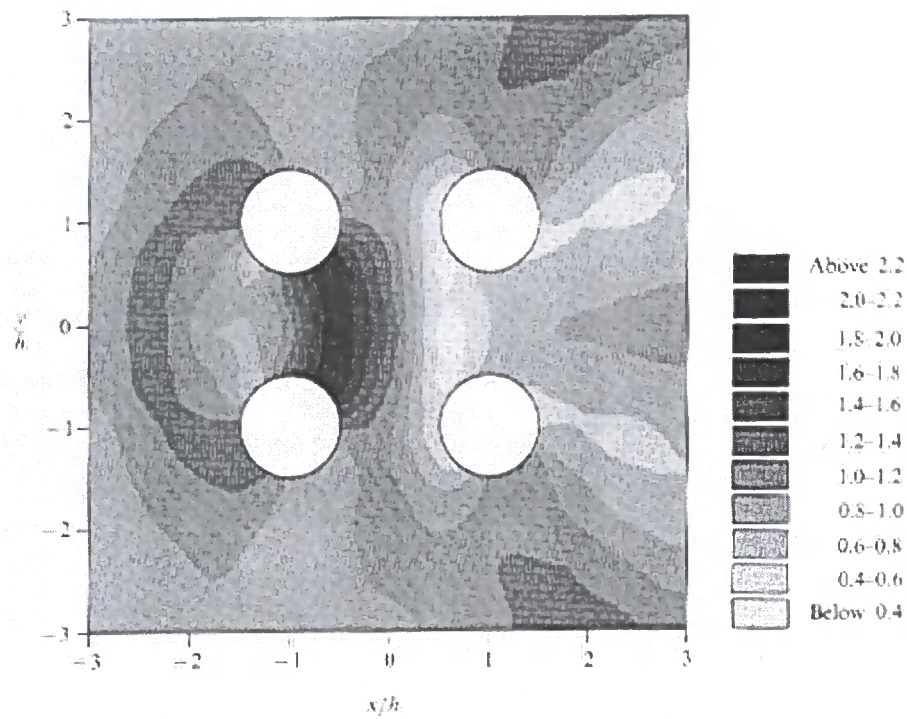
Diffraction of wave by a square array of vertical circular cylinders

Linton & Evans results, incident wave $0°$, kh $= 2\pi/4$

Figure 8.25 Linton and Evans results. Absolute part of wave elevations, $\theta = 0°$, kh $= 2\pi/4$
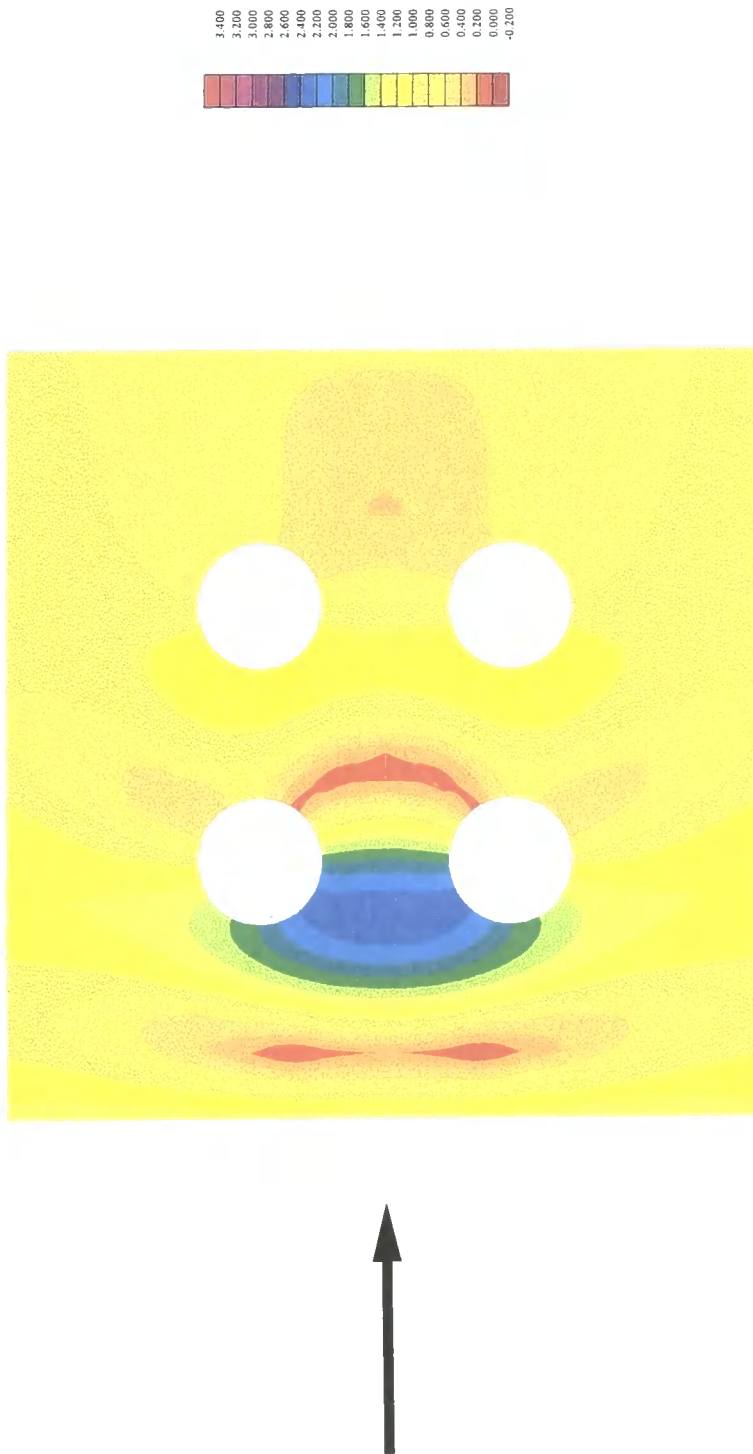
Figure 8.26 Coarse mesh, absolute part of wave elevations, incident wave = 0, kh = 2pi/4
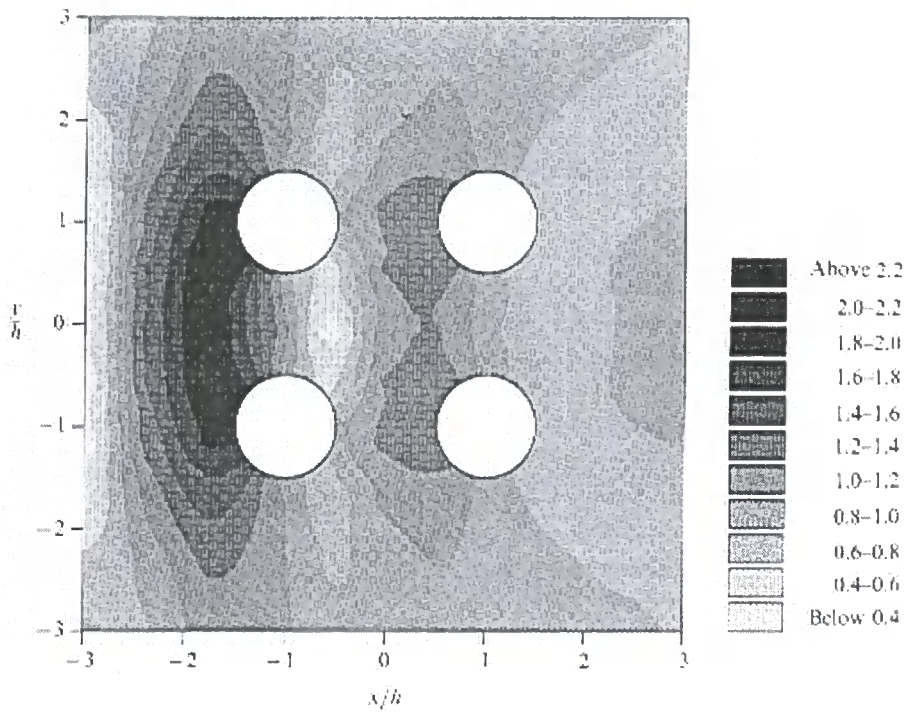
Diffraction of wave by a square array of vertical circular cylinders
Linton & Evans results, incident wave 0°, kh = 2π/5

Figure 8.27 Linton and Evans results. Absolute part of wave elevations, θ = 0°, kh = 2π/5
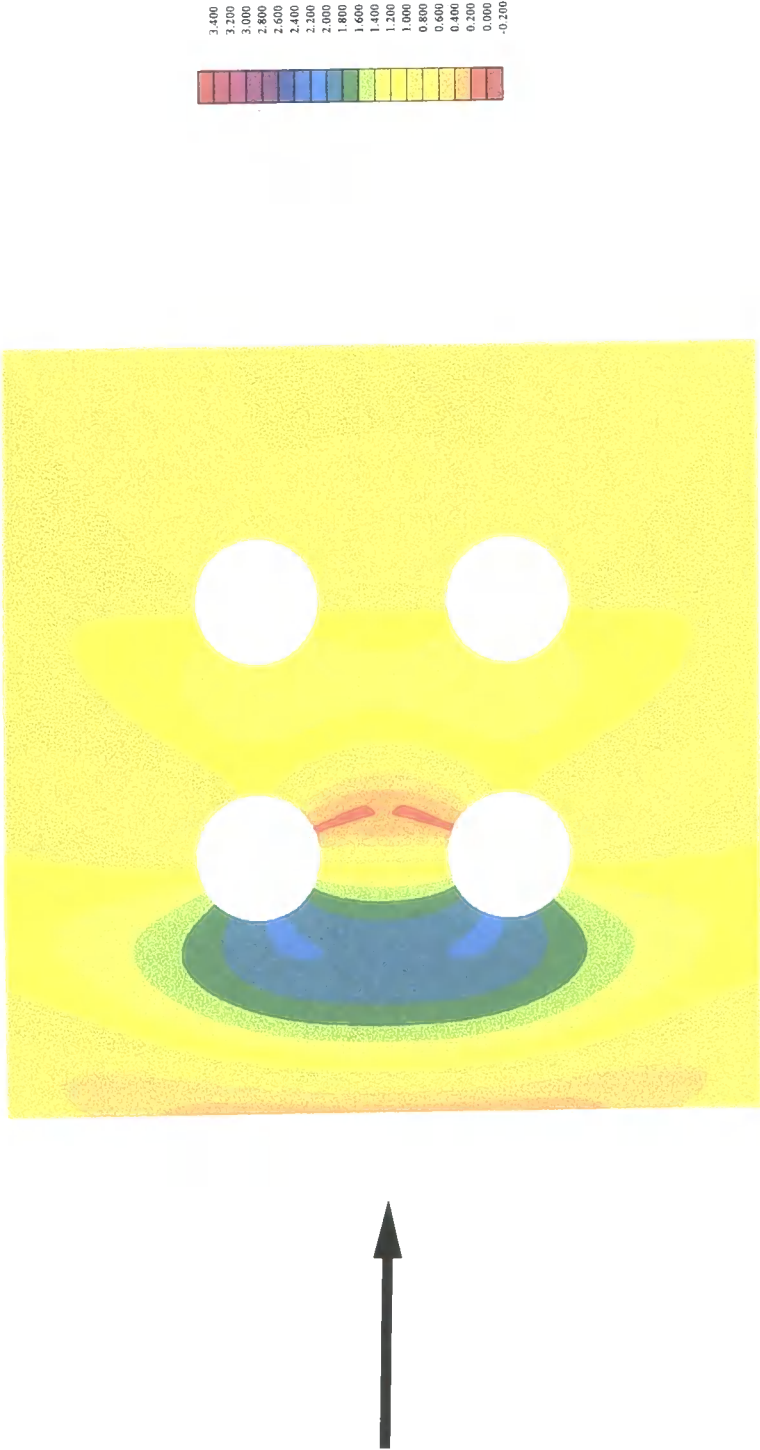
Figure 8.28 Coarse mesh, absolute part of wave elevations, incident wave = 0, kh = 2pi/5

8.12 Calculation of wave energy

As a preliminary to diffraction calculations, in this section we calculate the wave energy incident upon a vertical cylinder, and compare it with the energy dissipated by the cylinder, through the drag force. We also thus give an indication of whether the energy lost to viscous dissipation is significant, in relation to the wave energy.

8.13 Incident wave energy and power

We consider a plane monochromatic wave. For this case Kinsman[85] gives the expression 8.10 for the power incident upon a line parallel to the wave crest, per unit length of crest as

$$P_w = \left(\frac{\rho g^2}{32\pi}\right) H^2 T, \qquad\qquad 8.10$$

where P is the power, ρ is the density of the water, g is acceleration due to gravity, H is the wave height, crest to trough and T is the wave period. In water of intermediate depth expression 8.10 becomes

$$P_w = \left(\frac{\rho g H^2}{8}\right)\left(\frac{\omega}{k}\right)\left(\frac{1}{2}\right)\left[1 + \frac{2kh}{\sinh 2kh}\right]. \qquad\qquad 8.11$$

Expression 8.11 includes 8.10 as a special case, of course.

Now consider a specific wave, typical of the Rough Field in the southern North Sea, in which

Water depth	20 m
Water density	1025 kg/m^3
Wave frequency	1.0 s^{-1}
Wave period	6.283 s
Wave amplitude	4 m
Riser diameter	0.72 m

From these base parameters, others were calculated.

Wave length	59.817 m
Wave number	0.10504 m^{-1}

The power, P, can be calculated for the deep water case as

$$P_w = 1025\frac{\text{kg}}{\text{m}^3} \times \left(\frac{9.81\text{m}}{\text{s}^2}\right)^2 \times \left(\frac{1}{32\pi}\right)(8\text{m})^2 \times 2\pi\frac{\text{sNs}^2}{\text{kgm}}$$

$$P_w = 0.39457 \times 10^6 (\text{Nms}^{-1})\text{m}^{-1}$$

The more precise, intermediate depth water calculation gives

$$P_w = \left(\frac{1}{8} \times 1025 \times 9.81 \times 64\right)\left(\frac{1.0}{0.10504}\right) \times \frac{1}{2}\left[1 + \frac{2 \times 0.10504 \times 20}{\sinh 2 \times 0.10504 \times 20}\right]$$

$$P_w = 0.43110 \times 10^6 (\text{Nms}^{-1})\text{m}^{-1}$$

For a depth of 40m, a period of about 14 seconds and a wave amplitude of 10m, corresponding aproximately to a fifty year storm wave at the site of the Rough Field, we obtain

$$P_w = 0.65421 \times 10^7 (\text{Nms}^{-1})\text{m}^{-1}$$

8.14   Power absorbed by cylinder

Now consider a vertical cylinder in the wave flow, with water depth 20 m and diameter 0.72 m.

The drag force due to Morison's equation is

$$F = \frac{1}{2}\rho C_d D u |u| \qquad\qquad 8.12$$

per unit length, and this needs to be integrated with respect to the depth. The rate of doing work is

$$P = \frac{1}{2}\rho C_d D u^2 |u|. \qquad\qquad 8.13$$

The velocity, u, at a given point can be written as

$$u = \frac{kga_0}{\omega} \sin\omega t \frac{\cosh k(h+z)}{\cosh kh}. \qquad\qquad 8.14$$

The average power will have to be integrated over a wave cycle, and over the height of the cylinder. This evaluation of the work done, by the drag forces on the cylinder, will require two integrals, namely

$$\int_{t=0}^{t=T/2} \sin^3 \omega t\, dt = \frac{4}{3} \times \frac{T}{2\pi}$$

$$\int_{z=-h}^{z=0} \cosh^3 k(h+z)dz = \left(\frac{1}{k}\right)\left[\frac{1}{3}\sinh^3 kh + \sinh kh\right] = \alpha. \qquad\qquad 8.15$$

The integrals of the squared quantities are also needed. Details are given in Appendix D. The above expressions can now be used to evaluate the work done by the drag forces on the cylinder, in a half wave period as

$$W = \frac{1}{2}\rho C_d \times \frac{4}{3}\frac{T}{2\pi}\left(\frac{kga_0}{\omega}\right)^3 \times \frac{\alpha}{\cosh^3 kh}. \qquad\qquad 8.16$$

The power will thus be expression 8.16 divided by $T/2$, which gives

$$P = \frac{1}{2}\rho C_d \times \frac{4}{3}\frac{1}{\pi}\left(\frac{kga_0}{\omega}\right)^3 \times \frac{\alpha}{\cosh^3 kh}. \qquad\qquad 8.17$$

8.15 Incident and absorbed powers compared

Next the power incident upon the wave front, per unit length, and the power dissipated by the viscous forces on the cylinder calculated above are compared. A small fortran program called POWER has been written to evaluate the quantities, and its output has been checked by hand. This leads to the following result.

Wave front average power:

$$P_w = 0.43110 \times 10^6 (\text{Nms}^{-1})\text{m}^{-1}$$

Cylinder average power

$$P_c = 0.45241 \times 10^5 \text{Nms}^{-1}$$

Equivalent front width = 0.10494 m

The corresponding values for the Rough Field site, mentioned in section 8.13 are:

$$P_w = 0.65421 \times 10^7 (\text{Nms}^{-1})\text{m}^{-1}$$

$$P_c = 0.62361 \times 10^6 \text{Nms}^{-1}$$

and equivalent front width = 0.09532 m

The cylinder thus absorbs all the power from a wave front of width roughly 0.1m. This is a significant amount of power, and its abstraction from the waves should have an observable effect on the wave field.

There are many assumptions in the above calculation. A major uncertainty is the area over which the dissipation of the power, due to viscous forces takes place. The orbital excursion of the water particles in the wave can be calculated. We can assume that most of the dissipation will take place within that domain. This is an approximation since vortices in the wake can interact, and cause velocities which project them beyond the domain of the orbits, as calculated by linear wave theory. It is however, a reasonable working hypothesis.

8.16 Diffraction tests

The program SMAWAVE was run on the case of a small array of six risers, set out in a 2 by 3 pattern, associated with a British Gas jacket structure in the south of the North Sea. The geometry of the risers is shown in Figure 8.29.

The following problem and wave parameters were set up:

Water depth	20 m
Water density	1025 kg/m^3
Wave frequency	1.0 s^{-1}
Wave period	6.283 s
Wave amplitude	4 m
Riser diameter	0.72 m

From these base parameters, others were calculated.

Wave length	59.817 m
Wave number	0.10504 m^{-1}

As a test, the wave diffraction pattern was first computed with no damping. The frequency was increased in this case to 4 radians/s, in order to increase the diffraction effects. The analysis was done in three versions, as follows:
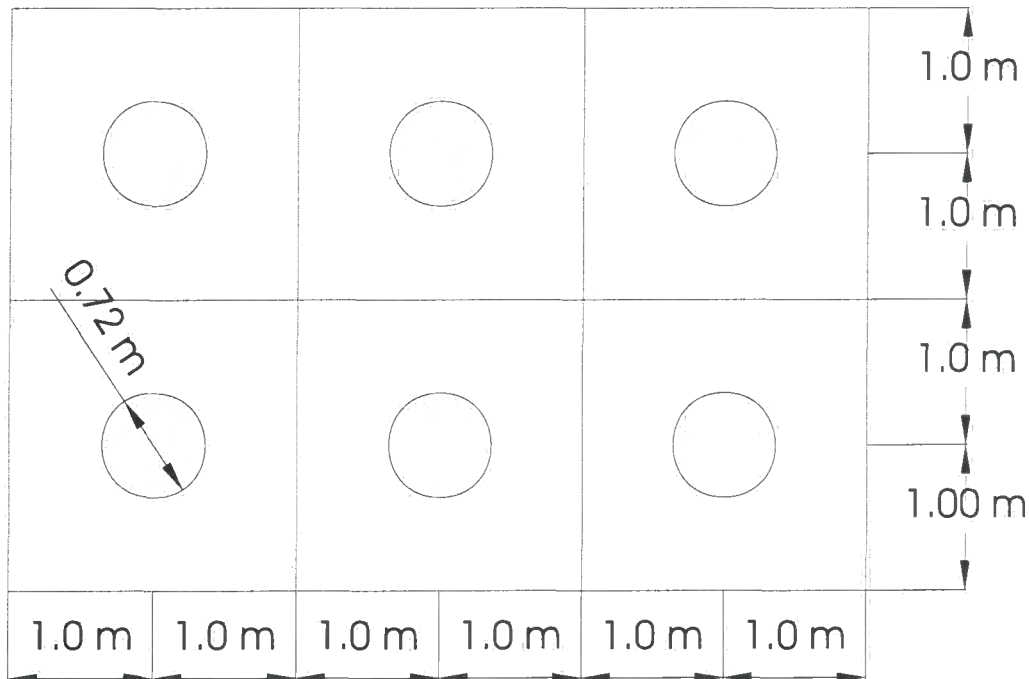
Figure 8.29   Array of risers - British Gas data

8.17 Risers absent

With no risers present the waves should continue as long crested progressive waves. This was indeed the case confirming the accuracy of the model. Contours of the real and imaginary parts of the wave elevation are plotted in Bettess and Bettess[46].

8.18 Mesh around invidual risers

The mesh generation program, CYLGEN was used to generate a mesh of finite elements around the risers, in which case all the risers were explictly modelled. Figures 8.30 to 8.32 show the mesh of elements and the contours of the real and imaginary parts of the wave elevation for this pure diffraction case. The wave elevations appear to be reasonable. As a check, the wave diffraction pattern was also calculated with the six cylinders shrunk down to very small radii. The wave diffraction pattern was, as expected, similar to that with no cylinders present.
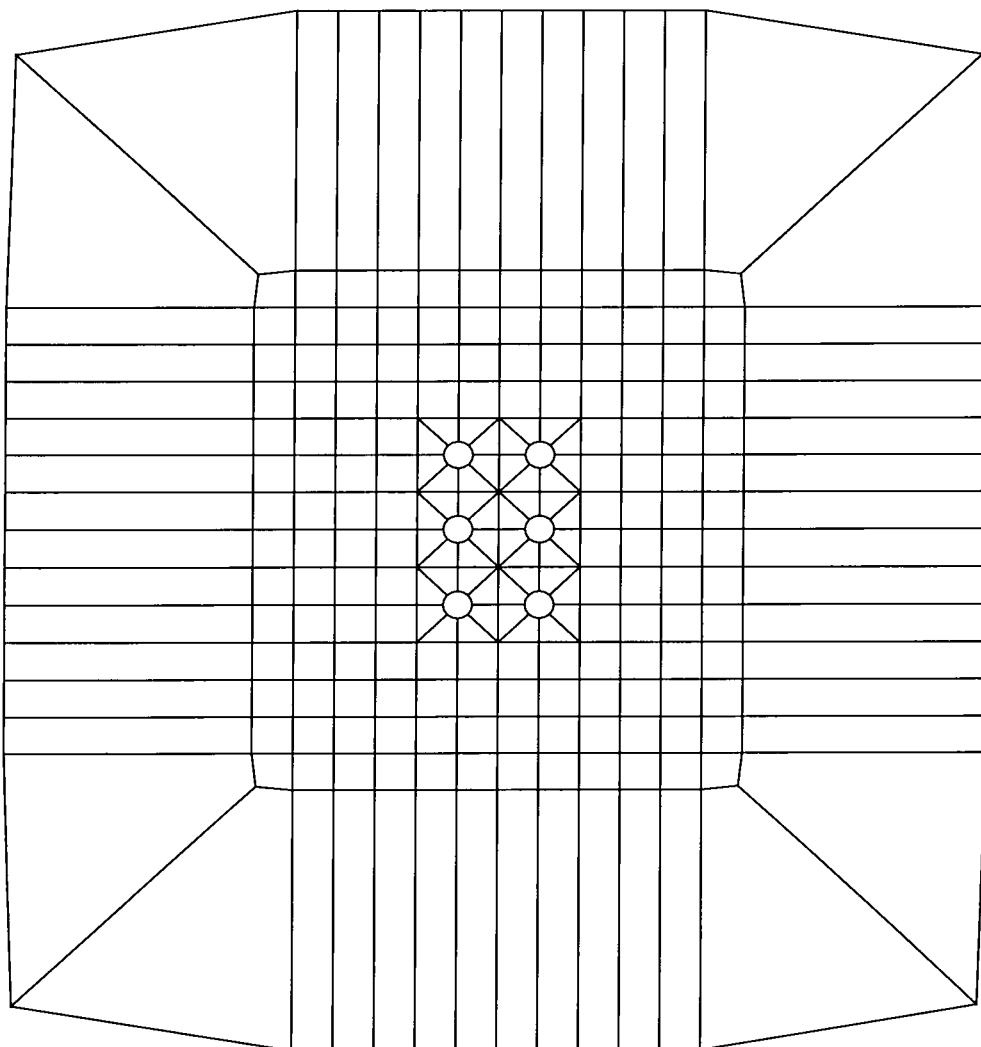
Figure 8.30 2 by 3 array of risers - generated mesh
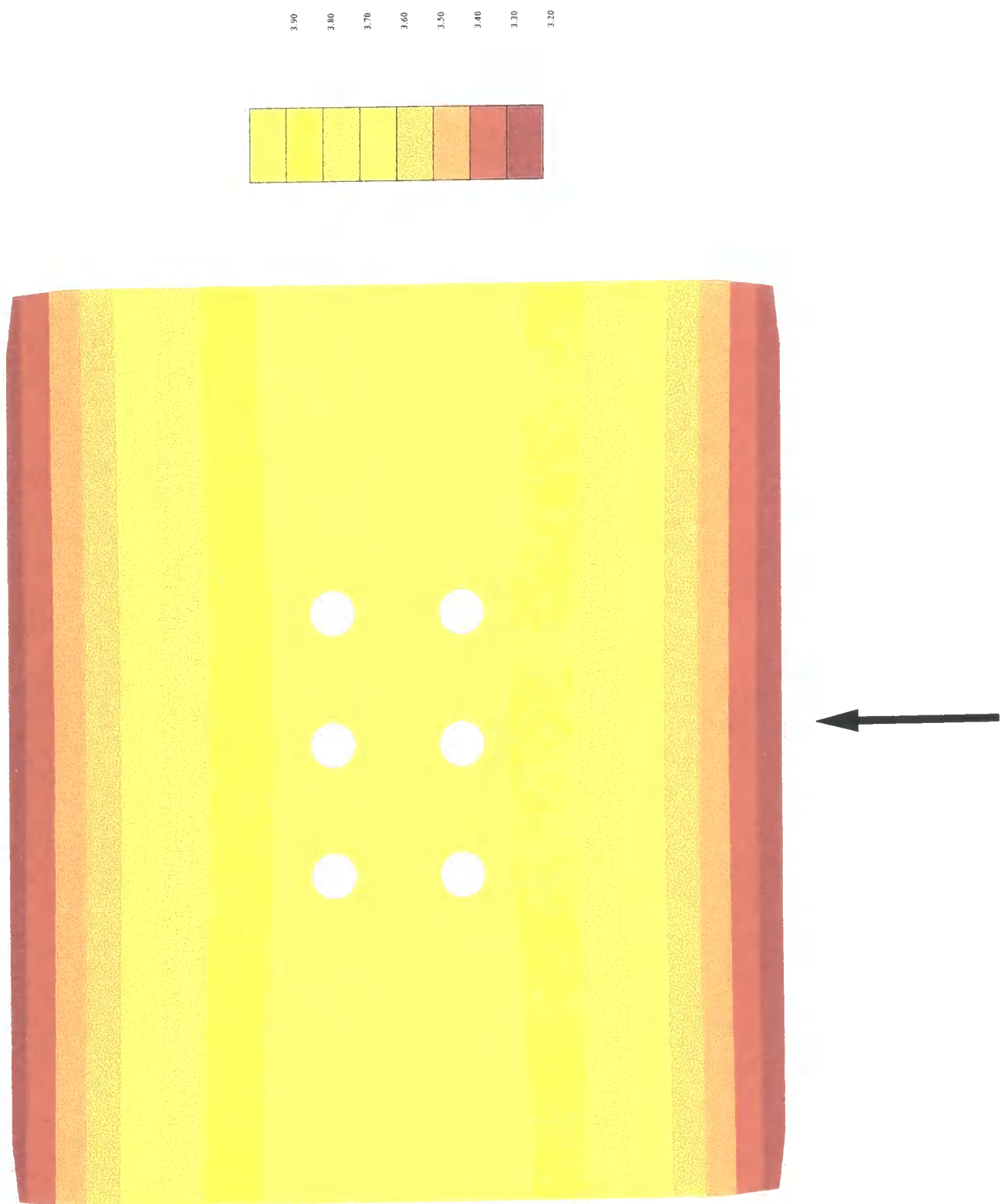
Figure 8.31 Real part of wave elevations, 2 x 3 array of risers, frequency = 1.0
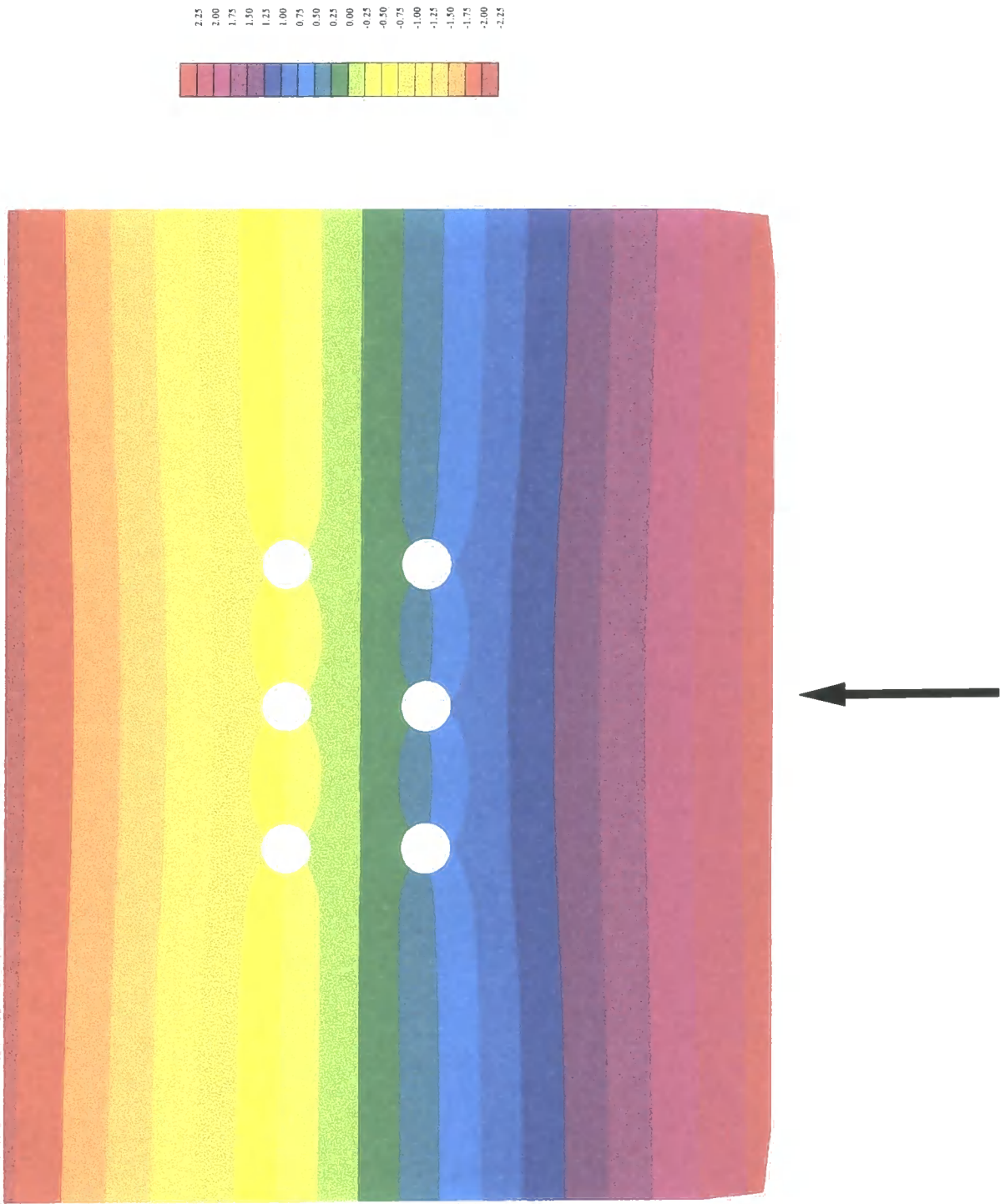
Figure 8.32 Imaginary part of wace elevations, 2 x 3 array of risers, frequency = 1.0

The mesh generation program SMAGEN was then used to generate a mesh where no risers were explicitly modelled, but the permeability of the riser zone was modified so as to account for the presence of the risers. In this case the permeability constant, β, see equations 8.1 to 8.9, was supposed to be of the order of the ratio of the rectangular area in which the risers were placed, divided by the area minus the area of the risers themselves. Each riser is located in an area, which has been slightly idealised as 2m by 2m, that is 4m^2. The diameter of the risers is 0.72 m, giving an area for each riser of 0.407 m^2 and thus a permeability constant of about 0.9. The program was run for several different permeability values, namely 0.9, 0.85, 0.8 and 0.6. The frequency was increased to $\omega = 4.0\mathrm{s}^{-1}$, since this would increase the diffraction effects. Figures 8.33 to 8.35 show the real, imaginary and absolute values of the wave elevation, using the precise finite element model of the risers, for the increased frequency value. The following figures show the wave elevations for the range of permeability values, again in sequence, real imaginary and absolute for the values of permeability as follows:

Figures 8.36 to 8.38 , permeability = 0.90
Figures 8.39 to 8.41 , permeability = 0.85
Figures 8.42 to 8.44 , permeability = 0.80
Figures 8.45 to 8.47 , permeability = 0.60

The results indicate that the permeability constant should be made rather larger than arguments based on equal area would suggest. The optimal value for comparison with the true cylinder results seems to be about 0.60, judging from the figures listed. The best comparisons for the two methods seem to be obtained from the absolute value of the wave elevation.
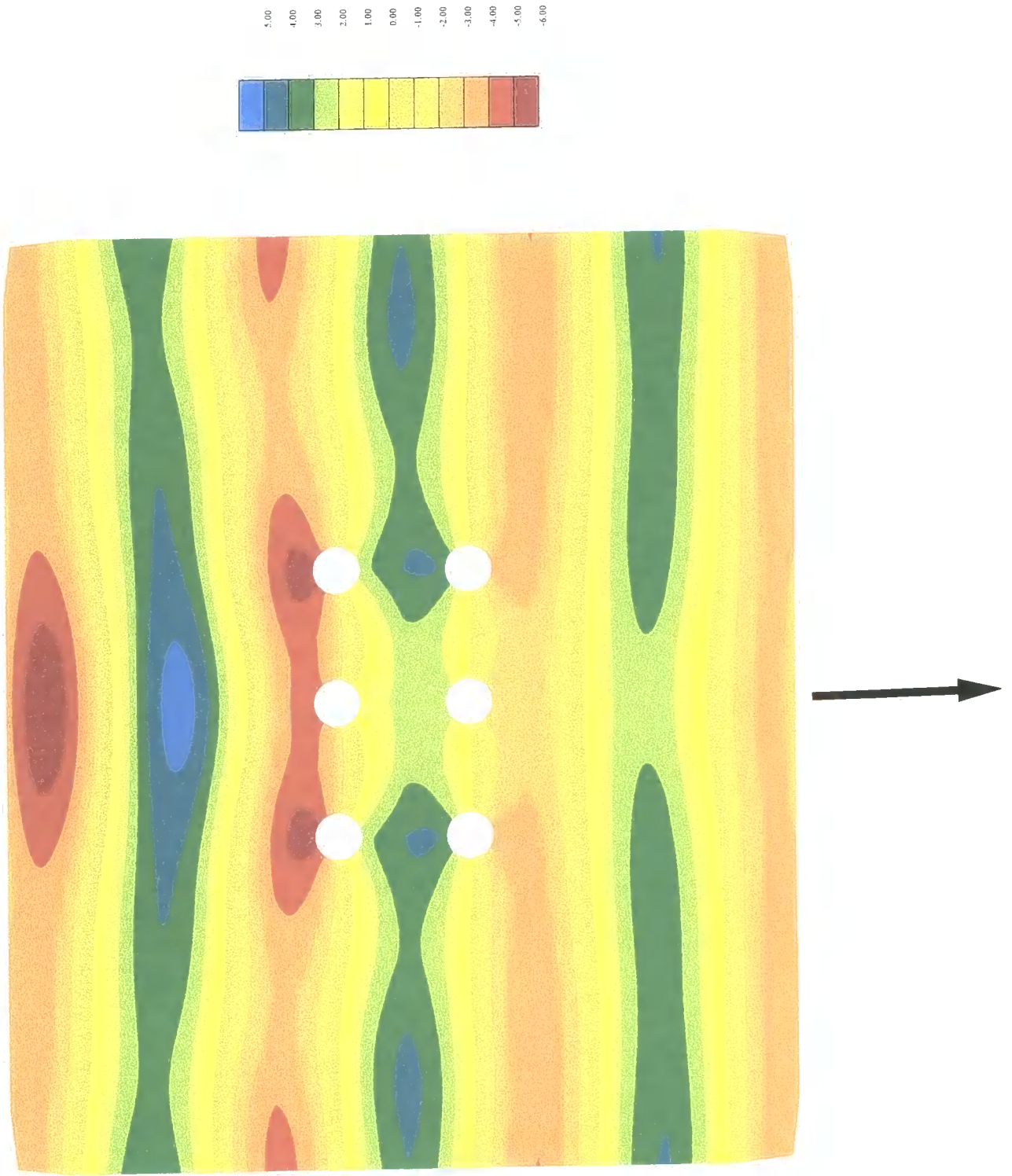
Figure 8.33   Real part of wave elevations, 2 x 3 array of risers, frequency = 4.0
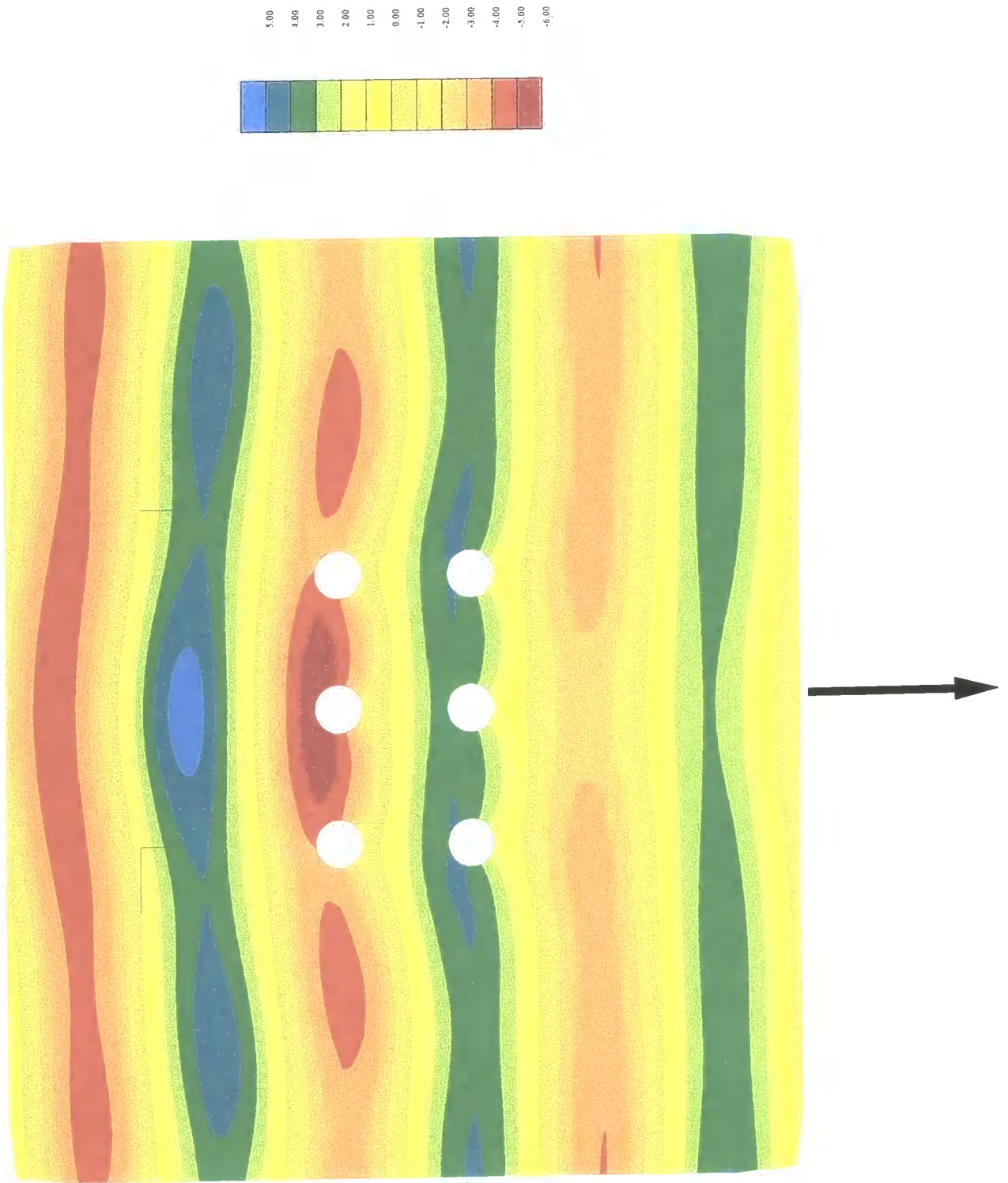
Figure 8.34   Imaginary part of wave elevations, 2 x 3 array of risers, frequency = 4.0
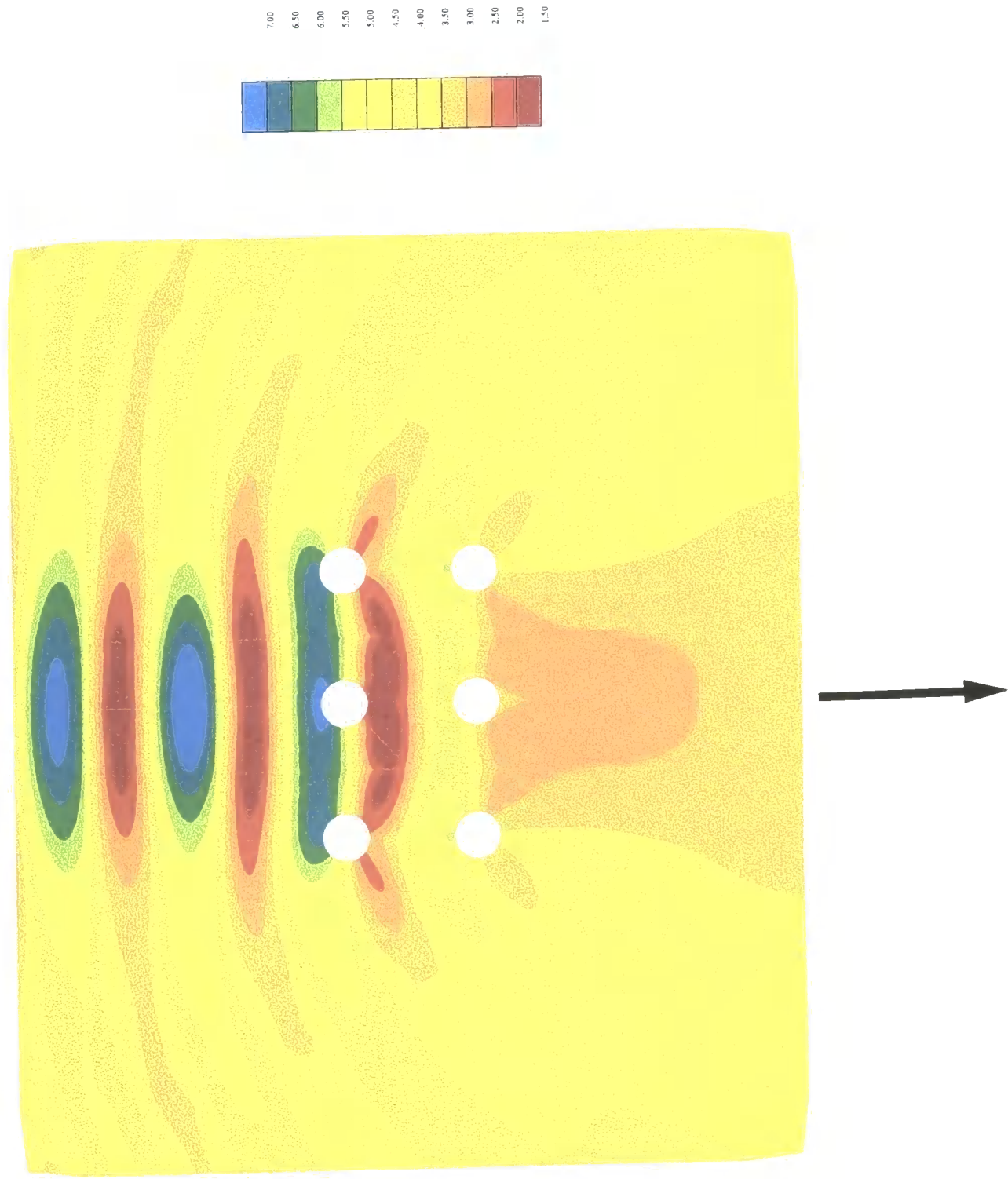
Figure 8.35   Absolute part of wave elevations, 2 x 3 array of risers, frequency = 4.0
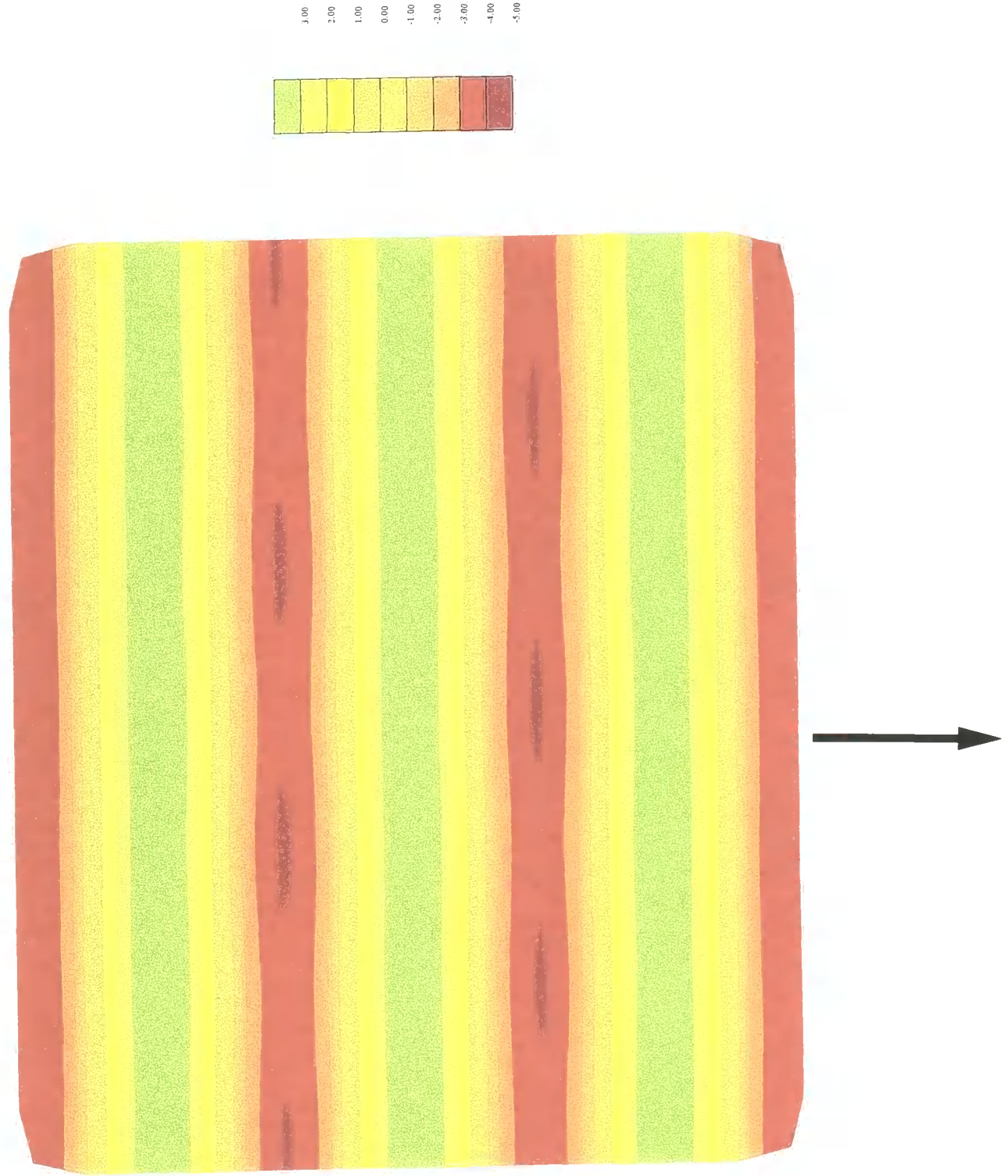
Figure 8.36   Real part of wave elevations, permeability = 0.9
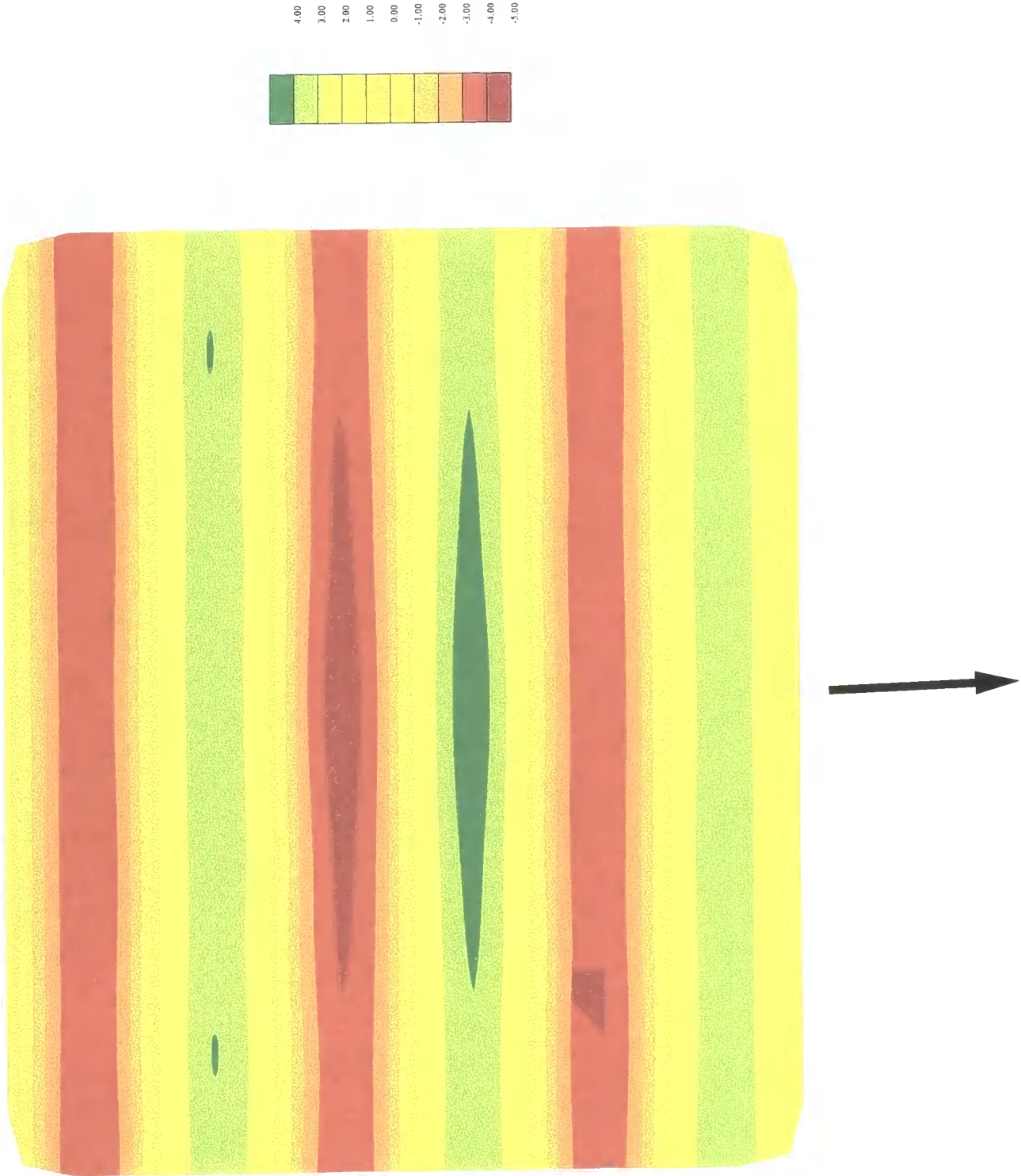
Figure 8.37   Imaginary part of wave elevations, permeability = 0.9
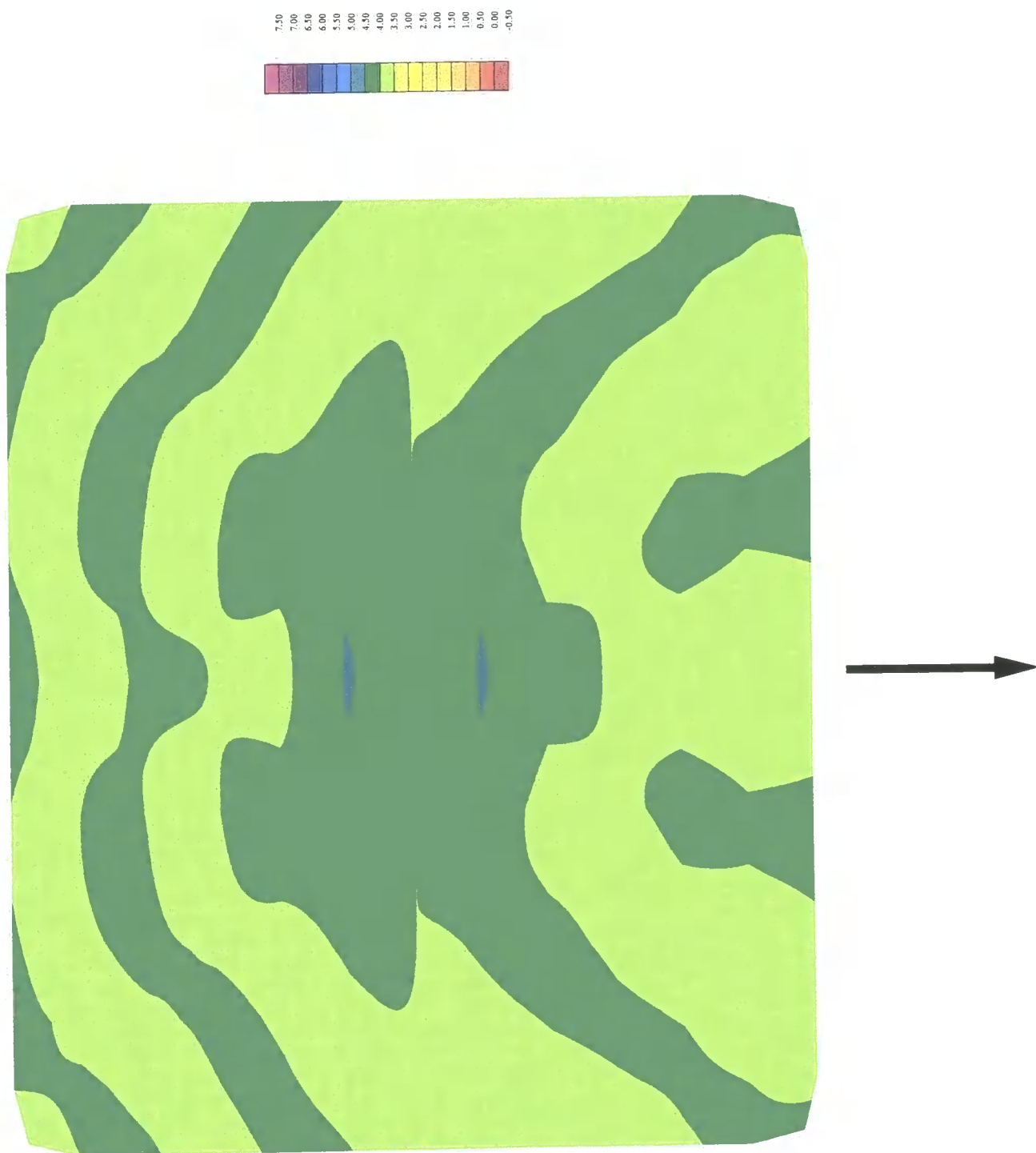
Figure 8.38 Absolute part of wave elevations, permeability = 0.9
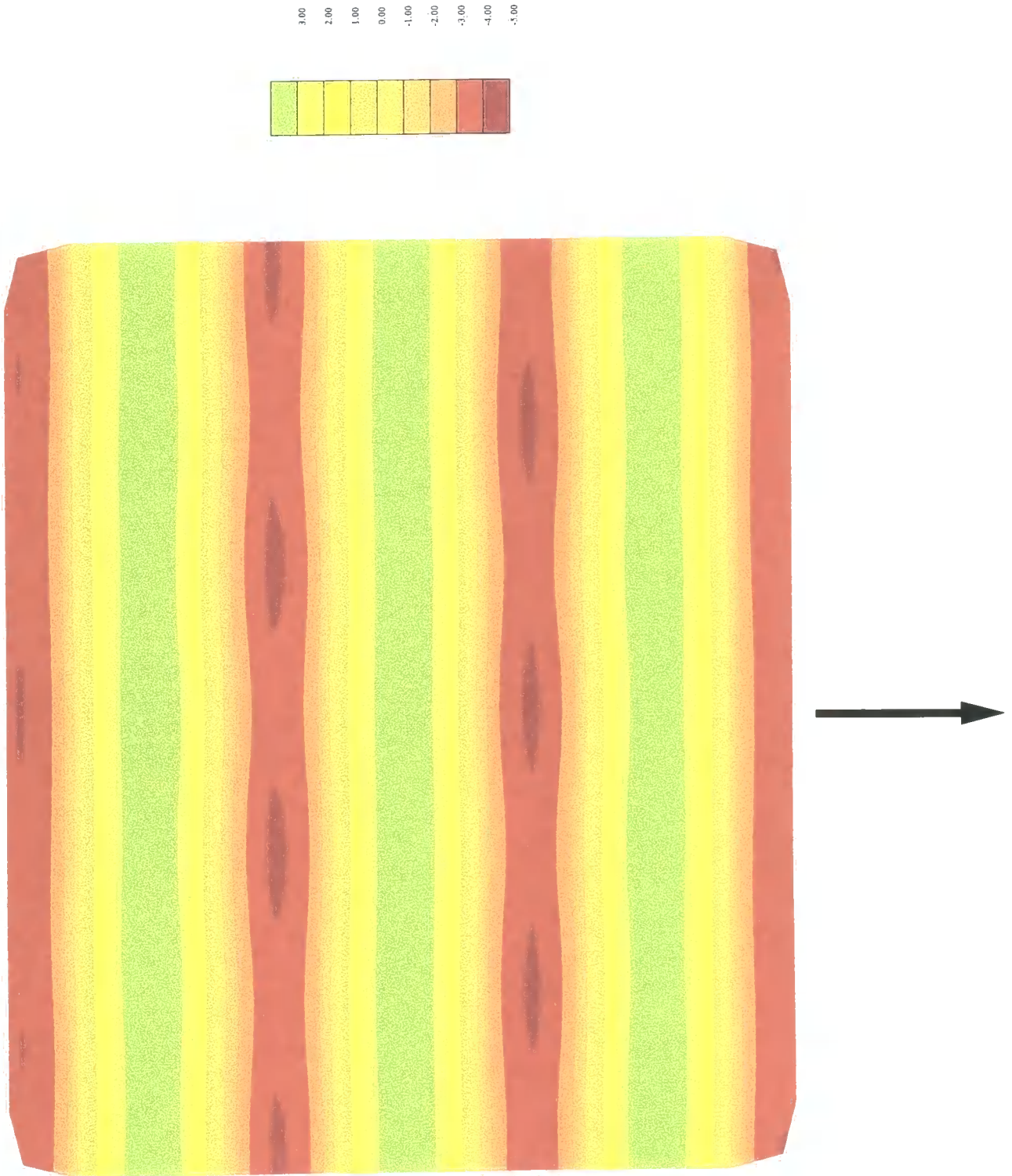
Figure 8.39   Real part of wave elevations, permeability = 0.85
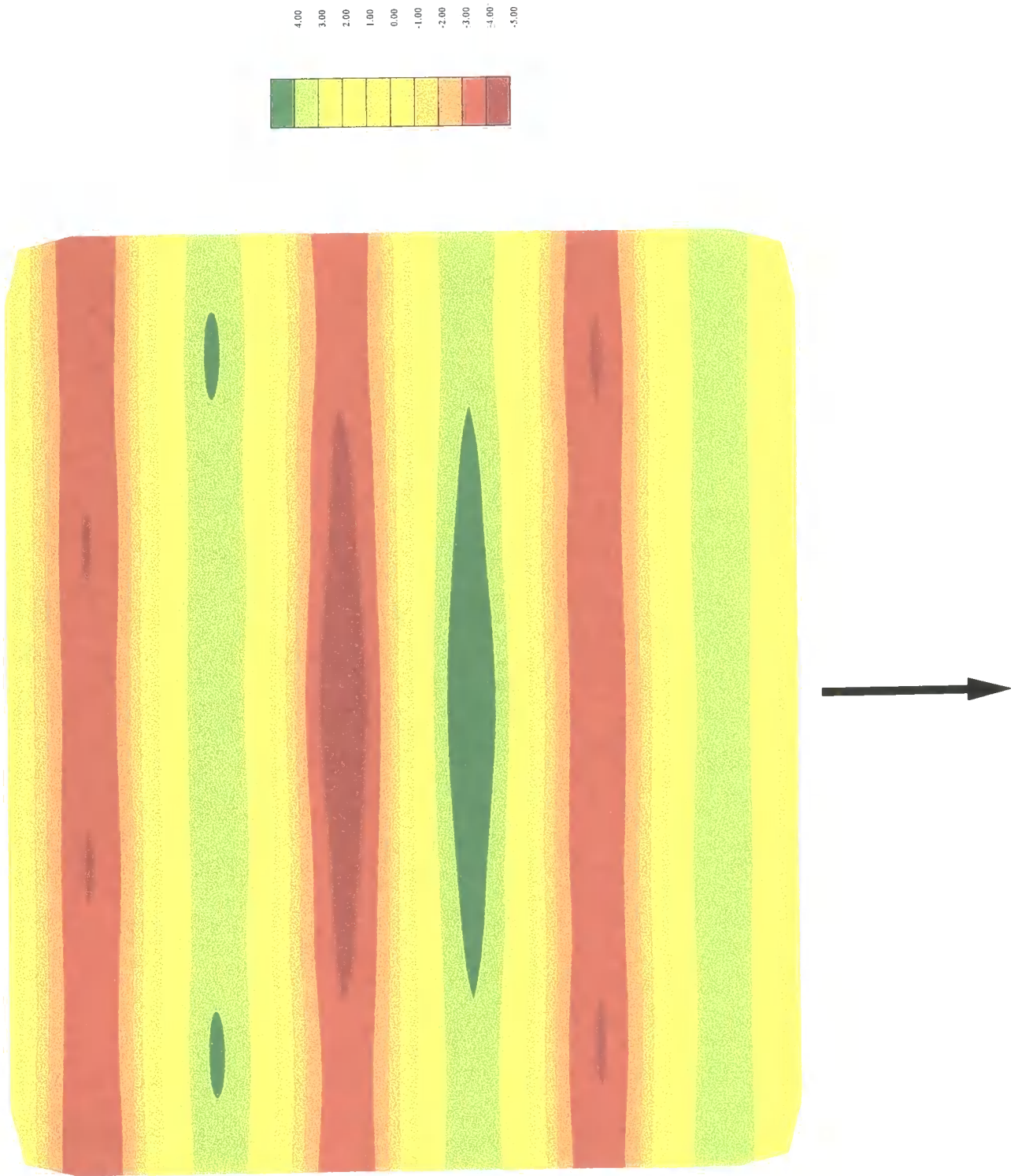
Figure 8.40   Imaginary part of wave elevations, permeability = 0.85
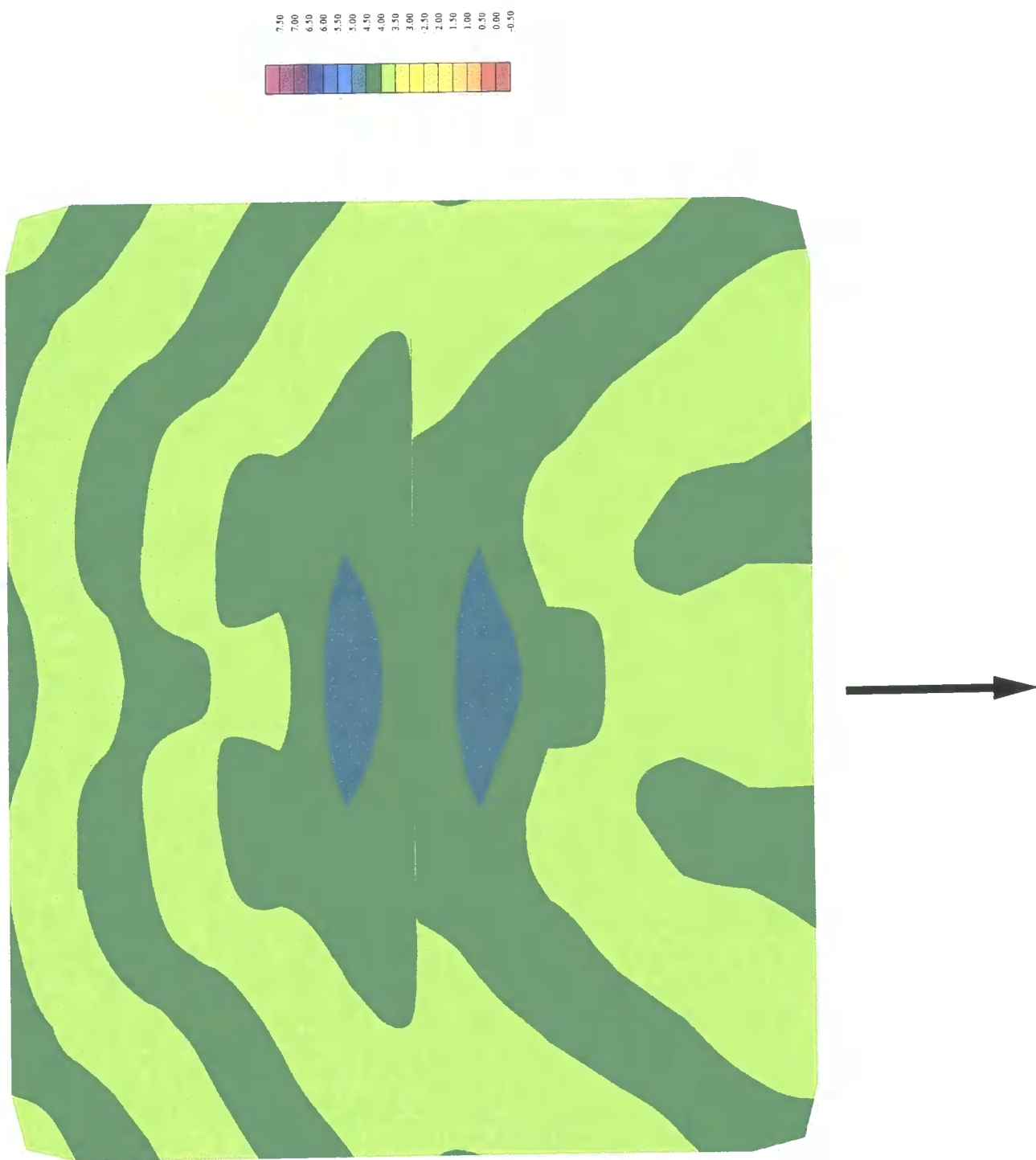
Figure 8.41   Absolute part of wave elevations, permeability = 0.85
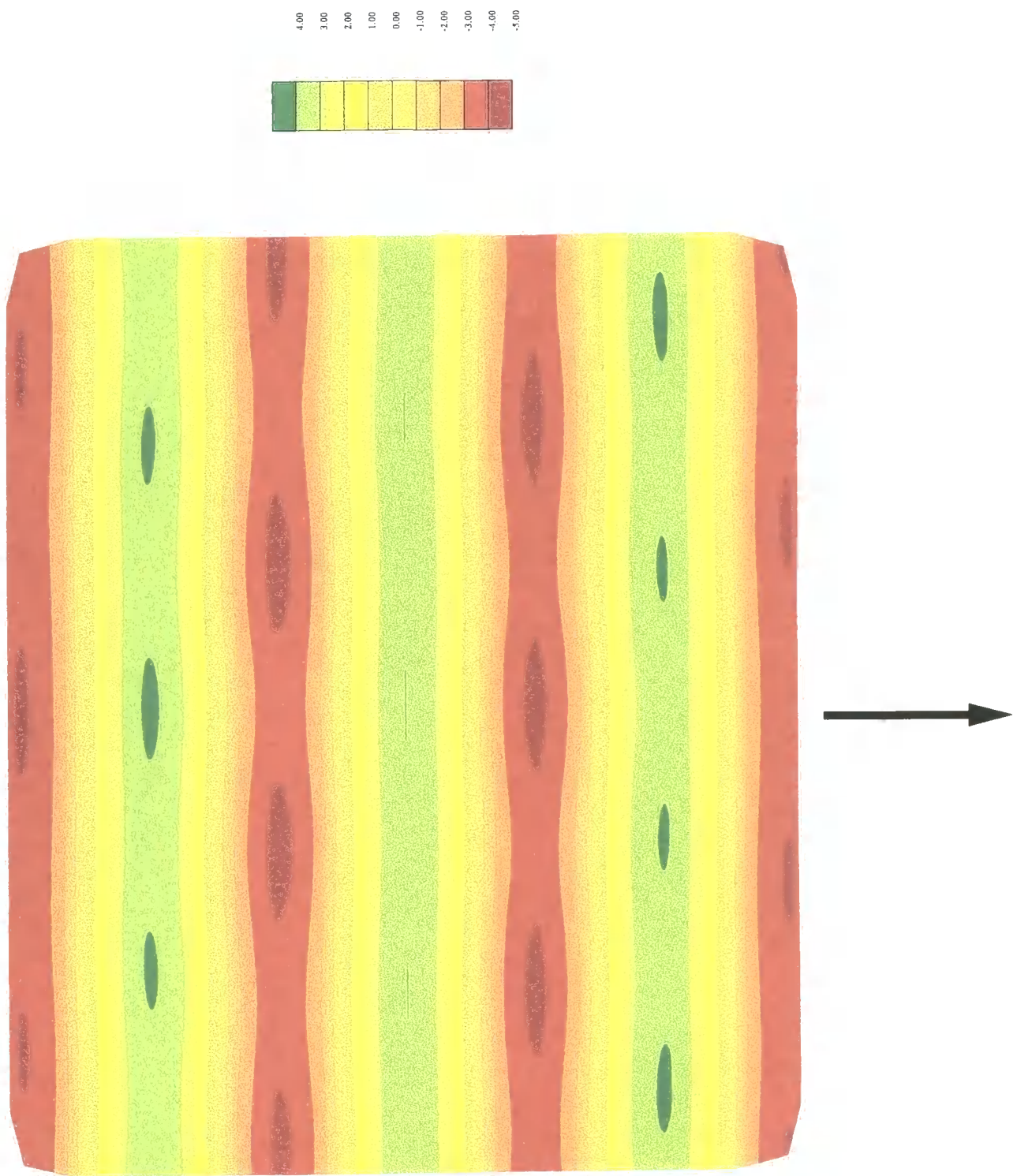
Figure 8.42   Real part of wave elevations, permeability = 0.8
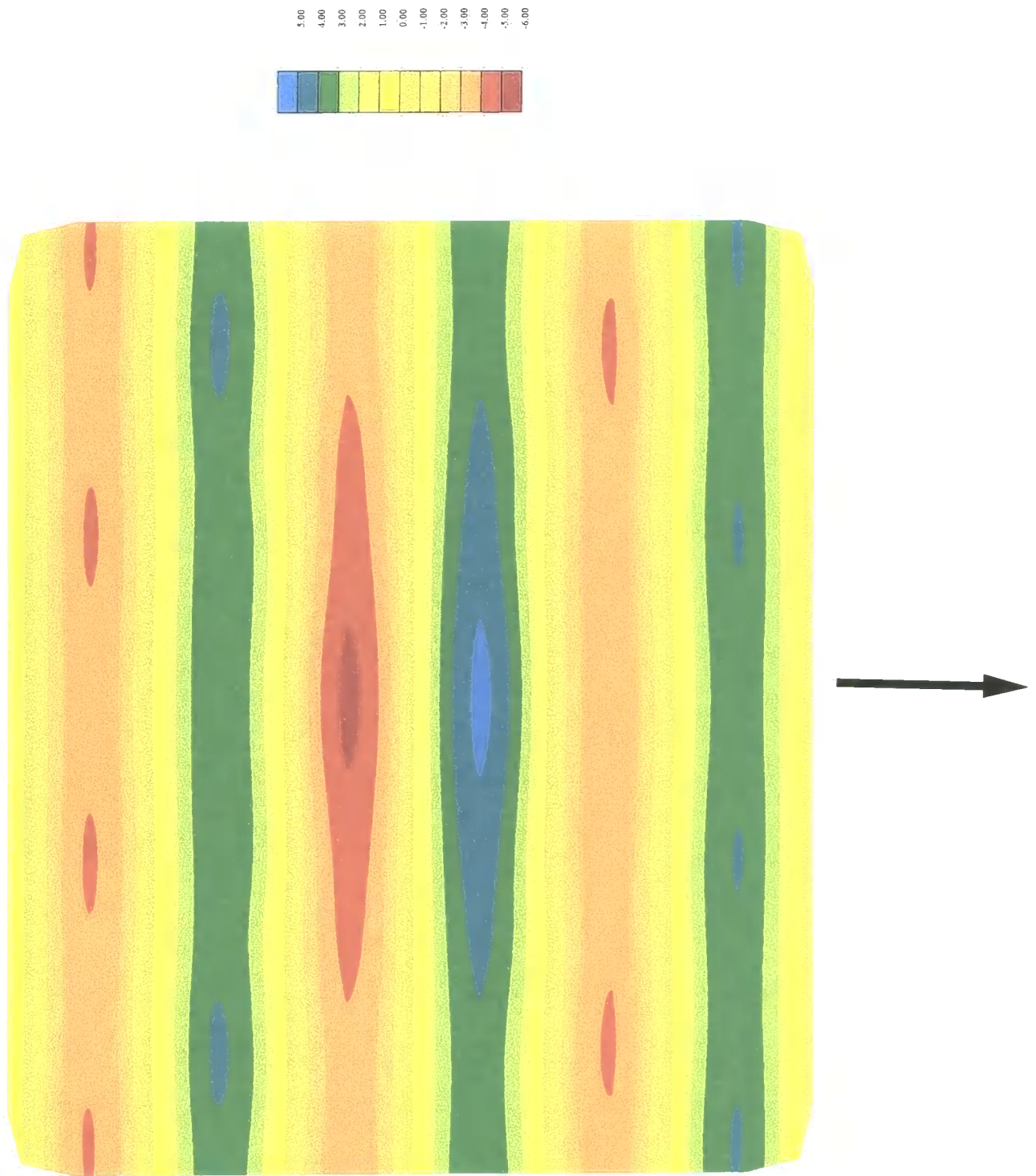
Figure 8.43   Imaginary part of wave elevations, permeability = 0.8
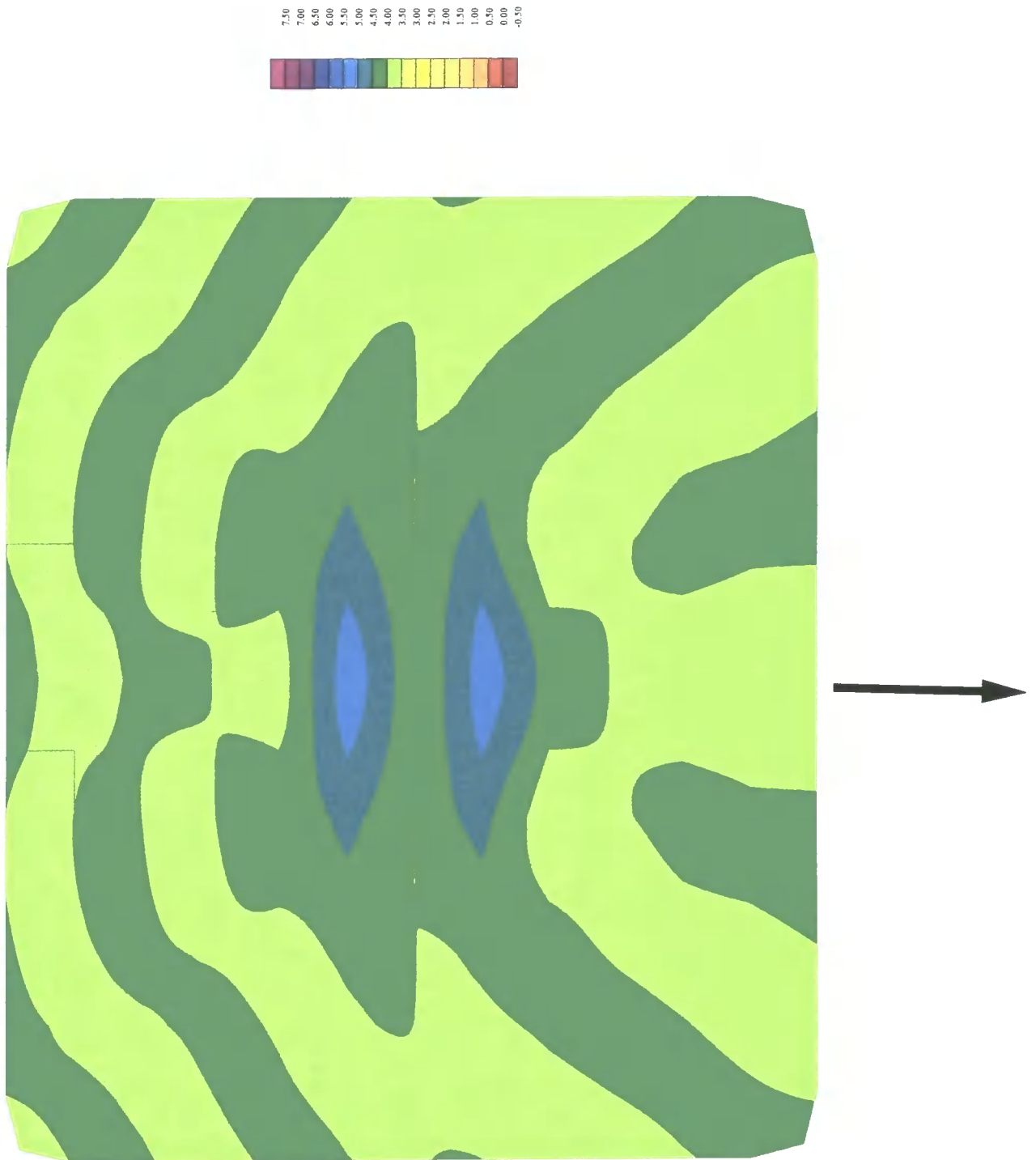
Figure 8.44   Absolute part of wave elevations, permeability = 0.8
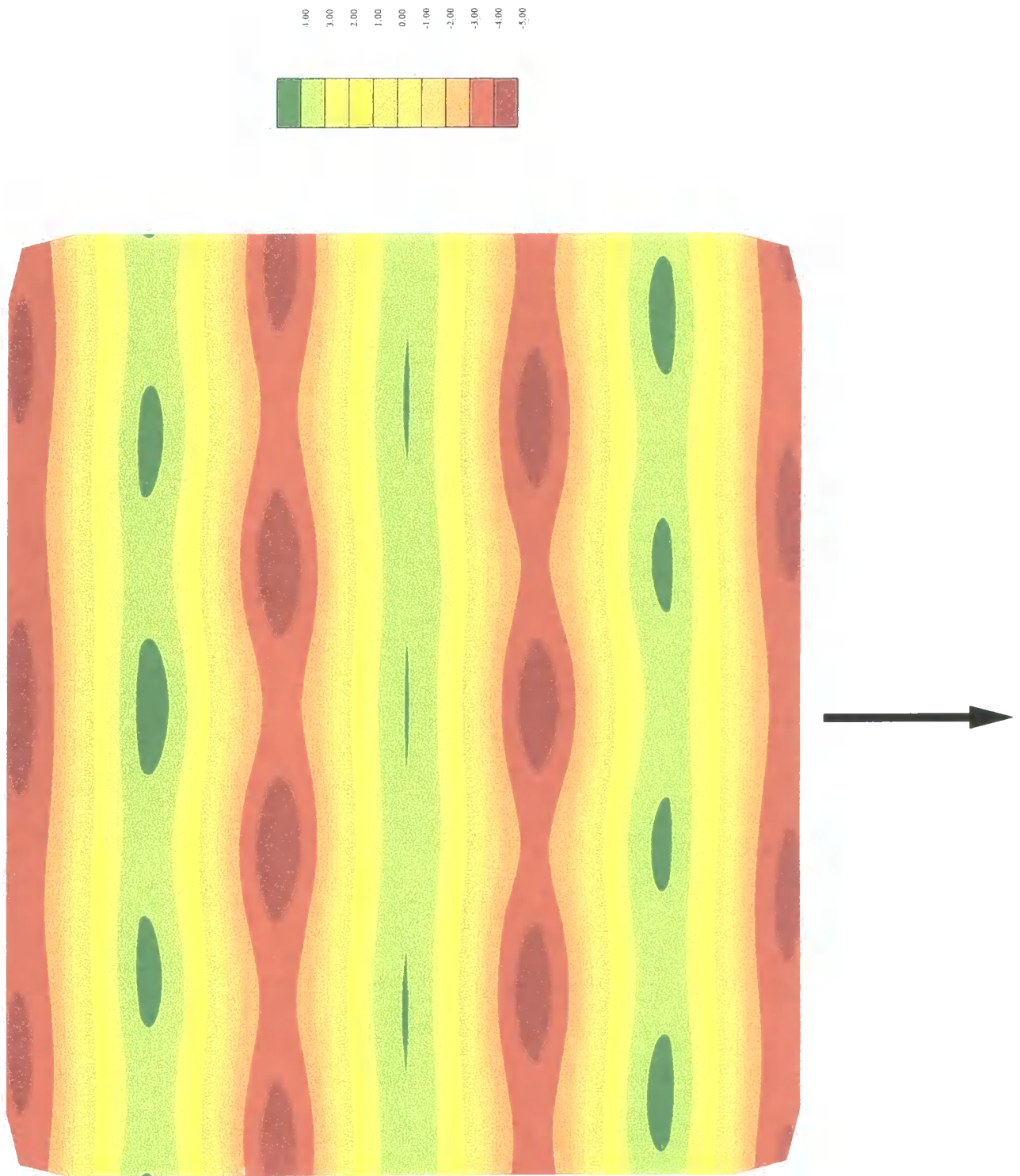
Figure 8.45   Real part of wave elevations, permeability = 0.6
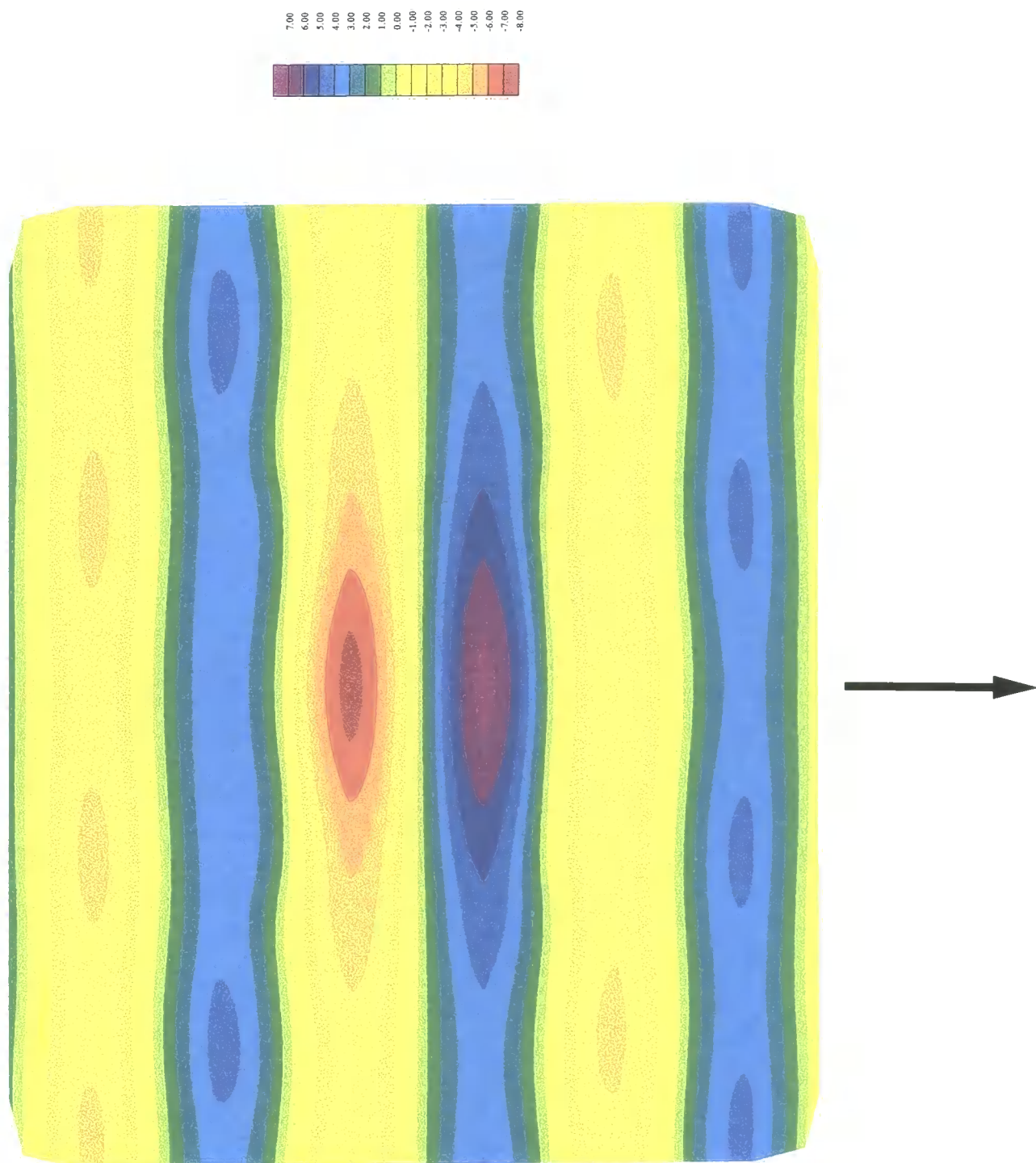
Figure 8.46   Imaginary part of wave elevations, permeability = 0.6
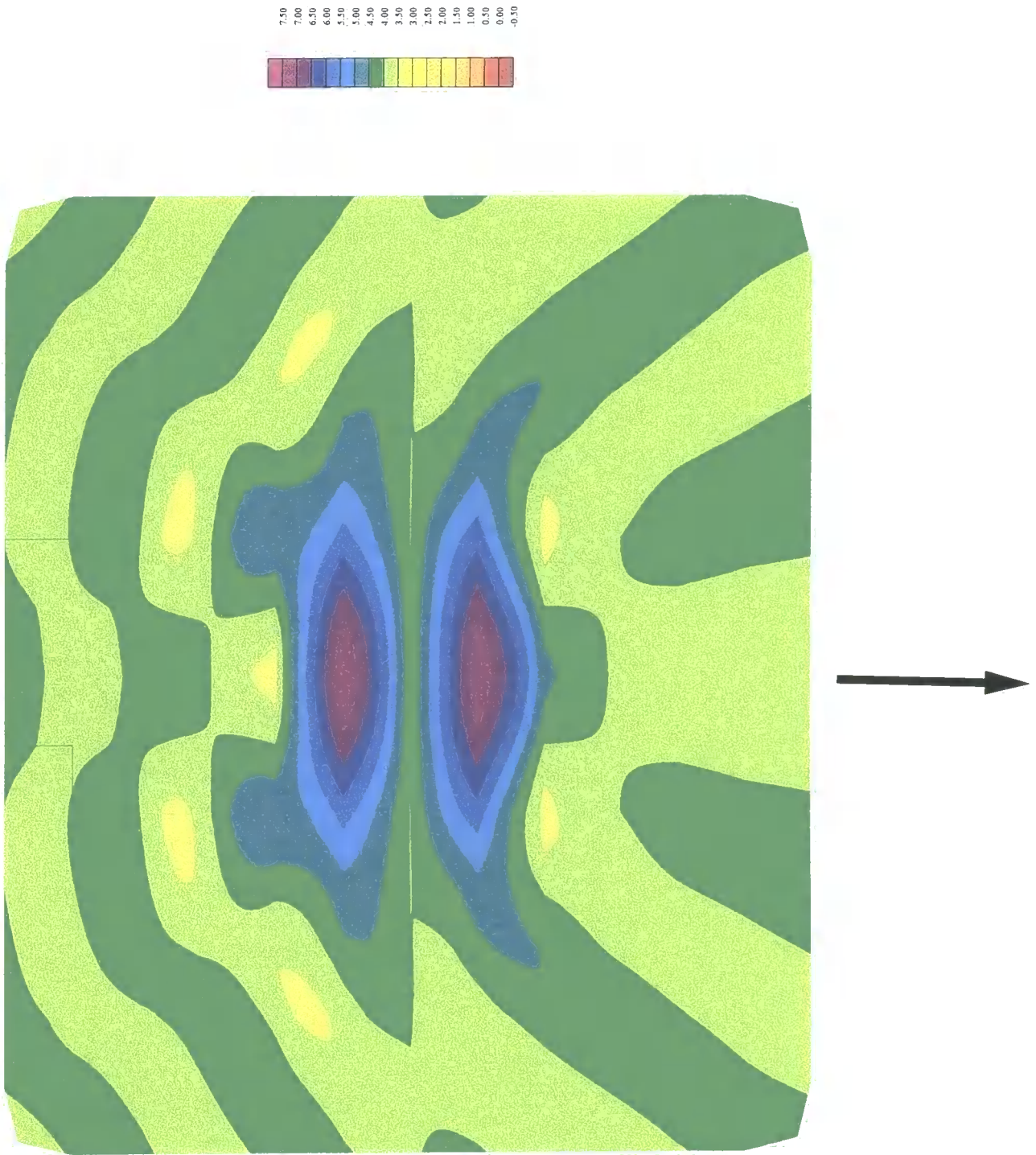
Figure 8.47   Absolute part of wave elevations, permeability = 0.6

Chapter 9

Wave drag force theory

Section 8.15 of Chapter 8 has demonstrated that the energy removed from the waves through viscous drag effects is significant. The next step is to incorporate this effect, in a crude way, into the wave diffraction program. The effect of the wake caused by viscous effects, boundary layers, separation and so on, cannot be incorporated into a simple numerical model in any detail. Instead the philosophy is to introduce into the model the same amount of energy dissipation, as that caused by viscous effects. That is, in each wave cycle, as much energy is abstracted from the system, as is known to be lost through the viscous drag. The global effect on the wave velocity field should be of the same order. This is a fairly sweeping assumption, but the same concept is well-known and widely accepted in dealing with bed friction. It was first intoduced in Holland in numerical simulation of flow around dykes, as mentioned in Chapter 1[81].

If the fluid were an ideal fluid, the only forces exerted on the cylinder would be due to fluid accelerations, that is the inertia parts of Morison's equation. All the drag part of Morison's equation is due to viscous flow, and the energy input into the flow, namely the drag force multiplied by the free stream velocity, is ultimately lost by viscous dissipation. The rate of energy loss is simply $F_d \times u$, where F_d is the drag force and u is the free stream velocity.

The drag force part of the Morison equation can be written

$$F_d = \frac{1}{2} C_d \rho D u |u|, \qquad\qquad 9.1$$

where ρ is the fluid density, u is the fluid velocity, C_d is the drag coefficient, and D is the cylinder diameter. Estimates of C_d are of course widely available. A value of 1.2 will be taken for C_d.

For a monochromatic wave the elevation can be written as

$$\eta = a_0 \sin(kx - \omega t), \q\qquad\qquad 9.2$$

where k is the wave number, given by $k = 2\pi/\lambda$, where λ is the wave length and ω is the angular frequency.

If the wave is linear, which is assumed here, then the velocity potential, ϕ can be written as

$$\phi = \frac{ga_0}{\omega} \sin(kx - \omega t).$$ 9.3

On differentiating, the velocities are obtained as

$$u = \frac{\partial \phi}{\partial x} = \frac{kga_0}{\omega} \cos(kx - \omega t).$$ 9.4

This can be substituted into the expression for the drag force.

$$F_d = \frac{1}{2}C_d \rho D \left(\frac{kga_0}{\omega}\right) \times \frac{\partial \phi}{\partial x}$$ 9.5.

In equation 9.5, the quadratic velocity has been linearised, using the maximum original free stream velocity. Also the velocity potential and velocity will vary with depth, as

$$\phi = \phi_{surface} \times \frac{\cosh k(z + h)}{\cosh kh}.$$ 9.6

This is true of both the linearised term and the remaining term in equation 9.5, so that a modification factor gives the effect of the length of the riser.

$$\int_{z=-h}^{z=0} \frac{\cosh^2 k(z + h)}{\cosh^2 kh} dz = \psi = \left[\frac{\sinh 2kh}{4} + \frac{kh}{2}\right]\left[\frac{1}{\cosh^2 kh}\right]\frac{1}{k}.$$ 9.7

The next step is to equate the work done on the cylinder, with an equivalent velocity proportional stress which can be applied on the free surface, in a manner analagous to bed friction.

Consider first the equation of balance of momentum on an element of fluid, with the pressure gradient and a surface stress, Su, acting, which will give

$$-\rho g \frac{\partial \eta}{\partial x}\delta x \delta y h - Su\delta x \delta y = \delta x \delta y h \rho \frac{\partial u}{\partial t}.$$ 9.8

The reader may find it relevant to refer to the section 1.4 concerned with bed friction.

The ρ term arises in the acceleration term from the mass of the element of fluid and in the surface gradient term from the expression for hydrostatic pressure. On dividing by $\delta x \delta y \rho h$, the equation becomes

$$\frac{\partial u}{\partial t} = -g \frac{\partial \eta}{\partial x} - \left(\frac{S}{\rho h}\right)u.$$ 9.9

This is similar to the the bed friction theory as given in Chapter 1, except that the bed friction term gM is replaced by $S/(\rho h)$. The corresponding equation, for a surface velocity proportional stress, S, is given by

$$-\omega^2\eta + i\left(\frac{\omega S}{\rho h}\right)\eta = g\left[\frac{\partial}{\partial x}(h\frac{\partial\eta}{\partial x}) + \frac{\partial}{\partial y}(h\frac{\partial\eta}{\partial y})\right], \qquad 9.10$$

creating a velocity proportional stress

$$\tau = Su \qquad 9.11$$

on the free surface, over which the stress is applied. The rate of doing work by the stress, (or power, P), will thus be

$$P = \text{Area} \times Su^2. \qquad 9.12$$

In this case the work done by S is equated to the work done by the drag forces on the cylinder. The cylinder has diameter, D, and stands in water of depth, h. The equivalent surface stress is spread over a free surface area A.

Thus

$$S \times A = \frac{1}{2}C_d\rho D\psi \times \left(\frac{kga_0}{\omega}\right) \qquad 9.13$$

or

$$S = \frac{1}{2}\frac{C_d\rho D\psi}{A} \times \left(\frac{kga_0}{\omega}\right). \qquad 9.14$$

The term needed in the wave element, to replace gM, that is $S/(\rho h)$, can be written as

$$\left(\frac{S}{\rho h}\right) = \frac{1}{2}\frac{C_dD}{A}\left(\frac{kga_0}{\omega}\right)\left(\frac{\psi}{h}\right)\frac{1}{\sqrt{2}}. \qquad 9.15$$

The constant, S, can be evaluated and incorporated into the finite element model, in the riser zone, and used in the wave analysis. It should ensure that the same amount of energy is absorbed over one wave cycle in both models. The $\sqrt{2}$ term incorporates a root mean square effect due to the linearised velocity. Of course this model is far too simple to predict the *details* of the flow.

It must be emphasised that whatever value is taken for the area, A, the same amount of energy should be absorbed from the system. The parameter A simply determines over how wide an area the energy is absorbed over, not the total energy absorption. Rational assessments for A are given in Appendix F. It is also shown that A can be changed, with minimal effect upon the resulting wave forces.

Chapter 10

Wave forces due to diffraction

The program, SMAWAVE, evaluates the force on each riser, using Morison's equation to obtain the sum of the inertia and drag loading effects. This is done for both the undisturbed or incident wave and the diffracted wave. The ratio of the two forces is also calculated, giving a measure of the effects of the diffraction. Usually Morison's equation is applied using the accelerations and velocities for the undisturbed wave, at locations along the centre line of the cylinders. However, this is not possible directly for the diffracted wave, since it is not calculated at these points which are, strictly speaking, outside the computational domain in which the diffracted wave is calculated.

10.1 Morison's equation

Before the details of the calculations are dealt with, Morison's equation will be described. Morison's equation is a semi-empirical method for calculating wave forces on cylinders. It makes the assumption that the wave forces arise from two causes:

- Viscous effects

- Inertia effects

The further assumption is made that these two effects can be superposed. The equation then rests on some plausible assumptions, followed by reasonably rigorous theory for the two force components. Although the equation has been often criticised since it was suggested in 1950, it has been used even more often, and it is widely accepted in the offshore industry, although it should always be used with caution.

10.1.1 Drag Forces

The drag force is supposed to correspond to fully developed turbulent flow for which it is known that the drag force, F_D is proportional to the square of the velocity, U, the fluid density, ρ and the cross sectional area, A. The velocity, U, is taken at the centre of the cylinder. Thus for a unit length of a cylinder of diameter, D,

$$F_D = \frac{1}{2}C_D\rho DU^2,\qquad\qquad 10.1$$

where C_D is the drag coefficient, experimentally shown to be about 1.2, although it varies with Keulegan-Carpenter number and Reynolds Number (See Chapter 1). Further information about C_D is given in Goldstein[68,69].

10.1.2 Inertia forces

The inertia force is supposed to correspond to the force required to accelerate the fluid in the space occupied by the cylinder. This is proportional to the volume of the cylinder, V, the fluid density, ρ and the acceleration, a, or $\dot{U} = dU/dt$. Thus for a unit length of a cylinder of diameter, D,

$$F_I = C_I \frac{\rho \dot{U} \pi D^2}{4},$$ 10.2

where C_I is the inertia coefficient, theoretically shown to be 2, provided that there are no diffraction effects, that is the wave length is large. For shorter waves it must be modified in the light of diffraction analysis. The velocities and accelerations needed for Morison's formula must be calculated using an appropriate wave theory.

Thus the total force, F, on a unit length of the cylinder is given by:

$$F = F_D + F_I = C_D \frac{\rho}{2} DU|U| + C_I \rho \frac{\pi}{4} D^2 \frac{dU}{dt},$$ 10.3

where

F	wave force per unit length, acting perpendicular to member	
F_D	drag force per unit length	
F_I	inertia force per unit length	
C_D	drag coefficient	
ρ	density of water	
D	is the diameter of the cylindrical members	
U	water particle velocity normal to member	
$|U|$	absolute value of U	
C_I	inertia (or mass) coefficient	
dU/dt	acceleration of water particle normal to the direction of the member $(= \dot{U})$	

10.1.3 Froude-Krylov Force

This force is calculated on the assumption that the only wave acting is the incident wave. That is, the cylinder does not change the waves at all. Such a calculation corresponds to an inertia coefficient, $C_I = 1.0$.

10.2 Calculation of wave forces

Because of the problems of calculating the diffracted wave forces, the following procedure is adopted. Some point in a finite element close to the cylinder is chosen and the velocities are found at that point by taking the derivatives of the nodal values of the velocity potentials, using the derivatives of the element shape functions. For the work described in this thesis, the point chosen in each case was the centroid of each of the finite elements which touched the cylinder. This choice of location can be criticised and clearly this procedure is an approximation, since the cylinder is not within the

element, but adjacent to it. If the wavelength is very short, then the velocities may be changing rapidly close to the cylinder, and errors could be introduced. However the finite elements which touch the cylinder are necessarily small, and no such errors were observed in any of the calculations. Any errors would tend to cancel out, because the velocities are calculated all round the cylinder. The accuracy of the calculations was also checked against conventional wave force evaluations, and gave good results. Several other methods for determining the best velocities at the cylinder were attempted. One method replaced the cylinder with a zone of very low permeability (in the same way as used for the riser zone, but with a much lower value of permeability), and the node at the centre of cylinder then gave a kind of smoothed average velocity, influenced by the velocities on the cylinder surface, around it. However for classical problems this gave worse force results than the method described above and the approach was not pursued. The forces are averaged for all the elements touching each cylinder.

The acceleration can easily be found from the velocities, because the problem is in the frequency domain, so that differentiation with respect to time corresponds to multiplication by $i\omega t$. The velocities and accelerations are then substituted into Morison's equation, using a suitable diameter for the cylinder and drag and inertia coefficients.

The acclerations and velocities are complex quantities, and since the drag force is a non-linear function of the velocities, it is necessary to evaluate the force at a range of time steps, throughout the periodic wave cycle, and to select the maximum force. It is actually possible to carry out the time integrations analytically, but it was easier to carry out a numerical integration in time.

In detail the procedure adopted here is as follows:

1. For all the cylinders in the problem considered all the finite elements touching the cylinder are processed.

2. For each finite element the *complex* velocities, in the x and y directions, U and V (and the corresponding complex velocities from the incident wave, U^i and V^i), are computed at the element centroid, from the derivatives of the total diffracted potential, ϕ and from the derivatives of the incident wave potential, ϕ_i. That is

$$U = \frac{\partial \phi}{\partial x} \quad \text{and} \quad V = \frac{\partial \phi}{\partial y},$$

$$U^i = \frac{\partial \phi_i}{\partial x} \quad \text{and} \quad V^i = \frac{\partial \phi_i}{\partial y}.$$

The corresponding complex accelerations are given by

$$\dot{U} = U \times i\omega \quad \text{and} \quad \dot{V} = V \times i\omega.$$

3. Again for each element, the instantaneous *true* velocities, u and v are calculated at 18 time steps through one wave period, for $t = 0$, $t = T/18$, $t = 2T/18$ etc. The number 18 was chosen arbitrarily. That is

$$u = \Re\left[U \exp(i\omega t)\right] \quad \text{and} \quad v = \Re\left[V \exp(i\omega t)\right].$$

4. For each time step Morison's equation, described above, is used to calculate the wave force.

5. The maximum wave force encountered in the wave period, for both the total diffracted wave and the incident wave is stored for each element.

6. The average value of the maximum force in the elements touching each cylinder is calculated, and this is taken as the maximum force on the cylinder.

It is possible to obtain more accurate values of the inertia forces on the cylinder by integrating the pressures over the surface of the cylinder, and this should be more accurate. This has been done elsewhere[39]. However it was not possible to implement this option with the resource and time scales of the work on this thesis. In any event, it is not possible to obtain more accurate values of the drag force through surface integration. The process was validated by comparison with known analytical solutions.

Something of an anomaly arises here. If we consider very long waves, that is the frequency, ω, is very small, then we should expect the wave forces to be the same as those derived from the incident wave. However, even for very long waves there is a distortion of the wave field close to the cylinders. Figure 10.1 is a contour plot of the imaginary part of the wave elevations for a wave of wavenumber, $k = 0.007164$ (1/m) and wavelength, $\lambda = 877.05$ m, and shows this effect. (The real part of the elevation is not interesting, and is not plotted.)

Table 10.1 shows the forces calculated for a 2 by 3 array of risers, with parameters as shown *. In this case the wavelength is long in comparison with the dimensions of the problem, $k = 0.10504$ m, and $\lambda = 59.82$ m. We could therefore expect the wave forces (due to inertia only) on the individual risers to be close to those for a cylinder on its own in a wave field. The wave forces were calculated by program CYL from the theoretical expressions of MacCamy and Fuchs, and were as follows:

Maximum diffracted wave force $= 31851.36$ N

Froude-Krylov wave force $= 15889.96$ N

As one would expect, the diffracted wave force is about twice the Froude-Krylov force, which is the theoretical ratio for small wavenumber, as discussed in section 10.2.

As stated, table 10.1 shows the force results obtained for the array of risers. The forces calculated from the rectangular elements surrounding the riser give an average force which gives a close agreement with the above solution. Because of this these results will be used with some confidence from now on. The agreement with the values calculated by the MacCamy and Fuchs program is excellent and gives added confidence.

---

* Some of the tabulated force results in Chapter 10 are given again in graphical form in Chapter 11, where they are compared with forces including viscous effects. The graphical form may be easier to interpret. An aide-memoire for the figures and tables in chapters 10 and 11 is given in Appendix C.
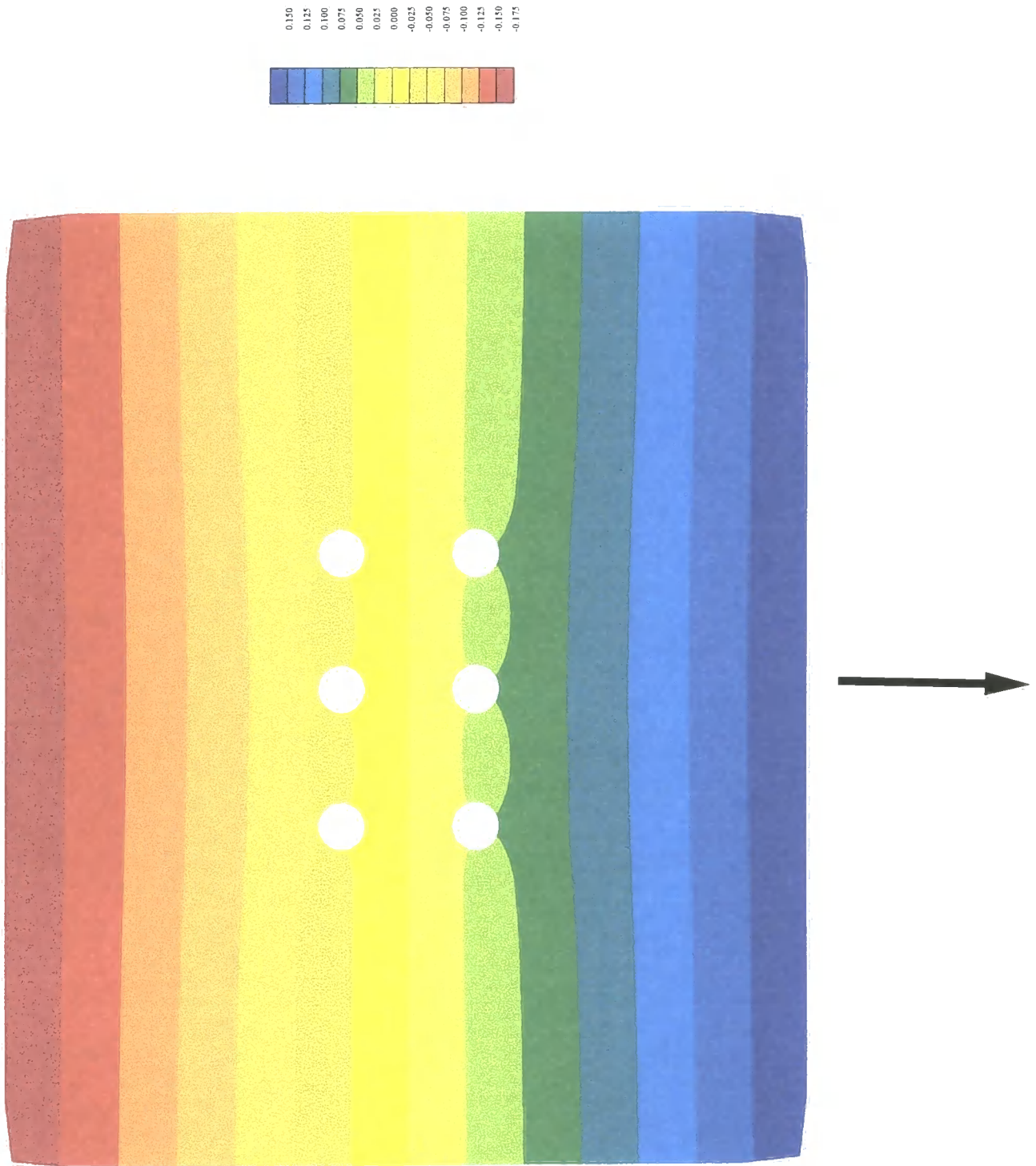
Figure 10.1   Imaginary wave elevations for very long wave

Incidentally, if the inertia coefficient were taken as 1.0 instead of 2.0, the Froude-Krylov results would be recovered.

		$x = -2.0$m	$x = 0.0$m	$x = 2.0$m
	a Diffracted	31367.55466	31873.40165	31367.55466
$y = 1.0$m	b Incident	31655.62895	31655.62895	31655.62895
	Ratio a/b	0.99090	1.00688	0.99090
	a Diffracted	31277.02140	31779.01569	31277.02140
$y = -1.0$m	b Incident	31655.62895	31655.62895	31655.62895
	Ratio a/b	0.98804	1.00390	0.98804

a Diffracted - forces given by elements surrounding the cylinders, using diffracted wave, b Incident - forces given by elements surrounding the cylinders, using the incident waves. Table of forces due to diffracted and incident waves 2 by 3 array of risers, no damping, only diffraction forces found.

Wave frequency, $\omega = 1.0$ s^{-1}, Depth, $h = 20.0$m, Drag coefficient, $C_d = 0.0$, Inertia coefficient, $C_i = 2.0$, Wavenumber, $k = 0.10504$ m^{-1}, Wave length, $\lambda = 59.82$ m, Wave period $T = 6.2832$ s, Wave amplitude, $a_0 = 4.0$ m, Acceleration due to gravity, $g = 9.81$ ms^{-2}, Angle of incident wave direction, $\theta_i = 90.0°$. All forces in N.

Table 10.1 Riser forces, no drag force, $\omega = 1.0$, $\theta_i = 90°$, $h = 20.0$

The results in table 10.1 give confidence in the method. Tables 10.2 and 10.3 show similar results for two other wave directions, that is the long direction of the array of six risers and at 45°. The results show that diffraction is having little effect at this frequency, $\omega = 1.0$ rads/sec, corresponding to a wave period of 6 seconds. All the results demonstrate that the approximation is quite good. They also give confidence in the force calculating procedure used by the program.

The next step is to include the viscous drag forces, in the force calculations. These cause considerable increases in the maximum forces on the cylinders.

Tables 10.4 to 10.6 show the results for a frequency of $\omega = 1.0$ rads/sec, corresponding to a wave period of 1.57 seconds, with angles of incidence of 0°, 45° and 90°. These are with the viscous drag contribution to the force on the cylinder calculated, but without the corresponding energy loss in the waves. There are modest changes in the maximum wave force, with increases of up to 6% and decreases of up to 6%. There are no systematic changes, which could be relied upon in design calculations.

		$x = -2.0$m	$x = 0.0$m	$x = 2.0$m
$y = 1.0$m	a Diffracted	30553.264	29833.579	30659.701
	b Incident	31712.191	31533.898	31712.191
	Ratio a/b	0.96345	0.94608	0.96681
$y = -1.0$m	a Diffracted	30553.264	29833.579	30659.701
	b Incident	31712.191	31533.898	31712.191
	Ratio a/b	0.96345	0.94608	0.96681

a Diffracted - forces given by elements surrounding the cylinders, using diffracted wave, b Incident - forces given by elements surrounding the cylinders, using the incident waves. Table of forces due to diffracted and incident waves 2 by 3 array of risers, no damping, only diffraction forces found.

Wave frequency, $\omega = 1.00$ s^{-1}, Wave period $T = 6.2832$ s, Depth, $h = 20.0$m, Waveno, $k = 0.10504$ m^{-1}, Wave length, $\lambda = 59.82$ m, Wave amplitude, $a_0 = 4.0$m, Drag coefficient, $C_d = 0.0$, Inertia coefficient, $C_i = 2.0$, Acceleration due to gravity, $g = 9.81$ ms^{-2}, Angle of incident wave direction, $\theta_i = 0.0°$.

Table 10.2 Riser forces, no drag force, $\omega = 1.0$, $\theta_i = 0°$, $h = 20.0$

		$x = -2.0$m	$x = 0.0$m	$x = 2.0$m
$y = 1.0$m	a Diffracted	31736.410	31187.346	30581.205
	b Incident	31574.150	31574.150	31696.534
	Ratio a/b	1.00514	0.98775	0.96481
$y = -1.0$m	a Diffracted	30469.699	31128.548	31793.277
	b Incident	31696.534	31574.150	31574.150
	Ratio a/b	0.96129	0.98589	1.00694

a Diffracted - forces given by elements surrounding the cylinders, using diffracted wave, b Incident - forces given by elements surrounding the cylinders, using the incident waves. Table of forces due to diffracted and incident waves 2 by 3 array of risers, no damping, only diffraction forces found.

Wave frequency, $\omega = 1.00$ s^{-1}, Depth, $h = 20.00$m, Waveno, $k = 0.10504$ m^{-1}, Wave length, $\lambda = 59.82$ m, Wave period $T = 6.2832$ s, Wave amplitude, $a_0 = 4.0$m, Drag coefficient, $C_d = 0.0$, Inertia coefficient, $C_i = 2.0$, Acceleration due to gravity, $g = 9.81$ ms^{-2}, Angle of incident wave direction, $\theta_i = 45°$.

Table 10.3 Riser forces, no drag force, $\omega = 1.0$, $\theta_i = 45°$, $h = 20.0$

		$x = -2.0$m	$x = 0.0$m	$x = 2.0$m
$y = 1.0$m	a Diffracted	43753.10608	42973.29798	44158.93699
	b Incident	45045.79443	45298.57222	45324.71592
	Ratio a/b	0.97130	0.94867	0.97428
$y = -1.0$m	a Diffracted	43753.10608	42973.29798	44158.93699
	b Incident	45045.79443	45298.57222	45324.71592
	Ratio a/b	0.97130	0.94867	0.97428

Table of forces due to diffracted and incident waves. 2 by 3 riser array, with no damping effects.

Wave frequency, $\omega = 1.0$ s^{-1}, Depth, $h = 20.00$m, Wave length, $\lambda = 59.82$ m, Wave period $T = 6.2832$ s, Waveno, $k = 0.10504$ m^{-1}, Wave amplitude, $a_0 = 4.0$m, Drag coefficient, $C_d = 1.2$, Inertia coefficient, $C_i = 2.0$, Acceleration due to gravity, $g = 9.81$ ms^{-2}, Angle of incident wave direction, $\theta_i = 0.0°$.

Table 10.4   Riser forces, $\omega = 1.0$, $\theta_i = 0°$, $h = 20.0$, no damping

		$x = -2.0$m	$x = 0.0$m	$x = 2.0$m
$y = 1.0$m	a Diffracted	46836.43398	45166.48076	43516.12416
	b Incident	45471.24411	45031.20782	45376.16977
	Ratio a/b	1.03002	1.00300	0.95901
$y = -1.0$m	a Diffracted	43031.36983	45201.08126	46867.74012
	b Incident	45024.36460	45471.24411	45031.20782
	Ratio a/b	0.95574	0.99406	1.04078

Table of forces due to diffracted and incident waves. 2 by 3 riser array, with no damping effects.

Wave frequency, $\omega = 1.0$ s^{-1}, Depth, $h = 20.00$m, Waveno, $k = 0.10504$ m^{-1}, Wave length, $\lambda = 59.82$ m, Wave period $T = 6.2832$ s, Wave amplitude, $a_0 = 4.0$m, Drag coefficient, $C_d = 1.2$, Inertia coefficient, $C_i = 2.0$, Acceleration due to gravity, $g = 9.81$ ms^{-2}, Angle of incident wave direction, $\theta_i = 45.0°$.

Table 10.5   Riser forces, $\omega = 1.0$, $\theta_i = 45°$, $h = 20.0$, no damping

		$x = -2.0$m	$x = 0.0$m	$x = 2.0$m
	a Diffracted	46141.77678	47563.12012	46141.77678
$y = 1.0$m	b Incident	45062.44317	45062.44317	45062.44317
	Ratio a/b	1.02395	1.05549	1.02395
	a Diffracted	45980.42968	47310.79855	45980.42968
$y = -1.0$m	b Incident	45432.15483	45432.15483	45432.15483
	Ratio a/b	1.01207	1.04135	1.01207

Table of forces due to diffracted and incident waves. 2 by 3 riser array, with no damping effects.

Wave frequency, $\omega = 1.0$ s^{-1}, Depth, $h = 20.00$m, Waveno, $k = 0.10504$ m^{-1}, Wave length, $\lambda = 59.82$ m, Wave period $T = 6.2832$ s, Wave amplitude, $a_0 = 4.0$m, Drag coefficient, $C_d = 1.2$, Inertia coefficient, $C_i = 2.0$, Acceleration due to gravity, $g = 9.81$ ms^{-2}, Angle of incident wave direction, $\theta_i = 90.0°$.

Table 10.6   Riser forces, $\omega = 1.0$, $\theta_i = 90°$, $h = 20.0$, no damping

Tables 10.7 to 10.9 show a repetition of the results shown in tables 10.4 to 10.6, but with a frequency of 4.0 s^{-1}. In this case the reductions in the maximum wave forces, caused by the diffraction are much more significant. The largest reduction can be seen in table 7, and is approximately 63% of the original value, whereas the biggest increase is of the order of 1%.

		$x = -2.0$m	$x = 0.0$m	$x = 2.0$m
	a Diffracted	1501.0	1147.7	987.49
$y = 1.0$m	b Incident	1558.0	1558.2	1558.0
	Ratio a/b	0.96344	0.73658	0.63382
	a Diffracted	1501.0	1147.7	987.49
$y = -1.0$m	b Incident	1558.0	1558.2	1558.2
	Ratio a/b	0.96344	0.73658	0.63382

Table of forces due to diffracted and incident waves. 2 by 3 riser array, with no damping effects.

Wave frequency, $\omega = 4.0$ s^{-1}, Depth, $h = 20.00$m, Waveno, $k = 1.63099$ m^{-1}, Wave length, $\lambda = 3.8524$ m, Wave period $T = 1.5708$ s, Wave amplitude, $a_0 = 0.2$m, Drag coefficient, $C_d = 1.2$, Inertia coefficient, $C_i = 2.0$, Acceleration due to gravity, $g = 9.81$ ms^{-2}, Angle of incident wave direction, $\theta_i = 0.0°$.

Table 10.7   Riser forces, $\omega = 4.0$, $\theta_i = 0°$, $h = 20.0$, no damping

		$x = -2.0$m	$x = 0.0$m	$x = 2.0$m
	a Diffracted	1574.5	1556.1	1447.3
$y = 1.0$m	b Incident	1572.4	1572.4	1569.0
	Ratio a/b	1.0014	0.98966	0.92242
	a Diffracted	1561.9	1547.0	1483.1
$y = -1.0$m	b Incident	1569.0	1572.4	1572.4
	Ratio a/b	0.99548	0.98388	0.94321

Table of forces due to diffracted and incident waves. 2 by 3 riser array, with no damping effects.

Wave frequency, $\omega = 4.0$ s^{-1}, Depth, $h = 20.00$m, Waveno, $k = 1.63099$ m^{-1}, Wave length, $\lambda = 3.8524$ m, Wave period $T = 1.5708$ s, Wave amplitude, $a_0 = 0.2$m, Drag coefficient, $C_d = 1.2$, Inertia coefficient, $C_i = 2.0$, Acceleration due to gravity, $g = 9.81$ ms^{-2}, Angle of incident wave direction, $\theta_i = 45.0°$.

Table 10.8   Riser forces, $\omega = 4.0$, $\theta_i = 45°$, $h = 20.0$, no damping

		$x = -2.0$m	$x = 0.0$m	$x = 2.0$m
	a Diffracted	1231.6	1075.1	1231.6
$y = 1.0$m	b Incident	1558.3	1558.3	1558.3
	Ratio a/b	0.79035	0.68995	0.79035
	a Diffracted	1460.30770	1374.9	1460.3
$y = -1.0$m	b Incident	1558.3	1558.3	1558.3
	Ratio a/b	0.93711	0.88233	0.93711

Table of forces due to diffracted and incident waves. 2 by 3 riser array, with no damping effects.

Wave frequency, $\omega = 4.0$ s^{-1}, Depth, $h = 20.00$m, Waveno, $k = 1.63099$ m^{-1}, Wave length, $\lambda = 3.8524$ m, Wave period $T = 1.5708$ s, Wave amplitude, $a_0 = 0.2$m, Drag coefficient, $C_d = 1.2$, Inertia coefficient, $C_i = 2.0$, Acceleration due to gravity, $g = 9.81$ ms^{-2}, Angle of incident wave direction, $\theta_i = 90.0°$.

Table 10.9   Riser forces, $\omega = 4.0$, $\theta_i = 90°$, $h = 20.0$, no damping

Tables 10.10 to 10.12 show the results repeated for a depth of 40m and a wave period of 14 seconds, and a wave height of 20m crest to trough, corresponding to a storm wave at the site of the Rough Field. These tables display only modest alterations in the maximum force on the cylinders, and indicate that diffraction is not, apparently, very significant.

		$x = -2.0$m	$x = 0.0$m	$x = 2.0$m
	a Diffracted	320038.65722	305622.53981	314273.70354
$y = 1.0$m	b Incident	332487.78394	330024.93800	325730.89513
	Ratio a/b	0.96256	0.92606	0.96483
	a Diffracted	320038.65722	305622.53980	314273.70353
$y = -1.0$m	b Incident	332487.78394	330024.93800	325730.89513
	Ratio a/b	0.96256	0.92606	0.96483

Table of forces due to diffracted and incident waves. 2 by 3 riser array, with no damping effects.
Wave frequency, $\omega = 0.45$ s^{-1}, Depth, $h = 40.00$m, Waveno, $k = 0.02635$ m^{-1}, Wave length, $\lambda = 238.451$ m, Wave period $T = 13.9626$ s, Wave amplitude, $a_0 = 10.0$m, Drag coefficient, $C_d = 1.2$, Inertia coefficient, $C_i = 2.0$, Acceleration due to gravity, $g = 9.81$ ms^{-2}, Angle of incident wave direction, $\theta_i = 0.0°$.

Table 10.10   Riser forces, $\omega = 0.45$, $\theta_i = 0°$, $h = 40.0$, no damping

		$x = -2.0$m	$x = 0.0$m	$x = 2.0$m
	a Diffracted	340293.61299	323752.35850	308097.40913
$y = 1.0$m	b Incident	331107.02045	328717.12558	325413.49832
	Ratio b/c	1.02775	0.98490	0.94679
	a Diffracted	313895.49828	326075.92955	338000.94393
$y = -1.0$m	b Incident	332579.86444	331107.02045	328717.12558
	Ratio a/b	0.94382	0.98481	1.02824

Table of forces due to diffracted and incident waves. 2 by 3 riser array, with no damping effects.
Wave frequency, $\omega = 0.45$ s^{-1}, Depth, $h = 40.00$m, Waveno, $k = 0.02635$ m^{-1}, Wave length, $\lambda = 238.451$ m, Wave period $T = 13.9626$ s, Wave amplitude, $a_0 = 10.0$m, Drag coefficient, $C_d = 1.2$, Inertia coefficient, $C_i = 2.0$, Acceleration due to gravity, $g = 9.81$ ms^{-2}, Angle of incident wave direction, $\theta_i = 45.0°$.

Table 10.11   Riser forces, $\omega = 0.45$, $\theta_i = 45°$, $h = 40.0$, no damping

		$x = -2.0$m	$x = 0.0$m	$x = 2.0$m
	a Diffracted	331199.20648	342536.41355	331199.20649
$y = 1.0$m	b Incident	328106.07054	328106.07054	328106.07054
	Ratio a/b	1.00943	1.04398	1.00943
	a Diffracted	334502.01605	345874.22562	334502.01605
$y = -1.0$m	b Incident	331485.68821	331485.68821	331485.68821
	Ratio a/b	1.00910	1.04341	1.00910

Table of forces due to diffracted and incident waves. 2 by 3 riser array, with no damping effects.

Wave frequency, $\omega = 0.45$ s^{-1}, Depth, $h = 40.00$m, Waveno, $k = 0.02635$ m^{-1}, Wave length, $\lambda = 238.451$ m, Wave period $T = 13.9626$ s, Wave amplitude, $a_0 = 10.0$m, Drag coefficient, $C_d = 1.2$, Inertia coefficient, $C_i = 2.0$, Acceleration due to gravity, $g = 9.81$ ms^{-2}, Angle of incident wave direction, $\theta_i = 90.0°$.

Table 10.12   Riser forces, $\omega = 0.45$, $\theta_i = 90°$, $h = 40.0$, no damping

Tables 10.13 to 10.15 show the same as above, but with a reduced wave height of 10m and a period of 7 seconds corresponding to smaller waves.

		$x = -2.0$m	$x = 0.0$m	$x = 2.0$m
	a Difffracted	60211.80551	59014.83806	60477.62565
$y = 1.0$m	b Incident	61967.30091	62651.70160	61888.15273
	Ratio a/b	0.97167	0.94195	0.97721
	a Diffracted	60211.80551	59014.83806	60477.62565
$y = -1.0$m	b Incident	61967.30091	62651.70160	61888.15273
	Ratio a/b	0.97167	0.94195	0.97721

Table of forces due to diffracted and incident waves. 2 by 3 riser array, with no damping effects.

Wave frequency, $\omega = 0.90$ s^{-1}, Depth, $h = 40.00$m, Waveno, $k = 0.08279$ m^{-1}, Wave length, $\lambda = 75.893$ m, Wave period $T = 6.9813$ s, Wave amplitude, $a_0 = 5.0$m, Drag coefficient, $C_d = 1.2$, Inertia coefficient, $C_i = 2.0$, Acceleration due to gravity, $g = 9.81$ ms^{-2}, Angle of incident wave direction, $\theta_i = 0.0°$.

Table 10.13   Riser forces, $\omega = 0.9$, $\theta_i = 0°$, $h = 40.0$, no damping

		$x = -2.0$m	$x = 0.0$m	$x = 2.0$m
$y = 1.0$m	a Diffracted	64480.48902	62291.04450	59349.26643
	b Incident	62662.44300	62310.05886	61956.97554
	Ratio a/b	1.02901	0.99969	0.95791
$y = -1.0$m	a Diffracted	59188.41730	62169.04854	64657.01322
	b Incident	61947.29668	62662.44300	62310.05886
	Ratio a/b	0.95546	0.99213	1.03767

Table of forces due to diffracted and incident waves. 2 by 3 riser array, with no damping effects.

Wave frequency, $\omega = 0.90$ s^{-1}, Depth, $h = 40.00$m, Waveno, $k = 0.08279$ m^{-1}, Wave length, $\lambda = 75.893$ m, Wave period $T = 6.9813$ s, Wave amplitude, $a_0 = 5.0$m, Drag coefficient, $C_d = 1.2$, Inertia coefficient, $C_i = 2.0$, Acceleration due to gravity, $g = 9.81$ ms^{-2}, Angle of incident wave direction, $\theta_i = 45.0°$.

Table 10.14 Riser forces, $\omega = 0.9$, $\theta_i = 45°$, $h = 40.0$, no damping

		$x = -2.0$m	$x = 0.0$m	$x = 2.0$m
$y = 1.0$m	a Diffracted	63581.95323	65529.08282	63581.95322
	b Incident	62061.48907	62061.48907	62061.48907
	Ratio a/b	1.02450	1.05587	1.02450
$y = -1.0$m	a Diffracted	63220.01714	65107.14609	63220.01714
	b Incident	62569.73800	62569.73800	62569.73800
	Ratio a/b	1.01039	1.04055	1.01039

Table of forces due to diffracted and incident waves. 2 by 3 riser array, with no damping effects.

Wave frequency, $\omega = 0.90$ s^{-1}, Depth, $h = 40.00$m, Waveno, $k = 0.08279$ m^{-1}, Wave length, $\lambda = 75.893$ m, Wave period $T = 6.9813$ s, Wave amplitude, $a_0 = 5.0$m, Drag coefficient, $C_d = 1.2$, Inertia coefficient, $C_i = 2.0$, Acceleration due to gravity, $g = 9.81$ ms^{-2}, Angle of incident wave direction, $\theta_i = 90.0°$.

Table 10.15 Riser forces, $\omega = 0.9$, $\theta_i = 90°$, $h = 40.0$, no damping

For the cases, given in tables 10.7 to 10.9, contours of wave elevation are shown in figures 10.2 to 10.7 and 8.33 to 8.35. The real and imaginary elevations represent two of the infinite number of instantaneous wave surfaces which occur during each wave cycle. The absolute plot represents the contours of the *maximum* water surface elevation achieved during a wave cycle. For this set of results, there are modest increases of the maximum load of up to 2.5% and significant reductions of up to 29%. This case, of a small wave with amplitude 0.2m and wave length of 4m, was the only one for which diffraction caused significant reductions in the wave loading. This is because the wave length is comparable with the cylinder spacing. For the case given in table 10.15, contours of wave elevations are shown in figures 10.8 to 10.10. The force reductions in this case were not significant.

10.3 Diffraction conclusions

In most of the cases calculated, the alterations in the maximum forces on the risers, due to diffraction are quite small. The largest increase, for the parameters considered is about 10%, though most increases are much less. The largest reduction is about 30%. The evidence indicates that in considering the wave climate, with respect to fatigue, *some* of the wave forces on the risers *might* be reduced significantly due to diffraction, but are not likely to be increased. Thus a systematic evaluation of the riser forces could give a pay-off in terms of increased fatigue life predictions of both risers and support frame. It is highly unlikely to predict a reduced fatigue life.
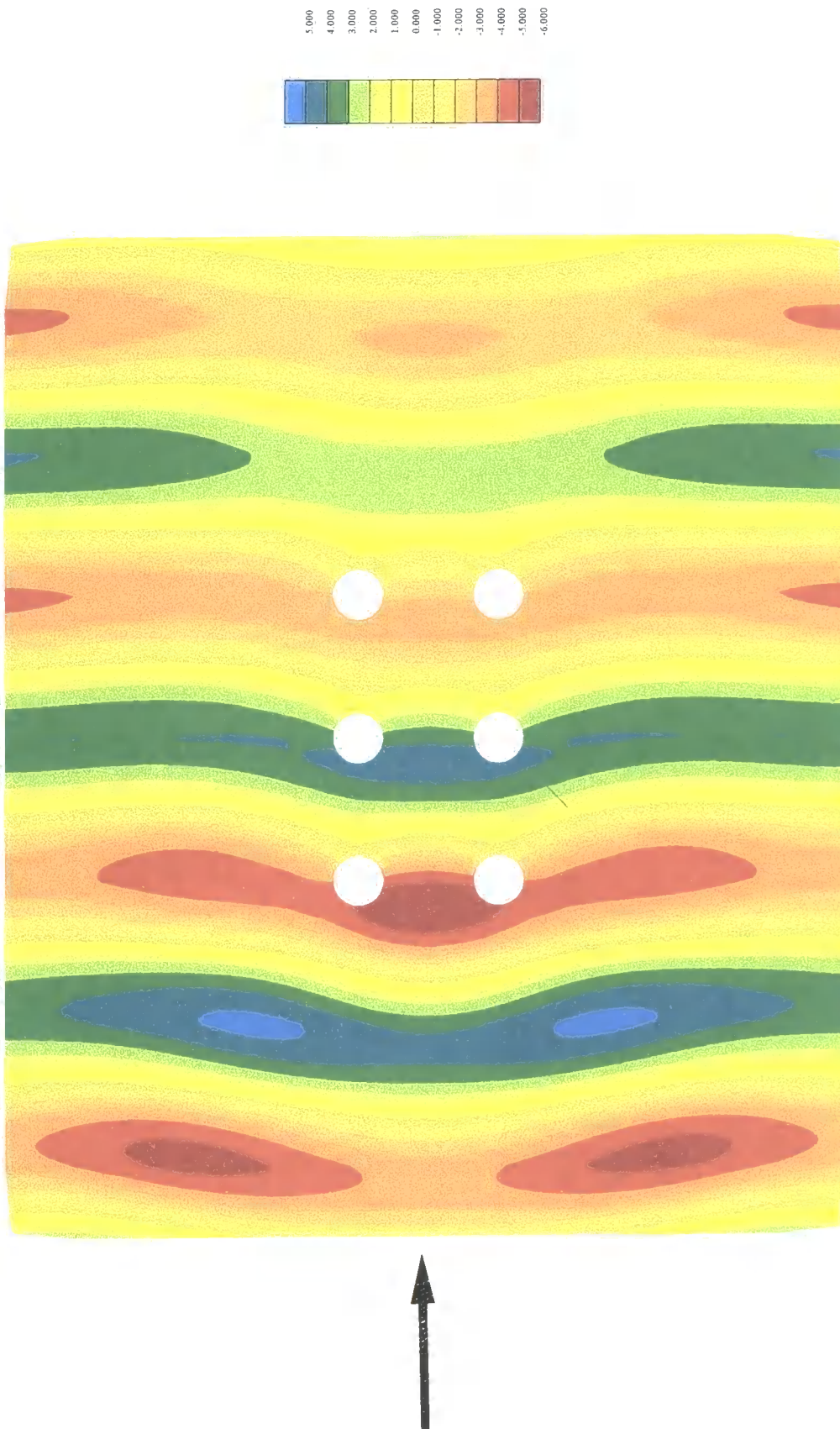
Figure 10.2   Real part of wave elevations, incident wave = 0 , frequency = 4.0
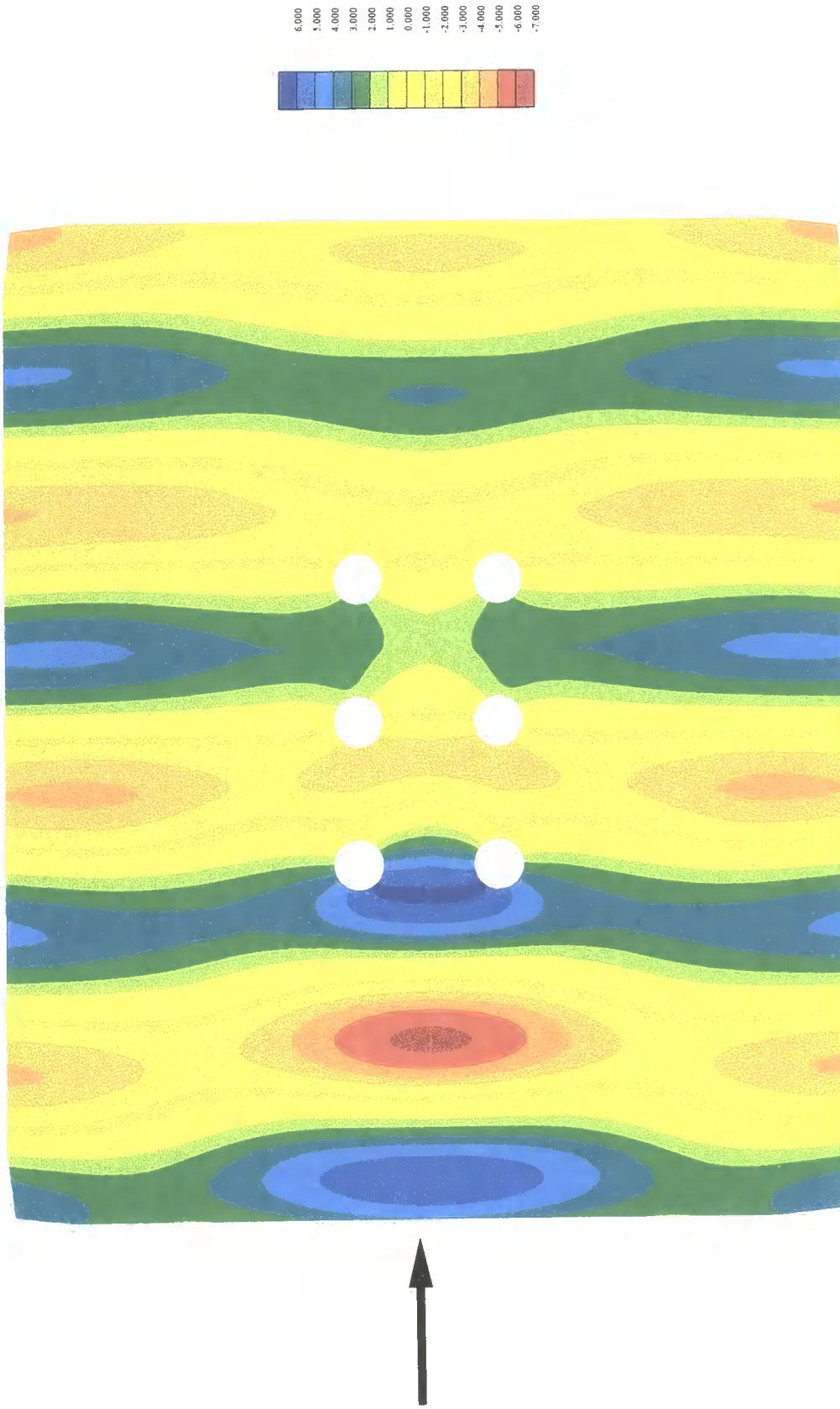
Figure 10.3   Imaginary part of wave elevations, incident wave = 0 ,frequency = 4.0

Figure 10.4   Absolute part of wave elevations, incident wave = 0 ,frequency = 4.0
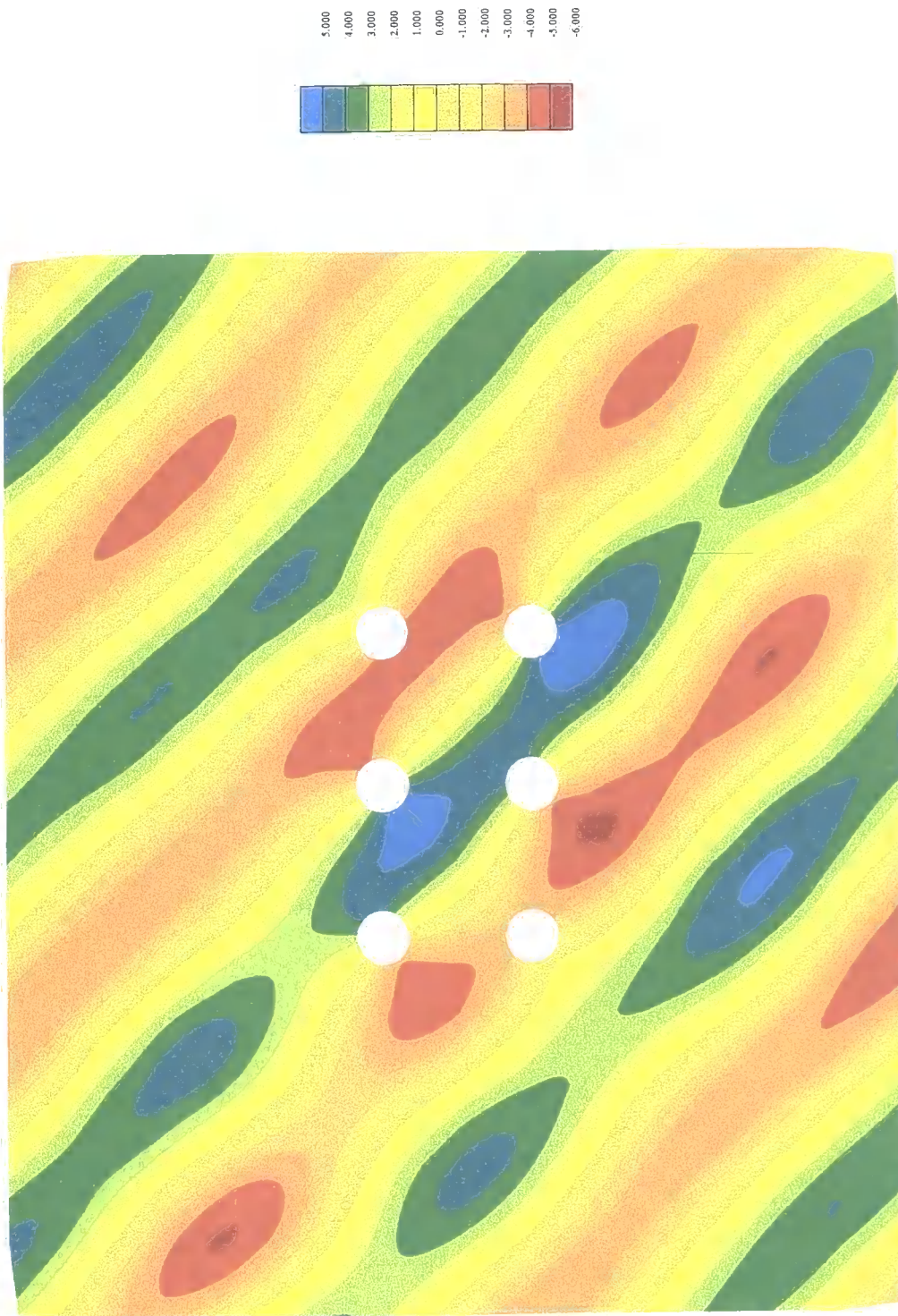
Figure 10.5 Real part of wave elevations, incident wave = 45 ,frequency = 4.0
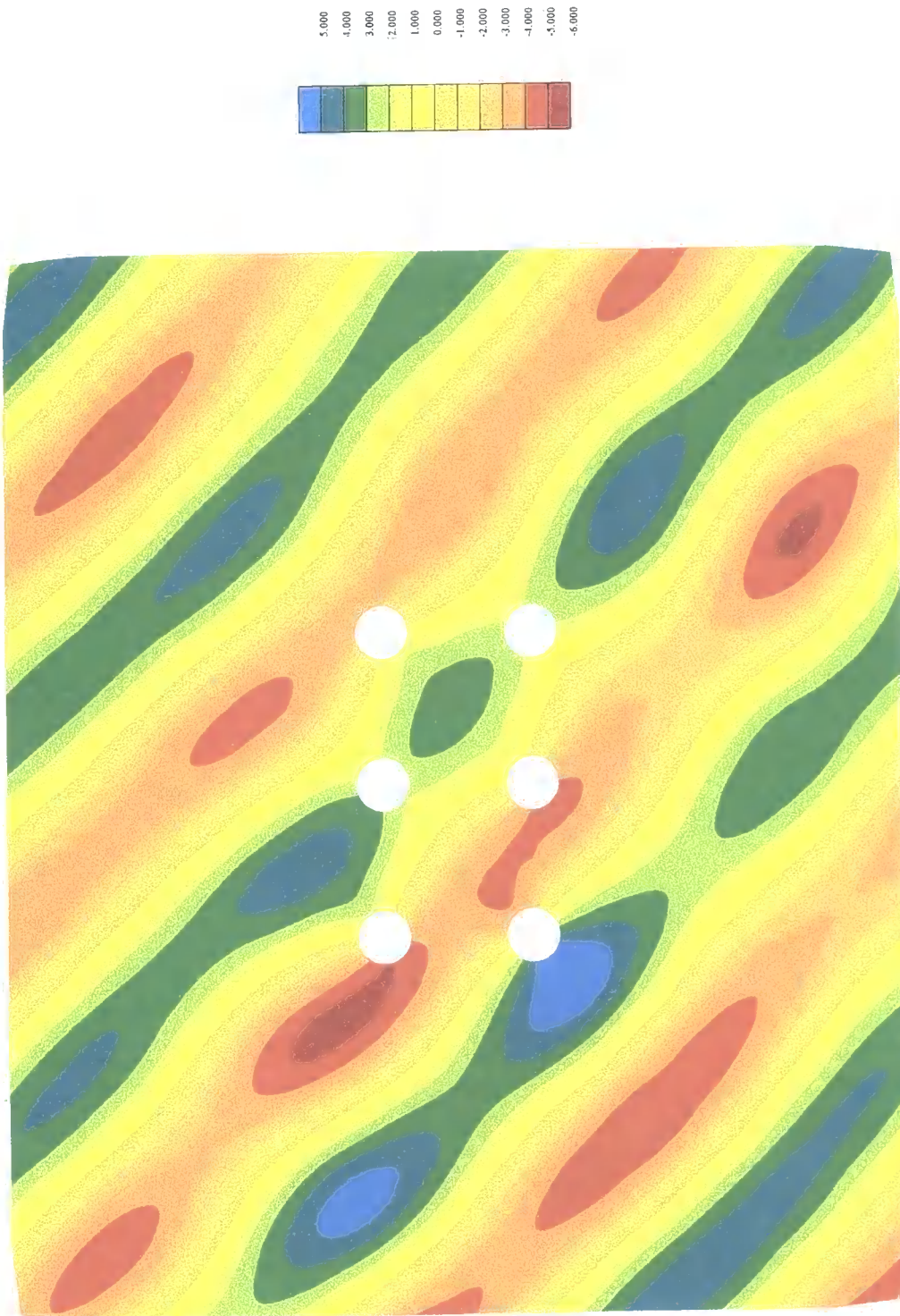
Figure 10.6   Imaginary part of wave elevations, incident wave = 45 ,frequency = 4.0
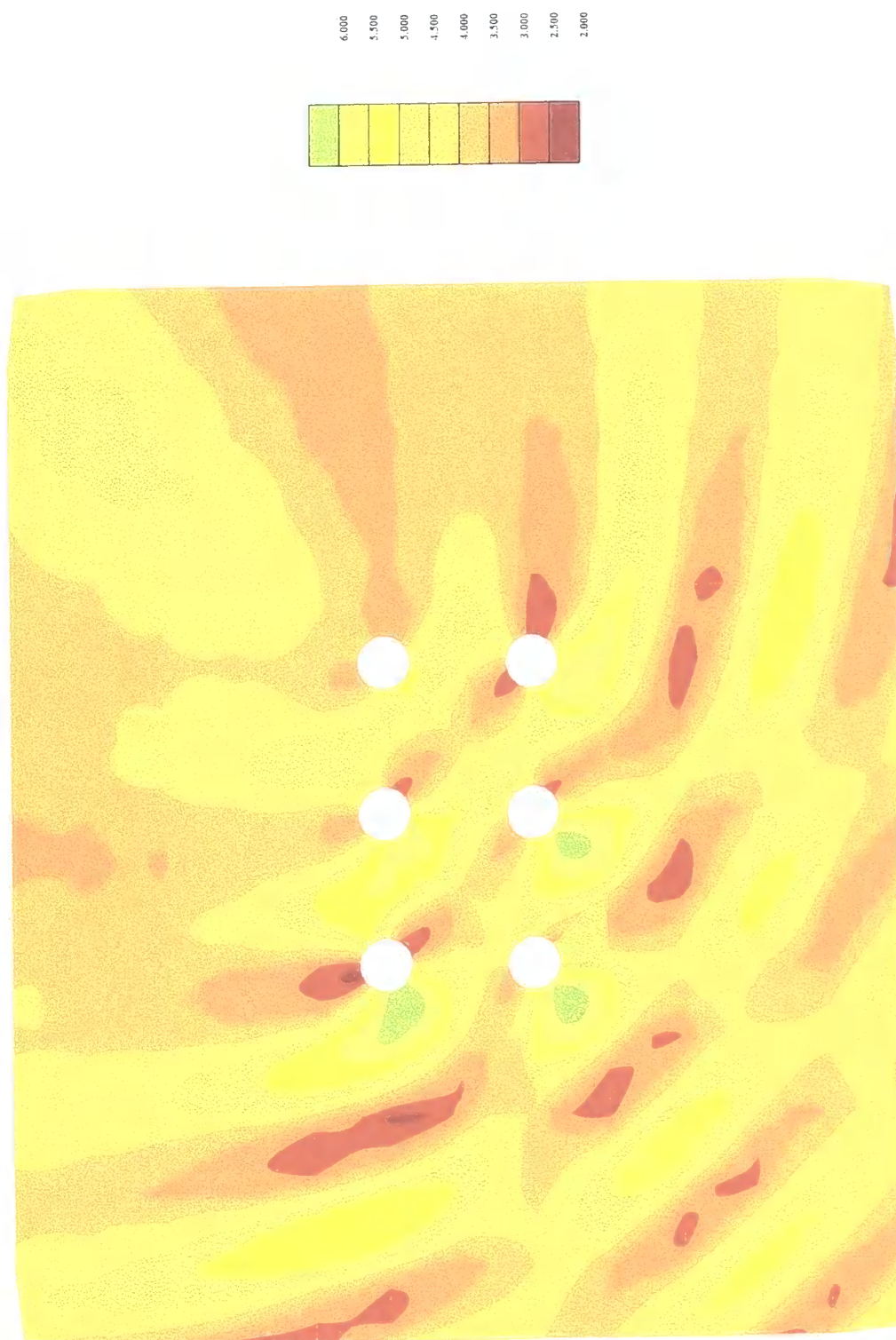
Figure 10.7   Absolute part of wave elevations, incident wave = 45 ,frequency = 4.0
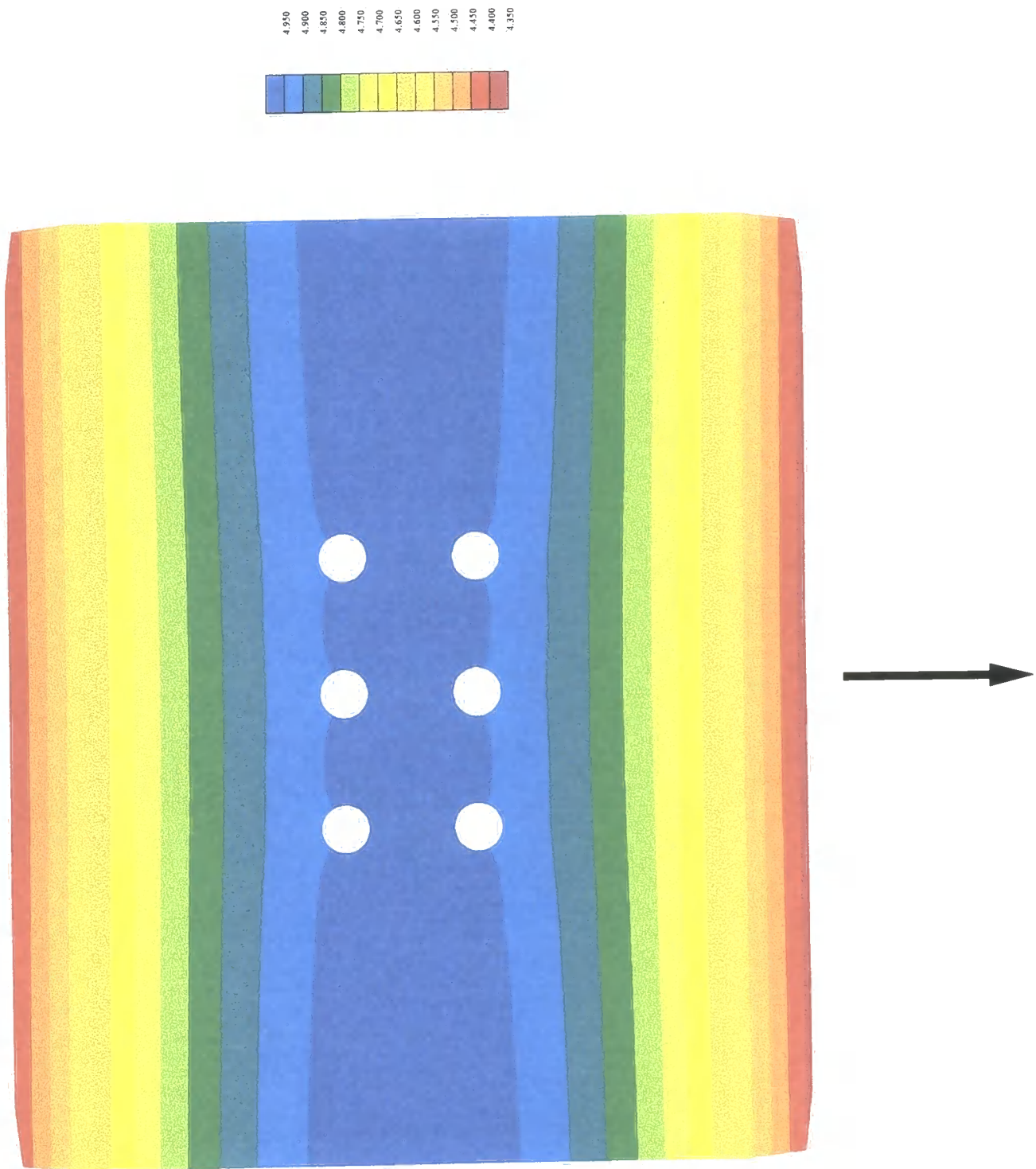
Figure 10.8   Real part of wave elevations, incident wave = 90 ,frequency = 0.9
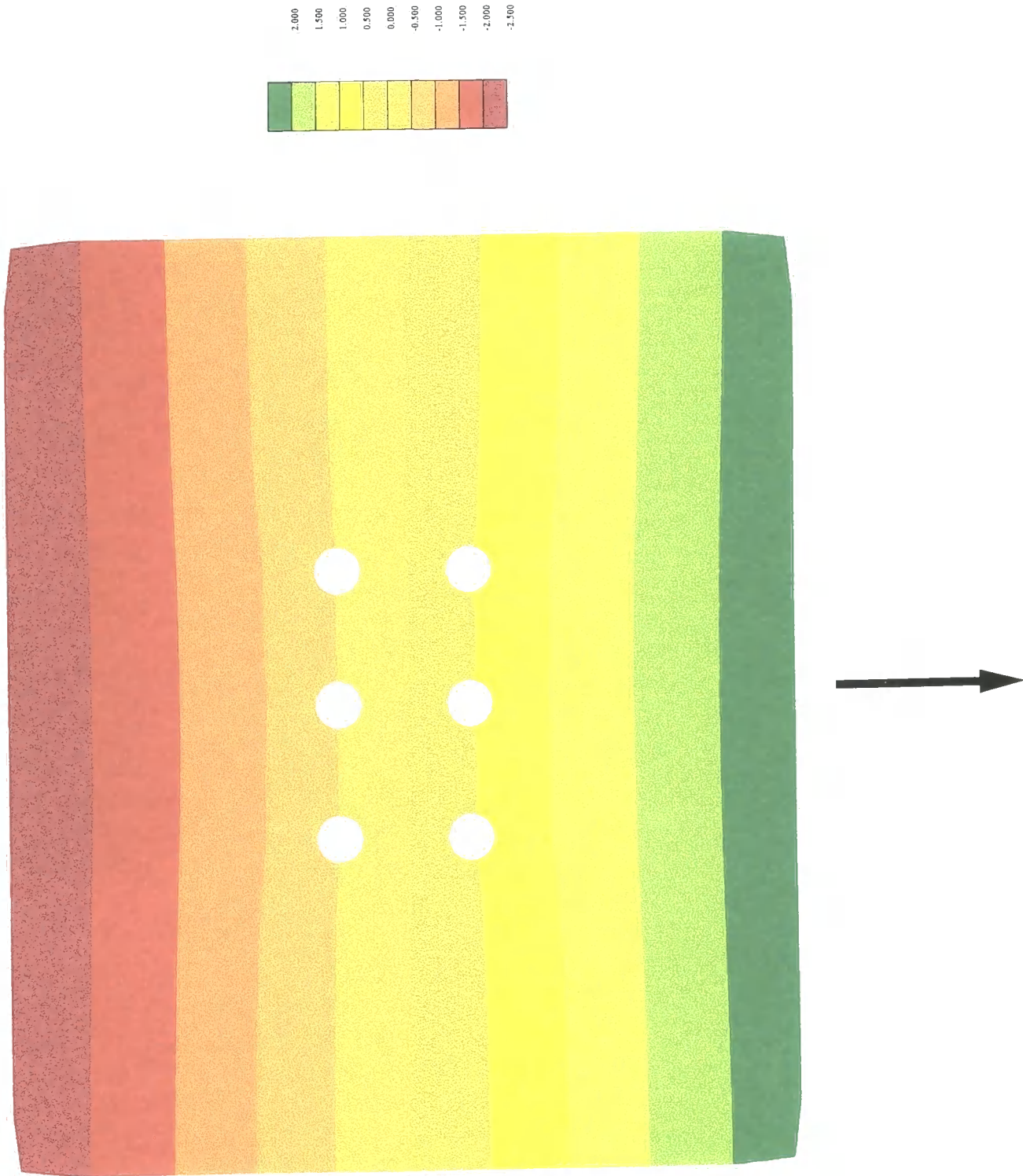
Figure 10.9   Imaginary part of wave elevations, incident wave = 90 ,frequency = 0.9
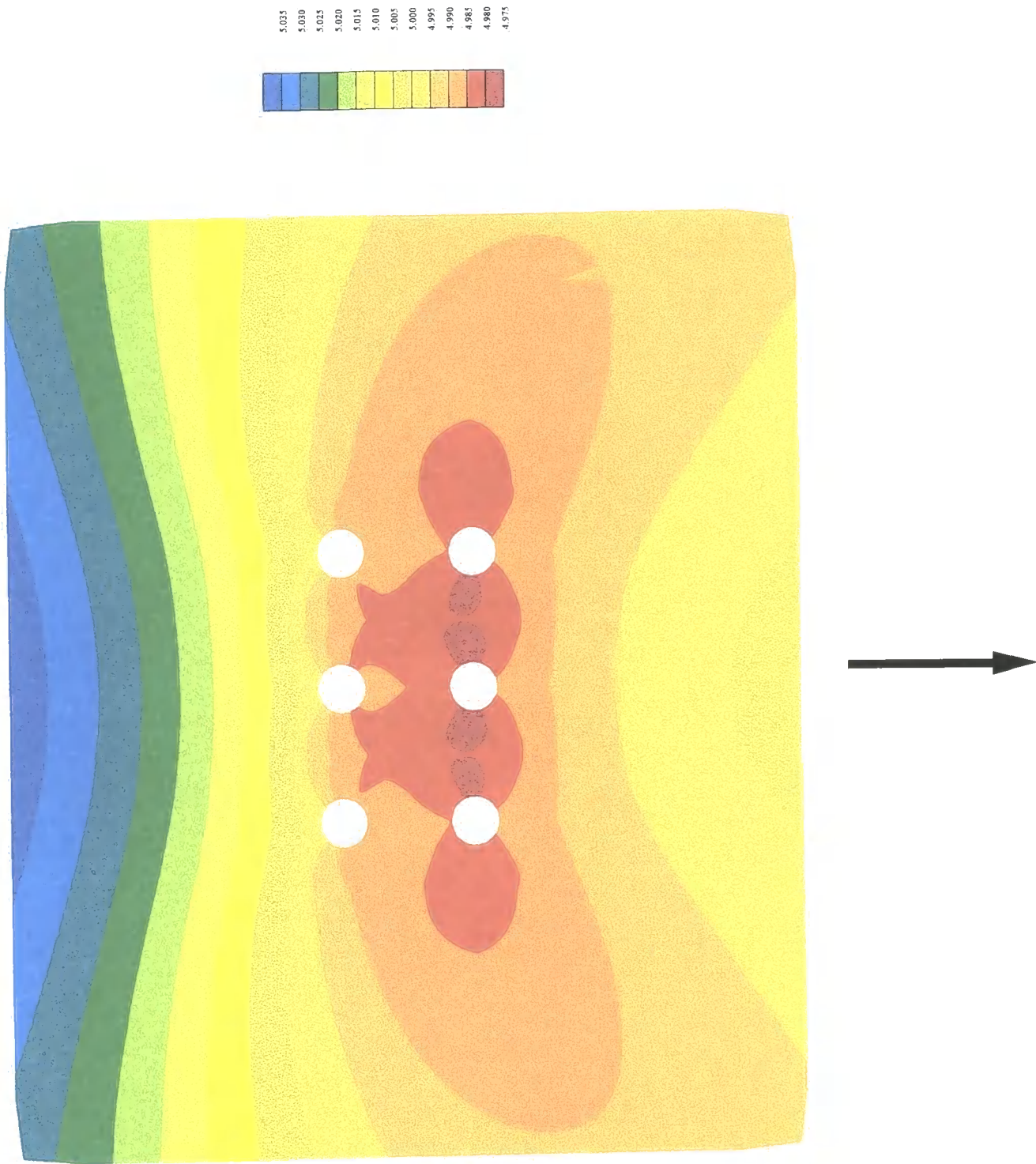
Figure 10.10   Absolute part of wave elevations, incident wave = 90 ,frequency = 0.9

Chapter 11

Wave force changes due to viscous energy losses

The program was modified so that all elements within the riser area foot print were given a damping constant, calculated from equation 9.15. In the program two parameters govern this effect. One is the area over which it is assumed the energy is dissipated, DAREA, which is in the third line of problem data. (See section A.5.1 and Appendix F). The second is the extent of the riser footprint area, which is specified by the minimum and maximum x and y values of the area containing the risers, XMIN, XMAX, YMIN, YMAX. These data must be consistent. Tables 11.1, 11.2 and 11.3 show a repetition of the results of tables 10.4, 10.5 and 10.6 but with a damping term in the wave equation, which absorbs energy from the waves. In order to have no effective energy loss due to damping, simply set DAREA to a large value. 1.0×10^{12} has been used in the present work. For damping to be present, set DAREA to a value representing the area over which it is felt that the viscous drag energy will be dissipated. In the current example a value of 3.59m^2 was used. This was because damping was applied in the region containing the risers of dimension 6m by 4m, giving a total area of 24m^2. The cross-sectional area of the six risers must be subtracted from this, i.e. $6\pi(0.36)^2$. The remaining area is divided equally between the six risers, giving a dissipation area of 3.59m^2. The actual choice of dissiation area is not critical (see Appendix F), as it governs only the area over which dissipation occurs, and *not* the total energy loss. The values of XMIN etc used to denote the area around the cylinders were:

$$\text{XMIN} = \text{-3.0}, \quad \text{XMAX} = 3.0, \quad \text{YMIN} = \text{-2.0}, \quad \text{YMAX} = 2.0$$

It would be desirable to carry out some parametric experimental and CFD studies, to evaluate the influence of different choices for the extent of the energy dissipation domain, although it is unlikely to be critical (see Appendix F).

Tables 11.1 to 11.3 show that the presence of the damping effects can both increase the maximum wave forces and also decrease them. The wave contours can rapidly attenuate in the wake of the first cylinder, and this gives rise to relatively large slopes of the water surface, and correspondingly high velocities, which generate large viscous drag forces. Table 11.1 demonstrates increases of 4% in the wave loading on the elements in the first row, and the forces are reduced by 10% in the back row. Similar effects are seen in the results for waves at angles of incidence of 45°, and 90°. Figures 11.1, 11.2 and 11.3 show the forces on the cylinders in a diagramatic form. In each case the height of the cylinder represents the maximum force obtained. In all the cases only the absolute maximum value of the force has been plotted.

		$x = -2.0$m	$x = 0.0$m	$x = 2.0$m
$y = 1.0$m	a Diffracted	47237.0	42980.0	40806.0
	b Incident	45046.0	45299.0	45325.0
	Ratio a/b	1.0486	0.94882	0.90029
$y = -1.0$m	a Diffracted	47237.0	42980.0	40806.0
	b Incident	45046.0	45299.0	45325.0
	Ratio a/b	1.0486	0.48829	0.90029

Table of forces due to diffracted and incident waves. 2 by 3 riser array, with damping effects

Wave frequency, $\omega = 1.0$ s^{-1}, Depth, $h = 20.00$m, Waveno, $k = 0.10504$ m^{-1}, Wave amplitude, $a_0 = 4.0$m, Drag coefficient, $C_d = 1.2$, Inertia coefficient, $C_i = 2.0$, Acceleration due to gravity, $g = 9.81$ ms^{-2}, Angle of incident wave direction, $\theta_i = 0.0°$. Area of dissipation, $DAREA = 3.59$ m^2

Table 11.1   Riser forces, $\omega = 1.0$, $\theta_i = 0°$, $h = 20.0$, with damping

		$x = -2.0$m	$x = 0.0$m	$x = 2.0$m
$y = 1.0$m	a Diffracted	47666.0	42745.0	39413.0
	b Incident	45471.0	45031.0	45376.0
	Ratio a/b	1.0483	0.94923	0.86858
$y = -1.0$m	a Diffracted	47295.0	47578.0	46209.0
	b Incident	45024.0	45471.0	45031.0
	Ratio a/b	1.0504	1.0463	1.0261

Table of forces due to diffracted and incident waves. 2 by 3 riser array, with damping effects

Wave frequency, $\omega = 1.0$ s^{-1}, Depth, $h = 20.00$m, Waveno, $k = 0.10504$ m^{-1}, Wave amplitude, $a_0 = 4.0$m, Drag coefficient, $C_d = 1.2$, Inertia coefficient, $C_i = 2.0$, Acceleration due to gravity, $g = 9.81$ ms^{-2}, Angle of incident wave direction, $\theta_i = 45.0°$. Area of dissipation, $DAREA = 3.59$ m^2

Table 11.2   Riser forces, $\omega = 1.0$, $\theta_i = 45°$, $h = 20.0$, with damping

		$x = -2.0$m	$x = 0.0$m	$x = 2.0$m
$y = 1.0$m	a Diffracted	43552.0	44151.0	43552.0
	b Incident	45062.0	45062.0	45062.0
	Ratio a/b	0.96649	0.97977	0.96649
$y = -1.0$m	a Diffracted	48645.0	50626.0	48645.0
	b Incident	45432.0	45432.0	45432.0
	Ratio a/b	1.0707	1.1143	1.0707

Table of forces due to diffracted and incident waves. 2 by 3 riser array, with damping effects

Wave frequency, $\omega = 1.0$ s^{-1}, Depth, $h = 20.00$m, Waveno, $k = 0.10504$ m^{-1}, Wave amplitude, $a_0 = 4.0$m, Drag coefficient, $C_d = 1.2$, Inertia coefficient, $C_i = 2.0$, Acceleration due to gravity, $g = 9.81$ ms^{-2}, Angle of incident wave direction, $\theta_i = 90.0°$. Area of dissipation, $DAREA = 3.59$ m^2

Table 11.3   Riser forces, $\omega = 1.0$, $\theta_i = 90°$, $h = 20.0$, with damping

		$x = -2.0$m	$x = 0.0$m	$x = 2.0$m
$y = 1.0$m	a Diffracted	1432.7	1086.9	911.41
	b Incident	1557.6	1558.2	1558.4
	Ratio a/b	0.91982	0.69756	0.58484
$y = -1.0$m	a Diffracted	1432.7	1086.9	911.41
	b Incident	1557.6	1558.2	1558.4
	Ratio a/b	0.919.82	0.69756	0.58484

Table of forces due to diffracted and incident waves. 2 by 3 riser array, with damping effects

Wave frequency, $\omega = 4.0$ s^{-1}, Depth, $h = 20.00$m, Waveno, $k = 1.63099$ m^{-1}, Wave amplitude, $a_0 = 0.2$m, Drag coefficient, $C_d = 1.2$, Inertia coefficient, $C_i = 2.0$, Acceleration due to gravity, $g = 9.81$ ms^{-2}, Angle of incident wave direction, $\theta_i = 0.0°$. Area of dissipation, $DAREA = 3.59$ m^2

Table 11.4   Riser forces, $\omega = 4.0$, $\theta_i = 0°$, $h = 20.0$, with damping

		$x = -2.0$m	$x = 0.0$m	$x = 2.0$m
$y = 1.0$m	a Diffracted	1483.0	1407.5	1283.5
	b Incident	1573.1	1571.6	1568.5
	Ratio a/b	0.94275	0.89555	0.81830
$y = -1.0$m	a Diffracted	1510.5	1467.7	1408.3
	b Incident	1569.6	1573.1	1571.6
	Ratio a/b	0.96234	0.93303	0.89609

Table of forces due to diffracted and incident waves. 2 by 3 riser array, with damping effects

Wave frequency, $\omega = 4.0$ s^{-1}, Depth, $h = 20.00$m, Waveno, $k = 1.63099$ m^{-1}, Wave amplitude, $a_0 = 0.2$m, Drag coefficient, $C_d = 1.2$, Inertia coefficient, $C_i = 2.0$, Acceleration due to gravity, $g = 9.81$ ms^{-2}, Angle of incident wave direction, $\theta_i = 45.0°$. Area of dissipation, $DAREA = 3.59$ m^2

Table 11.5 Riser forces, $\omega = 4.0$, $\theta_i = 45°$, $h = 20.0$, with damping

		$x = -2.0$m	$x = 0.0$m	$x = 2.0$m
$y = 1.0$m	a Diffracted	1159.1	990.53	1159.1
	b Incident	1557.9	1557.9	1557.9
	Ratio a/b	0.74397	0.63579	0.74397
$y = -1.0$m	a Diffracted	1420.6	1326.7	1420.6
	b Incident	1558.6	1558.6	1558.6
	Ratio a/b	0.91149	0.85121	0.91149

Table of forces due to diffracted and incident waves. 2 by 3 riser array, with damping effects

Wave frequency, $\omega = 4.0$ s^{-1}, Depth, $h = 20.00$m, Waveno, $k = 1.63099$ m^{-1}, Wave amplitude, $a_0 = 0.2$m, Drag coefficient, $C_d = 1.2$, Inertia coefficient, $C_i = 2.0$, Acceleration due to gravity, $g = 9.81$ ms^{-2}, Angle of incident wave direction, $\theta_i = 90.0°$. Area of dissipation, $DAREA = 3.59$ m^2

Table 11.6 Riser forces, $\omega = 4.0$, $\theta_i = 90°$, $h = 20.0$, with damping

	x=-2m	x=0m	x=2m
y=1.0m	43753	42973	44158
y=-1.0m	43753	42973	44158
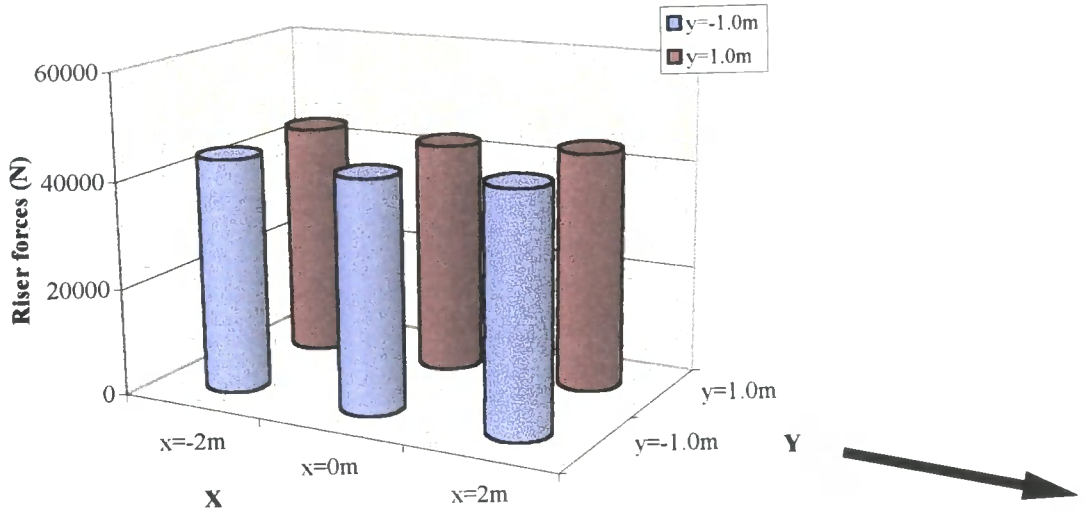
Riser forces - no damping (from table 10.4)

	x=-2m	x=0m	x=2m
y=1.0m	47237	42980	40806
y=-1.0m	47237	42980	40806
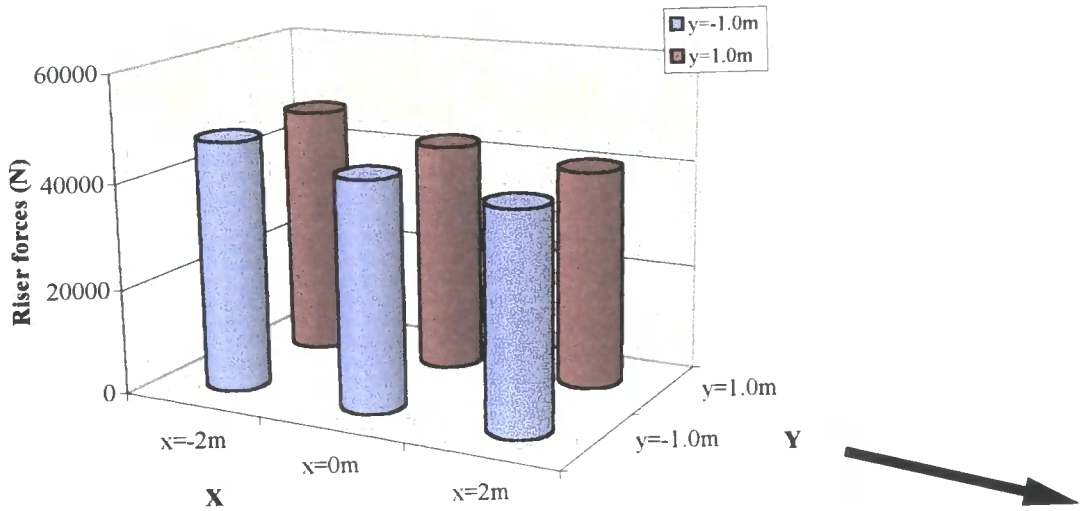
Riser forces - with damping (from table 11.1)

Fig. 11.1 Riser Forces comparing tables 10.4 and 11.1
Depth=20m, Frequency=1(1/s), Amplitude=4m, Wave no.=0.10504(1/m), Period=2π,
Wave length=59.82m, Angle of Incidence=0.0, Dissipation area=3.59sq.m

	x=-2m	x=0m	x=2m
y=1.0m	46836	45166	43516
y=-1.0m	43031	45201	46868
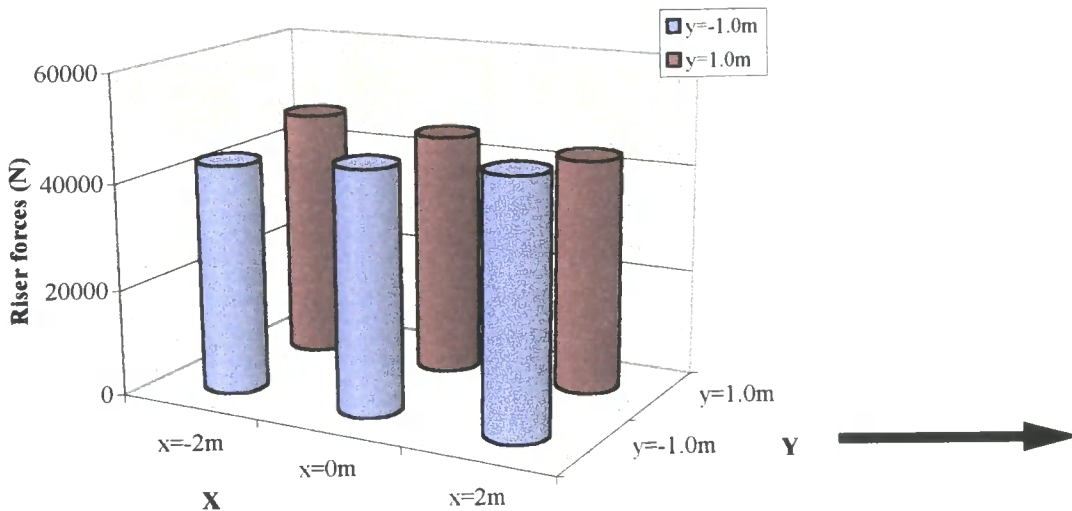
Riser forces - no damping (from table 10.5)

	x=-2m	x=0m	x=2m
y=1.0m	47666	42745	39413
y=-1.0m	47295	47578	46209
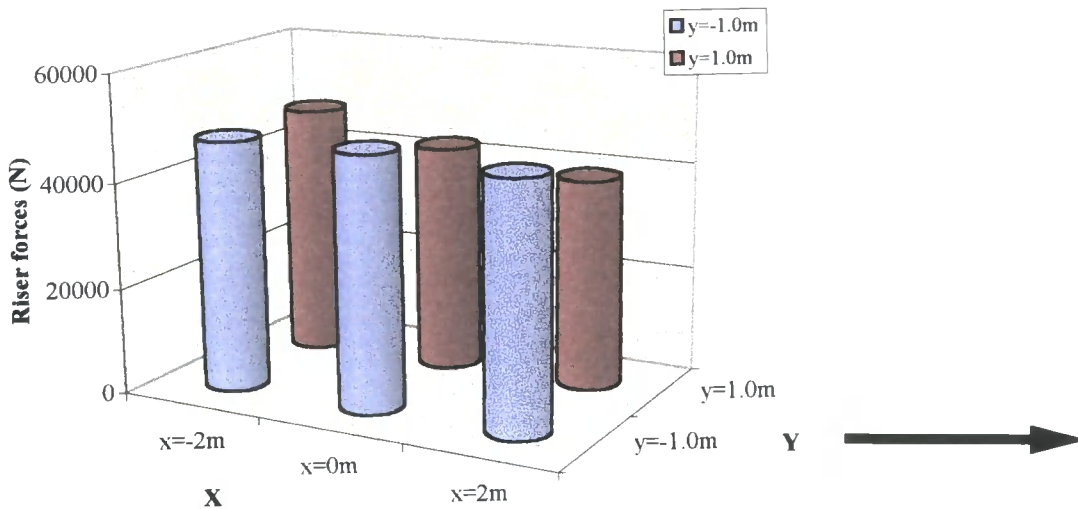
Riser forces - with damping (from table 11.2)

Fig. 11.2 Riser Forces comparing tables 10.5 and 11.2
Depth=20m, Frequency=1(1/s), Amplitude=4m, Wave no.=0.10504(1/m), Period=2π,
Wave length=59.82m, Angle of Incidence=45.0, Dissipation area=3.59sq.m

	x=-2m	x=0m	x=2m
y=1.0m	46142	47563	46142
y=-1.0m	45980	47311	45980
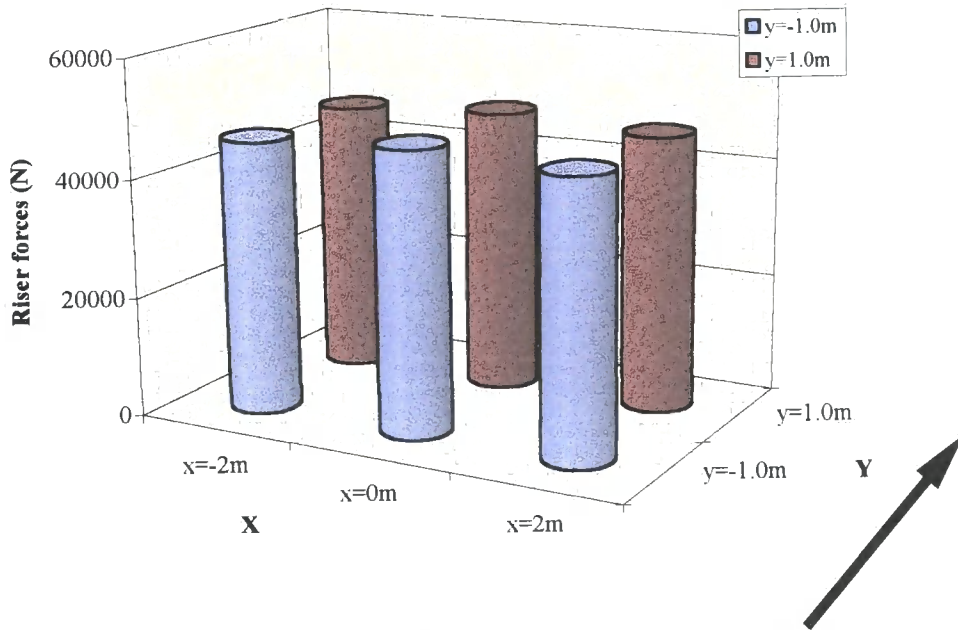
Riser forces - no damping (from table 10.6)

	x=-2m	x=0m	x=2m
y=1.0m	43552	44151	43552
y=-1.0m	48645	50626	48645
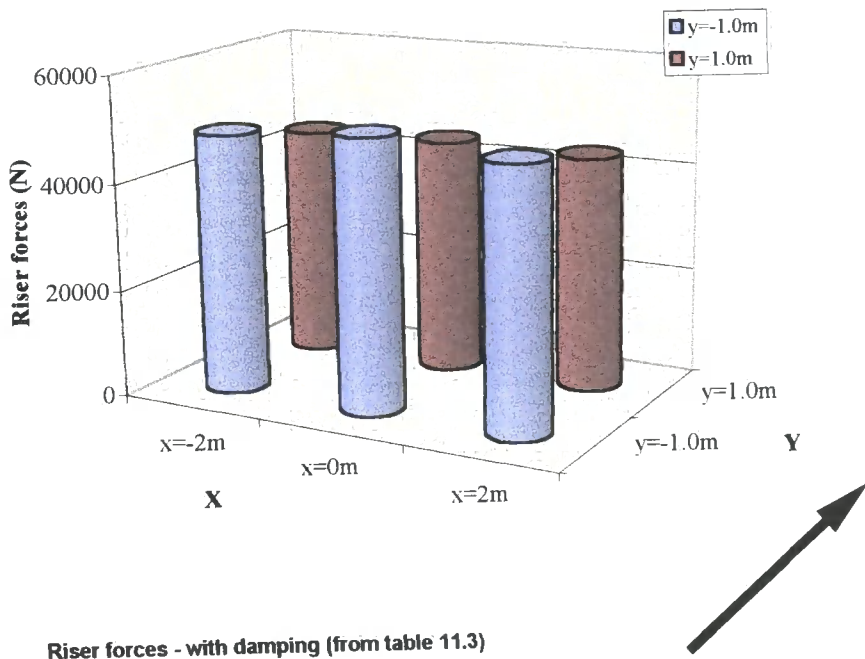
Riser forces - with damping (from table 11.3)

Fig. 11.3 Riser Forces comparing tables 10.6 and 11.3
Depth=20m, Frequency=1(1/s), Amplitude=4m, Wave no.=0.10504(1/m), Period=2π,
Wave length=59.82m, Angle of Incidence=90.0, Dissipation area=3.59sq.m

	x=-2m	x=0m	x=2m
y=1.0m	1501	1148	987
y=-1.0m	1501	1148	987
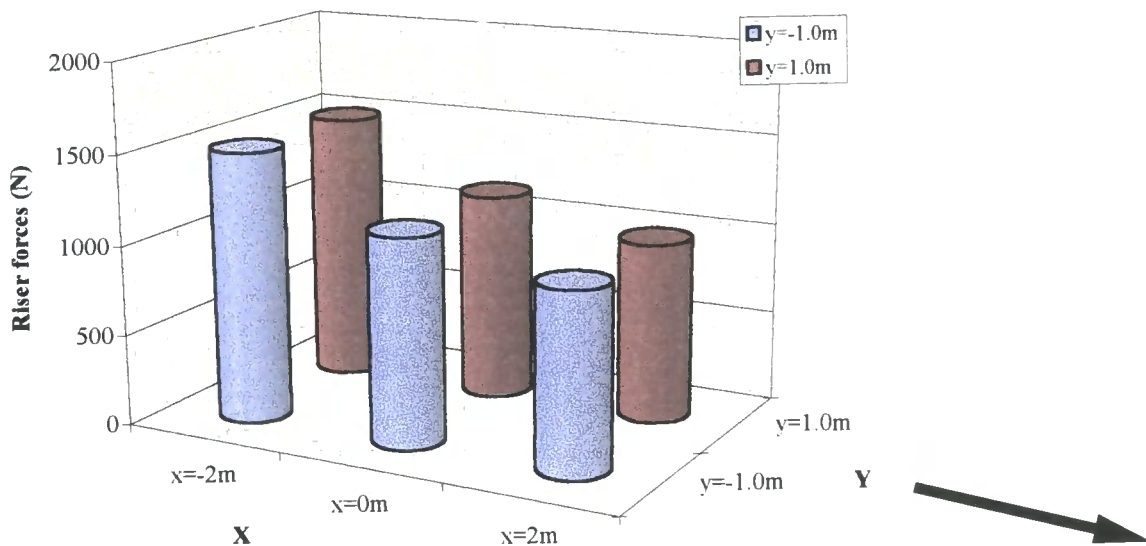
Riser forces - no damping (from table 10.7)

	x=-2m	x=0m	x=2m
y=1.0m	1433	1087	911
y=-1.0m	1433	1087	911
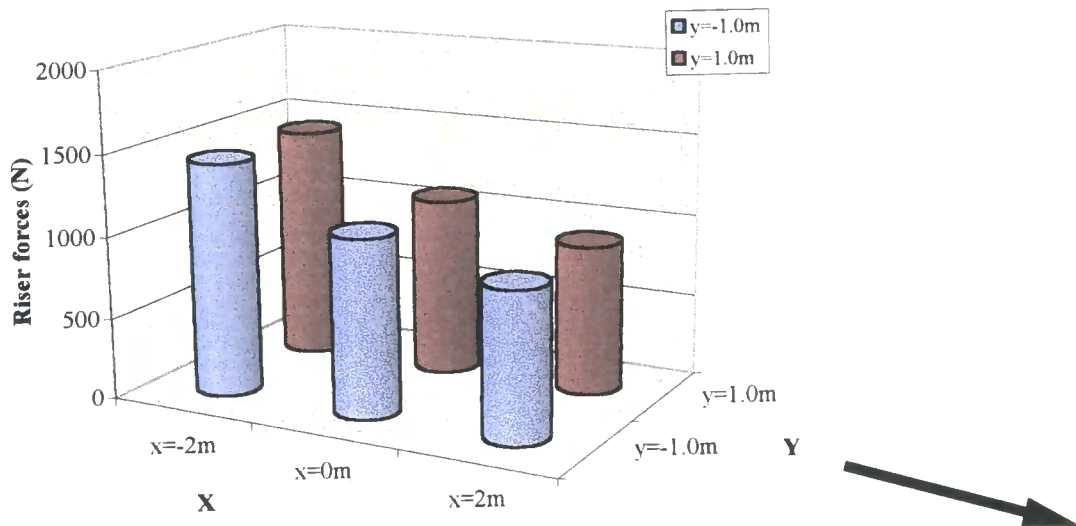
Riser forces - with damping (from table 11.4)

Fig. 11.4 Riser Forces comparing tables 10.7 and 11.4
Depth=20m, Frequency=4(1/s), Amplitude=0.2m, Wave no.=1.63099(1/m), Period=$\pi/2$,
Wave length=3.8524m, Angle of Incidence=0.0, Dissipation area=3.59sq.m

	x=-2m	x=0m	x=2m
y=1.0m	1575	1556	1447
y=-1.0m	1562	1547	1483
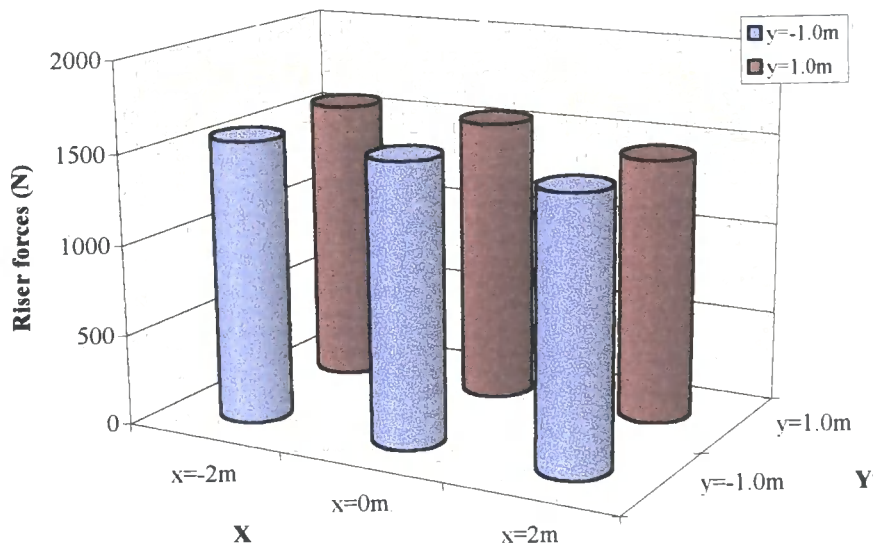
Riser forces - no damping (from table 10.8)

	x=-2m	x=0m	x=2m
y=1.0m	1483	1407	1284
y=-1.0m	1511	1468	1408
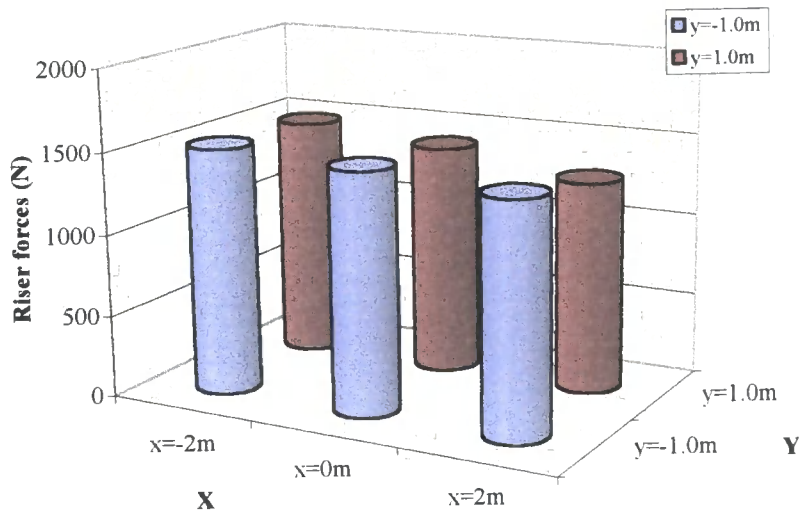
Riser forces - with damping (from table 11.5)

Fig. 11.5 Riser Forces comparing tables 10.8 and 11.5
Depth=20m, Frequency=4(1/s), Amplitude=0.2m, Wave no.=1.63099(1/m), Period=$\pi/2$,
Wave length=3.8524m, Angle of Incidence=45.0, Dissipation area=3.59sq.m

	x=-2m	x=0m	x=2m
y=1.0m	1232	1075	1232
y=-1.0m	1460	1375	1460
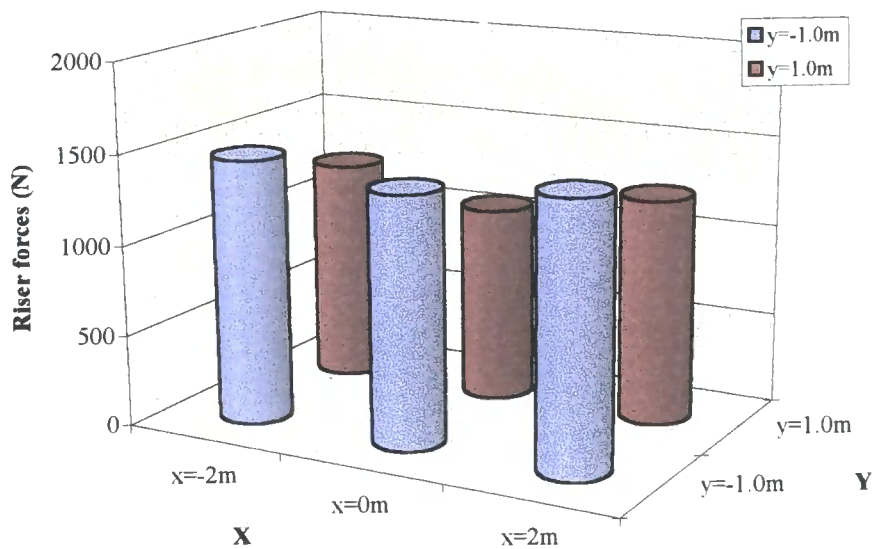
Riser forces - no damping (from table 10.9)

	x=-2m	x=0m	x=2m
y=1.0m	1159	991	1159
y=-1.0m	1421	1327	1421
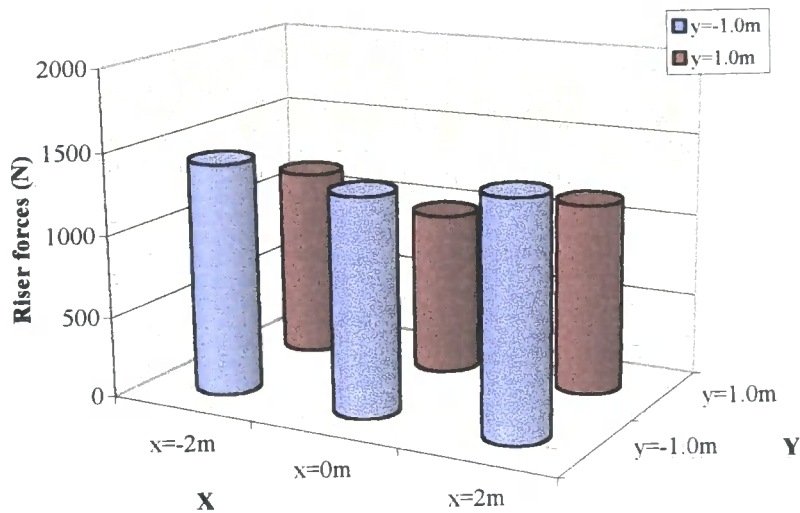
Riser forces - with damping (from table 11.6)

Fig. 11.6 Riser Forces comparing tables 10.9 and 11.6
Depth=20m, Frequency=4(1/s), Amplitude=0.2m, Wave no.=1.63099(1/m), Period=$\pi/2$,
Wave length=3.8524, Angle of Incidence=90.0, Dissipation area=3.59sq.m

Although the phase of the force and its variation through the wave cycle has been determined, it was not possible to plot these values without making the thesis even longer than it is currently.

Tables 11.4 to 11.6 and figures 11.4 to 11.6, show similar results for a shorter wave, with frequency, $\omega = 4.0$ s^{-1}. Here the reductions in the maximum wave force show a further reduction over those due to diffraction alone. The minimum maximum force due to the diffracted and damped wave is about 59% of the force due to the unaltered incident wave. Because these reductions are of such interest, they have been investigated more thoroughly. Figures 11.7, 11.8 and 11.9 show contour plots of real, imaginary and absolute values of the wave elevation, for the case of $\omega = 4.0$ (1/s), $a_0 = 0.2m$, $h = 20.0$ m, $\theta_i = 90°$ and viscous damping, corresponding to table 11.6.

These figures should be compared with figures 8.33, 8.34 and 8.35, which show the same case, but with no damping losses. The attenuation of the waves due to the damping is noticeable. The wave force reductions and the wave elevation reductions are consistent. The theory developed in this thesis is for small changes to the wave field, due to viscous effects. The relatively large effects which change the wave field significantly may not be modelled accurately. But the results do indicate that the energy loss to viscous drag is very important. The large attenuation is also consistent with a calculation of the power absorbed, using program POWER, which gives a wave absorption front width for each riser of about 1.5 m.

Two general conclusions can be drawn. The first is that the higher the frequencies and the shorter the waves, the larger the reduction in the wave forces. The second is that small maximum force increases are seen in the risers which bear the 'brunt' of the wave and large decreases in the maximum forces are seen on 'sheltered' risers.

Tables 11.7 to 11.12 show results comparable with Tables 10.10 to 10.15 for a depth of 40 m and wave frequencies of $\omega = 0.45$ s^{-1} and $\omega = 0.90$ s^{-1}. There are some increases of up to 8% in the maximum wave forces and there are decreases, of up to 14%, with respect to the forces for the unchanged or incident wave.

Figures 11.10 to 11.12 show the real and imaginary parts of the wave elevation corresponding to the wave forces given in table 11.12. These should be compared with figures 10.8, 10.9 and 10.10.

Although all the wave theory used is linear, some of the waves considered do not fall into the linear wave regime of Chapter 1. However, non-linear wave diffraction analysis is very difficult and has been attempted only for simple problems and for second order waves. The results obtained here using linear wave theory will still have an *indicative* value for non-linear regimes, but should, of course, be used with caution.
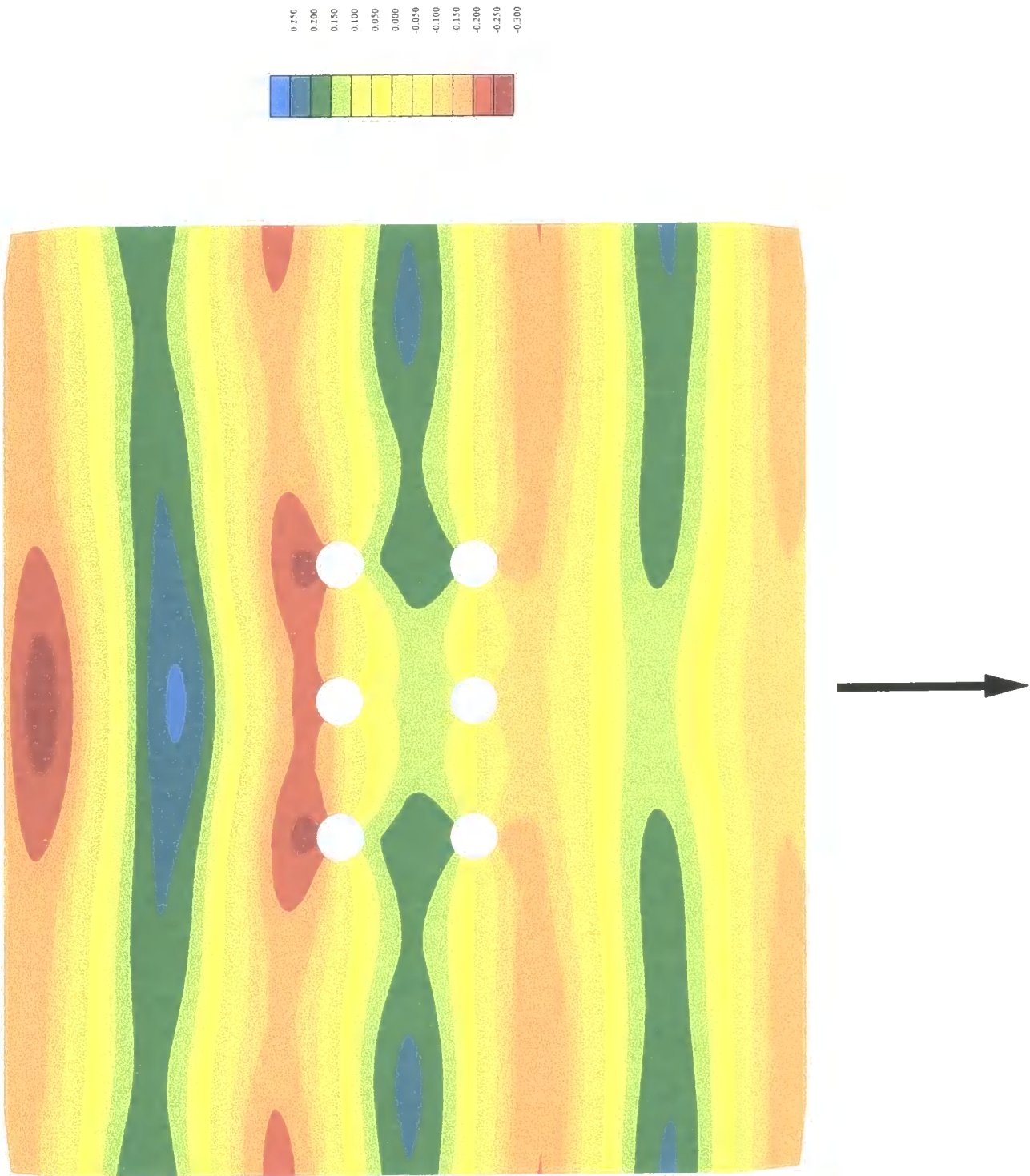
Figure 11.7 Real part of wave elevations, incident wave = 90, frequency = 4.0
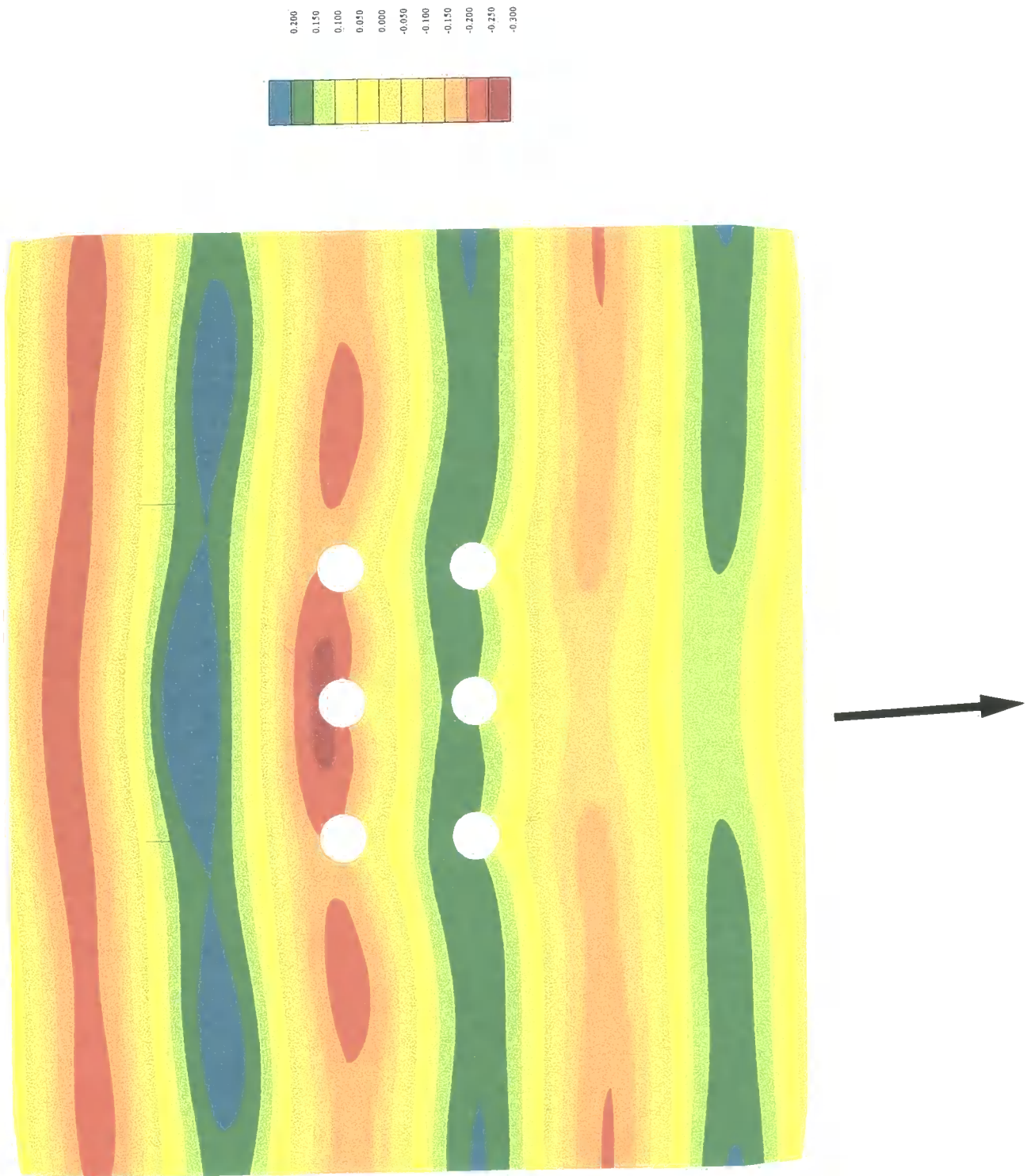
Figure 11.8 Imaginary part of wave elevations, incident wave = 90, frequency = 4.0
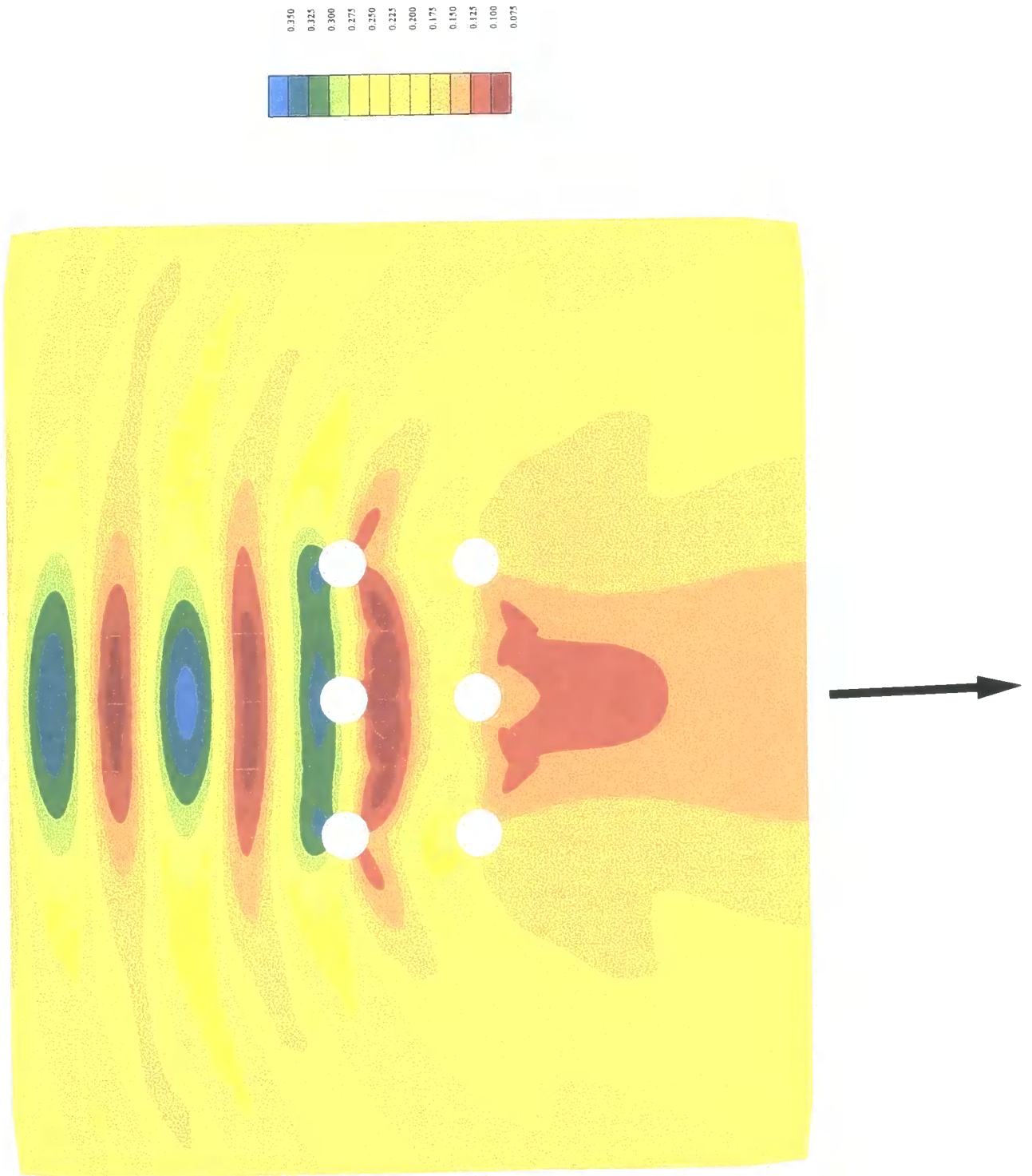
Figure 11.9 Absolute part of wave elevations, incident wave = 90, frequency = 4.0

		$x = -2.0$m	$x = 0.0$m	$x = 2.0$m
$y = 1.0$m	a Diffracted	337640.0	305740.0	297580.0
	b Incident	332490.0	330020.0	325730.0
	Ratio a/b	1.0155	0.92643	0.91356
$y = -1.0$m	a Diffracted	337640.0	305740.0	297580.0
	b Incident	332490.0	330025.0	325730.0
	Ratio a/b	1.0155	0.92643	0.91356

Table of forces due to diffracted and incident waves. 2 by 3 riser array, with damping effects

Wave frequency, $\omega = 0.45$ s^{-1}, Depth, $h = 40.00$m, Waveno, $k = 0.02635$ m^{-1}, Wave amplitude, $a_0 = 10.0$m, Drag coefficient, $C_d = 1.2$, Inertia coefficient, $C_i = 2.0$, Acceleration due to gravity, $g = 9.81$ ms^{-2}, Angle of incident wave direction, $\theta_i = 0.0°$. Area of dissipation, $DAREA = 3.59$ m^2

Table 11.7   Riser forces, $\omega = 0.45$, $\theta_i = 0°$, $h = 40.0$, with damping

		$x = -2.0$m	$x = 0.0$m	$x = 2.0$m
$y = 1.0$m	a Diffracted	343950.0	312460.0	287590.0
	b Incident	331110.0	328720.0	325410.0
	Ratio a/b	1.0388	0.95055	0.88378
$y = -1.0$m	a Diffracted	335340.0	337670.0	335040.0
	b Incident	332580.0	331110.0	328720.0
	Ratio a/b	1.0083	1.0198	1.0192

Table of forces due to diffracted and incident waves. 2 by 3 riser array, with damping effects

Wave frequency, $\omega = 0.45$ s^{-1}, Depth, $h = 40.00$m, Waveno, $k = 0.02635$ m^{-1}, Wave amplitude, $a_0 = 10.0$m, Drag coefficient, $C_d = 1.2$, Inertia coefficient, $C_i = 2.0$, Acceleration due to gravity, $g = 9.81$ ms^{-2}, Angle of incident wave direction, $\theta_i = 45.0°$. Area of dissipation, $DAREA = 3.59$ m^2

Table 11.8   Riser forces, $\omega = 0.45$, $\theta_i = 45°$, $h = 40.0$, with damping

		$x = -2.0$m	$x = 0.0$m	$x = 2.0$m
$y = 1.0$m	a Diffracted	319050.0	326540.0	319050.0
	b Incident	328110.0	328110.0	328110.0
	Ratio a/b	0.97239	0.97239	0.97239
$y = -1.0$m	a Diffracted	347440.0	362230.0	347440.0
	b Incident	331490.0	331490.0	331490.0
	Ratio a/b	1.0481	1.0928	1.0481

Table of forces due to diffracted and incident waves. 2 by 3 riser array, with damping effects

Wave frequency, $\omega = 0.45$ s^{-1}, Depth, $h = 40.00$m, Waveno, $k = 0.02635$ m^{-1}, Wave amplitude, $a_0 = 10.0$m, Drag coefficient, $C_d = 1.2$, Inertia coefficient, $C_i = 2.0$, Acceleration due to gravity, $g = 9.81$ ms^{-2}, Angle of incident wave direction, $\theta_i = 90.0°$. Area of dissipation, $DAREA = 3.59$ m^2

Table 11.9 Riser forces, $\omega = 0.45$, $\theta_i = 90°$, $h = 40.0$, with damping

		$x = -2.0$m	$x = 0.0$m	$x = 2.0$m
$y = 1.0$m	a Diffracted	65544.0	59117.0	55292.0
	b Incident	61967.0	62652.0	61888.0
	Ratio a/b	1.0577	0.94358	0.89342
$y = -1.0$m	a Diffracted	65544.0	59117.0	55292.0
	b Incident	61967.0	62652.0	61888.0
	Ratio a/b	1.0577	0.94358	0.89342

Table of forces due to diffracted and incident waves. 2 by 3 riser array, with damping effects

Wave frequency, $\omega = 0.90$ s^{-1}, Depth, $h = 40.00$m, Waveno, $k = 0.08279$ m^{-1}, Wave amplitude, $a_0 = 5.0$m, Drag coefficient, $C_d = 1.2$, Inertia coefficient, $C_i = 2.0$, Acceleration due to gravity, $g = 9.81$ ms^{-2}, Angle of incident wave direction, $\theta_i = 0.0°$. Area of dissipation, $DAREA = 3.59$ m^2

**Table 11.10** Riser forces, $\omega = 0.9$, $\theta_i = 0°$, $h = 40.0$, with damping

		$x = -2.0\text{m}$	$x = 0.0\text{m}$	$x = 2.0\text{m}$
$y = 1.0\text{m}$	a Diffracted	65717.0	58829.0	53150.0
	b Incident	62662.0	62310.0	61957.0
	Ratio a/b	1.0487	0.94414	0.85785
$y = -1.0\text{m}$	a Diffracted	65667.0	65732.0	63796.0
	b Incident	61947.0	62662.0	62310.0
	Ratio a/b	1.0600	1.0490	1.0600

Table of forces due to diffracted and incident waves. 2 by 3 riser array, with damping effects

Wave frequency, $\omega = 0.90 \text{ s}^{-1}$, Depth, $h = 40.00\text{m}$, Waveno, $k = 0.08279 \text{ m}^{-1}$, Wave amplitude, $a_0 = 5.0\text{m}$, Drag coefficient, $C_d = 1.2$, Inertia coefficient, $C_i = 2.0$, Acceleration due to gravity, $g = 9.81 \text{ ms}^{-2}$, Angle of incident wave direction, $\theta_i = 45.0°$. Area of dissipation, $DAREA = 3.59 \text{ m}^2$

Table 11.11   Riser forces, $\omega = 0.9$, $\theta_i = 45°$, $h = 40.0$, with damping

		$x = -2.0\text{m}$	$x = 0.0\text{m}$	$x = 2.0\text{m}$
$y = 1.0\text{m}$	a Diffracted	59886.0	60637.0	59886.0
	b Incident	62061.0	62061.0	62061.0
	Ratio a/b	0.96494	0.97705	0.96494
$y = -1.0\text{m}$	a Diffracted	67229.0	70078.0	67229.0
	b Incident	62570.0	62570.0	62570.0
	Ratio a/b	1.0745	1.1200	1.0745

Table of forces due to diffracted and incident waves. 2 by 3 riser array, with damping effects

Wave frequency, $\omega = 0.90 \text{ s}^{-1}$, Depth, $h = 40.00\text{m}$, Waveno, $k = 0.08279 \text{ m}^{-1}$, Wave amplitude, $a_0 = 5.0\text{m}$, Drag coefficient, $C_d = 1.2$, Inertia coefficient, $C_i = 2.0$, Acceleration due to gravity, $g = 9.81 \text{ ms}^{-2}$, Angle of incident wave direction, $\theta_i = 90.0°$. Area of dissipation, $DAREA = 3.59 \text{ m}^2$

Table 11.12   Riser forces, $\omega = 0.9$, $\theta_i = 90°$, $h = 40.0$, with damping
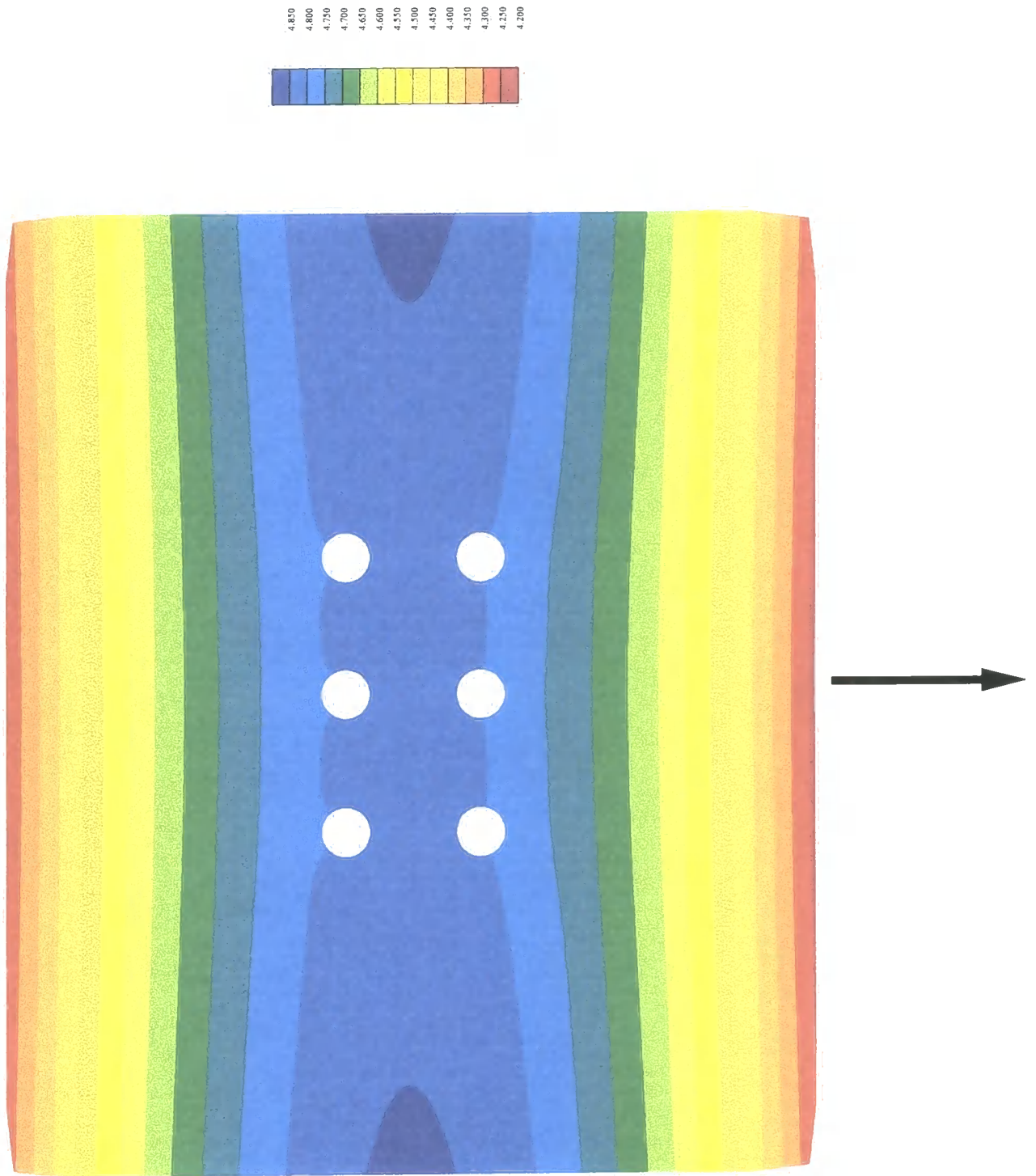
Figure 11.10 Real part of wave elevations, incident wave = 90, frequency = 0.9
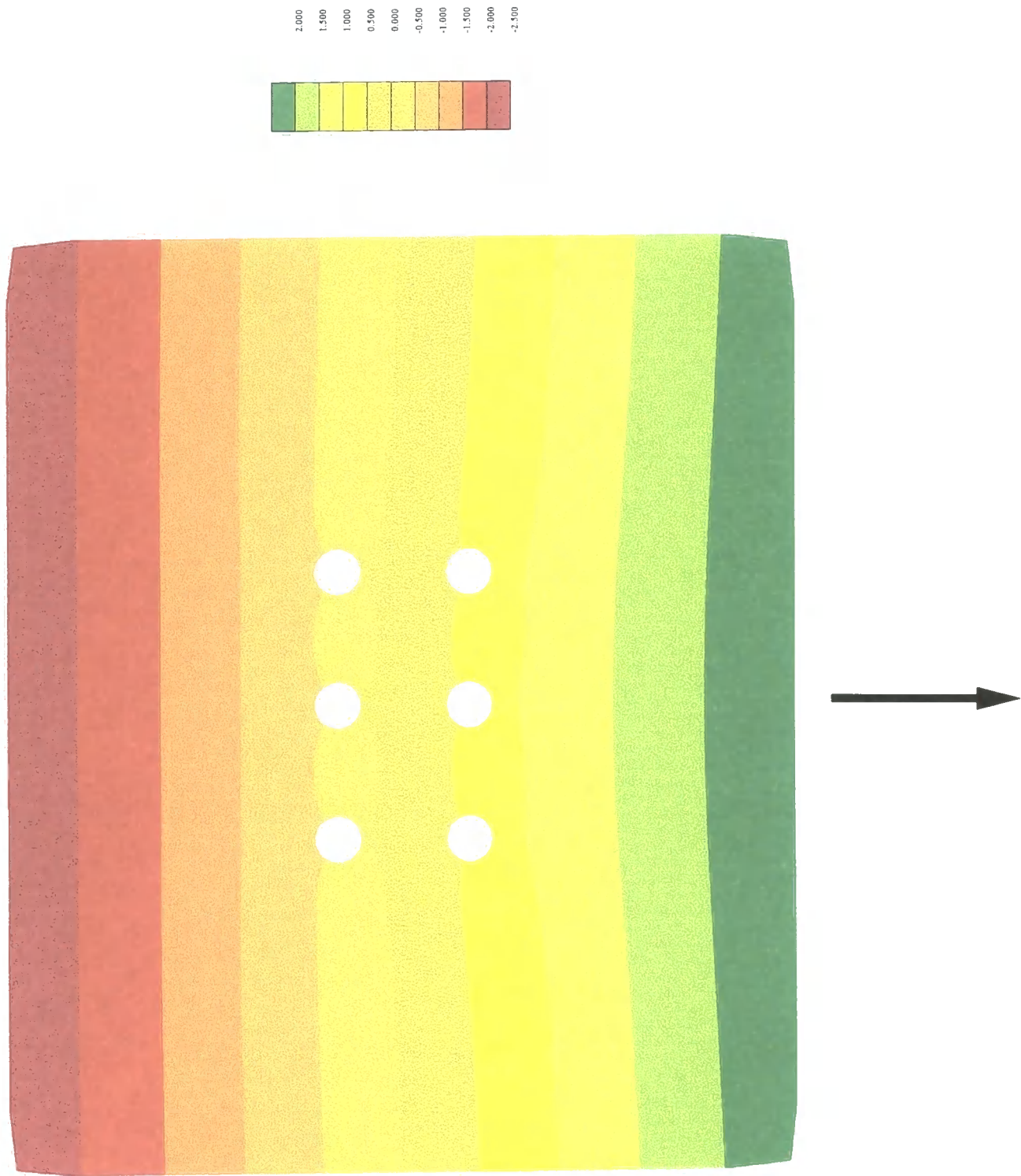
Figure 11.11 Imaginary part of wave elevations, incident wave = 90, frequency = 0.9
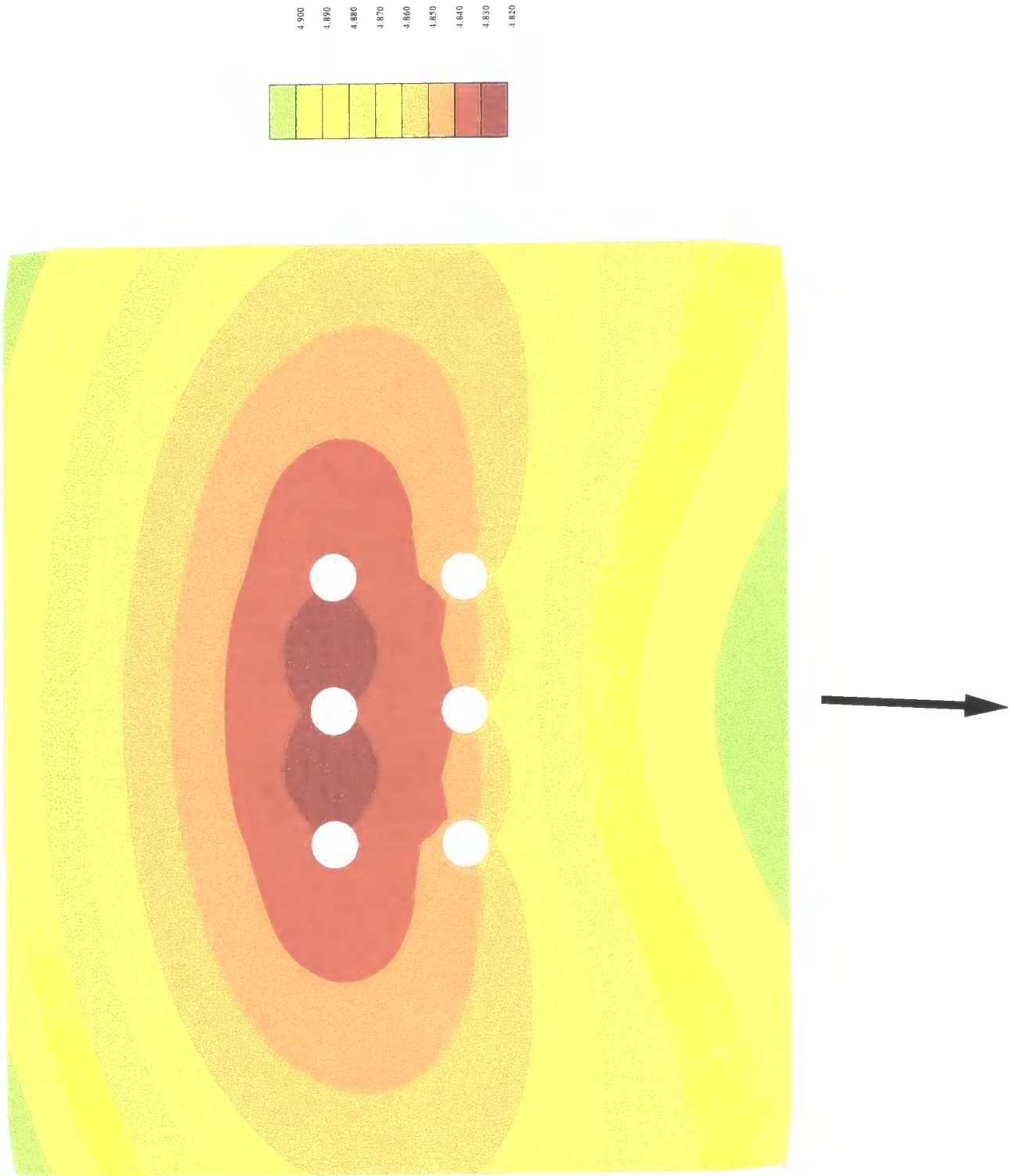
Figure 11.12 Absolute part of wave elevations, incident wave = 90, frequency = 0.9

Chapter 12

Conclusions

12.1 New infinite element

The results shown in Chapter 7 demonstrate that the new infinite element, together with conventional finite elements for wave problems, gives accurate results for the diffraction of waves around an ellipse, even for the case of ellipses with large aspect ratios.

The innovation introduced in the new infinite element is to allow the mapping parameter, A, to vary with the local co-ordinate, η, that is $A = A(\eta)$. The necessary theory is worked out and given in detail, and it is shown that the changes needed to the theory are relatively simple. The new mapping enables the meshes of finite and infinite elements to be shaped around the diffracting object, that is they no longer need to be radial. This gives considerable computational economies, for scattering objects of large aspect ratio, or indeed any object, which is not roughly circular. The extra complexites introduced to the theory by letting A be a function of η are easily incorporated into the infinite element program. The work demonstrates that at very little cost the range of problems that can be tackled efficiently with these infinite elements can be greatly extended.

The results further demonstrate that infinite elements do not need to be restricted to problems in which a circumcircle around the scattering object can be drawn entirely within the finite element mesh, since this rule is violated in several problems for which accurate results were obtained. The new infinite element can be thus be used with *considerable* confidence in problems with large aspect ratios.

It is of course still possible that two dimensional diffraction problems could be bounded by an ellipse, yet not converge in a hyperbolic-elliptical co-ordinate system, since there is no strict mathematical proof of convergence, but the results are highly suggestive that the new element is accurate for these types of problems.

It would be desirable to test the elements on probems such as diffraction of waves by two cylinders (and other problems with internal reflections), using an elliptical interface between the finite and infinite elements. However, this is beyond the scope of the present study. The techniques described in this thesis are easily extended to three dimensions, and to higher order infinite elements, having more terms in the multi-polar expansion.

12.2 Database, mesh generation and plotting software

I believe that the results throughout this thesis demonstrate that the software works and is efficient and effective. The programs have been used to generate a large numbers of finite element meshes for wave problems in many different applications, by a number of authors.

12.3 Riser wave diffraction and wave force calculations

It ought to be noted that the method used and described in this thesis is fairly crude, and can be subjected to a number of criticisms. Some of these have been outlined previously. Notwithstanding this caveat it is obvious from the calculations that some preliminary conclusions can be drawn. They are listed below.

It had originally been planned not to model the area containing the risers in any detail, but to represent them by a region of reduced permeability, as described in Chapter 8. However, on comparison of these results and those for the individually modelled risers, it became apparent that:

1. The extra work involved in modelling the risers was not excessive. The finest meshes run originally only took about 3 minutes to execute on a 486 66MHz PC. The program only utilised 640KB of memory. So now that PCs with clock speeds of 100s of MHz and memories of several hundred Mbytes are widely available, meshes of say 5 by 10 arrays of risers or even larger could very easily be modelled.

2. The comparisons between the results for the riser mesh and the zone of reduced permeability were not particularly impressive. Although this approach was originally considered as promising, on the grounds of simplicity and economy, it is not now recommended.

All subsequent work was therefore carried out on the wave forces using the finite element mesh which modelled the individual risers using special finite element meshes. Conclusions from these results are as follows:

1. The effects of diffraction close to the array of cylinders is relatively small. It has typically a modest effect on the maximum forces on the risers, which may be an increase or a decrease. There seems to be no systematic decrease in the force which the designer could rely upon.

2. The amount of energy abstracted from the waves, and lost as viscous dissipation is relatively small, compared to the amount of energy in the waves overall. In a given case the designer can compute the total energy lost to viscous dissipation by using the equations in Chapters 8 and 9 and an appropriate value of the drag coefficient, C_d. This would have to be estimated in any event if Morison's equation was to be used, which is the most usual case.

3. The procedure described in this report predicts that modest changes to the wave

field will result from the energy loss due to viscous effects around the risers, and that the neighbouring waves will attempt to diffract towards the riser zone, to 'fill the gap'.

4. The resulting changes in the forces on the risers are in the main, relatively small reductions. It would be unwise at this stage to rely upon the larger force reductions predicted. The shorter the wave length the more significant the reductions are. It could be that a comprehensive fatigue analysis would reveal quite large increases in fatigue life, due to the decreases in the wave loading at high frequencies.

5. The reductions in the wave forces are much more significant at small wave lengths, and in this case they can become quite large.

6. Diffraction and viscous drag effects on groups of risers will not, it is believed, have any significant effect on the wave forces due to large 'design' waves, at any rate for small numbers of risers. It would be desirable to carry out more computer simulations for large groups of closely spaced risers, for example an array of 5 by 10 risers with spacing equal to riser diameter.

7. The reductions in forces due to diffraction and viscous drag effects are significant, even for small arrays of risers, at low wave lengths, (or high frequencies). In cases where such small wave length waves make a significant contribution to the fatigue damage through the riser design life time, re-working of the calculations, using the methods described here, could lead to considerable extensions of predicted riser lifetimes.

8. Before relying on the reductions predicted, it would be desirable to develop more confidence in the proposed method, using the usual tools, of more detailed numerical simulations, full scale measurements and laboratory experiments. It would also be desirable for the computer program SMAWAVE to be run for a wider range of parameters, in particular the area over which the energy is dissipated by the viscous drag DAREA should be varied.

9. The economic savings given by extending fatigue lives are significant. Therefore the reductions in wave loading predicted here are worth more detailed examination. It would be economically worthwhile to carry out some detailed CFD investigations of the flow as the wave proceeds through the risers. This is probably just at the limit of current CFD capability. Such simulations could be compared with the results predicted in this thesis. If there was a good correlation, the program SMAWAVE could be used for fatigue life assessments.

10. The effects predicted are likely to be diminished, though not removed, in short crested waves.

12.4 Possible Future Work

1. It would be desirable if the findings of this thesis on wave forces could be scrutinised and critically reviewed by offshore industry experts, since at present they are tentative.

2. Studies could be used to determine the optimal strategy for determining the particle velocities around the cylinder, since the process for selecting these points is presently somewhat arbitrary.

3. A key parameter, about which little is presently known, is the area over which the viscous dissipation takes place. More detailed studies should be undertaken to develop a better way of determining this parameter, including comparisons with CFD simulations and with experiments. Experiments have the difficulty that they would really require both Froude number (wave similarity) and Reynolds number scaling. As is well known from ship models it is difficult to achieve both of these with the same model, unless full scale observations can be carried out.

4. The wave force calculations should be repeated, using the same velocity and acceleration values and a commercial and quality assured wave diffraction code. If this used a different method, such as boundary elements, so much the better.

5. It would be desirable for industry practitioners to work through a fatigue life prediction, which thus takes into account diffraction and viscous losses, for a typical riser array, and wave spectrum. The author expects that an increase of predicted fatigue life time of about 10% might well be obtained. As even quite modest offshore jacket installations may cost of the order of £100 million, even such a life extension would be very valuable. It should however be recalled that fatigue life times are developed ignoring the above effects, which are thus absorbed into the calibration of the design calculations. Such calculations are beyond the scope of this thesis.

6. As described above, comparisons with detailed CFD simulations could be carried out, which it is hoped would give additional confidence in the results.

Appendix A

Software

A.1 Overview

The software consists of four sets of programs - data generation programs, analysis programs, plotting programs and programs to calculate analytical solutions.

Data generation programs

SMACREA	Cylindrical mesh generator
SMAGEN	Rectangular mesh generator
CYLGEN	Riser mesh generator

Analysis program

SMAWAVE	Finite and Infinite element analysis program

Plotting programs

PLTELEV	Plots wave elevations around the risers
PLTOTF5	Plots contours of wave elevation

Analyticl programs

ELLIPSE	Analytical solution for flow around an elliptical body
CYL	Analytical solution for flow around a cylindrical body

All programs are written in ANSII standard Fortran 77 and are self-contained apart from the plotting programs, which use the Gino Graphics library to generate PostScript plotting files.

A.2 Program SMACREA

This program generates data for the wave program SMAWAVE. It generates sectorial meshes of triangular and quadrilateral elements divided radially and circumferentially. The sectors can be up to and include a complete circle. The mesh is divided radially into three parts, the middle of which is divided into two by a breakwater at some given radius. The program is designed so that it will operate in degenerate forms with, for example, the breakwater sector reduced to zero degrees (i.e. ALPHA=BETA in the data which follows).

A.2.1 Data preparation

Data preparation

Data line 1

ALPHA, BETA, GAMMA, BFLAG

ALPHA	Angle from 0° subtended by first sector
BETA	Angle from 0° subtended by first & second sector
GAMMA	Angle from 0° subtended by first, second & third sectors
BFLAG	= F ⇒ no breakwater, = T ⇒ breakwater present

Angles measured anti-clockwise from 0°, ALPHA ≤ BETA ≤ GAMMA ≤ 360°

Data line 2

P, Q, ECC1

P	Radius to breakwater
Q	Radius of outermost point
ECC1	Eccentricity

For cylindrical bodies, ECC1 = 0.0;
for elliptical bodies, ECC1 is derived from the aspect ration,
e.g. for aspect ratio of 4:1, ECC1=3.0

Data line 3

N1, N2

N1	Number of elements in radial direction before breakwater
N2	Number of elements in radial direction after breakwater

Note: The number of elements around the ellipse **must** result in an integer interval between nodes. (e.g. 12 elements ⇒ 30°; 36 elements ⇒ 10°).

Data line 4

M1, M2, M3, IT, ITYPEW, ELLTYP, INFTYP, NOR

M1	Number of radial subdivisions in first sector
M2	Number of circumferential subdivisions in second sector
M3	Number of circumferential subdivisions in third sector
IT	Indicator for singularities at breakwater tips (set to zero)
ITYPEW	Type of wave
	= 0 ⇒ shallow water wave
	= 1 ⇒ Berkhoff theory wave
	= 2 ⇒ deep water wave
ELLTYP	Type of elliptical mesh to generate
	= 1 ⇒ Distorted cylinder
	= 2 ⇒ Elliptical cylyndrical co-ordinates
INFTYP	Type of infinite element to generate
	= 3 ⇒ Exponential infinite element
	= 6 ⇒ 6-node mapped infinite element
NOR	Number of radii at which results are to be plotted

Data lines 5

    `R(I),I=1,NR`   where `NR=(N1+N2)*2+1`

    `R(I)`   Radius of ith node

Data lines 6

    `D(I),I=1,NR`   where `NR=(N1+N2)*2+1`

    `D(I)`   Depth at ith node

Data line 7

    Title   Data line 1 for program `SMAWAVE`

Data lines 8, 9 & 10

    Parameters & Data lines 3, 4 & 5 for program `SMAWAVE`

A.2.2 Sample data

Sample data

The sample data below is for a mesh of 36 elements around the ellipse and no breakwater. There are 4 finite elements radially, and one infinite element. Figure ??? shows mesh generated by data below.

```
  180.0      180.0      360.0        F
    2.6         5.6        1.0
    4    1
   18    0   18    0    0    2    6    5
   1.0        1.2        1.4      1.6      1.8      2.0      2.2      2.4
   2.6        5.2        5.6
   1.0        1.0        1.0      1.0      1.0      1.0      1.0      1.0
   1.0        1.0        1.0
Sample data for elliptical mesh, k=1, 18x(4+1), mapped inf.els.
   1.0        1.0        1.0      1.0      0.0      0.0      0.0
1025.0       0.72        0.0      0.0    1.0E12    0.0      0.0      0.0
   0.0        0.0        0.0      0.0
```

A.3 Program `SMAGEN`

This program generates data for the wave program `SMAWAVE`. It generates a rectangular mesh of 8-noded quadrilateral elements with the outer elements being 9-noded infinite elements. The depth (Z co-ordinate) is a given constant up to a specified Y ordinate and a (different) given constant beyond another specified Y ordinate. For constant depth over the whole domain, the given Y ordinates should be set equal. There is an option to have a breakwater along part of a specified Y ordinate, parallel to the X-axis.

A.3.1 Data preparation

Data preparation

Data line 1

```
NX1, NX2, NY1, NY2, NTYPEW, B                    (5I5,4X,A)
```

NX1	No.of elements in X direction before breakwater (≥ 2)
NX2	No.of elements in X direction after breakwater (≥ 2)
NY1	No.of elements in Y direction before breakwater (≥ 2)
NY2	No.of elements in Y direction after breakwater (≥ 2)
NTYPEW	Type of wave
	$= 0 \Rightarrow$ shallow water wave
	$= 1 \Rightarrow$ Berkhoff theory wave
	$= 2 \Rightarrow$ deep water wave
B	='B' if breakwater required, leave blank otherwise

Data line 2

```
NYD1, D1          (I5,F10.0)
```

NYD1	Y ordinate up to which depth is constant at D1
D1	Depth

Data line 3

```
NYD2, D2          (I5,F10.0)
```

NYD2	Y ordinate beyond which depth is constant at D2
D2	Depth

For constant depth over whole domain, set NYD1=NYD2 and D1=D2

Data lines 4

```
XG(I),I=1,NX      where NX=(NX1+NX2)*2+1          (8F10.0)
```

XG(I)	X co-ordinate of i-th X parallel

Data lines 5

```
YG(I),I=1,NY      where NY=(NY1+NY2)*2+1          (8F10.0)
```

YG(I)	Y co-ordinate of i-th Y parallel

Data line 6

Title	Data line 1 for program SMAWAVE

Data lines 7, 8 & 9

Parameters	Data lines 3, 4 & 5 for program SMAWAVE

A.3.2 Sample data

Sample data

```
7    9    7    7    1    A
1   20.0
1   20.0
-21.0    -7.0    -6.0    -5.5    -5.0    -4.5    -4.0    -3.5
 -3.0    -2.5    -2.0    -1.5    -1.0    -0.5     0.0     0.5
  1.0     1.5     2.0     2.5     3.0     3.5     4.0     4.5
  5.0     5.5     6.0     6.5     7.0     7.5     8.0     9.0
 23.0
-21.0    -7.0    -6.0    -5.5    -5.0    -4.5    -4.0    -3.5
 -3.0    -2.5    -2.0    -1.5    -1.0    -0.5     0.0     0.5
  1.0     1.5     2.0     2.5     3.0     3.5     4.0     4.5
  5.0     5.5     6.0     7.0    21.0
2 by 3 Risers Array Test Case - Finer Mesh Offset - origin not in ctr
  1.0     9.81    4.0    20.0   270.0     0.0     0.0     0.0
1025.0     0.72    1.2     2.0     1.0     0.0     0.0     0.0
```

A.4   Program CYLGEN

This program generates data for the wave program SMAWAVE. It generates a rectangular mesh of 8-noded quadrilateral elements around cylinders, surrounded by a given number of 8-noded quadrilateral elements and an outer ring of 9-noded infinite elements.

A.4.1 Data preparation

Data preparation

Data line 1

Title	Data line 1 for program SMAWAVE

Data line 2

R, H, NR, NH, NCX, NCY, NFE   (free format)

R	Radius of cylinder
H	Half-length of square
NR	Number no.of elements radially
NH	Number of elements in half-length
NCX	Number of cylinders in x direction
NCY	Number of cylinders in y direction
NFE	Number of rows of finite elements around cylinders

Data lines 3,4 & 5

Parameters	Data lines 3, 4 & 5 for program SMAWAVE

A.4.2 Sample data

Sample data

```
Linton & Evans - incident wave pi/4, kh=2*pi/2
0.5 1.0  2  2  2  2  4
3.14159    1.0     1.0     1.0    45.0     0.0     0.0
1025.0     0.72    0.0     0.0  1.0E12     0.0     0.0     0.0
   0.0     0.0     0.0     0.0
```

A.5 Program SMAWAVE

A program for the prediction of wave diffraction and refraction, using finite and infinite elements.

A.5.1 Data preparation

Data preparation

Data line 1

TITLE		(alphanumeric)
TITLE	Problem title	

Data line 2

NN, NE, NX, IREFL, ITYPEW, NTIREX   (6I5)

NN	Number of nodes
NE	Number of elements
NX	Order of integration for infinite elements (type 3) (if in doubt, set NX = 6)
IREFL	Introduces a straight infinite boundary through the origin of the co-ordinate system of the problem. The boundary is perfectly reflecting = 0 ⇒ no boundary = 1 ⇒ boundary present
ITYPEW	Wave type number = 0 ⇒ shallow water wave = 1 ⇒ Berkhoff theory wave = 2 ⇒ deep water wave
NTIREX	Type of output = 0 ⇒ forces and element by element = 1 ⇒ data for contour plotting

Data line 3

OMEGA, GRAV, AO, HINF, THETAI, EMMMM, ATTEN, ANGREF

(8F10.5)

OMEGA	Angular frequecy of waves
GRAV	Acceleration due to gravity
AO	Amplitude of incoming waves
HINF	Depth of water at infinity
THETAI	Angle of incidence of incoming waves, (measured in degrees, anti-clockwise from positive x-axis)
EMMMM	Linearised friction coefficient – not used
ATTEN	Attenuation length. This is difficult to estimate – see below.
ANGREF	Angle made by infinite boundary to positive x-axis, in degrees, used only if IREFL is non-zero. It should be only in multiples of 90° i.e. 90° or 270°

The amplitude of waves that are reflected, will be assumed to decay very roughly as $\exp(-r/ATTEN)$ where r is the distance from the inner nodes of the infinite elements, going out towards infinity. If r_1 is the radius of the inner nodes of infinite elements and r_2 is the radius of the ring of nodes, then $ATTEN$ can be estimated from

$$\exp\left(\frac{R1 - R2}{ATTEN}\right) = \frac{\sqrt{J_0(r_2)^2 + Y_0(r_2)^2}}{\sqrt{J_0(r_1)^2 + Y_0(r_1)^2}}$$

where J_0 and Y_0 are Bessel functions. See reference 12. If $ATTEN$ is left zero or negative, it will be calculated by the program from the above formula.

Data line 4

RHO, DIAM, CD, CI, DAREA, PERM   (5F10.5)

RHO	Water density
DIAM	Diameter of cylinders
CD	Drag coefficient used in both damping calculation and force calculation
CI	Inertia coefficient used in force calculation
DAREA	Area for dissipation set to very large, 10^{12} say, for no dissipation - for dissipation set to area around risers, e.g. in examples 1 m^2
PERM	Permeability

Data lines 5

XMIN, XMAX, YMIN, YMAX (4F10.5)

XMIN	x and y bounds for riser zone (if any)
XMAX	in which damping is to be applied and forces
YMIN	are to be calculated
YMAX	

Data lines 6

```
NNOD, X, Y, Z                                    (I5,3F10.5)
```

`NNOD`	Node number
`X`	X co-ordinate of node
`Y`	Y co-ordinate of node
	(rectangular right-handed cartesion co-ordinates)
`Z`	Depth of water

All nodes must be present in ascending numerical order of node number. No gaps are allowed – there **must** be `NN` lines of data.

Data lines 7

```
NETYPE, IFS, INTGR, NOD                          (11I5)
```

`NETYPE`   Element type

= 1 ⇒ 6-noded isoparametric triangular finite element
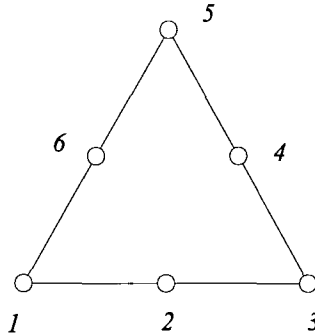
= 2 ⇒ 8-noded isoparametric quadrilateral finite element
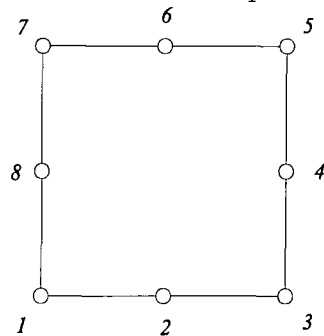
= 3 ⇒ 9-noded parametric quadrilateral infinite element
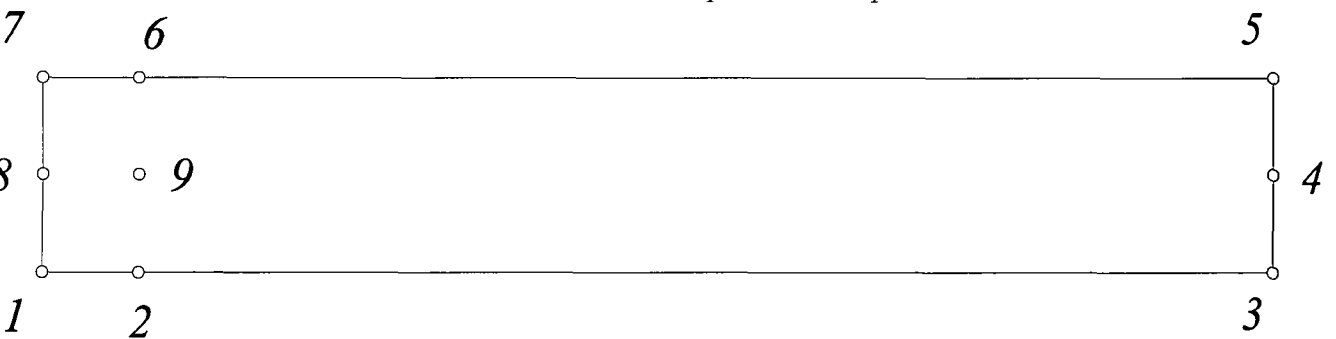
Distance ratio 1-3/1-2 must = about 15

Distance ratio 8-4/8-9 must = about 15
Distance ratio 7-5/7-6 must = about 15

IFS   Surface and edge load code

Any boundary of any element can be assumed to have the incident wave applied
to it. The problem is divided into inner and outer areas. The outer area has the only the
reflected wave as its variable and the incoming wave is ignored. If an infinite reflecting
boundary has been specified, the wave reflected from that boundary is treated as part of
the incoming wave. In the inner area, the variable is the total wave – i.e. both incoming
and reflected waves. This boundary is specified by naming some of the elements as
'loaded' infinite. The actual boundary can be on the surface of the obstacle in the
water – i.e. no inner area.

INTGR   Integration code for up to 5 areas

The total area and the integral of the magnitude of the elevation and the mag-
nitude of the elevation squared are calculated and output at the end of the results. For
example, this is a means of evaluating the overall response of a harbour. If an element
is in area 4, say, $INTGR$ should be set to 4 as it cannot be left as zero without ill-effect.
Infinite elements cannot be included in these areas.

NOD   Array of 6, 8 or 9 element node numbers, ordered as shown

Data line 8

ICYL

ICYL   Indicates whether risers are cylinders or ellipses
               = 0 ⇒ cylinder data
               = 1 ⇒ ellipse data

Data line 9

NCYL, R1, R2

NCYL   No.of cylinders/ellipses
R1   Radius of cylinders or semi-major axis of ellipses
R2   Semi-minor axis of ellipses

Data lines 10

CX, CY

CX   X co-ordinate of centre of cylinder/ellipse
CY   Y co-ordinate of centre of cylinder/ellipse

A.5.2 Sample data

Sample data

```
Single cylinder problem
```

```
 412  108    6    0    0    1
   2.0      1.0      1.0      1.0      0.0      0.0      0.0
1025.0      0.72     0.0      0.0      1.0E12   0.0      0.0      0.0
   0.0       0.0       0.0       0.0
     1   0.70700   0.70700   1.00000
     2   0.60900   0.79300   1.00000
.......
   410   6.13300   1.33300   1.00000
   411   6.13300   1.60000   1.00000
   412   5.52100   3.25400   1.00000
     3     4    0  221  285  349  350  351  287  223  222  286
     3     4    0  283  347  411  412  349  285  221  284  348
     3     4    0  223  287  351  352  353  289  225  224  288
     2     0    0  145  220  283  284  221  222  223  193    0
     2     0    0  145  193  223  224  225  194  147  146    0
     3     4    0  281  345  409  410  411  347  283  282  346
     3     4    0  225  289  353  354  355  291  227  226  290
     2     0    0  147  194  225  226  227  195  149  148    0
......
     3     4    0  255  319  383  384  385  321  257  256  320
     2     0    0   25   61   97   98   99   62   27   26    0
     2     0    0  169  206  251  252  253  254  255  207    0
     2     0    0  169  207  255  256  257  208  171  170    0
     2     0    0   97  133  169  170  171  134   99   98    0
     3     4    0  253  317  381  382  383  319  255  254  318
     0
     1      1.000
   0.00000   0.00000
```

A.6 Program PLOTF5

This program takes the plotting data output from program SMAWAVE and produces various plots defined by a control file (the control data has been separated from the data to make it easy to change). It is possible to plot the mesh and the wave elevations (real, imaginary and absolute parts). The elevations are plotted as solid colour filled contours.

A.6.1 Data preparation

Data preparation

Data line 1

    TITLE

    TITLE   Problem title

Data lines 2

    NODENO, X, Y, Z

`NODENO`	Node number
`X`	X co-ordinate of node
`Y`	Y co-ordinate of node
	(rectangular right-handed cartesion co-ordinates)
`Z`	Depth of water

The last node number must be preceded with a minus sign to indicate the end of the node data.

Data lines 3

```
ELENO, NETYPE, IFS, INTGR, ELSIZ, NODS
```

`ELENO`	Element number
`NETYPE`	Element type
`IFS`	Surface and edge load code (not used)
`INTGR`	Integration code (not used)
`ELSIZ`	No.of nodes in element
`NODS`	Array of 6, 8 or 9 element node numbers, ordered as shown

The last element number must be preceded with a minus sign to indicate the end of the node data.

Data lines 4 (one per node, in node order)

```
REALD, IMAGD
```

`REALD`	Real displacement
`IMAGD`	Imaginary displacement

A.6.2 Sample data - geometry and displacement data

Sample data - geometry and displacement data

```
Single cylinder problem
       1   0.70700E+00   0.70700E+00   0.10000E+01
       2   0.60900E+00   0.79300E+00   0.10000E+01
.......
     410   0.61330E+01   0.13330E+01   0.10000E+01
     411   0.61330E+01   0.16000E+01   0.10000E+01
    -412   0.55210E+01   0.32540E+01   0.10000E+01
     1   3   4   0   9  221  285  349  350  351  287  223  222  286
     2   3   4   0   9  283  347  411  412  349  285  221  284  348
     3   3   4   0   9  223  287  351  352  353  289  225  224  288
.......
   104   2   0   0   8   25   61   97   98   99   62   27   26
   105   2   0   0   8  169  206  251  252  253  254  255  207
   106   2   0   0   8  169  207  255  256  257  208  171  170
   107   2   0   0   8   97  133  169  170  171  134   99   98
  -108   3   4   0   9  253  317  381  382  383  319  255  254  318
         -0.164377D-01    0.635666D+00
```

```
          0.238501D+00     0.787637D+00
          0.519580D+00     0.840903D+00
  . . . . . .
          0.112861D-20    -0.414153D-21
          0.237035D-21     0.107085D-21
          0.437925D-21     0.681366D-21
```

A.6.3 Sample data - control file (normally output from SMAWAVE)

Sample data - control file (normally output from SMAWAVE)

The data input was originally driven interactively by a menu system but is now in a file. However, the original menu structure has been retained. The sample data below is described by annotation.

```
1                 ;data to be input
1                 ;initial data follows
Single cylinder   ;title
2                 ;number of dimensions
2                 ;number of degrees of freedom
2                 ;read co-ordinate data
3                 ;read element data
4                 ;read cylinder/ellipse data
0                 ;following data is for cylinders (1 for ellipses)
1 1.0             ;no. of cylinders, radius of cylinders
0.0 0.0           ;co-ords of centres of cylinders
7                 ;return to main menu
5                 ;read wave elevations
8                 ;goto plotting menu
1                 ;plot mesh
4                 ;plot contours
1                 ;plot elevations
1                 ;number of degree of freedom to be plotted (1st in this case)
4                 ;plot contours
1                 ;plot elevations
2                 ;number of degree of freedom to be plotted (2nd in this case)
4                 ;plot contours
1                 ;plot elevations
3                 ;number of degree of freedom to be plotted (3rd in this case)
9                 ;return to main menu
9                 ;end
```

Appendix B

Integration of the Inifnite Elements

B.1 Preliminary

In the original paper by Zienkiewicz, Bando, Bettess, Emson and Chiam[83], a special integration rule for the infinite elements was used. This was done, according to well-known procedures, by developing functions for each of the chosen integration points. These functions take on unit value at their own point, and zero at all the others. In the paper, these functions were developed from general polynomials with unknown coefficients, and a matrix inversion was carried out to determine the particular values of the polynomial coefficients. These could then be used in the integration of the functions over the required domain, and by summing the effects for all the coefficients, the integration weight for that particular point was found.

The procedure was described in the paper as follows

1. Choose n integration point abscissæ, which are quite arbitrary, $s_i, i = 1$, to n, where n is generally one greater than the highest power of s appearing in the polynomial. It would be possible to choose the Gauss-Legendre abscissæ, but for small n no special benefits would be gained.

2. Form the matrix $\mathbf{X}$.

$$\mathbf{X} = \begin{bmatrix} 1 & s_1 & s_1^2 & \ldots & s_1^{n-1} \\ 1 & s_2 & s_1^2 & \ldots & s_1^{n-1} \\ \vdots & \vdots & \vdots & \ddots & \vdots \\ 1 & s_n & s_1^2 & \ldots & s_1^{n-1} \end{bmatrix}, \qquad B.1$$

and since

$$\mathbf{y} = \sum_{i=1}^{n} \alpha_i s^{i-1}, \qquad B.2$$

where α_i are the unknown polynomial coefficients, it is clear that

$$\alpha = \mathbf{X}^{-1}\mathbf{y}, \qquad B.3$$

where $\mathbf{y}$ is the vector of values at the integration points. Setting

$$\mathbf{y} = 1, 0, 0, \ldots; 0, 1, 0, \ldots; \ldots; \ldots; \ldots, 0, 0, 1 \qquad B.4$$

corresponds to finding the polynomials which are equal to unity at each integration point in turn and zero at all the others.

The paper continues with the details of the integration process.

No problems were encountered in practice with the above procedure. However one of the reviewers pointed out that the matrix above, $\mathbf{X}$ could become ill-conditioned if the number of integration points were large. So a comment was added to the paper as follows:

'The procedure outline above can be criticized on two grounds. As n, the number of integration points becomes large then the matrix $\mathbf{X}$ will tend to become ill-conditioned. Also the computation of $\mathbf{X}^{-1}$ is potentially expensive. However it is intended that n would always be small, say less than 10, and the inversion of $\mathbf{X}$ would only be carried out one in each computer run. So neither of these criticisms carries much weight at present.

If one were trying to generate a scheme of optimal efficiency, one could generate the polynomial coefficients directly, by expanding Lagrange polynomials, say. '

The number of $n = 10$ was only inserted as a casual estimate, with no numerical experimentation. However, as is clear to any numerically aware reader it would be possible to develop the Lagrange polynomials directly, which is straightforward and does not involve any instability.

The reader is probably aware of the example from the First World War, in which a message is passed orally along the trench, in the course of which journey it mutates from

'Send re-inforcements, we're going to advance.'

to

'Send three and fourpence, we're going to a dance.'

In the course of several papers dealing with infinite elements, the mild precaution given above mutates in the paper by Moyer[142], into

'The procedure *requires* the inversion of an ill-conditioned matrix limiting the possible number of quadrature points to fewer than ten.' (my italics)

and in the paper by Burnett[117] paper it is stated that

'... the generation of the matrics for the mapped element *requires* inversion of an ill-conditioned matrix. This causes quadrature problems at very high frequencies.' (my italics)

Neither of the above statements is correct. The inversion can be completely eliminated by some simple re-coding, of the elementary theory of Lagrange polynomials. This will be explained below. The theory and the new code were developed and tested by the author as part of the present study. This is the version of the integration scheme which is used in the thesis. It should be noted that notwithstanding the dire warnings of Moyer and Burnett, no differences in element performance were observed.

B.2 Polynomial theory

It is simple to construct a Lagrange polynomial, which takes unit value at one point and is zero at a finite number of other points. If there are a total of n points, and their co-ordinates are x_i, $1 = 1$ to n, and we seek the Lagrange polynomial for the

i point, it is given by

$$L_i(x) = \prod_{j=1\,\mathrm{to}\,n\neq i}^{n} \left(\frac{x - x_j}{x_i - x_j} \right).$$ B.5

It is easy to verify that $L_i(x)$ is equal to 1 at $x = x_i$, and equal to 0 at $x = x_j$ where $i \neq j$.

For the integration the polynomial has to be expanded term by term. This is done by starting with all the polynomial coefficients set to zero. To expand the expression B.5, each numerator must be multiplied out to modify the polynomial coefficents. The polynomial coefficients are held in an array. When the existing polynomial is mulitplied by a typical term of the form $(x - x_j)$, this involves all the polynomial coefficients being modified. A new highest coefficient of value unity is introduced and all the others are multiplied by x_j and have the next lowest coefficient added to them. This is carried out for each term in the series B.5. At the end of this process, which is very quick, much quicker than the previous matrix inversion, the polynmial coefficients are in the array alpha. They can then be used in connection with the integration formulas given by Zienkiewicz *et al.*[83].

Code for the determination of the polynomial coefficients

```
      subroutine coeffs2(n,xin,max)
C***  subroutine to evaluate coefficients of polynomial from
C***  product((x-x(j)/(x(i)-x(j)), i=1,n j=1,n i not= j
C***  alpha (j,i), j=0,n-1 Coefficients for polynomial i
C***  denom product(x(i)-x(j))
C***  xin x(i), i=1,n
C***  x rearranged xin such that x(1) is always x(i)
      integer i,j,k,n
      double precision alpm, xin, x, denom
      dimension xin(*),x(100)
      COMMON /TOUCH/ ALPM(0:100,100), DENOM(100)
C*** set all alphas to 1.0
      do 3 j=1,max
      do 2 i=0,max
      alpm(i,j)=1.0
    2 continue
    3 continue
C***  rearrange xin such that x(1)=x(i) and all other vales close up
      do 50 i=1,n
      x(1)=xin(i)
      k=1
      do 5 j=1,n
        if(i.ne.j) then
          k=k+1
```

```
          x(k)=xin(j)
          endif
     5  continue
C       write(6,601)n,(x(j),j=1,n)
C601  format(' n, x(j)'/i5/(5x,8e13.5))
        call polmod(n,denom(i),alpm(0,i),x)
    50 continue
       return
       end
       subroutine polmod(n,denom,alpha,x)
C*** calculate the coefficients of the polynomial generated by the
C*** product of (x-x(j))/(x(1)-x(j)), j=1,n
C*** poly(n) is calculated from poly(n-1)
C*** n       number of x(i)'s
C*** alpha coefficients of polynomial (0:n-1)
C*** denom product(x(1)-x(j))
       parameter (maxn=20)
       integer i,ic,j,n
       double precision alpha,denom,prod,sum,x
       dimension alpha(0:*), x(*)
C      write(6,601)n,(x(i),i=1,n)
C 601 format(' in coeffs:  n, x(i)'/i5/(5x,8e13.5))
C*** calculate denominator
       denom=1.0
       do 5 i=2,n
       denom=denom*(x(1)-x(i))
     5 continue
C       write(6,600)denom
C 600 format(' denom =',e13.5)
C***   calculate alphas
       alpha(0)=-x(2)
       do 20 j=3,n
       do 10 i=j-2,1,-1
       alpha(i)=alpha(i-1) - alpha(i)*x(j)
    10 continue
       alpha(0)=-alpha(0)*x(j)
C       write(6,603)n,j,(alpha(i),i=0,n-1)
C603  format(' n, j =',2i5,' alpha(i) '/(5e13.5))
    20 continue
C      write(6,602)n,(alpha(i),i=0,n-1)
C602  format(' n =',i5,' alpha(i) '/(5e13.5))
       return
       end
```

Appendix C

Aide-memoire for figures and tables in chapters 10 and 11

	ω	θ_i	a_0	C_d	h	Table no.	Figures of Contours	Figures of Forces
Long wave	1.0	90	4.0	0.0	20	10.1	10.1	
		0				10.2		
		45				10.3		
No damping	1.0	0	4.0	0.0	20	10.4		11.1
		45				10.5		11.2
		90				10.6		11.3
	4.0	0	0.2			10.7	10.2, 10.3, 10.4	11.4
		45				10.8	10.5, 10.6, 10.7	11.5
		90				10.9	8.33, 8.34, 8.35	11.6
	0.45	0	10.0		40	10.10		
		45				10.11		
		90				10.12		
	0.9	0	5.0			10.13		
		45				10.14		
		90				10.15	10.8, 10.9, 10.10	
Damping area 3.5928	1.0	0	4.0	1.2	20	11.1		11.1
		45				11.2		11.2
		90				11.3		11.3
	4.0	0	0.2			11.4		11.4
		45				11.5		11.5
		90				11.6	11.7, 11.8, 11.9	11.6
	0.45	0	10.0		40	11.7		
		45				11.8		
		90				11.9		
	0.9	0	5.0			11.10		
		45				11.11		
		90				11.12	11.10, 11.11, 11.12	

Appendix D

Vertical variations in wave force

D.1 Shallow water

In this case the velocities do not vary with depth and thus the wave force (both inertia and drag) is simply

$$\text{force per unit length} \times \text{depth}$$

D.2 Intermediate depth

In this case the velocity varies as the velocity potential, as $\cosh k(h + z) / \cosh kh$. So the drag force will vary with depth as the square of that term, and the inertia force will vary as the term itself. Hence three integrals are needed:

$$\int_{z=-h}^{z=0} \frac{\cosh k(h + z)}{\cosh kh} dz, \quad \int_{z=-h}^{z=0} \frac{\cosh^2 k(h + z)}{\cosh^2 kh} dz \quad \text{and} \quad \int_{z=-h}^{z=0} \frac{\cosh^3 k(h + z)}{\cosh^3 kh} dz$$

The three integrals can be shown to be

$$\int_{z=-h}^{z=0} \frac{\cosh k(h + z)}{\cosh kh} dz = \frac{\tanh kh}{k}$$

$$\int_{z=-h}^{z=0} \frac{\cosh^2 k(h + z)}{\cosh^2 kh} dz = \frac{1}{\cosh^2 kh} \left(\frac{1}{k} \right) \left[\frac{\sinh 2kh}{4} + \frac{kh}{2} \right]$$

and

$$\int_{z=-h}^{z=0} \frac{\cosh^3 k(h + z)}{\cosh^3 kh} dz = \left(\frac{1}{k} \right) \left[\frac{1}{3} \sinh^3 kh + \sinh kh \right] \times \frac{1}{\cosh^3 kh}$$

D.3 Deep water

Here the velocity varies as e^{kz}, and the depth is infinite.

$$\int_{z=-h}^{z=0} e^{kz} dz = \frac{1}{k} \left[e^{kz} \right]_{-\infty}^{0} = \frac{1}{k}, \quad \int_{z=-h}^{z=0} e^{2kz} dz = \frac{1}{2k} \left[e^{2kz} \right]_{-\infty}^{0} = \frac{1}{2k}$$

$$\int_{z=-h}^{z=0} e^{3kz} dz = \frac{1}{3k} \left[e^{3kz} \right]_{-\infty}^{0} = \frac{1}{3k}$$

Appendix E

Interface conditions in zones of different permeability

This appendix explains the interface conditions between the zones of different permeability, the theory of which was developed in Chapter 8. It might be thought that the β term could simply be cancelled in the wave equation for the zone of reduced permeability, since it appears throughout equation 8.9. However it is not correct to do this, because if the β term is cancelled the correct interface term between regions of different permeability is not obtained. This will be demonstrated, for clarity, for a very simple one dimensional case, but it is quite generally true. First the correct interface condition will be derived and then it will be shown that this is consistent with retaining the β factor in the weighted residual statement and hence the element matrices. The demonstration relates entirely to the governing equations and their equivalent weighted residual and variational statements, and is not dependent upon finite element concepts.

E.1 The inter region continuity equation in 1 dimension
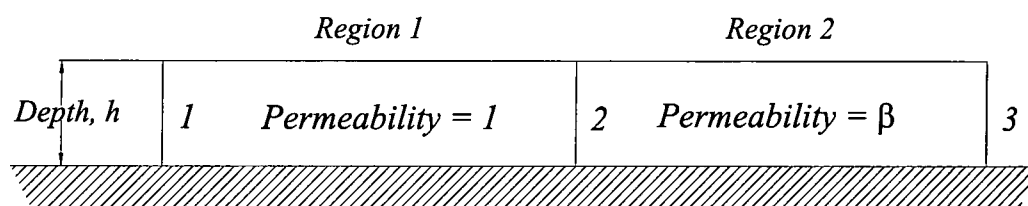
Elevation of one dimensional wave problem with varying permeability, β

Figure E.1   General arrangement of one dimesional wave problem

Consider the case shown in Figure E.1. there are two regions, labelled 1 and 2, delimited by 3 points, 1, 2 and 3. In region 1 the factor β is unity, and in region 2 it is some other value β. The flow out of region 1 is given by the product of the depth of water, h, the perpendicular distance, taken as unity, and the velocity at point 2, in region 1, which is denoted at u_{12}. At point 2 the flow into region 2 is the same product except that the effective perpendicular distance will now be unity multiplied by β, and the velocity is u_{22}, being the velocity in region 2 at point 2. * Hence on equating the two flows

$$u_{12} \times h \times 1 = u_{12} \times h \times 1 \times \beta \qquad\qquad E.1,$$

or

$$u_{12} = \beta u_{22}. \qquad\qquad E.2.$$

---

* The wave elevations and wave potentials must be continuous between regions, but the particle velocities can be discontinuous, indeed must be, if there are permeability changes.

This is the correct interface condition. It can be re-written in terms of wave elevations, for periodic problems, because of the simple relations between velocity, velocity potential, surface elevation and their derivatives, (equations 1.9 - 1.11), to become

$$\frac{d\eta_{12}}{dx} = \beta \frac{d\eta_{22}}{dx}.$$
<div align="right">*E.3*</div>

E.2   Weighted residual statement

Now consider the weighted residual statement for both the regions, where the wave elevation, η is given by a shape, or trial function, $\mathbf{N}_j$, so that

$$\eta = \mathbf{N}_j \eta_i,$$
<div align="right">*E.4*</div>

where i are the set of nodes in the problem, which we do not need to specify. The subscript j is 1 for region 1, and 2 for region 2. The identical function is used as a weighting, or test, function

Helmholtz equation in 1 dimension is given by

$$\frac{d^2\eta}{dx^2} + k^2\eta = 0,$$
<div align="right">*E.5,*</div>

where as usual, k is the wave number.

On multiplying by the weighting function, $\mathbf{N}_j^T$, and integrating over the entire domain, that is both regions, Ω_1 and Ω_2, we obtain

$$\int_{\Omega_1} \left\{ \mathbf{N}_1^T \frac{d^2\mathbf{N}_1}{dx^2} + k^2\mathbf{N}_1\mathbf{N}_1 \right\} d\Omega\eta_i + \int_{\Omega_2} \beta \left\{ \mathbf{N}_2^T \frac{d^2\mathbf{N}_2}{dx^2} + k^2\mathbf{N}_2\mathbf{N}_2 \right\} d\Omega\eta_i = 0$$
<div align="right">*E.6*</div>

On integrating by parts we find

$$\int_{\Omega_1} \left\{ d\frac{\mathbf{N}_1^T}{dx}\frac{d\mathbf{N}_1}{dx} + k^2\mathbf{N}_1\mathbf{N}_1 \right\} d\Omega\eta_i + \left[\mathbf{N}_1^T \frac{d\mathbf{N}_1}{dx} \right]_1^2 \eta_i \quad +$$

$$\int_{\Omega_2} \beta \left\{ d\frac{\mathbf{N}_2^T}{dx}\frac{d^2\mathbf{N}_2}{dx^2} + k^2\mathbf{N}_2\mathbf{N}_2 \right\} d\Omega\eta_i + \left[\mathbf{N}_2^T \frac{d\mathbf{N}_2}{dx} \right]_2^3 \eta_i = 0$$
<div align="right">*E.7*</div>

The two terms in square brackets represent end terms, and those which arise at point 2, give the interface condition

$$\left(\frac{d\mathbf{N}_1}{dx} \right)\eta_i - \beta\left(\frac{d\mathbf{N}_2}{dx} \right)\eta_i = 0.$$
<div align="right">*E.8*</div>

But by definition

$$\left(\frac{d\mathbf{N}_1}{dx} \right)\eta_i = \frac{d\eta_{12}}{dx} \quad \text{and} \quad \left(\frac{d\mathbf{N}_2}{dx} \right)\eta_i = \frac{d\eta_{22}}{dx},$$
<div align="right">*E.9*</div>

and so equation E.9 reduces to

$$\frac{d\eta_{12}}{dx} = \beta \frac{d\eta_{22}}{dx}, \qquad\qquad E.10,$$

which has already been derived as the interface condition, equation E.3. However, if the factor β is cancelled from the weighted residual statement for region 2, in equation E.6, (and hence from any finite element matrices), it will also disappear from equation E.10, and an *incorrect* interface condition will arise. This explains why the β term *must* be retained in zones of reduced permeability.

Appendix F

Dissipation areas

In Chapter 11 it was originally assumed that the viscous dissipation for each cylinder took place over a domain of 1 m^2 area. This was because contiguous squares of 1 m side could be drawn around each riser, but was otherwise an arbitrary choice. In reality, the zone over which the dissipation takes place will be broadly related to the size of the orbits of the orbits of the water particles in the cylinder vicinity. It must be emphasized that the area chosen, does *not* affect the amount of energy absorbed, merely the area over which it is absorbed. A numerical experiment, given later, shows that the effect on the wave forces of doubling the area, is minimal, of the order of 1%.

The extent of the orbit for the incident wave is closely related to the Keulegan-Carpenter number. The necessary formulas are given by Lamb[87], page 365. First recall that all quantities are complex and have an implicit time dependence of $\exp i\omega t$.

Consider a simple incident wave whose elevation, η, is given by

$$\eta = a_0 \times \exp ikx. \qquad F.1$$

The corresponding velocity potential, ϕ, is given by

$$\phi = \frac{iga_0}{\omega} \times \exp ikx. \qquad F.2$$

The velocity of a particle is given by $\partial\phi/\partial x$, that is

$$u = \frac{\partial\phi}{\partial x} = \frac{igka_0}{\omega} \times \exp ikx, \qquad F.3$$

and the maximum velocity in a wave period will be

$$u_{max} = \frac{gka_0}{\omega}. \qquad F.4$$

Now according to Lamb, the velocity can be equated to the rate of change of the particle displacement, denoted here by $\mathbf{x}$. Thus we have

$$\frac{d\mathbf{x}}{dt} = u = \frac{igka_0}{\omega} \times \exp ikx. \qquad F.5$$

Equation F.5 can be integrated with respect to time, using the implicit $\exp i\omega t$ term to give an expression for

$$\mathbf{x} = \frac{igka_0}{\omega} \times \frac{-i}{\omega} \times \exp ikx. \qquad F.6$$

Clearly the maximum displacement $\mathbf{x}_{max}$ in a wave period will be

$$\mathbf{x}_{max} = \frac{gka_0}{\omega^2}. \qquad F.7$$

It will be recalled that the definition of the Keulegan-Carpenter number is

$$KC = \frac{u_{max}T}{D}. \qquad F.8$$

On substituting for the period, T, and the maximum velocity, u_{max}, KC can be written as

$$KC = \frac{gka_0}{\omega D} \times \frac{2\pi}{\omega} = \frac{2\pi gka_0}{\omega^2 D}. \qquad\qquad F.9$$

Clearly then the Keulegan-Carpenter number (apart from the factor 2π), gives the ratio of the water particle excursions to the cylinder diameter, for the incident wave. This then suggests a simple way of calculating the area over which the dissipation can be assumed to take place. It can be taken that the dissipation will take place in a cylinder of radius equal to the maximum particle excursion, that is the area of this cylinder, A_{diss}, will be given by

$$A_{diss} = \pi \times \mathbf{x}_{max}^2 = \left(\frac{1}{4\pi}\right) \times (KC \times D)^2. \qquad\qquad F.10$$

It is probable that equation F.10 will form a more rational basis for the selection of the area over which dissipation should be allowed to take place. The following points should be noted

1. The zone of dissipation will depend upon the wave direction

2. A more accurate model would use the true velocities, not those of the incident wave.

3. The zones of dissipation of adjacent risers may overlap, and it is not clear what the best assumption is, for that case.

4. The area of dissipation should be calibrated by experiments and detailed CFD simulations.

In the following examples the case of the wave used in Table 10.7 and Figure 11.4 is revisited. The problem parameters are given by each table of results. Comparisons are made using two different areas over which the viscous force is dissipated. The areas are shown in Figure 1. Table F.1 shows the wave forces for the case when the viscous force is distributed around the risers over an area 6m by 4m, excluding the actual cross sections of the risers themselves (as in Figure 11.4). In Table F.2, the same calculation is repeated with the viscous forces being distributed over an area 8m by 6m, again excluding the risers, i.e. over twice as large. The forces are compared in Figure F.2. The changes are of the order of 1 to 2%, and indicate that the choice of the area is not critical.

b Dissipation area 7.59 square metres per cylinder

a Dissipation area 3.59 square metres per cylinder
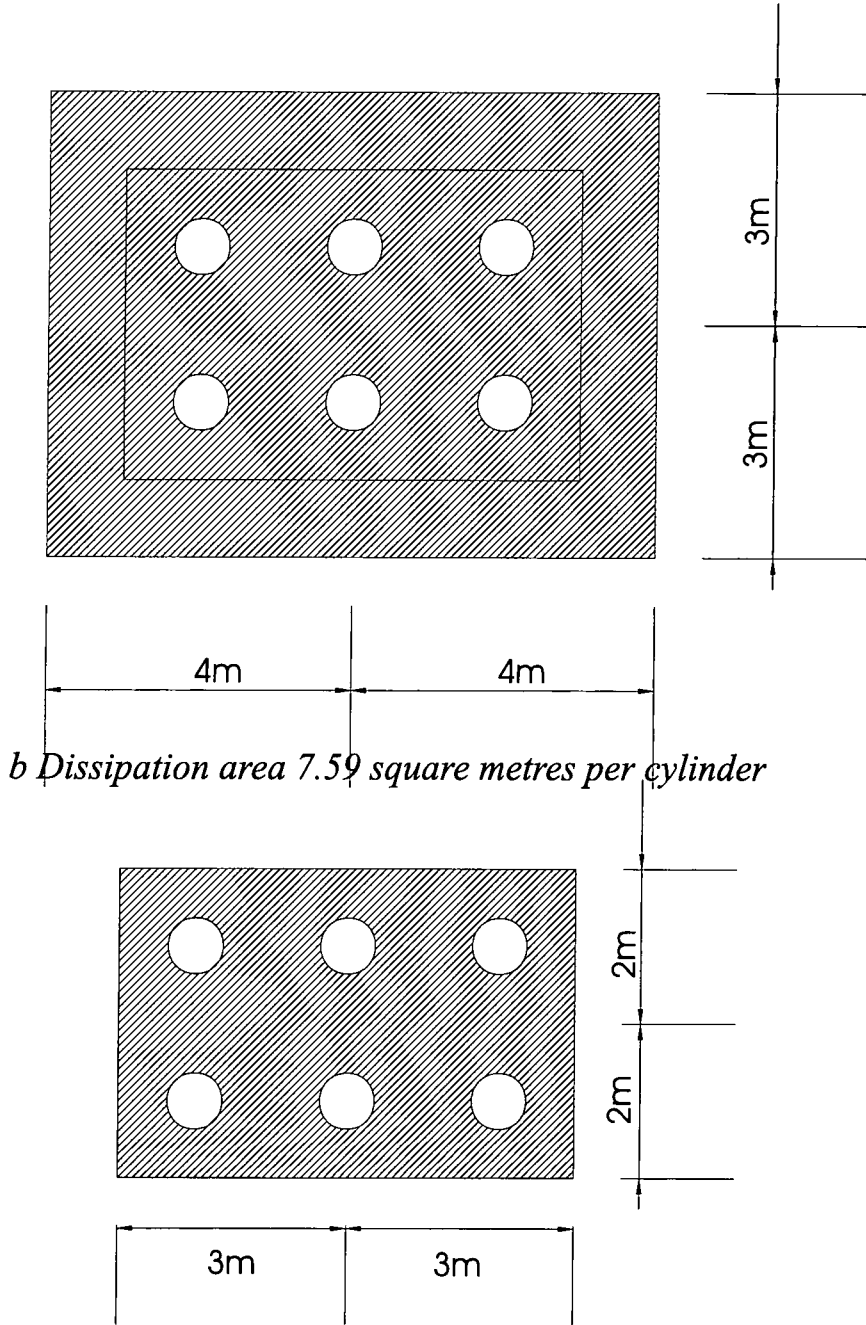
Figure F.1 Areas of dissipation around risers

		$x = -2.0$m	$x = 0.0$m	$x = 2.0$m
	a Diffracted	1432.7	1086.9	911.4
$y = 1.0$m	b Incident	1557.6	1558.2	1558.4
	Ratio a/b	0.91982	0.69756	0.58484
	a Diffracted	1432.7	1086.9	911.4
$y = -1.0$m	b Incident	1557.6	1558.2	1558.4
	Ratio a/b	0.91982	0.69756	0.58484

Table of forces due to diffracted and incident waves. 2 by 3 riser array, with damping area of 3.5928m^2

Wave frequency, $\omega = 1.0$ s^{-1}, Depth, $h = 20.00$m, Wave length, $\lambda = 59.82$ m, Wave period $T = 6.2832$ s, Waveno, $k = 0.10504$ m^{-1}, Wave amplitude, $a_0 = 4.0$m, Drag coefficient, $C_d = 1.2$, Inertia coefficient, $C_i = 2.0$, Acceleration due to gravity, $g = 9.81$ ms^{-2}, Angle of incident wave direction, $\theta_i = 0.0°$.

Table F.1   Riser forces, $\omega = 1.0$, $\theta_i = 0°$, $h = 20.0$, damping area $= 3.5928$m^2

		$x = -2.0$m	$x = 0.0$m	$x = 2.0$m
	a Diffracted	1450.9	1104.1	934.5
$y = 1.0$m	b Incident	1557.6	1558.2	1558.4
	Ratio a/b	0.93154	0.70854	0.59957
	a Diffracted	1450.9	1104.1	934.5
$y = -1.0$m	b Incident	1557.6	1558.2	1558.4
	Ratio a/b	0.93154	0.70854	0.59957

Table of forces due to diffracted and incident waves. 2 by 3 riser array, with damping area of 7.5928m^2

Wave frequency, $\omega = 1.0$ s^{-1}, Depth, $h = 20.00$m, Waveno, $k = 0.10504$ m^{-1}, Wave length, $\lambda = 59.82$ m, Wave period $T = 6.2832$ s, Wave amplitude, $a_0 = 4.0$m, Drag coefficient, $C_d = 1.2$, Inertia coefficient, $C_i = 2.0$, Acceleration due to gravity, $g = 9.81$ ms^{-2}, Angle of incident wave direction, $\theta_i = 0.0°$.

Table F.2   Riser forces, $\omega = 1.0$, $\theta_i = 0°$, $h = 20.0$, damping area $= 7.5928$m^2

	x=-2m	x=0m	x=2m
y=1.0m	1433	1087	911
y=-1.0m	1433	1087	911
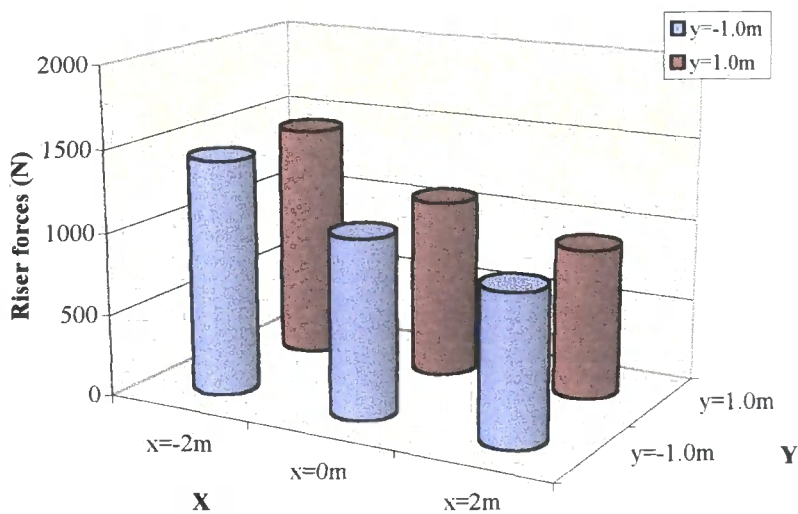
Riser forces - damping area 3.5928 (from table F.1)

	x=-2m	x=0m	x=2m
y=1.0m	1451	1104	934
y=-1.0m	1451	1104	934
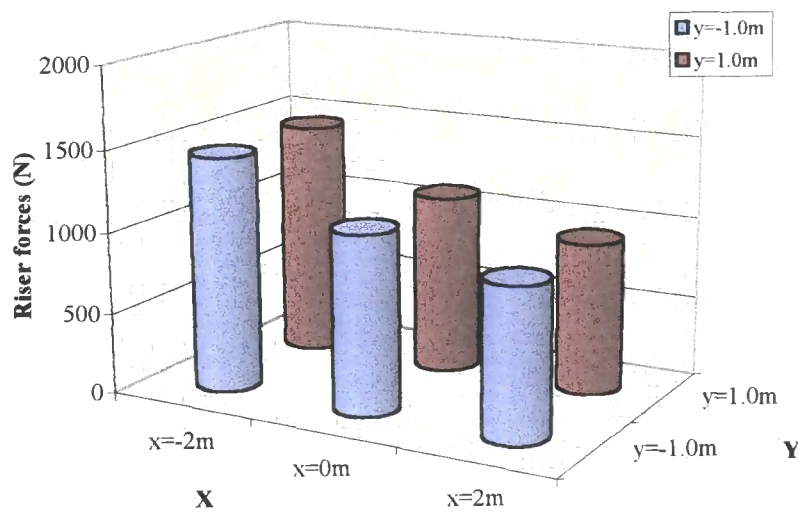
Riser forces - damping area 7.5928 (from table F.2)

Fig. F.2 Riser Forces comparing tables F.1 and F.2
Depth=20m, Frequency=1(1/s), Amplitude=4m, Wave no.=0.10504(1/m), Period=2π,
Wave length=59.82m, Angle of Incidence=0.0

References

1. M. Abramowitz and I.A. Stegun, 1972, *Handbook of Mathematical Functions with Formulas, Graphs and Mathematical Tables*, John Wiley, New York, tenth printing.

2. J. E. Akin and W. H.Gray, 1977, 'Contouring on isoparametric surface', *Int. J. Num. Meth. Eng.*, **11**, pp 1893 - 1897.

3. J. E. Akin and W. H.Gray, 1979, 'An improved method for contouring on isoparametric surface', *Int. J. Num. Meth. Eng.*, **14**, pp 451 - 472.

4. D. L. Anderson and R. L. Ungless, 1977, 'Infinite finite elements', *Int. Symp. Innovative Num. Anal. Appl. Eng. Sci.*, France.

5. R. J. Astley and W. Eversman, 1981, 'A Note on the Utility of a Wave Envelope Approach in Finite Element Duct Transmission Studies', *Journal of Sound and Vibration*, **76**, pp 595-601

6. R. J. Astley, 1983, 'Wave Envelope and Infinite Elements for Acoustical Radiation', *Int. Journ. Num. Meth. Fluids*, **3**, pp 507-526.

7. R. J. Astley and W. Eversman, 1983, 'Finite Element Formulations for Acoustical Radiation', *Journal of Sound and Vibration Research*, **88**(1), pp 47-64.

8. R. J. Astley and W. Eversman, 1984, 'Wave Envelope and Infinite Element Schemes for Fan Noise Radiation from Turbofan Inlets ' *A.I.A.A. Journal*, **22**(12), pp 1719-1726.

9. R. J. Astley, 1986, 'A Finite Element Wave Envelope Formulation for Acoustical Radiation in Moving Flows', *Journal of Sound and Vibration*, **103**, pp 471-485.

10. R. J. Astley and W. Eversman, 1988, 'Wave Envelope Elements for Acoustical Radiation in Inhomogeneous Media' *Computers and Structures*, **30**(4), pp 801-810.

11. R. J. Astley and J. P. Coyette, 1991, 'Applications of Wave Envelope Elements to Acoustical Scattering', to appear, *Proc. third IMACS International Symposium on Computational Acoustics*, Harvard, Mass., June 26-28, 1991.

12. R. J. Astley and J. P. Coyette, 1991, 'Mapped Wave Envelope Elements of Infinite Extent: Applications to Acousto-Structural Scattering' to appear, *Proc. Fourth International Conference on Recent Advances in Structural Dynamics*, I.S.V.R., Southampton University, U.K., 15-18 July, 1991.

13. R. J. Astley, P. Bettess and P. J. Clark, 1991, Letter to the editor concerning Ref. 128, *Int. Journ. Num. Meth. Engng.*, **32**(1), pp 207 - 209.

14. R. J. Astley, G. J. Macaulay and J. P. Coyette, 1994, 'Mapped Wave Envelope Elements for Acoustical Radiation and Scattering', *Journal of Sound and Vibration*, **170**(1), pp 97 - 118.

15. R. J. Astley, 1996, 'A Transient Infinite Element for Multi-dimensional Acoustic Radiation', *Proceedings of the ASME 15th. Biennial Conference on Mechanical Vibration and Noise*

16. R. J. Astley, 1997, 'Mapped Spheroidal Wave-Envelope Elements for Unbounded Wave Problems', to appear, *International Journal for Numerical Methods in Engineering.* Need further details.

17. Christos Andreas Atalianis, 1990, *Wave Forces on a Vertical Cylinder of Elliptical Shape*, Final Year, B.Eng. Thesis, Department of Marine Technology, University of Newcastle upon Tyne

18. Christos Andreas Atalianis, 1995, *Hydrodynamic Analysis of Structures by a Hybrid Method*, Ph.D. Thesis, Department of Marine Technology, University of Newcastle upon Tyne

19. C. Barbier, P. J. Clark, Peter Bettess and Jacqueline A. Bettess, 1990, 'Automatic generation of shape functions for finite element analysis using REDUCE', *Engineering Computations*, **7**(4), pp 349 - 358.

20. C. Barbier, P. Bettess and J. A. Bettess, 1992, 'Automatic Generation of Mapping Functions for Infinite Elements using REDUCE', *Journal of Symbolic Computation*, **14**, pp 523-534.

21. A. Bayliss and E. Turkel, 1979, 'Radiation boundary conditions for wave-like equations', ICASE Report, Number 79 - 26.

22. A. Bayliss, M. Gunzberger and E. Turkel, 1980, 'Boundary conditions for the numerical solution of elliptic equations in exterior regions', ICASE Report, Number 80 - 1.

23. A. Bayliss and E. Turkel, 1980, 'Radiation Boundary Conditions for Wave-Like Equations', *Communications on Pure and Applied Mathematics*, **33**, pp 707-725.

24. G. Beer and J. L. Meek, 1981, 'Infinite domain elements', *Int. J. Num. Meth. Eng.*, **17**(1), pp 43-52.

25. G. Beer and J. O. Watson, 1992, *Introduction to Finite and Boundary Element Methods for Engineers*, John Wiley, Chichester, England.

26. J. C. W. Berkhoff, 1970, 'Wave refraction: derivation and numerical solution of the refraction equations', Delft Hydraulics Laboratory, *Report on Mathematical Investigation, S5-11.*

27. J. C. W. Berkhoff, 1972, 'Computation of combined refraction-diffraction', *Proceedings of the 13th. International Conference on Coastal Engineering*, Vancouver.

28. J. C. W. Berkhoff, 1975, 'Linear Wave Propagation Problems and the Finite Element Method', in *Finite Elements in Fluids*, 1, Eds. R. .Gallagher *et al.*, Wiley, Chichester, pp 251-280.

29. P. Bettess, 1977, 'Infinite elements', *Int. J. Num. Meth. Eng.*, **11**, pp 53-64.

30. P. Bettess and O. C. Zienkiewicz, 1977, 'Diffraction and refraction of surface waves using finite and infinite elements', *Int. J. Num. Meth. Eng.*, **11**, pp 1271-1290.

31. P. Bettess and J. A. Bettess, 1977, 'WAVE, A Finite Element Program for Solving the wave Equation', *Computer Report No. 81*, Department of Civil Engineering, University College of Wales, Swansea.

32. P. Bettess (Ed.), 1978, 'Fluid-structure interaction', Special edition of *Int. Journ. Num. Meth. Engng.*, **13**(1).

33. P. Bettess and O. C. Zienkiewicz, 1978, 'Report on Infinite Elements for Laplace's Equation, compatible with the SESAM-69 Finite Element Program System', Report to IRCN Paris.

34. P. Bettess, 1980, 'More on infinite elements', *Int. J. Meth. Eng.*, **15**, pp 1613-1626.

35. P. Bettess, C. R. I. Emson, and K. Bando, 1982, 'Some useful techniques for testing infinite elements', *Appl. Math. Modelling*, **6**, pp 436-440.

36. P. Bettess, S.-C. Liang and J. A. Bettess, 1984, 'Diffraction of Waves by Semi-Infinite Breakwater using Finite and Infinite Elements' *Int. Journ. Num. Meth. Fluids*, **4**(9), pp 813-832.

37. P. Bettess and J. A. Bettess, 1984, 'Infinite Elements for Static Problems', *Engineering Computations*, **1**, pp 4-16.

38. P. Bettess, C. R. I. Emson and T, C. Chiam, 1984, 'A New Mapped Infinite Element for Exterior Wave Problems', Chapter 17 of *Numerical Methods in Coupled Systems*, eds R. W. Lewis, P. Bettess and E. Hinton, John Wiley, Chichester.

39. Peter Bettess and Jacqueline A. Bettess, 1984, 'Infinite Elements for Dynamic Problems: Part 1', *Engineering Computations*, **8**, pp 99 - 124.

40. Peter Bettess and Jacqueline A. Bettess, 1984, 'Infinite Elements for Dynamic Problems: Part 2', *Engineering Computations*, **8**, pp 125 - 151.

41. P. Bettess, 1987, 'A Simple Wave Envelope Test Example', *Communications in Applied Numerical Methods*, **3**, pp 77-80.

42. Peter Bettess and Jacqueline A. Bettess, 1987, 'Automatic Generation of Shape Function Routines', *Proceedings of the International Conference on Numerical Methods in Engineering, NUMETA '87*, Martinus Nujhoff, Dordrecht, pp s20/1, 1 - 9.

43. P. Bettess, 1987, 'Finite and Infinite Elements for Fluid Loading on Offshore Structures - An Assessment of Accuracy', Chapter 5 of *Integrity of Offshore Structures - 3*, edited by D.Faulkner, M.J.Cowling and A.Incecik, Elsevier Applied Science, 1987, pp 95-114.

44. Peter Bettess, 1992, *Infinite Elements*, Penshaw Press, Sunderland, U.K., ISBN 0-9518806-0-8.

45. Jacqueline A. Bettess and Peter Bettess, 1997, 'New Mapped Infinite Element for Diffraction of Waves by General Object', *Proceedings of the ACME Conference, Imperial College, April, 1997*, 6 pages.

46. J. A. Bettess and P. Bettess, 'New Mapped Wave Infinite Element and Diffraction of Waves by Elliptical Cylinders of Varying Aspect Ratio', *Proceedings of the IUTAM Symposium on Computational Methods for Unbounded Domains*, July 27 - 31, 1997, University of Colorado, Boulder.

47. J. A. Bettess and P. Bettess, 1998, 'A New Mapped Infinite Wave element for General Wave Diffraction Problems and Its Validation on the Ellipse Diffraction Problem', *Computer Methods in Applied Mechanics and Engineering*, **164**, pp 17 - 48.

48. G. Blanch and D. S. Clemm, 1965, 'Tables Relating to Radial Mathieu Functions', Vols 1 and 2, Aerospace Research Laboratories, Office of Aerospace Research, United States Air Force.

49. D. S. Burnett, 1994, 'A three-dimensional acoustic infinite element based on a prolate spheroidal multipole expansion', *Journal of the Acoustical Society of America*, **95**(5), pp 2798 - 2816.

50. D. S. Burnett, and R. L. Holford, 1998, 'Prolate and oblate spheroidal acoustic infinite elements', *Computer Methods in Applied Mechanics and Engineering*, **158**, pp 117 - 141.

51. D. S. Burnett, and R. L. Holford, 1998, 'An ellipsoidal acoustic infinite element', *Computer Methods in Applied Mechanics and Engineering*, **164**, pp 49 - 76.

52. H. S. Chen and C. C. Mei, 1969, 'Scattering and Radiation of Gravity Waves by an Elliptical Cylinder' Parsons Laboratory, Department of Civil Engineering, M.I.T. Technical Report No. 140, July.

53. H. S. Chen and C. C. Mei, 1973, 'Wave Forces on a Stationary Platform of Elliptical Shape', *Journal of Ship Research*, **17**(2), pp. 61 - 71.

54. H. S. Chen and C. C. Mei, 1974, 'Oscillations and wave forces in a man-made harbor in the open sea', *Proc. Tenth Naval Hydrodynamics Symposium*

55. H. S. Chen and C. C. Mei, 1974, 'Oscillations and wave forces in an offshore harbor', *Ralph M. Parsons Laboratory for Water Resources and Hydrodynamics, M.I.T.*, Report No. 190.

56. H. S. Chen, 1990, 'Infinite elements for water wave radiation and scattering', *Int. J. Num. Meth. Fluids*, **11**, pp 555-569.

57. Y. K. Chow and I. M. Smith, 1981, 'Static and periodic infinite solid elements, *Int. J. Num. Meth. Eng.*, **17**(**4**), pp 503-526.

58. D. S. Clemm, 1969, 'Algorithm 352, Characteristic Values and Associated Solutions of Mathieu's Differential Equation (s22)', *Communications of the Association for Computing Machinery*, **12**(7), July.

59. R. Courant and D. Hilbert, 1953, *Methods of Mathematical Physics*, Volumes 1 and 2, Wiley Interscience.

60. L. Cremers, K. R. Fyfe and J. P. Coyette, 1994, 'A Variable Order Infinite Acoustic Wave Envelope Element', *Journal of Sound and Vibration*, **171**(4), pp 483 - 508.

61. L. Cremers and K. R. Fyfe, 1995, 'On the use of variable order infinite wave envelope elements for acoustic radiation and scattering', *Journal of Acoustical Society of America*, **97**(4), pp 2028 - 2040.

62. E. Cuthill and J. McKee, 1969, 'Reducing the bandwidth of sparse symmetric matrices', presented at the *1969 Conference of the Association for Computing Machinery* , San Francisco, California.

63. P. J. Davis and P. Rabinowitz, 1975, *Methods of Numerical Integration*, Academic Press, New York.

64. R. G. Dean, and L. E. Borgman, 1986, 'Wind and Wave Forces', Chapter 12 of Bramlette McClelland and Michael D. Reifel, *Planning and Design of Offshore Platforms*, Van Nostrand Reinhold, New York, pp 317 - 363.

65. C. R. I. Emson, and P. Bettess, 1981, 'Application of infinite elements to external electromagnetic field problems', *Proc. Int. Conf. Numerical Methods for Coupled Problems*, Pineridge Press, Swansea, pp. 887-902.

66. C. J. Garrison 1966, 'Hydrodynamic Loading of Large Offshore Structures. Three Dimensional Source Distribution Methods', Chapter 3 of O. C. Zienkiewicz, R. W. Lewis and K. G. Stagg, *Numerical Methods in Offshore Engineering*, John Wiley and Sons, Chichester, pp 87 - 140.

67. D. Givoli, 1992, *Numerical Methods for Problems in Infinite Domains*, Elsevier, Amsterdam.

68. S. Goldstein, 1938, *Modern Developments in Fluid Mechanics - Volume I*, Oxford University Press, Dover reprint, 1965.

69. S. Goldstein, 1938, *Modern Developments in Fluid Mechanics - Volume II*, Oxford University Press, Dover reprint, 1965.

70. J. P. E. Goransson and C. F. Davidsson, 1987, 'A three dimensional infinite element for wave propagation', *Journal of Sound and Vibration*, **115**(3), pp 556 - 559.

71. G. Green, 1828, *An Essay on the Application of Mathematical Analysis to the Theories of Electricity and Magnetism*, privately printed booklet.

72. The Group Numerical Analysis at Delft University of Technology, 1972, 'On the computation of Mathieu Functions', *Journal of Engineering Mathematics*, **7**(1), January.

73. R. W. Hamming, 1973, *Numerical Methods for Scientists and Engineers*, Second edition, McGraw Hill, New York.

74. H. Hara, 1978, 'Coupled Oscillation of Bodies in Fluid with a Free Surface and an Infinite Element using Finite Elements and Boundary Integral Elements', *M.Sc. thesis*, University of Wales, Swansea, (C/M/134/78).

75. H. Hara, O. C. Zienkiewicz and P. Bettess, 1979, 'Application of Finite Elements to Determination of Wave Effects on Offshore Structures' Paper 31, *Proceedings of BOSS '79*, published by B.H.R.A.

76. H. Hara, K. Kanehiro, H. Ashida, T. Sugawara and T. Yoshimura, 1983, 'Numerical Simulation System for Wave Diffraction and Response of Offshore Structures', *Mitsui Technical Bulletin*, **TB 83-07**, October, pp 1-9. (Published by Technical Research and Development H. Q., Mitsui Engineering and Shipbuilding Co. Ltd., 6-4, Tsukiji 5-Chome, Chuo-ku, Tokyo, Japan.)

77. T. H. Havelock, 1950, 'The Pressure of Water Waves on a Fixed Obstacle', *Proceedings of the Royal Society of London* **A**, **175**, pp 409 - 421.

78. S. Homma, 1950, 'On the behaviour of seismic seas round circular island', *Geophysical Magazine*, **XXI**, pp 199 - 208.

79. J. R. Houston, 1981, 'Combined refraction and diffraction of short waves using the finite element numerical model', *Applied Ocean Research*, **3**, pp 163-170. (See also ref. 255.)

80. E. L. Ince, 1932, 'Tables of the Elliptic-Cylinder Functions', *Proceedings of the Royal Society of Edinburgh*, **52**(4), pp 25 - 433.

81. A. T. Ippen, and D. R. F. Harleman, 1966, 'Tidal Dynamics in Estuaries', Chapter 10 of A. T. Ippen, *Estuary and coastline hydrodynamics*, McGraw-Hill, New York, pp 493 - 454.

82. S. Karaiosifidis, 1976, 'A Comparison of Solution Methods for Exterior Surface Wave Problems', *M.Sc. thesis*, University of Wales, Swansea, (C/M/ 120/ 76).

83. S. N. Karp, 1961, 'A Convergent 'Farfield' Expansion for Two-Dimensional Radiation Functions', *Communications on Pure and Applied Mathematics*, **XIV**, pp 427 -434.

84. Steve Kay and Peter Bettess, 1996, 'Revised Mapping Functions for Three-Dimensional Serendipity Infinite Elements', *Communications in Numerical Methods in Engineering*, **12**, pp 181 - 184.

85. B. Kinsman, 1965, *Wind Waves* Prentice-Hall, Englewood Cliffs, New Jersey.

86. D. E.Knuth, 1969, *The Art of Computer Programming, Volume 1 - Fundamental Algorithms*, Addison-Wesley.

87. Sir Horace Lamb, 1932, *Hydrodynamics*, Sixth Edition, reprinted 1974, Cambridge University Press, Cambridge.

88. S. L. Lau and Z. Ji, 1989, 'An Efficient 3-D Infinite Element for Water Wave Diffraction Problems', *Int. Journ. Num. Meth. Engng.*, **28**, pp 1371-1387.

89. B. LeMehauté, 1970, *An Introduction to Hydrodynamics and Water Waves*, Springer Verlag, Berlin.

90. H. Y. Leung, 1981, *Contour Plotting for Finite Element*, B.Sc. Thesis, Department of Civil Engineering, University of Wales, Swansea, CP/752/81.

91. James Lighthill, 1978, *Waves in Fluids*, Cambridge University Press.

92. C. M. Linton and D. V. Evans, 1990, 'The interaction of waves with arrays of vertical circular cylinders', *Journal of Fluid Mechanics*, **215**, pp 549-569.

93. R. C. MacCamy and R. A. Fuchs, 1954, 'Wave Forces on Piles. A Diffraction Theory' *Beach Erosion Board Tech. Mem. No. 69.*

94. J. M. M. C. Marques, and D. R. J. Owen , 1984, 'Infinite elements in quasi-static materially non-linear problems', *Computers and Structures*, **18**(4), pp 739-751.

95. J. M. M. C. Marques and D. R. J. Owen, 1984, 'Implicit-Explicit Time Integration in Quasistatic Elastoviscoplasticity using Finite and Infinite Elements', *Computer Methods in Applied Mechanics and Engineering*, **42**(2), pp 167-182.

96. C. C. Mei, 1983, *The Applied Dynamics of Ocean Surface Waves*, Sixth Edition, Wiley Interscience, New York.

97. E. Thomas Moyer, Jnr., 1992, 'Performance of Mapped Infinite Elements for exterior Wave Scattering Applications', *Comms. in Applied Numerical Methods*, **8**, pp 27-39.

98. H. W. McLachlan, 1960, *Theory and Application of Mathieu Functions*, Oxford University Press.

99. Sir Isaac Newton, 1687, *Philosophiæ Naturalis Principia Mathematica*, translated into English by Andrew Motte, 1729, as *The Mathematical Principles of Natural Philosophy*, facsimile published in 1968 by Dawsons of Pall Mall, London.

100. B. Nicolas-Vullierme, 1984, 'Study of harmonic vibrations of fluid-structure coupled systems of revolution by means of the Bettess-Zienkiewicz mapped infinite element', *Int. Conf. Numerical Methods for Transient and Coupled Problems*, Pineridge Press, Swansea, pp. 887-902.

101. D. R. J. Owen and E. Hinton, 1980, *Finite Elements in Plasticity - Theory and Practice*, Pineridge Press, Swansea.

102. E. S. Page and L. B.Wilson, 1973, *Information Representation and Manipulation in a Computer*, Cambridge.

103. W. G. Penney and A. T. Price, 1952, 'Diffraction of sea waves by breakwaters', *Phil. Trans. Royal Society of London, Series A*, **244**(882), pp 231-253.

104. J. D. Pos, 1983, 'Wave Diffraction using Finite and Infinite Elements', *Computer Methods in Applied Mechanics and Engineering*, **41**(2), pp 219-235.

105. J. D. Pos, 1984, 'A Study of Breakwater Gap Wave Diffraction Using Close Range Photogrammetry and Finite and Infinite Elements', *Ph. D. thesis*, University of Cape Town.

106. J. D. Pos, 1985,'Asymmetrical Breakwater Gap Wave Diffraction using Finite and Infinite Elements', *Coastal Engineering*, **9**, pp 101-123.

107. J.D. Pos, F.A. Kilner, P.G. Fischer, 1987, 'Combined refraction-diffraction of water waves by an island', *Int. Jou. of Eng. Sci.*, **25**(5), pp 577-590.

108. F. Rellich, 1943, 'Über das Asymptotische Verhalten der Lösungen von $\Delta u + \lambda u = 0$ in Unendlichen Gebeiten', *Jahresbericht der Deutschen Mathematiker Vereinigung*, **53**, pp 57-65.

109. L. F. Richardson, 1911, 'The approximate arithmetical solution by finite differences of physical problems involving differential equations, with an application to the stresses in masonry dam', *Trans. Roy. Soc.*, **A210**, pp 307 - 357.

110. A. Sommerfeld, 1896, 'Theorie mathematique de la diffraction', *Math. Ann.*, **47**, pp 317-374.

111. A. Sommerfeld, 1949, *Partial Differential Equations in Physics*, Academic Press, New York.

112. J. J. Stoker, 1957, *Water Waves*, Interscience, New York.

113. A. H. Stroud and D. Secrest, 1966, *Gaussian Integration Formulas*, Prentice-Hall, Englewood Cliffs, New Jersey.

114. C. Taylor, B. S. Patil and O. C. Zienkiewicz, 1969, 'Harbour Oscillation - A Numerical Treated for Undamped Natural Modes', *Proc. Inst. Civil Engineers*, **43**, pp 141 - 156.

115. E.Trefftz, 1926, 'Gegenstuck zom rits schen verfahren', *Proc. Sec. Int. Congress Applied Mechanics*, Zurich, 1926.

116. R. L. Ungless, 1973, *An infinite finite element*, M A Sc Thesis, University of British Columbia.

117. A. C. Vastano and R. O. Reid, 1967, 'Tsunami response for islands: verification of a numerical procedure', *Journal of Marine Research*, **25**, pp 129 - 139.

118. G. B. Whitham, 1973, *Linear and Nonlinear Waves*, John Wiley, New York.

119. C. H. Wilcox, 'An Expansion Theorem for Electromagnetic Fields' 1956, *Communications in Pure and Applied Mathematics*, **IX**, pp 115 - 134.

120. A. N. Williams, 1985, 'Wave Forces on an Elliptic Cylinder' *Journal of the Waterway, Port and Coastal Engineering, Proceedings of the A.S.C.E.*, **3**(2), March, pp 433 - 449.

121. A. N. Williams, 'The Linear Theory of Wave Diffraction by a Vertical Cylinder of Elliptic Cross-Section in Water of Finite Depth', *Fluid Dynamics Report 3/82*, Department of Mathematics, University of Reading, Whiteknights, Reading, RG6 2AX.

122. O. C. Zienkiewicz and P. Bettess, 1975, 'Infinite elements in the study of fluid structure inter-action problems', *Proc. 2nd Int. Symp. on Comp. Methods Appl. Sci.*, Versailles, also published in *Lecture Notes in Physics*, Vol. 58, Eds. J.Ehlers *et al.*, Springer-Verlag, Berlin, 1976.

123. O. C. Zienkiewicz, D. W. Kelly and P. Bettess, 1977, 'The Coupling of the Finite Element Method and Boundary solution Procedures', *Int. Jour. for Num. Meth. in Engng.*, **11**, pp 355-365.

124. O. C. Zienkiewicz, P. Bettess and D. W. Kelly, 1978, 'The Finite Element Method for Determining Fluid Loadings on Rigid Structures: Two- and Three- Dimensional Formulations', Chapter 4 of *Numerical Methods in Offshore Engineering*, Eds. O. C. Zienkiewicz, R. W. Lewis and K. G. Stagg, pp 141-183, John Wiley.

125. O. C. Zienkiewicz, P. Bettess, T. C. Chiam and C. R. I. Emson, 1981, 'Numerical methods for unbounded field problems and a new infinite element formulation', ASME, *AMD*, **46**, pp 115-148, New York.

126. O. C. Zienkiewicz and P. Bettess, 1982, Letter discussing Ref. 79, *Applied Ocean Research*, **4**(2), p 124.

127. O. C. Zienkiewicz, C. R. I. Emson, and P. Bettess 1983, 'A novel boundary infinite element', *Int.J. Num. Meth. Eng.*, **19**, pp 393-404.

128. O. C. Zienkiewicz, K. Bando, P. Bettess, C. R. I. Emson and T, C. Chiam, 1985, 'Mapped Infinite Elements for Exterior Wave Problems', *Int. J. Num. Meth. Eng.*, **21**, pp 1229-1251.

129. O. C. Zienkiewicz and R. L. Taylor, 1989, *The Finite Element Method*, **1**, 4th edition, McGraw-Hill, Maidenhead. (And first three editions).

130. O. C. Zienkiewicz and R. L. Taylor, 1992, *The Finite Element Method*, **2**, 4th edition, McGraw-Hill, Maidenhead. (And first three editions).